Republic of Iraq
Ministry of Higher Education and Scientific Research
University of Babylon
College of Engineering

Development of Electroplating Zn-Ni Base System for Aerospace Industries

A Thesis Submitted to

Materials Engineering Department
College of Engineering
University of Babylon
In Partial Fulfillment of the Requirements for the Degree of
Doctor of Philosophy

In
Materials Engineering

Submitted by

Mohammed Abdul-Mahdy Mohammed Hussein

Supervised by

Dr.Abdul-Alwahid Rajih
Professor

Dr.Fadhel M.Hussoun
Ass.Professor

Dr.Fraqud F.M Saeed
Ass.Professor

2007 1428

بسم الله الرحمن الرحيم

﴿ وَفَوْقَ كُلِّ ذِي عِلْمٍ عَلِيمٌ ﴾

صدق الله العلي العظيم

[يوسف : ٧٦]

Dedication

To My Family

Mohammed

Abstract

It is well established recently that Zn-Ni coatings possess significant applications like aerospace industry.

This work represents an attempt to introduce further improvement in the properties of theses coatings, although the Zn-Ni deposition is known to be an anomalous electrodeposited process and yet poorly understood.

Also, it appears so difficult to design an electrolyte in such away to obtain a sacrificial coatings, i.e. ~ 14% Ni content. In addition, it is required to verify whether or not the same simple relations would be obtained from the solutions containing other pairs of metal ions.

Carbon steel samples were coated with Zn-Ni, Zn-Ni-Cu and Zn-Ni-SiO_2 by using potentiostatic technique under nitrogen atmosphere. After electroplating, these samples were analyzed by X-ray fluorescent to confirmed all the content for each alloy.

This work adopted an attempt to develop Zn-Ni and not Ni-Zn to minimize the cost. The addition of SiO_2 ,however, introduces a further decrease in cost and weight(density for SiO_2 2.6gm/cm^3) which represent the main target in the aerospace industries.

In addition these coatings are free of toxicity and an environmentally friendly compared with Cd and Cr.

Microhardness tests were conducted for all coatings and the base metal, the result was a significant superiority of Zn-Ni-SiO_2 layer.

Corrosion test by salt spray chamber (5% NaCl) at 35 °C for 24 hrs 1 bar carried out the base metal(carbon steel) ,Zn-Ni, Zn-Ni-Cu and Zn-Ni-SiO_2 before and after heat treatment at 200°C 1 hr. The corrosion rate (mpy) for Zn-Ni-SiO_2 coatings was only 3%,7% and 10% with respect to the corresponding value of the base metal, Zn-Ni and Zn-Ni-Cu respectively.

Polarization curves for (Tafel slope) were carried out by potentiostatic technique for (5% NaCl) a medium and produce all data by computerize. The observed corrosion current for Zn-Ni-SiO_2 was only 9%,15%and 18% compared with base metal and other coatings.

In 1% sulfuric acid, however, the corrosion current (Tafel slope) was only 5%,22% and 23% compared with base metal, Zn-Ni and Zn-Ni-Cu respectively, this result observed again a protective layer in a different medium.

The test were carried out by 1% HCl a medium at ambient temperature (15°C),35°C,45°C and 55°C before and after heat treatment. The corrosion rate(mpy) at 55 °C was only 7%,9% and 11% when compared with base metal, Zn-Ni and Zn-Ni-Cu respectively.

In humidity environment, after heat treatment for example, the weight loss for Zn-Ni-SiO_2 at 55°C 24 hrs was only 10%and 13% compared with Zn-Ni and Zn-Ni-Cu respectively.

Thermal shock test was carried out at various temperature ranges (250,300,350,400,450,500 and 550°C) at interval of 50 °C and these samples were water quenched after 15 min at each

temperature. Zn-Ni-SiO_2 coating appeared to have a good plasticity and adhesion with Zn-Ni rich coating. The weight loss (measure for cracking and spalling) for Zn-Ni-SiO_2 was only 3% and 5% compare with Zn-Ni and Zn-Ni-Cu respectively.

Surface roughness tests were carried out for Zn-Ni, Zn-Ni-Cu and Zn-Ni-SiO_2.The addition of SiO_2 to the surface layer did not effect the surface roughness.

Reflectivity-Transmissivity tests were also conducted to measure the absorption and reflective for all coating. The result indicated that the addition of SiO_2 increased transmissvity and decreased reflectivity (for first layer) i.e. more absorption.

List of Tables

List of Figures

Nomenclature

ΔG	Change in Gibbs free energy
ΔH	Change in enthalpy
ΔS	Change in entropy
T	Temperature
$\Delta G°$	Free energy change at standard state
R	Gas constant 8.314 J/mole.K
K_{eq}	Equilibrium constant
$G`$	Electrochemical free energy
q	Electric charge
Φ	Electric potential energy
ΔG_M	Chemical free energy change
z	Valancy of metal
F	Faradays constant (96487 coulomb/mole)
$\Delta \Phi_M$	Potential change
E_M	e.m.f of the cell
$\Delta \Phi_H$	Potential change (reference to hydrogen)
E	The electrode potential at equilibrium
$E°$	The standard electrode potential
Q	Charge created by ionization of M mole of material
j	Flux of substance
η	Overpotential
E_i	Polarized potential
E_{eq}	Equilibrium potential
i_{app}	Applied current density
$\overrightarrow{i}$	Partial current
E_c	Potential of cathode direction
E_a	Potential of anode direction
$\grave{E}_c$	Potential of cathode direction (open circuit)
$\grave{E}_a$	Potential of anode direction (open circuit)
f_c	Polorization function of the cathode
f_a	Polorization function of the anode
A_c	The area of the cathode
A_a	The area of the anode
i	Current density
a,b	Tafel constant

α	The symmetry factor
i_o	Echange current density
i_a, i_c	Net anodic and cathodic current respectively
η_a	Anodic overpotential
η_c	Cathodic overpotential
b_a	Anodic Tafel slope
b_c	Cathodic Tafel slope
i_{Lm}	Maximum rate of a possible reaction for a given system (limiting current density)
η^c	Concentration polarization
D	Diffusion confficient of reaction ion
C_b	Bulk concentration of reaction ion
δ_m	Thickness of diffusion layer
n	Number of electrons transfer
η_r	Resistance of overpotential
R_{solu}	The electric resistance of solution
R_f	The electric resistance produced by film or coatings
E_{corr}	Corrosion potential
CR	Corrosion rate
d_{Me}	Density of the metal
t_a	Year in seconds
t_n	Transference number
c_s	Concentration of electrode surface
∂x	The velocity moving along the axis
O	Pertaining to species O in O+ nē →R
R	Pertaining to species R in O + nē →R
μ_i	Charge of species i
Φ	Potential
θ_j	The surface covered by specie j
W_a	Wagner number
ρ_e	The electrode resistivity
LCD	Low corrosion current
UPD	Underpotential deposition
SCE	Saturated calomel electrode
EUT	The equipment under test
SHE	Standard hydrogen electrode

List of Contents

Introduction

For many years, zinc has been the most widely used corrosion resistance coatings for steel and other ferrous materials. This is direct result of its ability to provide efficient and reliable corrosion protection at low cost. Regardless of the production method ,zinc coatings generally need to be thick (typically up to 25 μm) in order to achieve good corrosion resistance because the zinc is consumed sacrificially at a relatively high rate while under exposure to corrosive conditions. Thick coatings are problematic, however, due their poor formability and weldability [(1)].

Its also difficult to obtain a high specular protective thick layer[(2)].This has prompted the search for techniques to further improve the corrosion resistance of zinc, thereby permitting the use of thinner coatings while still maintaining a high level of performance. Reduction in corrosion susceptibility by a factor of 5-7 times, for example, have been claimed for Zn coatings alloyed with 9-17 Wt.% Ni, as compared to those having no alloying additions at all[(3)].

Due to the attractive properties of Zn-Ni coatings, the introduction of this alloy into industrial practice has been extremely successful. Zn-Ni electrodeposits performance, however, the beneficial influence of alloying is not fully understood. Several hypotheses have been advanced assuming that corrosion inhibition may be related to the structural and /or electronic properties of the passive oxide film.

At this time, approximately 75% of market demand for zinc alloy coatings come from automotive industry[(4)],steel autobody

panels[5],fuel tanks[6],and fasteners[7] are a few of the products that well suited to the thinner and lighter Zn-Ni coatings.

Zn-Ni coating has recently using to replace cadmium plating, which is widely used in the aerospace industry for the corrosion protection of steel[8]. Cadmium plating, is used to protect steel components on aircraft primarily because of its excellent corrosion resistance and its electrochemical compatibility with any of aluminum alloys used in aircraft construction[9].Despite the advantages of cadmium plating, however, alternatives are required due to the toxicity of the metal and its compounds.

Chrome(Cr^{6+}) is used, as a passivating layer on zinc alloys, the chromate layer offers good corrosion protection properties, to the fact that chrome (Cr^{6+}) is very active and can migrate over the surface,thus providing self-healing properties. Due to that reactivity, hexavalent chrome is also toxic and carcinogenic. When replacing hexavelent chrome with a chrome (Cr^{6+}) free product, the passivating properties are reduced. One of the alternatives is to replace by coating Zn-Ni alloys, this coating shows great promise from the corrosion resistance point of view.

Steady growth in the usage of Zn-Ni coatings has also been seen in the household appliance[10], electrical component[11],metal building, construction and (heating ventilation and air conditioning) HVAC industries[12].Potential exists, as well, for Zn-Ni to be used as electrodes for electrocatalytic water electrolysis [13]. This work i.e. Zn-Ni coatings represents an alternative for Ni-Zn coatings. This attempt is however, represents a real challenge.

Aim of The Research

Composite coatings used in this work for electroplating process technology provides an environmentally friendly solution for chromium or cadmium (both considered as toxic metal) replacement in corrosion protection application for steels, tacking into consideration that incorporation of Zn and SiO_2 into the sacrificial coatings decreases cost, density and enhancing corrosion resistance.

The main targets of this work include:

1-Low carbon steel is main alloy to be plated. Carbon steel is considered the most applicable alloy and widely used in industry as well as this alloy is considered to be the cheapest among other steel alloys.

2-Preparing new combination of coatings consist of enriching Zn coatings, Ni, Cu and SiO_2.

3- Fabricating new electrochemical cell to be used for electroplating.

4-Appling new procedure tailored to introduce the effective parameters (time and current),in order to optimize (zinc/nickel/ceramic) system.

5-Investigating the ability of the new coating (zinc/nickel/ceramic)to combat sever corrosion environmental conditions.

These coatings systems find a wide range of advanced applications in aerospace industries such as landing gear, hydraulic actuators, high performance fasteners, break and fuel lines, as well as other industries like marine industry, electrical power transmitting equipment, computerize lock components, electrocatalysis and storing energy.

Chapter One

CORROSION

Chapter One

Corrosion

1.1 Definition of corrosion

The word corrosion comes from the Latin - corrodene to gnaw away .Corrosion is the destructive attack of a metal by chemical or electrochemical reaction with its environment[14] , which leads to change of characteristics of the metal and substantial impairments of the function of the metal, the metal ceases to be an element , and becomes a compound [15].

They are reduced to metallic state by the expenditure of energy during smelting operation which involves the removal of the bulk of the combining elements.

Such extracted metals are inherently unstable and show a general tendency to revert to the natural or oxidized condition by combining with the constituents of their environment. This reverse process requires no supply of energy so it occurs readily and spontaneously in order to reach a stable state, the result is seen as corrosion [16, 17].

Deterioration by physical cause is not called corrosion, but described as erosion , galling , or wear .In some instances , chemical attack accompanies physical deterioration as described by terms , corrosion-erosion, corrosive wear or fretting corrosion[18].

Electrochemical corrosion is an industry cancer with direct costs estimated to at 2.5 to 3.5% of the gross nation product in industrialized countries [19].

A recent survey on the costs of corrosion showed that the direct cost of corrosion was $276 billion in the United States for 2002 , which is approximately 4% of their National product [20] (see appendix A) [21] , Although currently the ability to reliably quantify corrosion in the field is limited to a threshold of about 10% loss of the original material thickness[22].

Corrosion is a complex problem due to the many variables involved , the Factor governing the rate of corrosion may by broadly divided into those relating to the metal and the environment.

The main factors relating to the metal or alloy include, the position of the metal in the electro – chemical series , contact with dissimilar metals , microstructure, e.g. the presence of impurities or of a second constituent and the presence of internal stress.

Other factors involved when considering the effect of environment include , the acidity or alkalinity of the liquid, rate of supply and distribution of oxygen, rate of flow of liquid, relative humidity, presence of external stress ,and presence of impurities in the atmosphere[23], see figures (1.1-1.6).

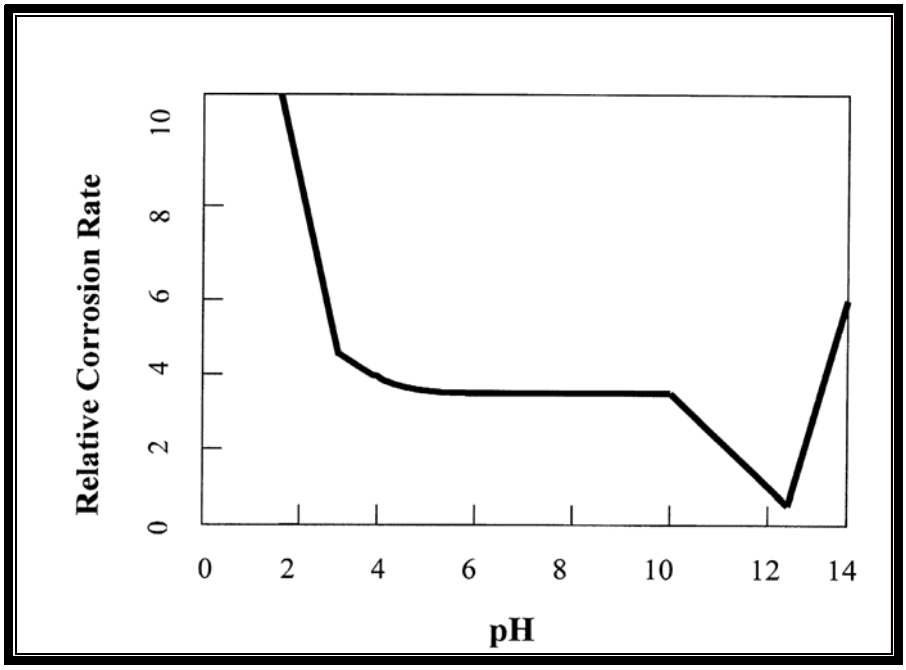

Figure (1.1) Effect of pH on the corrosion rate of iron [24].

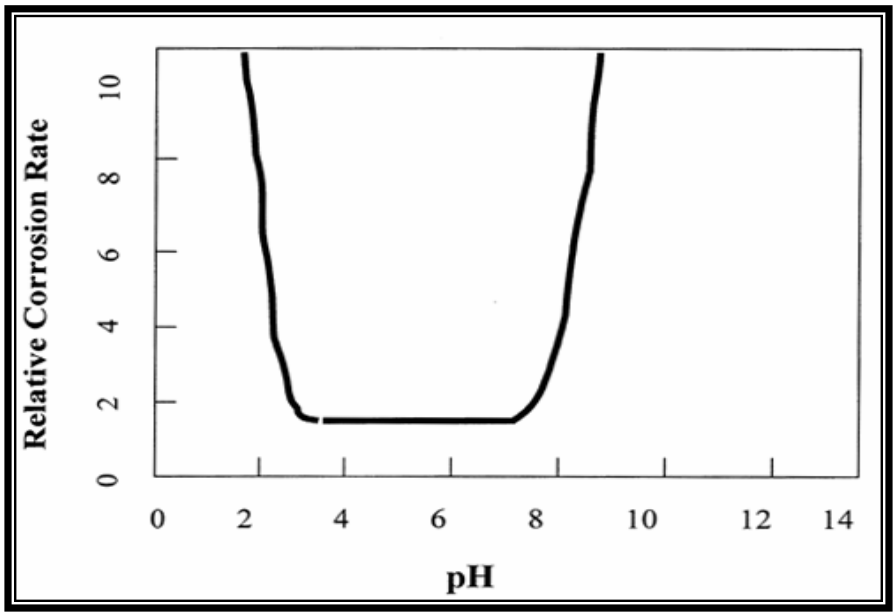

Figure (1.2) Effect of pH on the corrosion rate of amphoteric metals (aluminum and zinc)[24]

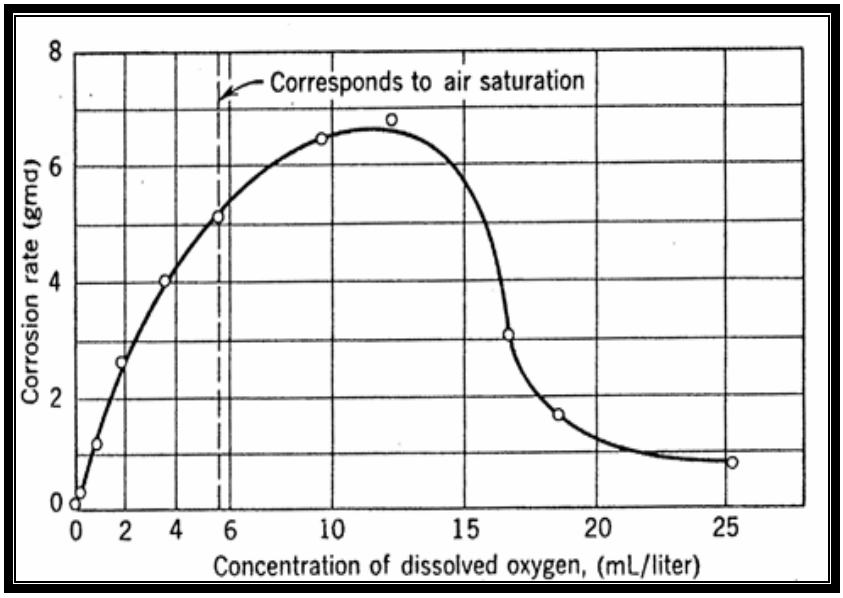

Figure (1.3) Effect of oxygen concentration on corrosion of mild steel in slowly moving distilled water, 48 hr test , 25°C[18].

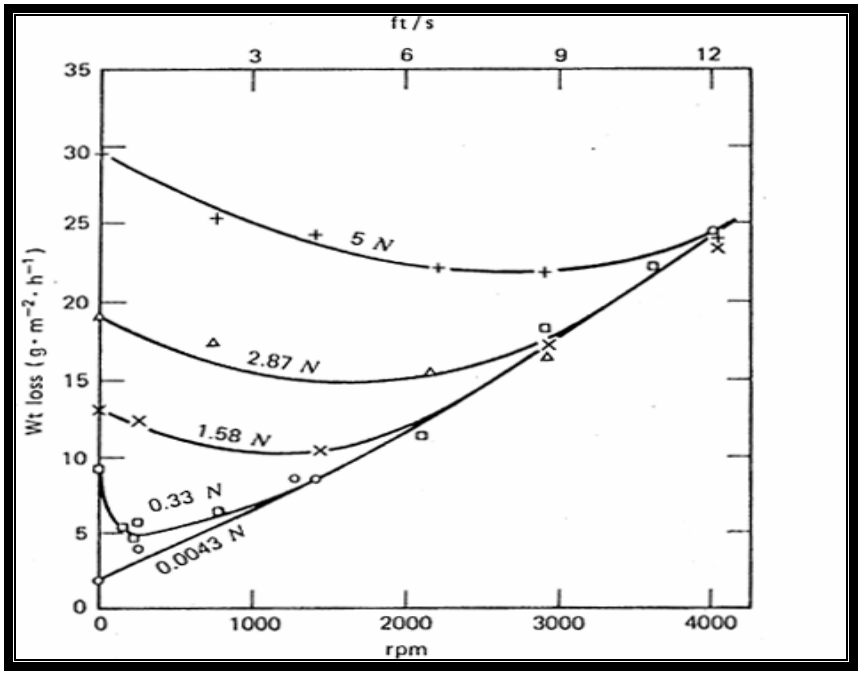

Figure (1.4) Effect of velocity on corrosion of mild steel (0.12 % C) in sulfuric acid under air (23 ± 2°C,45 min test , rotating space , 18-mm diameter , 56 mm long) [18]

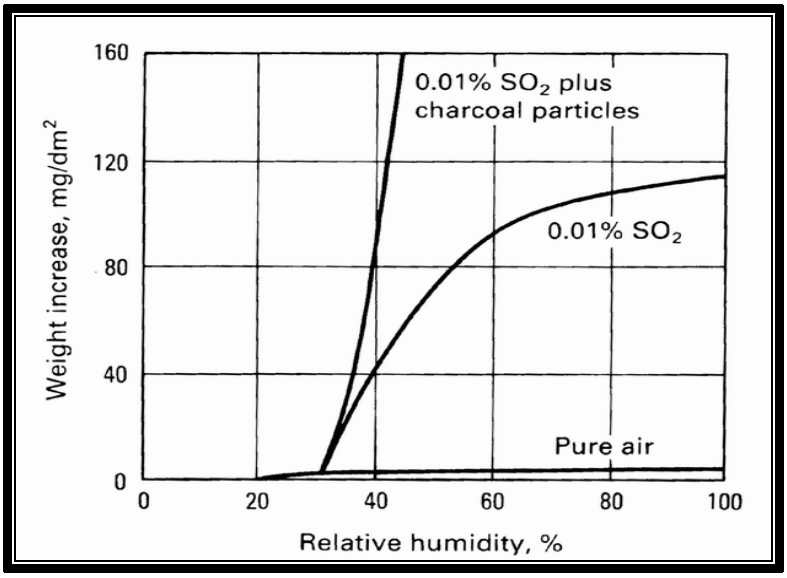

Figure (1.5) Relationship between the corrosion rate of iron and the relative humidity in an environment containing 0-01% SO_2.Exposure period :55 days the corrosion rate of iron exposed for 55 days at 100% relative humidity is shown for comparison [25]

\

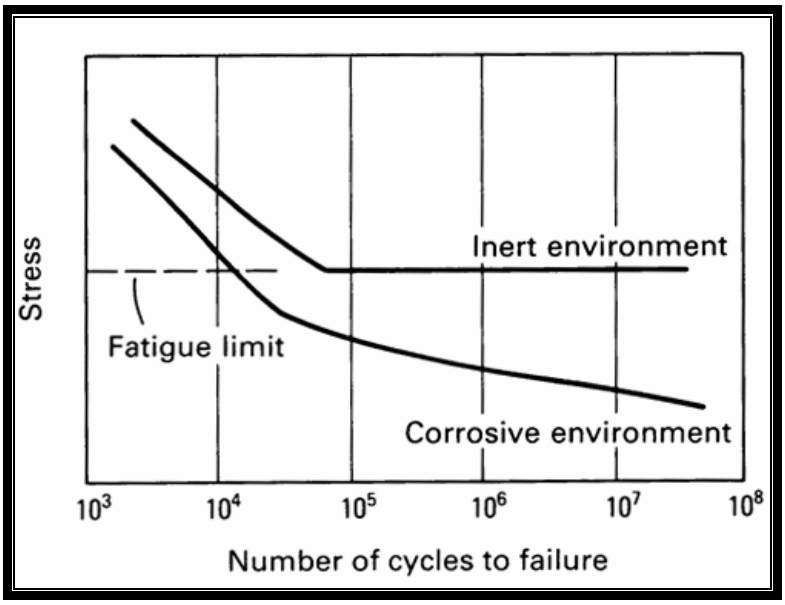

Figure (1.6)Elimination of the fatigue limit due to the presence of a corrosion environment [25]

1.2 Mechanism of Aqueous Corrosion

When metal atoms are exposed to an aqueous environment they can release electrons, thus becoming positively charged ions, this is the anodic reaction of the electrochemical process. It can only happen if the electric circuit is completed by electron consumption at some other place, as shown schematically in figure (1.7) for iron in acid environment.

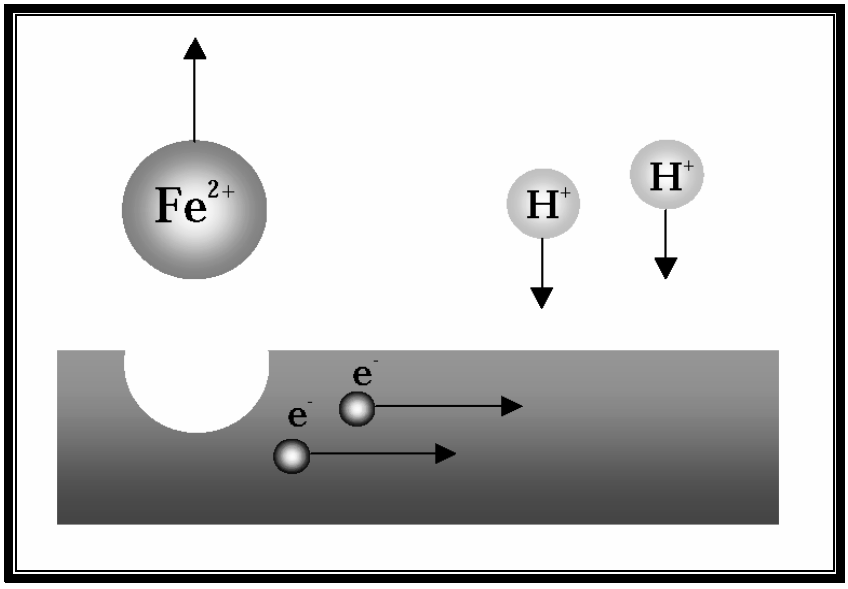

Figure (1.7) Corrosion of iron in acid environment [26]

At the cathode side the electrons and protons first form atomic hydrogen and after that molecular hydrogen gas . The free metal ions can form different compounds with the species in the environment , predominantly oxides and hydroxides , thus returning to their lower energy levels.

The conductivity of the environment is also of a great importance , since the electric circuit must be closed in the environment side by the transfer of charged particles . The

presence of various salts would provide anions that increase the conductivity and facilitate the corrosion process.

1.3 Gibbs Energy

The driving force for chemical reactions depends not only on chemical formulas of species involved but also on the activities of the reactants and products. Free energy is the thermodynamic property that has been assigned to express the resultant enthalpy of substance and inherent probability. At constant temperature, free energy can be expressed as:

$$\Delta G = \Delta H - T\Delta S \quad \text{.....(1.1)}$$

Where ΔG is the change in free energy (Gibbs free energy) ΔH is the change in enthalpy , T is the absolute temperature , and ΔS is the change in entropy.

When reaction is at equilibrium and there is no apparent tendency for a reaction to proceed either forward or backward, so free energy could be expressed as follows: [27].

$$\Delta G^{\circ} = - RT \ln K_{eq} \quad \text{…….(1.2)}$$

Where ΔG° is the free energy change under the special conditions when all reactants and products at a standard state, R is the gas constant, and k_{eq} is the equilibrium constant.

The change in free energy ΔG is a direct measure of the work capacity or maximum electric energy available from a system.

If the change in free energy accompanying the transition of a system from one state to another is negative, this indicates a loss in free energy and spontaneous reaction direction of the system. In other word, if no external forces act on the system, the system will tend to transform to its lowest energy state.

If the change in free energy is positive, this indicates that the transition represents an increase in energy, and this requires that additional energy to be added to the system [28].

These principles are illustrated in figure(1.8) by a mechanical analogy. If the ball moves from position 1 to position 2, this represents a decrease in free energy.

The transition from position 1 to position 2 is the spontaneous direction for this particular system.

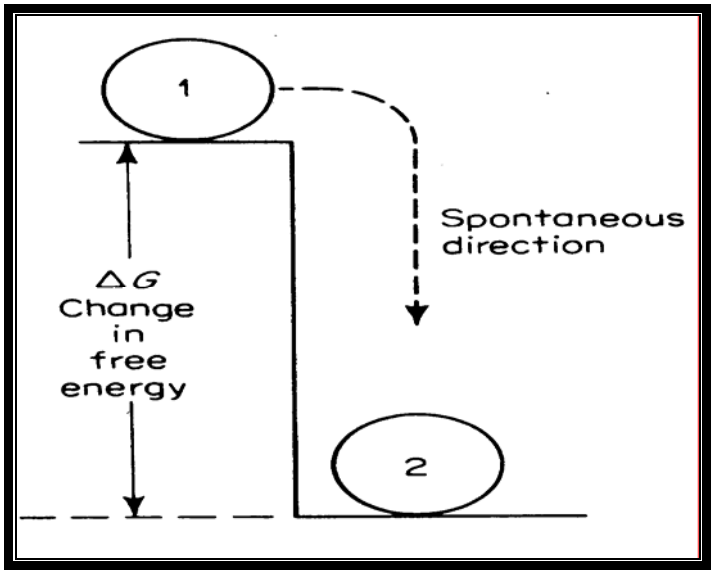

Figure (1.8) Mechanical analogy of free energy charge[29]

The reverse transformation from position 2 to position 1 is not spontaneous direction and requires the application of energy.

The change in free energy is a state function and is independent of the reaction path. This is illustrated in figure(1.9) , which is similar to figure (1.8) except that there are two possible reaction path A and B.

For either path, free-energy change for the transition from state 1 to state 2A or 2B is exactly the same. It is obvious, however, that the transformation along path B will require more time and will be slower than along path A. Chemical and corrosion reactions behave exactly in the same fashion.

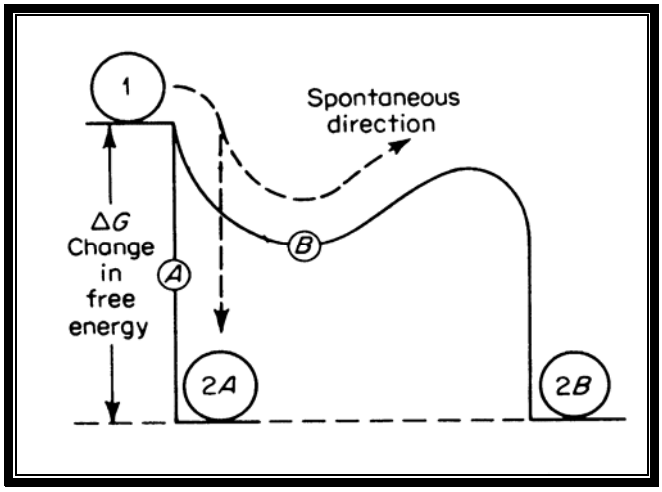

Figure (1.9) Effect of reaction path on reaction rate[29]

It is impossible to predict accurately the velocity of a reaction from the change in free energy.

This parameter reflects only the direction of reaction by its sign, and any prediction of velocity based on the magnitude of the change in free energy.

If the extent of reaction is small enough not to change the activities of reactants and products, the potential remains constant, and the energy dissipatal by an infinitesimal passage of charge [25].

Thus if the chemical reaction leads to the production or elimination of ions or electrons, the driving force then becomes the electrochemical free energy:

$$G` = G+q\Phi \quad \ldots\ldots\ldots\ldots\ldots\ldots(1.3)$$

G` is called electrochemical free energy, q is the electric charge and $\Phi$ is electric potential energy ,the reaction will proceed in such a direction $\Delta G`$ is negative figure (1.10) .At equilibrium , there is no net driving force and $\Delta G`$ is zero.

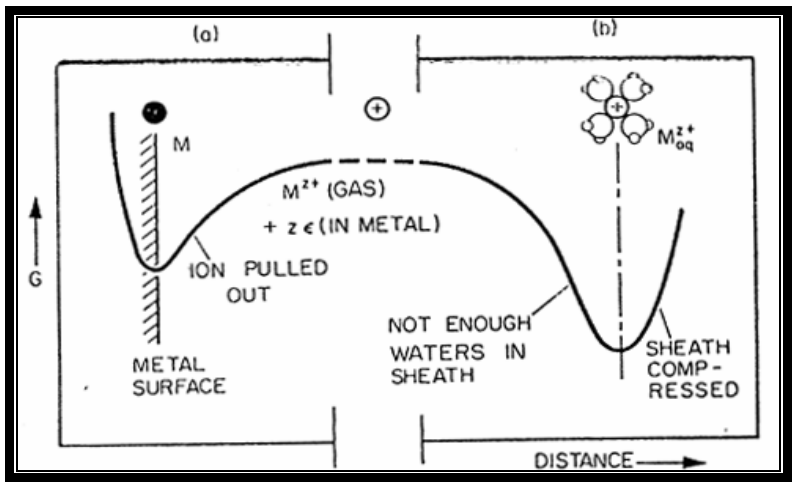

Figure (1.10) The chemical free energy of a family of metals ions[30].

a) Pulled out of the metal surface.

b) Subsequently solvated.

As the metal M dissolves to form aqueous-ions M^{Z+} , there occurs an increasing separation of electric charge , the metal will have a net negative charge and the aqueous solution will be adjacent to the positive side of the metal. Such system is called an electrode.

At equilibrium, when the net changes in electrochemical free energy accompanying, either dissolution or deposition will be zero and equation (1.3) leads to,

$$\Delta G_M = - zF \Delta \Phi_M \text{ …….(1.4)}$$

Where

ΔG_M …. Chemical free energy change

F …… Faraday's constant (96487 Coulomb/ mole)

z …… Valency of metal

$\Delta \Phi_M$ …… Potential change

It is impossible to measure the metal / solution potential directly, but if the system is coupled back –to-back with a second arbitrarily chosen electrode system, it is possible to obtain a relative potential difference.

This arbitrarily reference electrode, which is almost invariably used , is the standard hydrogen electrode (S.H.E). It is assumed that Φ_H is zero. The e.m.f of the cell is then as follows [31] .

$$E_M = \Delta\Phi_M - \Delta\Phi_H \text{ …….....(1.5)}$$

and

$$\Delta G = -zF\, E_M \text{ ……(1.6)}$$

The equation expresses the e.m.f of a cell in terms of the concentrations of reactants and products is:

$$E = E^\circ - \frac{RT}{zF} \ln \frac{[pro]}{[red]} \text{.....(1.7)}$$

Equation.(1.7) is called Nernst equation

Where

E… The electrode potential at equilibrium

E°... The standard electrode potential in which all the products and reactants are in unit concentration.

[ox] and [red]….The concentrations of oxidized and reduced species respectively.

1.4 The Electrical Double Layer

If the charges tend to line up opposite to one another similar test the way that electric charges do on the plates of radio condenser, referred as the double layer. It is illustrated schematically in figure (1.11) and figure (1.12) .

The double layer consists of two parts: a compact layer and a diffuse layer. The compact layer, or Helmholtz layer, is closest to the surface in which the distribution of charge, and hence, potential changes linearly with the distance from the electrode surface. The diffuse outer layer, or Gouy – Chapman layer , occurs where the potential changes exponentially.

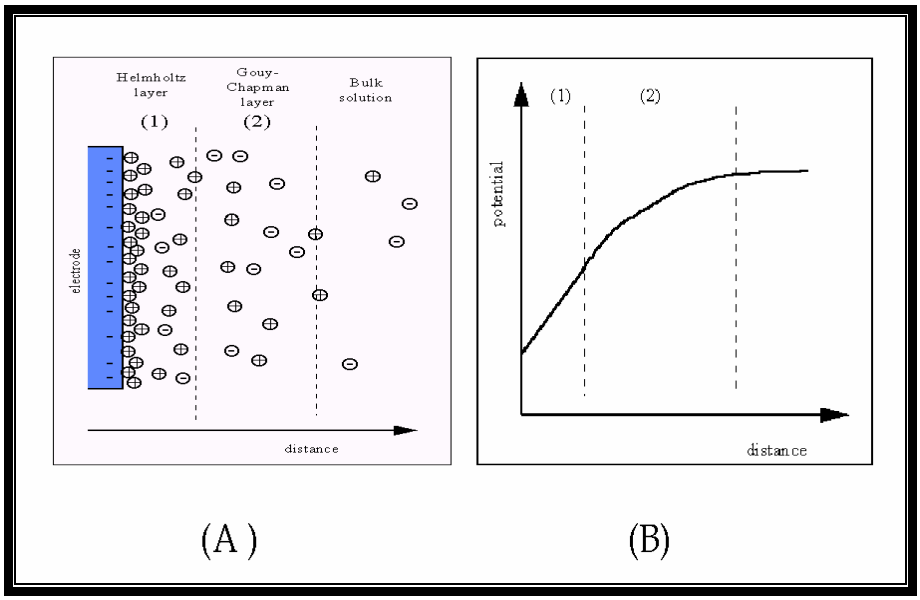

Figure (1.11) The double layer[32]

A: Distribution of ions as a function of distance from electrode behaving as an anode.

B: Variation of potential with distance for the model in A

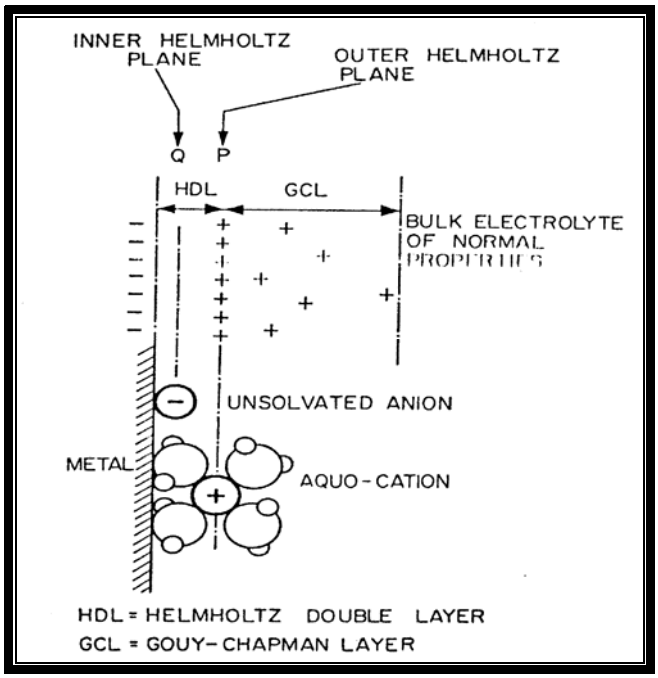

Figure (1.12) The structure of the electrical double layer [30].

Faraday's law of electrolysis states that [32]

$$Q = zFM \quad \text{…….....(1.8)}$$

Q is the charge created by the ionization of M moles of material.

Differentiating with respect to time

$$\frac{dQ}{dt} = zF\,\frac{dM}{dt} \quad \text{……. (1.9)}$$

The rate of flow of charge is current(I) , or if the charge passes a cross unit area of cross-section the current (I) becomes current density (i). then $\frac{dM}{dt}$ becomes (J),

the flux of substance , and equation (1.9) becomes

$$I = z\,F\,j \quad \text{……...(1.10)}$$

The flux of substance is another name of corrosion rate per unit area. The value of double layer capacitance depends on many variables including electrode potential , temperature ionic concentrations , type of ions , oxide layers , polish of the electrode surface , adsorption of impurities , etc. [33].

1.5 Polarization

It is defined as the change in potential of an electrode which results from current flow to or from the surface [34].

Reactants and products jump back and forth at a very real rate, but since there is no accumulation of product, direct measurement of this rate is difficult. The equilibrium exchange rate for an electrochemical reaction, called the exchange current density (i_o).

So polarization could be defined as the extent of the change in potential of an electrode from its equilibrium potential caused by a net current flow to or from the electrode, galvanic or impressed.

When a reaction is forced a way from equilibrium i.e. when one direction of the reaction is favored over the other, the potential at which the reaction is occurring changes. The amount by which the potential changes is the over voltage which is defined as follows [26]:

$$\eta = E_i - E_{eq} \quad \text{……(1.11)}$$

Where

η Is the overpotential.

E_{eq} Is the equilibrium potational.

E_i Is the polarized (current flowing) potential.

Polarization of the anode causes a shift of potential in the positive direction and is the result of an increase in the concentration of ions of the dissolving metal in the vicinity of the electrode, as well as, the formation of protective film covering the anode [35].

Polarization of the cathode displaces the potential of the latter in the negative direction, this shift of potential is brought about by insufficiently rapid removal of the electrons coming from the anodic area,i.e. by accumulation of electrons figure (1.13) shows anodic and cathadic polarization curves.

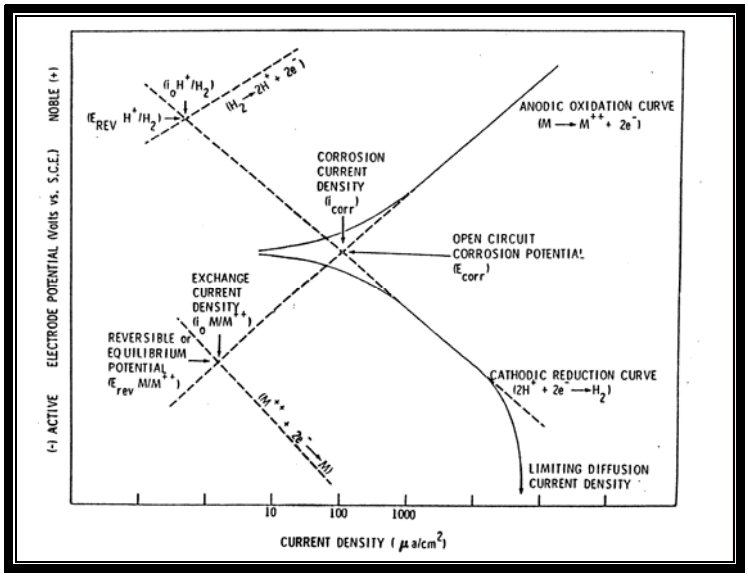

Figure (1.13) Anodic and cathodic polarization curves of a corroding metal[35]

The current applied to cause the departure from equilibrium is the net rate of reaction , thus:

$$i_{app} = \Sigma i^{\rightarrow} - \Sigma i^{\leftarrow} \quad \ldots\ldots\ldots\ldots (1.12)$$

Where

$i^{\rightarrow}$, $i^{\leftarrow}$ and i_{app} are the anodic , cathodic and applied current density respectively.

Also, polarization, defined as the change of potential of an electrode resulting from current flow, alters the potential of the anode in the cathodic direction and the potential of the cathode in the anodic direction. The terms E_c and E_a can be written as functions of the open circuit potentials $È_a$ and $È_c$ in the following way :

$$E_c = È_c - f_c \frac{I}{A_c} \quad \ldots\ldots\ldots (1.13)$$

$$E_a = È_a + f_a \frac{I}{A_a} \quad \ldots\ldots\ldots (1.14)$$

Where f_c and f_a the polarizing functions of the cathode and anode ; A_c and A_a the area of the cathode and anode ; I total current of the cell .

If the current (positive electricity) leaves the electrode and enters the electrolyte, the electrode is functioning as an anode , the electrode will polarize anodically, and its potential will be altered in the cathodic direction (curves 1A , 2A , or 4A in fig.1.14) unless $f_a \quad I/A_a$ is zero (that is , the electrode does not anodically polarize).

In the latter event , the potential will not change with increased current flow and is represented by the horizontal line AC. It is very important to note that if the electrode does polarize anodically , the area of the electrode as well as the amount of current flowing influences the amount of polarization .

If the current leaves the electrolyte and enters the electrode, the electrode is functioning as a cathode, the electrode will polarize cathodically , and its potential will be altered in anodic direction (curve 1C,2C,or 4C figure 1.14) unless $f_c \ I/A_C$ is zero .

In the latter instance , the potential again will not change with the increase of current and the potential curve will be the horizontal line AC.

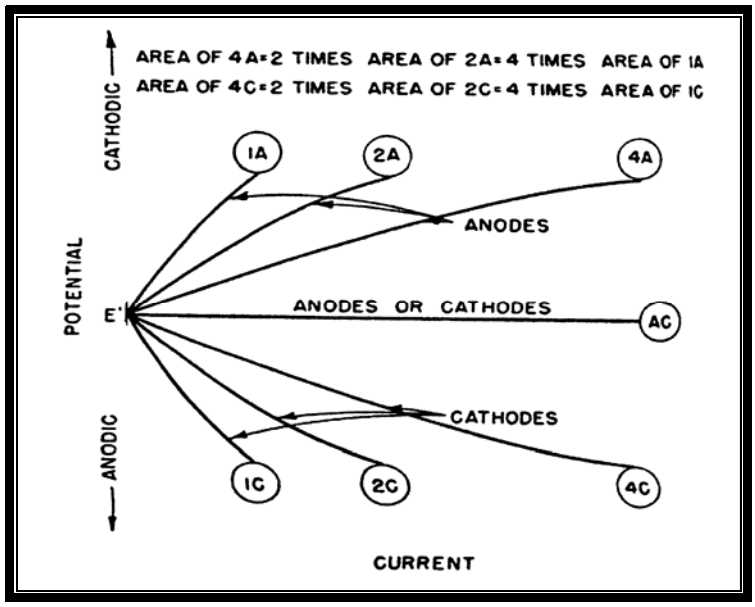

Figure (1.14) Change of potential of anodes or cathodes with flow of current [36].

1.6 Types of polarization

The cause of electrode polarization falls into three different types:

1.6.1 Activation polarization

This polarization refers to an electrochemical process which is controlled by the reaction sequence at the metal–electrolyte interface [29] , or stated in another way in which the reaction at the electrode requires an activation energy in order to go. Activation polarization is usually the controlling factor during corrosion in strong acids.

This is easily illustrated by considering hydrogen evolution reaction on zinc during corrosion in acid solution; figure(1.15) shows some of the possible steps in hydrogen reduction on zinc surface and as follows [29]:

Step (1) : Occurs rapidly and the species must be adsorbed or attached to the surface before the reaction.

Step (2) : Electron transfer (resulting in reduction of the species).

Step (3) : Two hydrogen atoms then combine to form hydrogen molecule.

Step (4) : Hydrogen bubbles are formed.

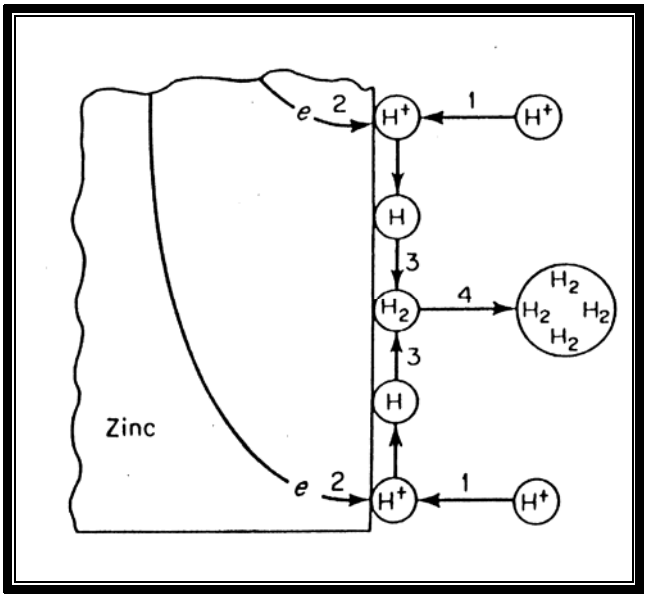

Figure (1.15) Hydrogen evolution reaction steps [29]

Activation polarization is a function of the nature and concentration of the species being reduced , surface roughness and composition , and temperature . In addition it is sensitive to traces of reducible impurities in the system[37].

For any given electrode process under specified conditions , charge transfer at a finite rate will involve an activation overpotential η_A ,which provides the activation energy required for the reactant to surmount the energy barrier that exists between the energy states of the reactant and product.

The activation over potential , and hence the activation energy varies exponentially with the rate of charge transfer per unit area of the electrode surface ,as defined by Tafel Equation [38]

$$\eta_A = a \pm b \log i \quad \text{……(1.15)}$$

Where

i = current density

a,b = Tafel constants

The current density corresponding to the anodic and cathodic processes are related to the over potential as follows :

$$i_a = i_{oa} \left[\exp\left(\frac{\alpha_a z F \eta_a}{RT}\right) - \exp\left(-\frac{(1-\alpha_a) z F \eta_a}{RT}\right) \right] \quad \text{…….(1.16)}$$

$$i_c = i_{oc} \left[\exp\left(-\frac{(1-\alpha_c) z F \eta_c}{RT}\right) - \exp\left(\frac{\alpha_c z F \eta_c}{RT}\right) \right] \quad \text{……..(1.17)}$$

Where

α …. The symmetry factor

z …. Valancy of the metal

F ….. Faraday's constant (96487 coulomb/mole)

R ….. Gas constant

T ….. Temperature

i_o ….. Exchange current density

i_a, i_c ..… Anodic and cathodic current respectively

η_a, η_c ….. Anodic and cathodic overpotential respectively

The above equations may be expressed in the form:

$$\eta_a = b_a \log \frac{i_a}{i_{oa}} \quad \text{……....(1.18)}$$

$$\eta_c = b_c \log \frac{i_c}{i_{oc}} \quad \text{……(1.19)}$$

Where

b_a = Anodic Tafel slope $= \frac{2.3\ RT}{\alpha\ zF}$

b_c = Cathodc Tafel slope $= -\frac{2.3\ RT}{(1-\alpha)\ zF}$

One immediate consequence of Equations (1.18,1.19) is that the activation overpotential measures the extent of the interference with equilibrium at the electrode , the larger the exchange current density then the smaller is η for a given net external current i_a or i_c.

The constant b_a,b_c and exchange current density i_o are constants for a given metal and environment and are both dependent on temperature [18].

The larger the value of i_o and the smaller the value of b , the smaller the corresponding overpotential figure (1.16) shows typically the positions of Tafel slopes , i_{corr} and E_{corr} .

At the reversible potential for the hydrogen electrode (-0.059 pH) , for example , overpotential is zero.

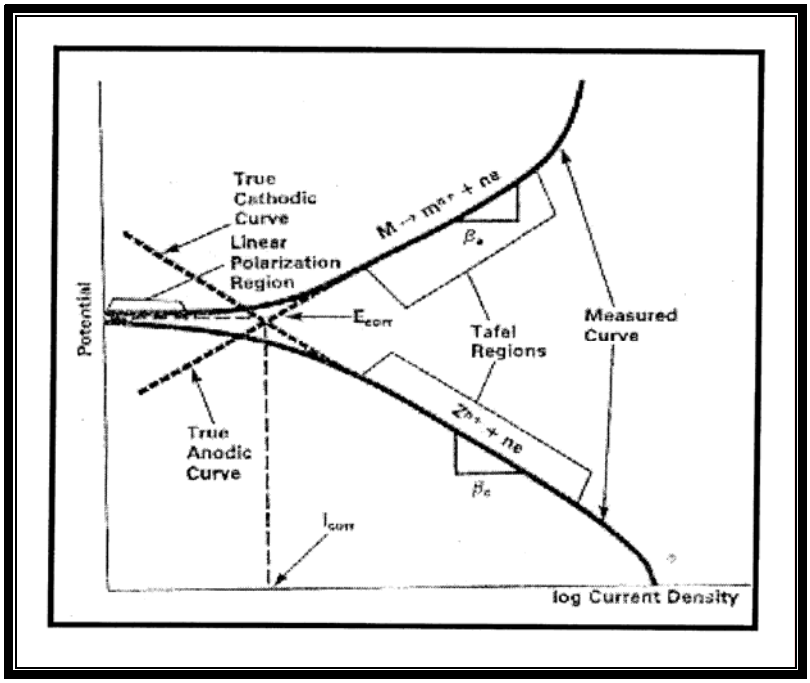

Figure (1.16) Tafel extrapolation [24]

1.6.2 Concentration Polarization

Concentration polarization refers to the electrochemical reactions which are controlled by the diffusion process in the electrolyte. It is obtained when the rate of an electrode reaction is dependent on mass transfer. In another way, the rate of the reduction of substance at a cathode may be limited by the rate of diffusion of the reaction species to the surface, the change in potential under these conditions is called concentration polarization[34].

Concentration polarization occurs when one of the reactants is consumed at an electrode faster than it can be supplied from the bulk of the solution [39,18].

The relationship between the reaction rate and concentration polarization is given in the following equation:

$$i = i_{Lm} [1- \exp (- \frac{nF}{RT} \eta^c)] \quad \text{……(1.20)}$$

Where

i_{Lm} = the maximum rate of a possible reaction for a given system, under which all the transferred species to the electrode react very soon.

η^c = concentration polarization

The maximum rate is known as the limiting current and can be defined mathematically by the following :

$$i_{Lm} = \frac{D_n F C_b}{\delta_m} \quad \text{……(1.21)}$$

Where

D = diffusion cofficient of reacting ion (m^2/s)

C_b = bulk concentration of reaction ion (moles/m^3)

δ_m = thickness of the diffusion layer (m)

Equation (1.20) can be expressed in term of η^c as:

$$\eta^c = - \frac{2.303 RT}{n . F} \log \left(1 - \frac{i}{i_{Lm}} \right) \quad \text{…….(1.22)}$$

The diffusion layer thickness δ is dependent on the velocity of the solution past the electrode surface.

As the velocity increases, δ decreases and the limiting current increases. The time interval required to set up the

diffusion layer varies with the current density and limiting diffusion rate, but it is usually of the order of one second or more.

The diffusion layer reaches a thickness of 100-500 μm depending upon concentration, agitation and temperature [10] .

It has been observed that concentration polarization is the controlling factor during reduction process where the supply of reducible species is limited [29] as shown in figure (1.17).

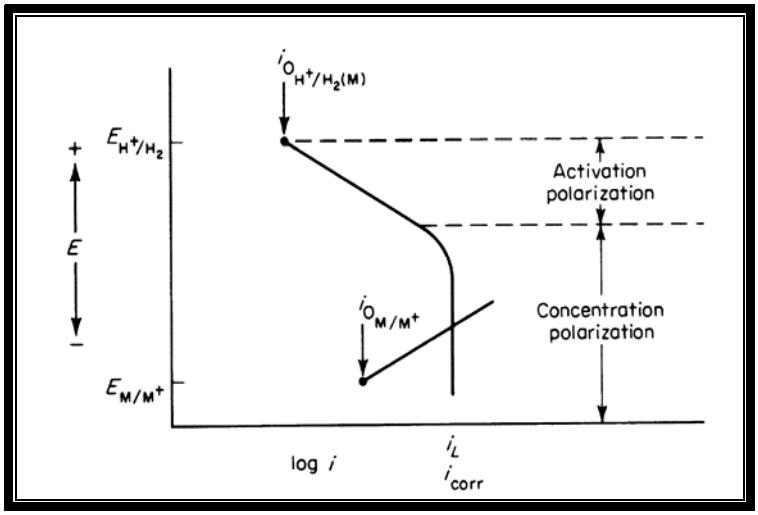

Figure (1.17) Corrosion of metal M under reduction –diffusion control[29]

1.6.3 Resistance polarization (IR Drop)

Polarization measurements include a so-called ohmic potential drop through a portion of electrolyte surrounding the electrode and through a metal-reaction product film on the surface, or both[18].

Since in corrosion the resistance of the metallic path for charge transfer is negligible, resistance overpotential η_r , is

determined by factors associated with the solution or with the metal surface. Thus, resistance overpotential may be defined as[38].

$$\eta_r = I (R_{solu.} + R_f) \quad \ldots\ldots\ldots (1.23)$$

Where, $R_{solu.}$ is the electrical resistance of solution, which is dependent on:

1- The electrical resistivity (ohm.cm) of the solution.

2- The geometry of the corroding system.

And R_f is the resistance produced by films or coatings formed on or applied to the surface of the sites.

Thus , in addition to resistivity of the solution , any insulating film deposited either at the cathodic or anodic sites that restricts or completely blocks contact between the metal and the solution will increase the resistance overpotential ,although the resistivity of the solution is unaffected.

Resistance polarization is merely an error produced by the potential measuring circuit. It is important only at high current densities or in high resistance solutions [39].

All the above types of polarization are presented to a greater or a lesser extent in most corrosion reactions, but if one is more significant than the others it will control the rate of the reaction .

This leads to a classification of corrosion reaction according to whether the cathodic or anodic reaction is rate determing (cathodic control or anodic control) which can be made even more specific by including the terms," activation", " concentration" and "resistance" .The total overpotential at a metal electrode then becomes:

η_T = Total overpotential = $\eta_a + \eta_c + \eta_r$ …….(1.24)

The last two terms are often insignificant in corrosion reaction in comparison with activation overpotential, but η_c, and η_r become important in electrode reactions subject to diffusion control, as occurred in electroplating process[30].

1.7 Passivation

The corrosion product is allowed to build up at the surface, supersaturation with regard to solid oxides and hydroxides can occur , leading to film formation reactions.

The effects of film formation have been referred to above. It can be seen that very substantial corrosion rates would be achieved if the kinetics of both the anodic and cathodic reactions were fast .

In many cases , the metal dissolution rate decreases to low values once the potential is raised above a critical value. The metal is said to be passivated.

A metal is passive if, on increasing the electrode potential toward more noble values, the rate of anodic dissolution in a given environment under steady state conditions become much less than the rate at some less noble potential , a metal is passive if ,on increasing the concentration of an oxidizing agent in an adjacent solution , the corrosion rate , in the absence of external

current , is much less than the rate at some lower concentration of oxidizing agent [40].

Passivation can occure when the corrosion potential exceeds (becomes more noble than) the potential corresponding to equilibrium between the metal and one of its oxides / hydroxides

$E_{corr} < (E_e)_{M/MO}$

Inspection of the pourbaix diagram for the particular metal /metal oxide / aqueous solution system shows that this condition moves the potential into the oxide stability region figure(1.18).

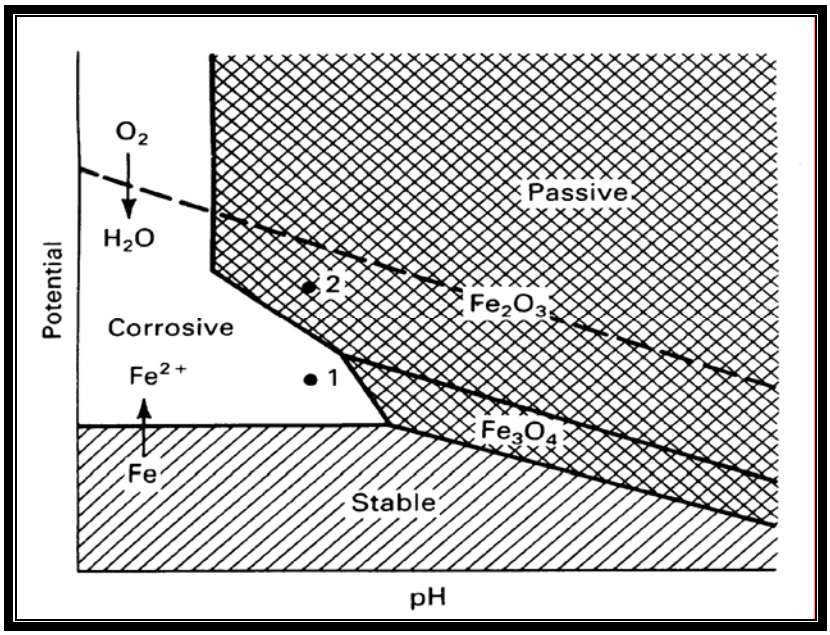

Figure (1.18) Pourbaix diagram of iron /water / dissolve oxygen system showing the effect of potential in moving the system from corrosive (active) region (point 1) to passive region (point 2) [25]

For point 1, $E_{corr} > (E_e)_{M/Mo}$ and corrosion of bare metal is expected , but for point 2. $E_{corr} < (E_e)_{M/MO}$,the metal should be oxide

covered and passive .Under passive conditions , the corrosion rate will be dependent on the oxide film properties.

The current –potential , or polarization curve for the anodic process is shown in figure(1.19) and can be divided into a number of regions.

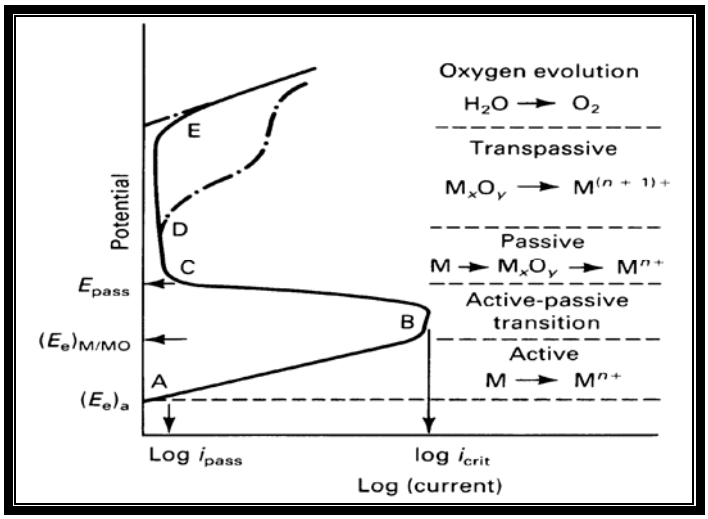

Figure (1.19) Polarization curve for metal / metal ion system that undergoes an active passive transition[25]

In region AB, the active region ,metal dissolution occurs unimpeded by the presence of surface films. $(E_e)_a$ would yield a value of $(i_o)_a$. At a potential B, to coincide with $(E_e)_{M/Mo}$, there is a departure from the Tafel relationship that becomes more pronounced as the potential increases, leading eventually to a decrease in current to a low value. The electrode is said to have undergone an active –passive transition and , by point c , has become passive.

For $E>E_{pass}$, the metal is said to be in the passive region , for potentials greater than point E , oxygen evolution can occur on the outside of the oxide film by the reaction:

$$4OH^- \rightarrow O_2+2H_2O+4\bar{e} \quad \text{…….(1.25)}$$

For this last reaction to occur, the film must be electronically conducting. This is possible because the passive films formed are commonly thin and possess semiconducting or even metallic properties .

The dashed – dotted line in figure (1.19), in the potential region D to E, corresponds to the phenomenon of transpassivity.

Three possible situations are shown in figure (1.20)the dashed – dotted line shows the anodic polarization curve for the metal dissolution ($M \rightarrow M^{n+} + n\bar{e}$) , and lines 1,2 , and 3 show the cathodic polarization curves for three different cathodic processes ($On + n\bar{e} \rightarrow Rn$) .

Consider cathodic reaction 1 , in which $(E_e)_{cl}<E_{pass}$, Because the corrosion potential must lie between $(E_e)_a$ and $(E_e)_{cl}$ for the two reaction to form a corrosion couple from this equation

$$E_{H+/H2} = - 0.059\ pH - \frac{0.059}{2} \log P_{H2} \quad \text{…….(1.26)}$$

The required condition for passivation , $E_{corr}>E_{pass}$, can not be achieved .Therefore ,the corrosion potential stays in active region , and the metal will actively corrode.For cathodic reaction 2 the condition $(E_e)_{c2}>E_{pass}$ is met , but the two polarization curves intersect at an anodic current less than i_{crit} .

A gain $E_{corr} > E_{pass}$, and the metal corrodes in the active region at a higher corrosion current than before .For cathodic

reaction 3 the condition $(E_e)_{c3}<E_{pass}$ and $i>i_{crit}$ are both matel therefore $E_{corr} < E_{pass}$ and the metal passivates.

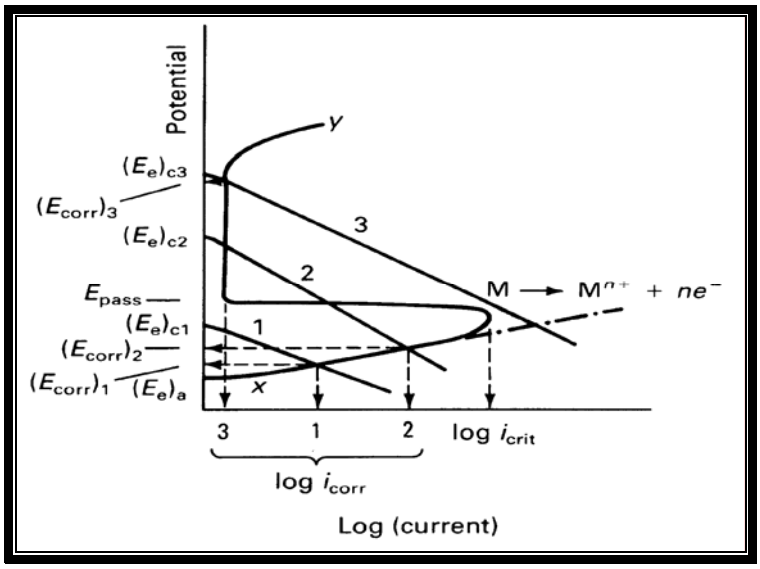

Figure (1.20) Impact of various cathodic reactions on the corrosion current and potential for a metal capable of undergoing an active-passive transition [25]

1.8 Galvanic Corrosion

Corrosion occurs when two or more dissimilar metals are in contact [41], it is that corrosion damage and accidents connected with galvanic corrosion happen frequently and that galvanic corrosion greatly contributes to stress corrosion cracking, pitting corrosion, crevice corrosion, hydrogen adsorption etc [42].

Galvanic corrosion is a persistent problem faced by design engineers because of the need to utilize a variety of different metals to construct complex structures as dictated by the large number of mechanical , metallurgical , and economical requirements .

An aircraft handler experienced difficulty in operating a magnesium alloy fuel pipe coupling during aircraft refuelling. The application of graphite grease proved to be a very short-term remedy, for the galvanic action between the graphite and the alloy caused seizure of the coupling soon after in next rained [43] .

The more active metal (base metal), anode, is corroded more rapidly than it would if it was uncoupled in the same medium, the less active metal (noble metal), a cathode, generally corrode as less, than would be the case if it was uncoupled in the medium or it could be made a resistance to corrosion .This effect is referred to as galvanic or cathodic protection [44] .

The basic requirement necessary for bimetallic (galvanic) corrosion are:

a- The presence of an electrolyte.

b- Electrical connection between metals.

c- A difference in potential between the two metals.

The principles of galvanic corrosion, cathodic protection of a metal structure by making it the cathodic of a galvanic cell.

Cathodic protection can be applied in practice, protection can be applied in practice to protect metals such as steel, copper, lead and brass against corrosion in all soils and all aqueous media.

If the auxiliary anode is composed of a metal more active in galvanic series than the metal to be protected , a galvanic cell is set up with current direction, and the impressed source of current (i.e. the rectifier) can then be omitted and the electrode is called a sacrificial anode [18,45] .

magnesium , zinc, and aluminum galvanic (sacrificial) anodes are used in a wide range of cathodic protection applications [46] .

1.9 Galvanic Series

There is an absolute value of electro-potential of metal independent of the factors that influence the corrosive characteristics of the solution in which the potential is measured.

Values of potential can be changed from one solution to another or in any solution when influenced by such factors as temperatures, aeration, and velocity of movement.

Consequently, there is no way, other than by potential measurements in the exact environment of interest in which to predict the potentials of metals and the consequent direction of a galvanic effect in that environment [47].

A galvanic series can be derived for metals in any desired medium or electrolyte solution. Most galvanic corrosion effects result from the electrical connection of two corroding metals.

Also, since most engineering materials are alloys, galvanic couples usually include one (or two) metallic alloys. Under these conditions, the galvanic series yield a more accurate prediction of galvanic relationships than the e.m.f series. Initially [48] the standard reduction potentials table was used to predict which metal of an electrically or physically connected couple would act as the anode or the cathode. This approach turns out to be dangerous and often incorrect; in addition, the behavior of alloys can not be predicted using the e.m.f Table.

A number of investigators have assembled and constructed tables that predict corrosion tendencies of commonly used metals and alloys in seawater as shown [41,49] in Table(1.1).

The potential variation with time in a particular environment is another concern when constructing the galvanic series[50]. The relative position of metals in the series may change , depending on the time of immersion.

For example in figure (1.21) the measured corrosion potentials for types 304 and 316 stainless steel vary considerably even after 10 or 15 month immersion in seawater .The relative position of nickel, type 304 stainless steel , and copper-nickel alloy clearly depends on the time of potential measurement .[51]

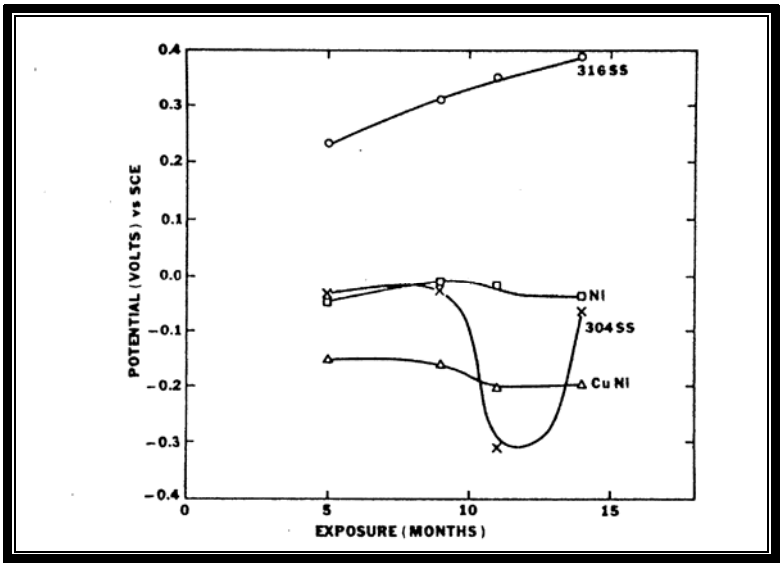

Figure (1.21) Variation of corrosion potential with time for nickel 90 to 10 "copper-nickel" , types 304 and 316 stainless steel in seawater[51]

Table.(1.1) Galvanic series[41,49]

Anodic (Least Noble, Corroded)	Magnesium Magnesium Alloys Zinc Beryllium Aluminum 1100, 3003, 3004, 5052, 6053 Cadmium Aluminum 2017, 2024, 2117 Mild Steel 1018, Wrought Iron HSLA Steel, Cast Iron Chrome Iron (Active) 430 Stainless (Active) 302, 303, 321, 347, 410, 416 Stainless Steel (active) Ni-Resist 316, 317 Stainless Steel (active) Carpenter 20cb-3 Stainless (Active) Aluminum Bronze (CA687) Hastelloy C (Active) Inconel 625 (Active) Titanium (Active) Lead/Tin solder Lead Tin Inconel 600 (active) 60 % Ni 15 % Cr (Active) 80 % Ni 20 % Cr (active) Hastelloy B (active) Navel Brass (CA464, Yellow) Brass (CA230) Red brass (CA268) Admiralty brass (CA443) Copper (CA102) Manganese bronze (CA675) Tin bronze (CA903, 905) 410, 416 stainless (passive) Phosphor bronze Nickel silver Cupro nickel 90-10 Cupro nickel 80-20 Monel 400, k500 Chrome iron (passive) 302, 303, 321, 347, 410, 416 Stainless Steel (passive) 316, 317 Stainless Steel (passive) Silver Titanium Graphite Zirconium Gold Platinum
Direction of Attack	
Cathodic (Most Noble, Protected)	

The process of predicting galvanic corrosion from polarization behavior can be illustrated by the example of a steel – copper system .Steel has the more negative corrosion potential and will therefore suffer increased corrosion upon coupling to copper , but the amount of this corrosion must be predicted from polarization curves.

If the polarization of each material is plotted as the absolute value of the log of current density versus potential and if the current density axis of each of these curves is multiplied by the wetted surface area of that material in the service application , then the result will be a plot of the total anodic current for steel and the total cathodic current for copper in this application as a function of potential figure (1.22).

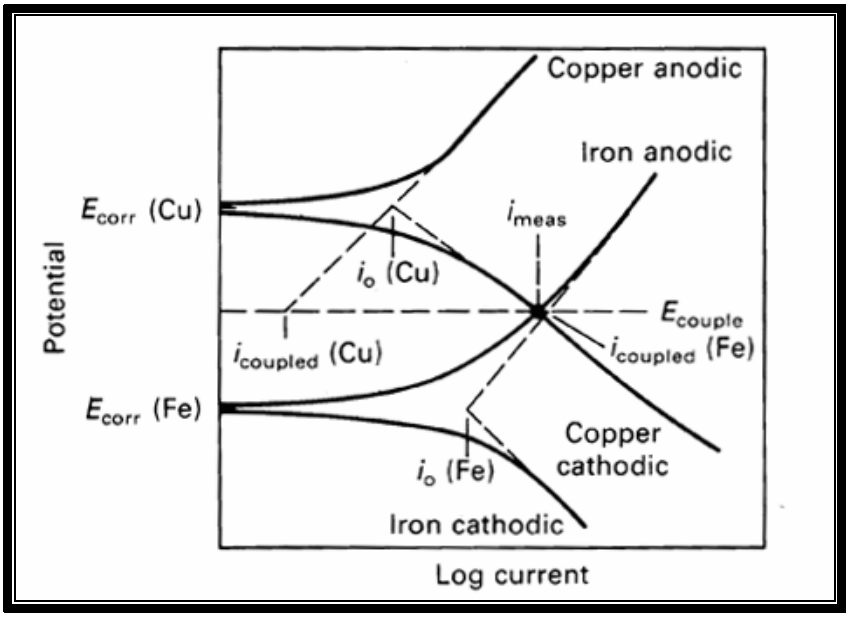

Figure (1.22) Prediction of coupled potential and galvanic current from polarization diagrams . i, current ; i_o , exchange current ; E_{corr},corrosion potential [25]

1.10 Corrosion Rate

Various measurements techniques are available for tackling this problem giving different and complementary in formation, the most important electrochemical test method used to identify and evaluate metallic corrosion reaction are: [52,53]

1- Potentiostatic or galvanostatic polarization.
2- Potentiodynamic and or/ galvanodynamic polarization.
3- Liner polarization.
4- Tafel extrapolation.
5- Potential versus pH (pourbaix diagrams).
6- Immersion test.
7- Ultimatate tensile strength.
8- Depth of corrosion pentration.

The corrosion rate CR is then proportional to the sum of the partial anodic currents (corrosion current) causing metal dissolution. CR is defined as the loss of the corroding metal in micrometers per year [μm/a]
and can be calculated by:

$$CR = \frac{i_{corr}.t_a.M_{Me}}{zF\,.\,d_{Me}}.10^6[\mu_m/a] \quad \text{…….(1.27)}$$

With

i_{corr} ….. Corrosion current density[A/m^2]

t_a …… Year in seconds (31557600 s/a)

M_{Me} …. Molar weight of the metal (for iron 55.847 gm/mol)

z ….. Number of electrons (for Fe z=2)

F …… Farday's constant (96487 Coulomb/mole)

d_{Me} …. Density of the metal (for iron d_{Me}= 7.86 gm/cm^3)

A corrosion current density of 1 mA/m^2 iron surface is therefore equal to a corrosion rate of 1.16 μm/a .

If a rebar with diameter of 16 mm is corroding with 100 mA/m^2 surface for 20 years, which can locally be the case –the cross section would have reduced to ~ 11.4mm [54] .

Chapter Two

Electroplating ZnNi system

Chapter Two

Electroplating Zn-Ni System

2-1 Electroplating

2-1-1 Historical of Electroplating

The history of the deposition of precious metals can be traced to William Nicholson and Johann, English chemists in 1800 succeeded in decomposing water into hydrogen and oxygen by electrolysis .Soon thereafter, Johann discovered the process of electroplating .He also observed the amount of metal deposited and the amount of oxygen produced during an electrolytic process that depended on the distance between the electrodes.By 1801 Ritter observed thermoelectric currents(55).

By 1802 Allisndro Volta , who had just discovered the chemical principles that would later lead to the development of "Voltaic" electrical batteries.Volta's first practical demonstration of this was called "a Voltaic pile" .As a result , Brugnatelli's early work using voltaic electricity enabled him to experiment with various metallic-plating solutions,as a decorative plating , however, an insult from Napoleon Bonaparte caused by Brugnatelli to confine the publication of his works to his own journal,causing the loss of this information for almost forty years(56).

Michael Faraday began , in 1832 , what promised to be rather tedious attempt to prove that all electricities had precisely the same properties and caused precisely the same effects,the key effect was electrochemical decomposition(55).

Voltaic and electromagnetic electricity posed no problems , but static electricity did. As Faraday delved deeper into the problem , he made two starting discoveries .

First, electrical force did not , as had long been supposed , act at a distance upon chemical molecules to cause them to dissociate.

It was passage of electricity through a conducting liquid medium that caused the molecules to dissociate , even when the electricity merely discharged into the air and not pass into a "Pole" or centre of action in a voltaic cell.

Second , the amount of the decomposition was found to be related in a simple manner to the amount of electricity that passed through the solution , these findings led Faraday to a new theory of electrochemistry .

Hermann Nernst's developed the theory of electromotive force of the voltaic cell in 1888.He developed methods for measuring dielectric constants and was the first to show that solvents of high dielectric constants promote the ionization of substances. Nernsts' early studies in electrochemistry were inspired by Arrhenius dissociation theory which first recognized the importance of ions in solution.

Nernst applied the principles of thermodynamics to the chemical reactions proceeding in a battery .In 1889,he showed how the characteristics of the current produced could be used to calculate the free energy change in the chemical reaction producing the current ,he constructed an equation , known as

Nernst equation , which related the voltage of a cell to its properties.

The first handbook ,published in 1889 by Canning for nickel plating .In 1910 Canning offered a proprietary mixture which contained nickel sulphate ,sodium chloride and boric acid and was to be maintained slightly acid[57].

The two world wars and the growing aviation industry gave impetus to further developments and refinements including such process as , hard chromium plating ,bronze alloy plating , sulfamate nickel plating , along with numerous other plating processes. Plating equipment evolved from manually operated tar-lined wooden tanks to automated equipment, capable of processing thousands of pounds per hour of part[58].

Despite the expansion of electroplating process to other industries ,no significant scientific developments were discovered until the emergence of the electronics industry in the 1940's.The 1970's lead to numerous regulatory laws for waste water emissions and disposal that set the direction for the electroplating industry for the next 30 years[59].

2.1.2 Electroplating Technique

Electroplating is often called electro-deposition. It is a process of producing a coating on a metallic surface by the action of electric current ,and is now a conventional technique for plating gold , rhodium , nickel , tin , silver etc.

When electrical potential is applied to the copper electrodes submerged in an acidified copper sulfate solution, copper ions from the anode move to the cathode due to the electric field , copper ion density difference within the solution , and the convective motion .This results in an evenly coated layer of copper on the cathode .At this time, the electric current between the electrodes offers information about the mass transfer(60).

2.1.3 The Nature of Electrode Reactions

Electrode reactions are heterogeneous and take place in the interfacial region between electrode and solution .the simplest electrode reaction could inter-convert at an inert surface, two species , O and R ,which are completely stable and soluble in the electrolysis medium containing an excess of an electrolyte:

$O^{z+} + z\bar{e} \rightleftarrows R$ …..(2.1)

The electrode reaction is a sequence of more basic steps. To maintain a current it is essential to supply reactant to the electrode surface and also to remove the product, as well as for the electron transfer reaction at the surface to occure. For example, in experimental conditions where O is reduced to R, the electrode reaction must have three steps:

$O_{bulk} \rightarrow O_{electrode}$ [mass transfer]

$O_{electrode} \rightarrow R_{electrode}$ [charge transfer]

$R_{electrode} \rightarrow R_{bulk}$ [mass transfer]

Since the rate of reduction, and hence cathodic current , is determined by the rate of the overall sequence , the rate must depend on the slowest step .

Thus, to understand the characteristics of an electrode reaction both mass transfer and electron transfer have to be considered [61] .

2.1.4 Mass Transfer in Electroplating System

The movement of copper ions, which are discharged from the anode and move to the cathode when an electric potential is applied to the electrodes figure (2.1)

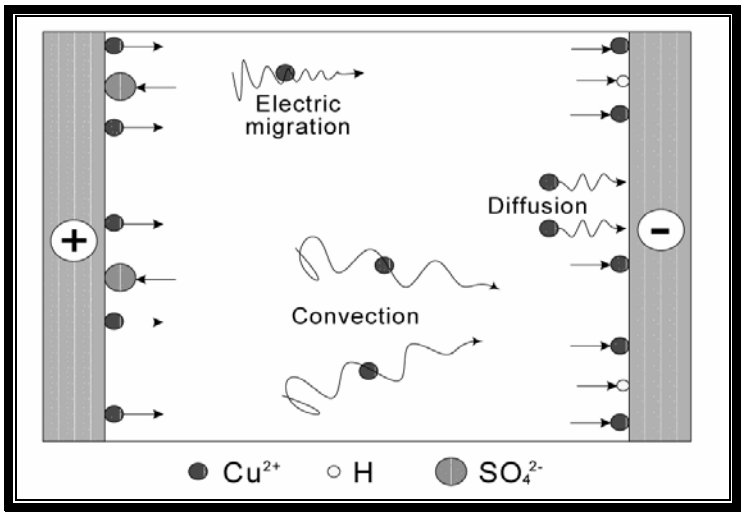

Figure (2.1) Schematic diagram of mass transfer in electric field[60]

In the absence of significant temperature gradients and external accelerations other than those resulting from gravitational or electrical forces, the mass transfer of copper ions occurs through the following primary mechanisms :

(1) An electric migration under a potential gradient.

(2) A diffusion by ion density difference .

(3) A convective motion of solution.

The total rate of transfer of a given component at particular point within a body of solution per unit area perpendicular to the direction of transfer may be expressed by:

$$N_t = N_m + N_d + N_c \ [\text{kmol}/\text{m}^2.\text{s}] \quad \ldots\ldots(2.2)$$

Where N_t , N_m , N_d , N_c represent the total rate of mass transfer , rate of electric migration, rate of diffusion and rate of convection , respectively[62].

For steady-state processes , it is convenient to express the rate of electric migration as a function of the current flow per unit area [63] :

$$N_m = \frac{t_n I}{zF} \quad \ldots\ldots(2.3)$$

Where t_n is transference number for the given species , I is the current density (A/m^2) , z is valence charge of the ion and F is the faraday constant (96,500A.S/mol) thus, the quantity of electric migration can usually be evaluated from equation (2.3)

and hence ,may be considered separately from the diffusion and convection processes.

In simulating heat transfer systems , an electric migration doesn't appear and the convective mass transfer should concentrate on simultaneous diffusion and convection.

Thus , it is convenient to define the rate of mass transfer , N_m by subtracting the electric migration rate from the total rate of transfer and the mass transfer coefficient h_m , corresponding to heat transfer coefficient , h:

$$N_m = N_d + N_c = h_m (c_b - c_s) \quad \text{……..(2.4)}$$

Where c_b and c_s are the copper ion concentration in the bulk and the electrode surface , respectively .Based upon Faraday's law , the mass transfer rate N_m can be presented by

$$N_m = \frac{(1-t_n)\, I}{zF} \quad \text{……..(2.5)}$$

Thus,from Eqs,(2.4) and (2.5) ,h_m can be evaluated by:

$$h_m = \frac{(1 - t_n)\ I}{zF(c_b - c_s)} \quad \text{……..(2.6)}$$

Mass transfer to an electrode is governed by the Nernst-Planck equation , which is written for one-dimensional mass transfer along the x-axis as [64] .

$$J_i(x) = -D_i \frac{\partial c_i(x)}{\partial x} - \mu_i c_i \frac{\partial \Phi(x)}{\partial x} + c_i \upsilon_x(x) \quad \text{……(2.7)}$$

Where $J_i(x)$ is the flux of species i (mole s^{-1} m^{-2}) at distance x from the surface, D_i is the diffusion coefficient (m^2 s^{-1}) , $\partial c_i(x)/\partial x$ is the concentration gradient at distance x ,$\partial \Phi(x)/\partial x$ is potential gradient ,μ_i and c_i are charge and concentration of species i, respectively ,and $\upsilon_x(x)$ is the velocity (ms^{-1}) with which a volume element in solution moving along the axis.

The three terms on the right hand side of the equation (2.7) represent the contribution of diffusion , migration , and convection , respectively , to the flux .

Mass transfer is the movement of metal atoms which are ionized and hydrated at the anode, and move to the cathode under the imposed external electrical field. The electrical field is applied to the electrodes to provide a driving force for the mass transfer.

Convection can be another factor for the mass transfer since it also governs the migration of ions through the electrolyte. As the electrodepostion proceeds, the metal ions can be depleted near the cathode. As a consequence, the density of the solution at the face of the cathodes becomes lower than the density of the bulk solution .

To avoid this inhomogeneity of the density of the solution , convection of the electrolyte is required either by natural or artificial method. For instance, heating or cooling coils are used to create temperature gradients for aid in convective mass

transport. In continuous plating, the cathode is moved through the solution at a relatively high speed to enhance the convection effect.

Once metal ions reach the vicinity of the cathode surface, the effect of convection becomes negligible, and diffusion becomes an important factor for ionic migration. Since diffusion is the movement of substances as a result of a concentration gradient, the depletion of metal ions near the cathode causes a movement of ions from the bulk of the solution toward the cathode .The metal ion approaches the surface of the cathode, is then discharged and becomes as so called ad-atom(65).

Consequently, this ad-atom diffuses through the surface and is incorporated into the site where the local free energy due to the accommodation of an ad-atom can be minimized figure(2.2).

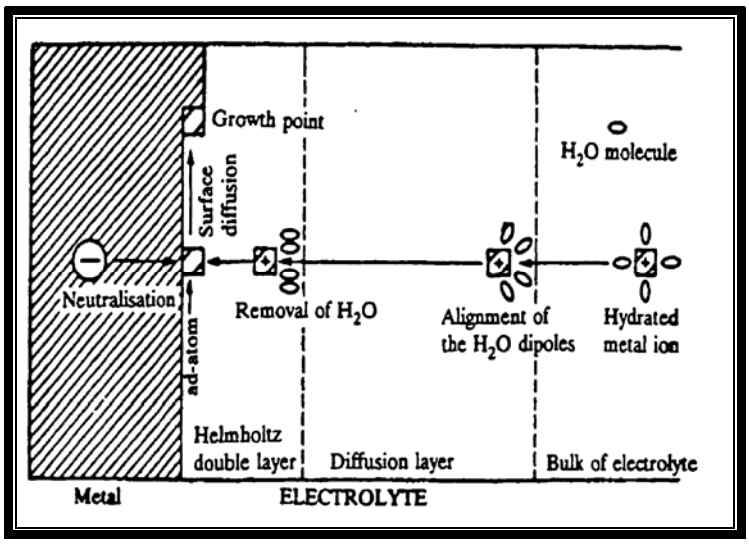

Figure (2.2) Schematic representation of the mechanism of cathodic metal deposition (65).

2.1.5 Mass Transport and Current Distribution for Theoretical Model

The microstructure, composition and uniformity of electroplated metals depend not only on kinetic and thermodynamic factors, but also on mass transport and current distribution conditions at the cathode.

It is useful to distinguish different electrochemical phenomena according to the length scale (distance from the model surface to the bulk solution) as shown in figure(2.3) .

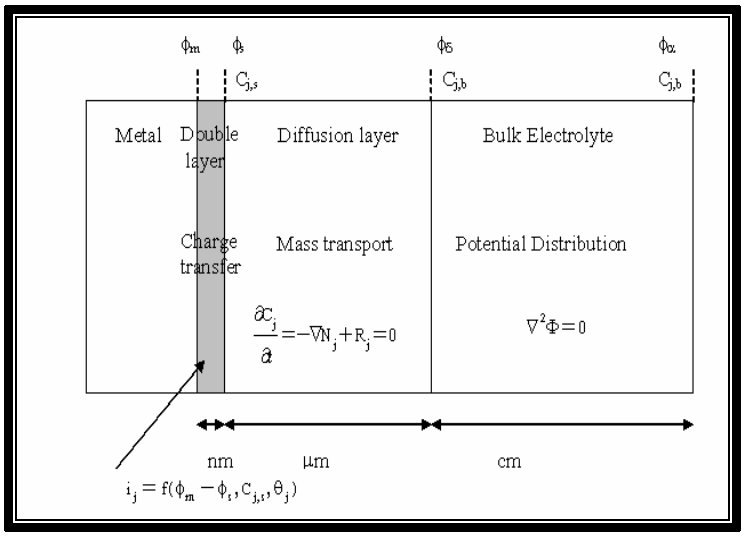

Figure (2.3) Length scales of electrochemical phenomena entering into theoretical modeling [66].

Charge transfer reactions are responsible for the formation of metallic deposits at the metal electrolyte interface. Their characteristic length is on the order of two to three nanometers , corresponding to the thickness of the electrical double layer.

The partial current density i_j of species j is a function of its overpotential (η_j) and its concentration at the electrode surface ($c_{j,s}$) .

In addition , i_j may depend on the surface coverge θ_j of different electrolyte species , or reaction intermediates adsorbed on the surface

$$i_j = f(\eta_j , c_{j,s} , \theta_j) \quad \text{……..(2.8)}$$

For given applied current or cell voltage , the value of local current density i_j at the cathode may be influenced by mass transport conditions and by the potential distribution in the bulk electrolyte.

The characteristic length for mass transport corresponds to the thickness of the diffusion layer and is typically on the order of a few micrometers. This is much larger than the double layer thickness, and for this reason charge transfer kinetics enter as a boundary condition into theoretical models when consideration of mass transport phenomena near the cathode.

According to the Nernst diffusion layer concept, a stagnant diffusion layer is assumed to exist near the electrode ,and mass transport in this region proceeds due to diffusion and migration only.

For each species j, a mass balance equation can be formulated, which may include a variation of time dependent concentrations and chemical reaction R_j .

$$\frac{dC_j}{dt} = -\nabla N_j + R_j \quad \text{……(2.9)}$$

At the steady state , outside the diffusion layer ,the electrolyte concentration is uniform. The potential distribution in the electrolyte in this case can be calculated from the Laplace equation(66).

$$\nabla^2 \phi = 0 \quad \text{……(2.10)}$$

From the potential distribution, the current density at each point is evaluated using ohm's law. The characteristic dimension for the potential distribution is that of the electrochemical cell, typically in the centimeter range. This is much larger than the diffusion layer thickness. Current distribution calculations based on Laplace's equation are linked with electrode kinetics.

A non-uniform potential distribution in the electrolyte normally leads to current distribution on the cathode, and can be distinguished into three cases, firstly, if the influence of electrode polarization and mass transport is unimportant, the so called primary current distribution prevails, which depends only on the geometry of the electrochemical cell.

Secondly, in the absence of non-negligible electrode polarization, the so called secondary current distribution prevails. The uniformity of the current density on the cathode, depends on cell geometry and on the value of electrode polarization.

Wanger number (W_a) expresses the ratio of the polarization resistance at the interface over the ohmic resistance in the electrolyte.

$$W_a = \frac{d\eta/di}{\rho_e L} \quad \ldots\ldots\ldots\ldots\ldots\ldots(2.11)$$

ρ_e is the electrolyte resistivity (Ωm) and L is a characteristic length of the system (m).The secondary current distribution is always more uniform than the primary current distribution .

Under conditions where the polarization resistance becomes dominating, i.e. when the Wanger number goes to infinity, the current distribution on the cathode become perfectly uniform, independent of cell geometry. The primary current distribution corresponds to Wanger number approaching to zero, which is attained when ρ_e L is high.

Finally, in presence of significant mass transport and polarization effects, the tertiary current distribution prevails. The current distribution on the cathode in this case will depend on the both the potential distribution and the local rate of mass transport and geometry of the cell[67] .

2.1.6 Nucleation Process

When metal ions arrive on the cathode surface, the discharged ions eventually migrate into the most favorable sites of the metal lattice .The sites may be the steps or kinks where the free energy increase due to the accommodation of the metal atoms can be minimized ,the sequence of the incorporation of growth units at a kink and step site figure (2.4).

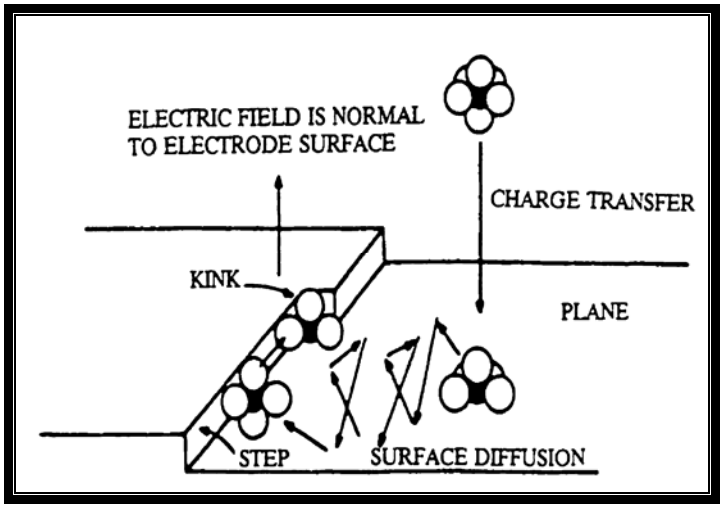

Figure (2.4) Steps and kinks are preferred sites for ad-atoms to get incorporated into the metal lattice[68].

These steps or kinks may result from two dimensional nucleation, screw dislocations or some other defects on the surface .The idea of two dimensional nucleation is suggested by kossel and stranski and has been largely accepted ,their model assumes the crystal growth occurring in repeated monatomic layers after two dimensional nucleation [69,70].

The model is based on the hypothesis that the probability of incorporation of an atom at the surface of a crystal is greater at

the sites which have higher surface energy. A single cubic lattice showing different possible sites of incorporation of an atom in the lattice figure (2.5).

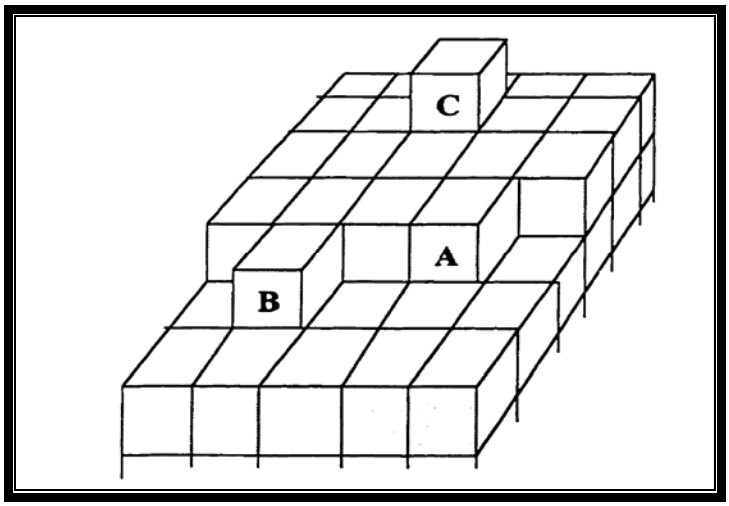

Figure (2.5) Schematic drawing of a single cubic lattice showing different possible sites of incorporation of an atom in the lattice[70].

It is evident that the most favorable incorporate site is the kink site A, which is at the same time a repeatable step. Once the row is completed , the next possible site is B.

Creating a new one dimensional nucleus along the developing plane .The next favorable site is C where a new two dimensional nucleus starts to form .

Therefore, the deposits grow through the competition between vertical growth ,depending on two dimensional nucleation rate, and horizontal growth ,depending on the rate of repeatable step.

2.1.7 Micro Throwing Power

Good micro throwing power is the ability to deposit a uniform thickness of coating at all points on the surface profile. As the name implies , it is associated with small scale surface irregularities but these can be of greater dimensions than those normally termed micro.

Diffusion of metal-ions is the most important process concerned with micro throwing power since this associated with surface irregularities of such size that effective differences in the thickness of the cathode layer may be established at various parts of the profile .To obtain good micro throwing power it is essential to have an electrolyte solution with a high concentration of dischargeable metal ions so that the regions where the cathode film is thickest, i.e. the recesses , are not depleted of metal ions.

If flow that there must be at a high concentration of dischargeable metal ions in the bulk solution,the diffusion can readily occur to all parts of the profile .If the electrolyte solution has a low concentration of dischargeable ions (dilute solution or complex formation) concentration differences can occur within the cathode film. High concentration overpotential will occur in the recesses, the current density will be reduced and so less metal will be deposited.

All factors which reduce concentration overpotential (increase in metal ion concentration , increase in agitation and

increase in temperature) are improving micro throwing power but reduce macro throwing power.

Solutions must have a good micro throwing power if the substrate contains pits and pores , otherwise these can eventually become bridged over and cavities remain below the coating .This can obviously result in early failure of the coating in service [57].

2.1.8 Theoretical Aspect of Alloy Plating

Alloy can be defined as "A substance that has metallic properties and is composed of two or more chemical elements of which at least one is a metal [71] .

2.1.9 Plating Variable

The functional properties of electrodeposition alloys depend on their chemical composition and on their structure in the micro and nano scales. Many factors could effect the composition and microstructure of electrodeposition alloy as in figure (2.6)

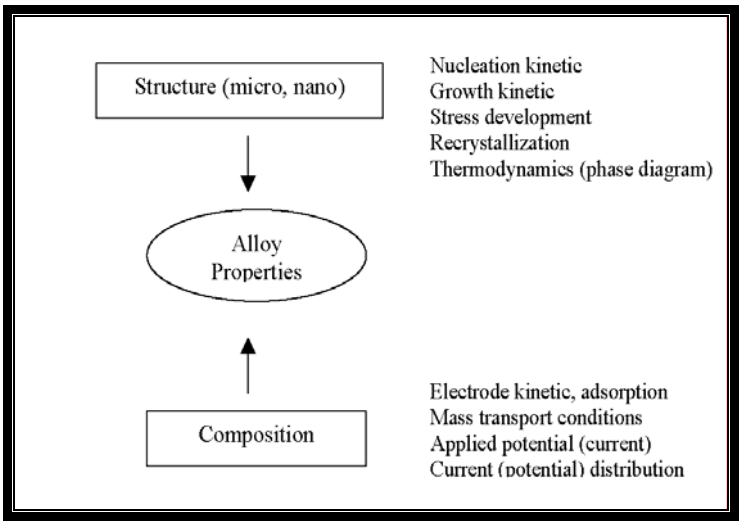

Figure (2.6) Factors influencing the composition and structure of electroplated alloy [66].

2.1.10 Alloy System Classification

The electrodeposition alloys have been comprehensively classified alloy systems into various types depending on their behavior [71].

A major distinction exists between "normal" system, in which more noble species deposits preferentially, and "Anormal" system , in which the less noble species is favored. (The term more noble refers to a more positive rest potential). "Anormal" behavior includes "anomalous" and "induced" codeposition. Anomalous deposition is typically observed during codeposition of the iron group metals: iron, nickel and cobalt, with each other or with zinc .

Induced codeposition indicates that a metal which can not be deposited in pure form can be codeposited as an alloy, well known example being the codeposition of molybdenum or tungsten with iron group metals.

2.1.11 Mixed Electrodes

The theory of mixed electrodes was originally developed by Wagner and Traud (1938) and later by Stern and Geary (1957) to describe uniform corrosion.

It states the measured current density at a mixed electrode is the sum of the partial current densities of all anodic and cathodic reactions (anodic partial current densities are taken as positive value and cathodic partial current densities as a negative one).

Normally, during alloy deposition at least two electrochemical reactions proceed simultaneously on to the cathode such as the deposition of the alloy constituents and sometimes the formation of hydrogen. For deposition of a binary alloy of metals A and B yields.

$$i=i_A+i_B+i_{H2} \quad \ldots\ldots\ldots\ldots\ldots\ldots \quad (2.12)$$

where i_A and i_B are the partial current densities of alloy components A and B, respectively ,and i_H is the current density for hydrogen formation. The current efficiency for alloy deposition regarding a binary alloy AB yields

$$\xi = \frac{i_A + i_B}{i} \quad \text{……(2.13)}$$

and for the alloy composition , X_B (expressed as mole % of B)

$$X_B = \frac{i_B/n_B}{i_A/n_A + i_B/n_B} \times 100 \quad \text{…….(2.14)}$$

n_A is the electron number involved in the deposition of component A of the alloy, and n_B for deposition of B . These equations give a plating condition of electrodeposited alloys and the current efficiency are uniquely determined by the value of the partial current densities.

2.2 Electroplating Zn-Ni Base System

2.2.1 Technology Developments

The electrodeposition of Zn-Ni has generated amount of interest in past 15 years[72].This has been in response to industry's demand for increasingly effective corrosion resistance coating on steel. Alloying with nickel is a common technique employed to augment zinc's protective properties. In addition , it has been observed that varying the electroplating bath chemistry, conditions and deposition parameters may give rise to a wide variation in properties of the resulting deposits.

In a severe corrosion environment , zinc is consumed rapidly. For this reason , it is the usual practice to increase the thickness of the zinc coating. This is not commercially cost effective and the thick coating cause problems during formation and welding of the steel. With the improvement in science and technology , the requirement for protection of products is increasing . Monometallic plating can no longer satisfy the needs of industry , therefore, more and more study is devoted to alloy plating , and especially studying zinc - alloys[73].

The early commercialization of the UK zinc nickel market occurred in the mid-1980's ,with the installation of the first acidic based technology[74] . This was chloride based using ammonia as the nickel complexing agent [75],and operated with a dual anode system having separate anodes and rectifiers for the zinc and nickel metals. The electrolyte produced high plating efficiency with excellent deposition rates.

Although the deposit was highly decorative in nature, poor alloy current density distribution led to premature low current density (LCD) corrosion failures. These nickel rich (LCD) areas were extremely difficult to passivate which lead to further processing and performance figure (2.7).

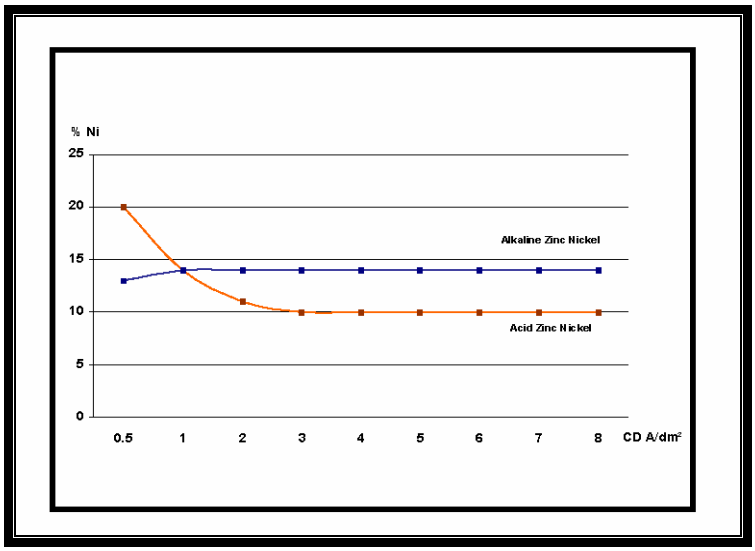

Figure (2.7) Zinc Nickel alloy distribution as a function of current density[76]

The first major UK commercial development of the electrodeposited alkaline zinc nickel alloy occurred during 1992[77],with the installation of a large production volume of low alloy having a typical deposit composition of 5-7% nickel. This installation was established to service the needs of the growing Japanese automotive presence within Europe. The electrolyte based upon sodium hydroxide and zinc, contains proprietary amine polymers as the complexing agents , the chemistry having being patented in 1989 [78].

The alkaline nature of this chemistry produced superior deposit throw and alloy distribution compared to that of the earlier acidic chloride based systems, which helped to improve the overall neutral salt spray corrosion performance of the electrodeposits [79].

However, this improvement was sacrificed at the expense of lower efficiency and longer processing times. These new systems were production user friendly ,and the deposits were more receptive to chromate passivation. However , there appearance is "technical" , i.e. matt to semi-bright in nature (the highly lustrous finish from acidic formulations is not realized).

The next major advancement in zinc nickel technology occurred with the development of the alkaline high alloy,i.e. 12-15% nickel .This was patented in 1995[80].The formulation produces very stable and reliable chemistry, which is not based upon traditional alkaline zinc technology and so does not blister or burn .Developed through research into alternative strategies for Cr (VI) passivation replacement , the new alloy has proven to be the most suitable medium for accepting these alternatives enhanced wear and corrosion resistance[81].

The first UK commissioned installation of this new system occurred in 1997[77].By early 2001[77], the total volume of electrolyte in production installations has exceeded that of the original low alloy zinc nickel systems.

2.2.2 Alternative for Cadmium Technologies

Cadmium has been extensively used as a barrier coating for steel in aerospace , electrical , and fastener industries owing to its excellent corrosion resistance and other engineering properties[82], especially salt water corrosion resistance, low coefficient of friction, and a low electrical contact resistance

plating of cadmium poses considerable challenges ,due to the toxicity of the metal and its salts[83].

Cadmium is one of the metals on the " black-list"[84].Acute poisoning of cadmium usually results from the inhalation of cadmium dust and fumes, specially cadmium oxide. Such poisonings are relatively rare but dangerous.

At present , one major public concern is the association between exceptionally high environmental exposure to cadmium and lung cancer .Early and recent studies provide consistent evidence that the risk of lung cancer is increased among workers exposed to cadmium .

Cadmium can accumulate in certain organs, particularly the kidneys. In Japan, kidney failure has been observed in individuals whose food and water intakes were affected by high levels of cadmium[85]. An inspection of an Estern Airlines landing gear shop revealed employee exposures to 85 times the ceiling limit ($0.5mg/m^3$).Unventilated grinding activities to cadmium plated landing gear components were the cause[86].

Further , during cadmium deposition , huge amounts of hydrogen are introduced into the substrate , thus making the substrate susceptible to hydrogen emberittlement failure[87,88].

Hence for environmental and hydrogen embrittlement reasons , alternate coating to cadmium are being actively explored .The most commonly used sacrificial coating in place of cadmium is zinc and its alloy.

Zinc-Nickel has a potential similar to cadmium and has attracted interest in the aircraft industry, excellent corrosion resistance and absence of voluminous white corrosion products and low hydrogen embrittlement makes zinc nickel an attractive candidate for aerospace usage[84,89].

Non-cyanide plating technologies alternatives are available for cyanide based copper , zinc ,and cadmium plating processes. These substitute processes can reduce regulatory and reporting requirements, lower risks to workers ,decrease environment impact ,and reduce coporate liability (See Appendix B) [90].

2.2.3 Alternative for Chromium Technologies

For chrome plating, the problem is not the chromium itself, but the hexavalent chrome (Cr^{6+}) from the chromic acid used in its deposition [91].

Hexavalent chrome passivated have been used for improving the corrosion resistance of sacrificial zinc ferrous substrate for many years[92].

Chromium plating provides a wear resistance surface and good barrier against external corrosive substances[93].

The problem of chromium is absorbed by mammals either through oral or dermatological routes. It is toxic on account of its high oxidation potential and a structural similarity of chromate with sulfate, allowing the chromate to penetrate sulfate channels in cell membranes.

A possible scheme discussing the manner in which (Cr^{6+}) acts on the cell leading to cancer is given in figure (2.8).

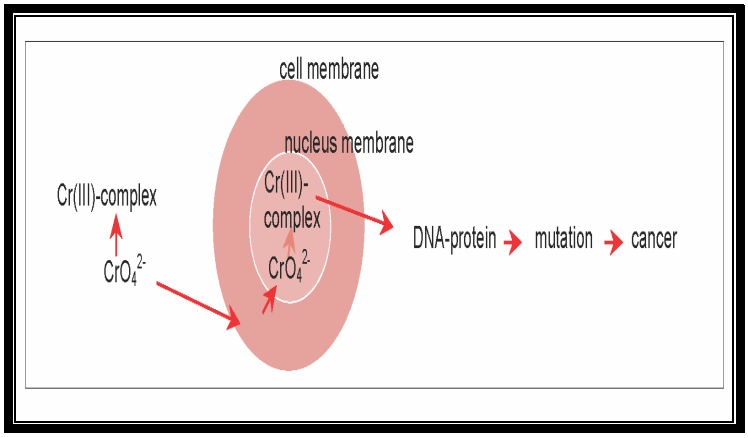

Figure (2.8) Schematic showing possible route leading to cancer inducting by (Cr^{6+}) in mammals[94] .

For this reason the end-of-life-vehicle directive, restricts the use of (Cr^{6+}),in automobiles since 1st July 2003.For corrosion preventation coatings (Cr^{6+}) has to be removed from the coatings after 1st July , 2007[95,96].

2.2.4 *Zn-Ni Phase Diagram*

The equilibrium phase diagram for the zinc-nickel binary system is presented in figure (2.9).It is notable that the electrodeposition alloys are metastable with respect to the equilibrium alloys shown in the Zn-Ni phase diagram. This is demonstrated schematically in figure (2.10) .

Here ,the phases that are found in electrodeposited Zn-Ni coating are compared to those given by the equilibrium phase diagram. Electrodeposited Zn-Ni alloy generally exhibit fewer phases which exist over larger ranges of nickel composition[97].

For the vast majority of Zn-Ni industrial applications, the single γ-phase is the alloy of interest. This is a result of its excellent performance in corrosive media, but the η phase is ductile and improves the pass formability[98].

The phase found in the current diagram are outlined in (Table 2.1).

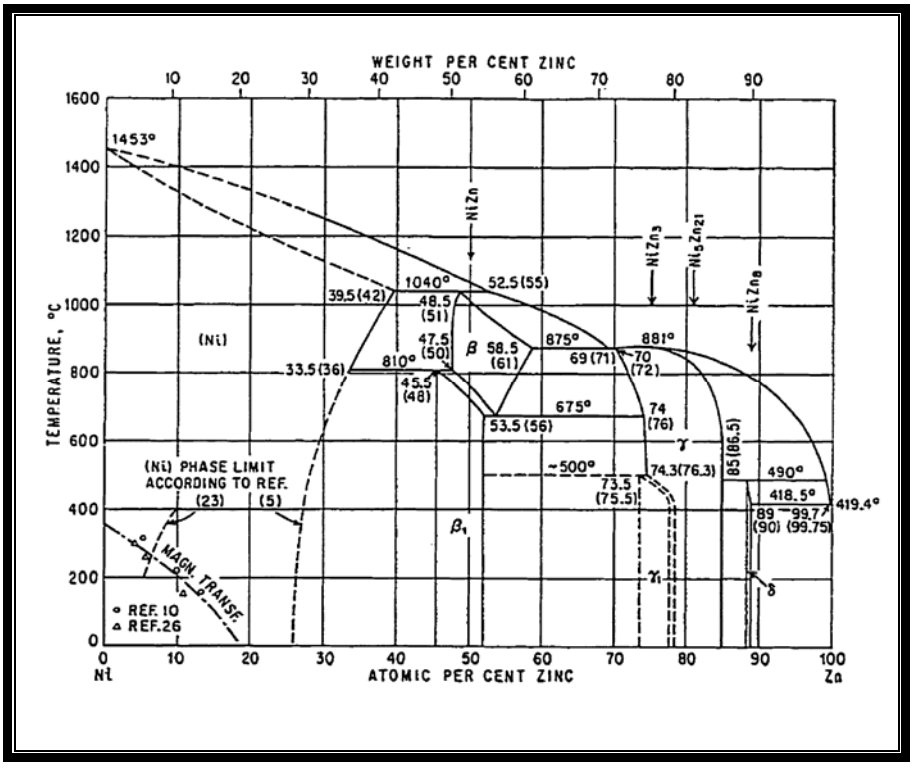

Figure (2.9) Equilibrium phase diagrams of Zinc-Nickel binary systems[99].

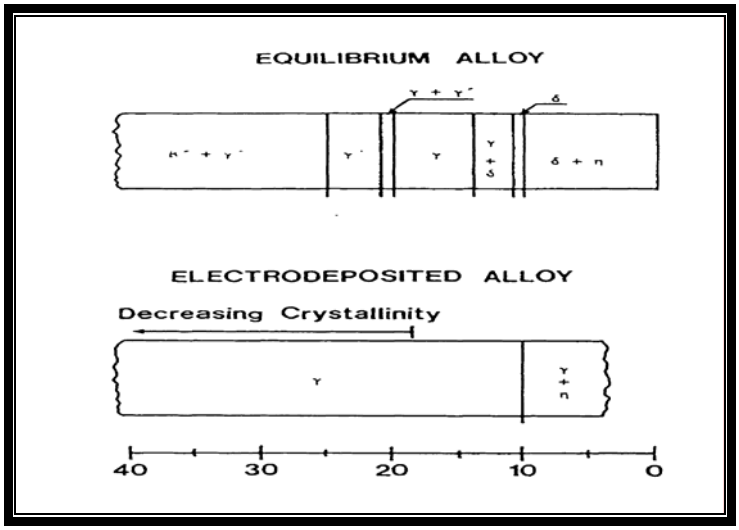

Figure (2.10) Phased in electrodeposited Zn-Ni alloy coatings compared to those given by the equilibrium phase diagram[97].

Table(2.1) Crystal structure , lattic parameter and the chemical formula of Zn-Ni intermetallic phase[100].

Phases (Zn-Ni)			
δ	$Zn_{22}Ni_3$	tetragonal	a=8.922, c=9.254
γ	$Zn_{21}Ni_5$	bcc	a=8.920
α-Ni	Ni	fcc	a=3.52

The deposition of zinc-nickel alloys involves the so called anomalous codeposition of zinc [101]. Since the less noble metal zinc deposits preferentially. So the ratio of this metal is higher in the deposit than in the electrolyte.

A second phenomenon during zinc-nickel deposition is depolarization which is a positive shift in the equilibrium potential of zinc in the alloy due to the free energy of alloy formation[102] .

The term "underpotential deposition" (UPD) is used below for the deposition of metal species on a foreign substrate in a more positive potential region than the equilibrium potential of the bulk deposit [103].

2.2.5 Structure of Zinc-Nickel alloy electrodeposits :

The structure and microstructure change of as-deposited alloys versus the nickel content in the deposits , which the substitution of Zn and Ni atoms in η or γ structure induces a lattice distortion has been defined .In contrast to the thermodynamic phase diagram ,the δ phase does not appear in as-deposited coatings. Two composition ranges have been defined , the first of which corresponds to the formation of a solid solution saturated in nickel(η_d) for the alloys containing up to 7.4 wt% of nickel. The second, corresponds to the formation of a γ phase out of equilibrium unsaturated in nickel.

For an increase in nickel, the added atoms are preferentially incorporated into this unsaturated γ phase , and the η_d phase gradually disappears up to 13% wt of nickel . The δ phase is obtained in electrodeposited alloy only after heat treatment at 200°C. This δ phase recrystallized from metastable phase η_d and γ_d [104].

Moreover, thermodynamically, the Zn-Ni η phase only appeared up to about 1wt% Ni and δ-phase (Ni_3Zn_{22} intermetallic compound) exists in a wide composition

range[105].The metallurgical alloy phase of zinc nickel electrodeposits have been reported as a function of composition[106] figure (2.11)

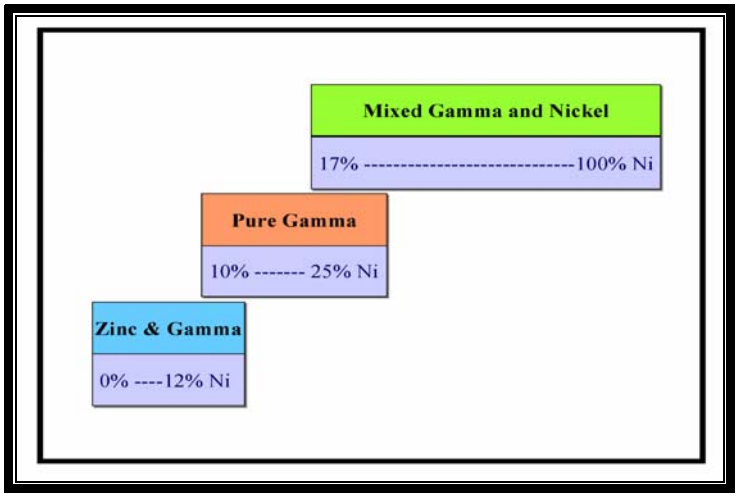

Figure (2.11) Zinc Nickel alloy phases reported as a function of composition[107].

2.2.6 The characteristics of the deposits Zn-Ni

Three potential zones could be defined for Zn-Ni deposition figure (2.12).

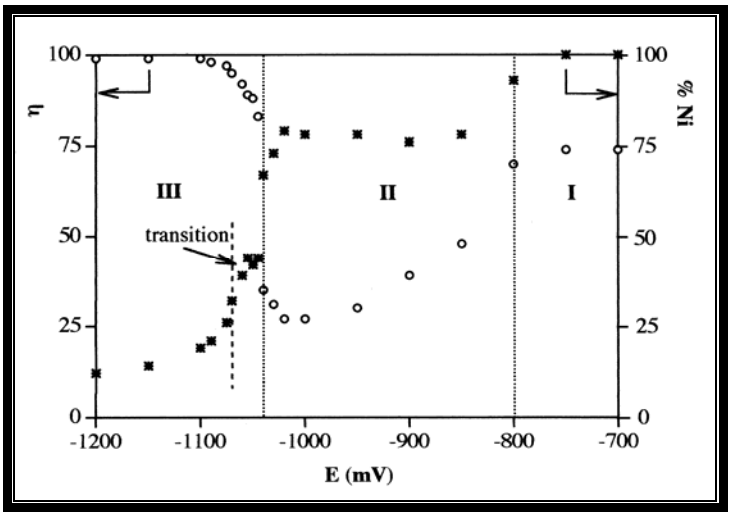

Figure (2.12) Variation of Nickel content and current efficiency with deposition potential for alloys obtained on a Ni electrode (Ammonium bath) [108]

The zones obtained with bath for industrial electrolyte, zone I corresponded to the most positive potentials in the polarization curve (- 700/-800 mV),where the deposit grew at low current densities (i<0.5 $mAcm^{-2}$) in this zone the potentiodynamic stripping response showed only one peak at potentials corresponding to nickel oxidation figure (2.13 (a)).

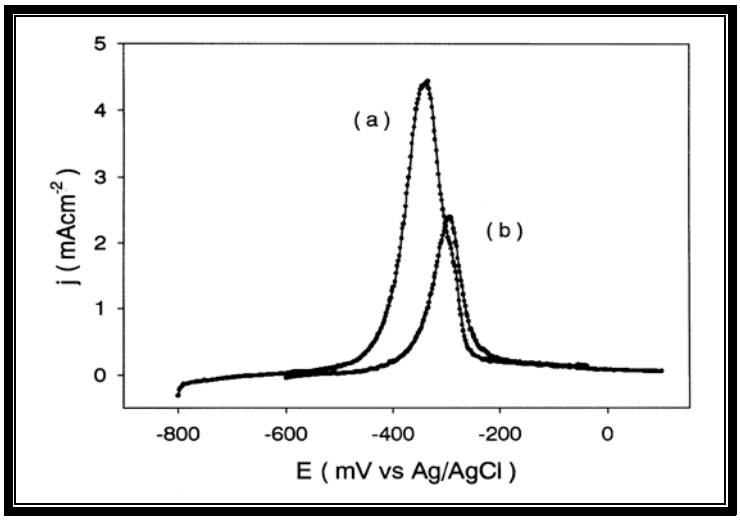

Figure(2.13) Potentiodynamic stripping response obtained on a nickel substrate after deposition at-750 mV for 1500s: Curve (a) Zn-Ni alloy from Ammonum bath (b) Nickel deposited from a bath with the same nickel content. Scan rate 5 mVs^{-1}. (108)

Analysis of deposits obtained in this zone indicated that they consisted of practically pure nickel with a maximum zinc content of about 5% .The deposits were formed of aggregates of various sizes, similar to nickel deposits figure (2.13(a)).

It is interesting to note that this low zinc content led to important changes in the electrochemical behavior of the deposits figure (2.13(b)) also includes the oxidation response of

pure nickel deposit, under the same deposition conditions, the main oxidation peak was obtained at very positive potentials.

In this case, the alloy obtained in this zone of potentials, although practically all nickel, had a sufficiently different structure to be easier oxidized and with a high current efficiency.

In this zone the deposition of nickel was inhibited by under potentially deposited zinc[109].When the deposition of pure zinc was studied on nickel electrode, it was observed that no deposition took place at these potentials, which indicated that zinc was only deposited on the nickel clusters and not on the nickel substrate.

Zone II corresponded to the interval of potentials prior to the maximum of the polarization curve (-850/-1040 mV).In this zone the deposition process took place at intermediate current densities(0.5-1.5 $mAcm^{-2}$) and was accompanied by a high hydrogen evolution.

The potentidynamic stripping response showed a separate peak for zinc oxidation figure (2.14),although the response was complex ,with the peaks not clearly separated, and deconvolution was needed to calculate the composition of the alloys .

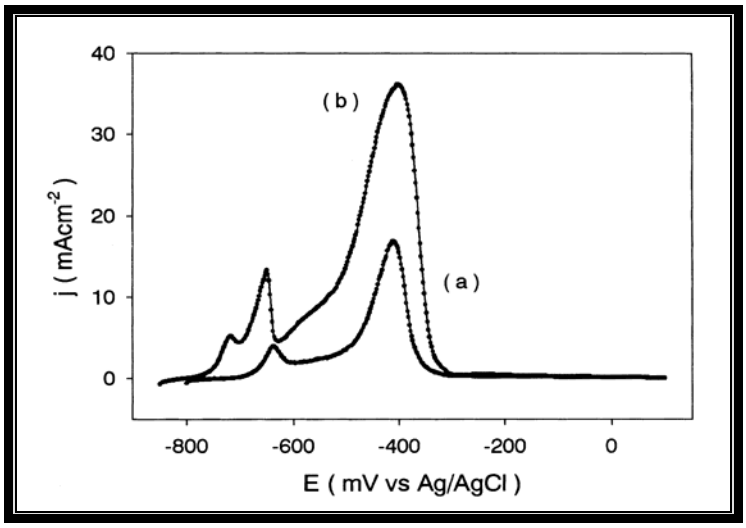

Figure (2.14) Stripping response obtained on a nickel substrate , after deposition of alloy (a) at -850 mV for 1500s ; (b) at - 1000 mV 1500s, scan rate 5mVs^{-1} [108].

For more positive potentials, the percentage of nickel in the alloys was fairly constant at about 75% and current efficiency gradually decreased as polarization increased .The morphology and structure of the coatings in this zone also evolved with potential ,for the most positive potentials, nodular grains could be distinguished at all deposition stages, but on increasing potential the grains were more difficult to distinguish and become broader and less intense.

For the most negative potentials in this zone the nickel content of the alloys was about 65%, which corresponded to the equilibrium composition of α-phase.

Therefore, in zone II ,as the deposition potential was increased , more zinc was deposited and an α-phase was gradually formed.

The structural change from a nickel-like deposit to an α-phase structure was accompanied by an increase in hydrogen evolution, in this region the presence of oxygen in the inner part of the coatings and also indicated that the amount of oxygen increased at more negative potentials. Therefore, the deposits in this zone must contain some oxygen-containing species [110] .

At about -1045mV (the exact potential depended on the substrate and bath composition) zone III, the composition of the alloy was maintained during a short interval of potentials between 40-45%Ni and then, as polarization increased, the nickel decreased to values less than 15%,the potentiodynamic stripping response in this zone indicated that this sharp change coincided with the appearance of the oxidation peak corresponding to γ-phase figure (2.15).

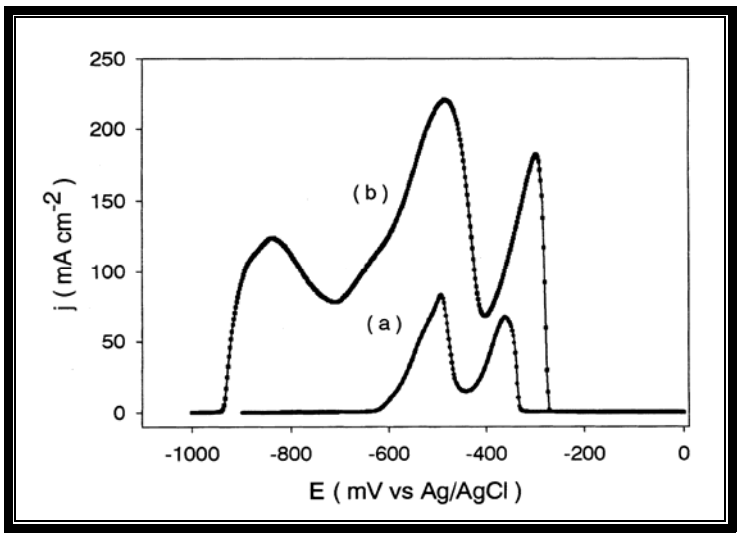

Figure (2.15) Stripping response obtained on a nickel substrate, after deposition of alloys from bath A : (a) at-1060mV for 1000 s; (b) at-1100mV for 500s.Scan rate 5 mV^{-1}. [108]

At low polarizations in this zone the peak caused by the oxidation of zinc from γ -phase appeared as a shoulder of the α-phase peak figure(2.15(a)).As the deposition potential was made more negative ,the Ni content of the alloys decreased and the oxidation peak of γ and η phase were observed in the stripping voltammograms at more negative potentials figure(2.15b).

Zone III could be considered as the γ-phase domain, as the appearance of this phase entailed an abrupt change in alloy composition and deposition current efficiency. It was observed that the appearance of a γ-phase coincided with the minimum of current density in the polarization curves. By plotting the partial current densities for zinc, nickel and hydrogen during deposition figure(2.16),it could be seen that this minimum and the following increase in current density were due to a big drop in hydrogen current density, in line with the fact that hydrogen evolution is very low when γ-phase is deposited [111].

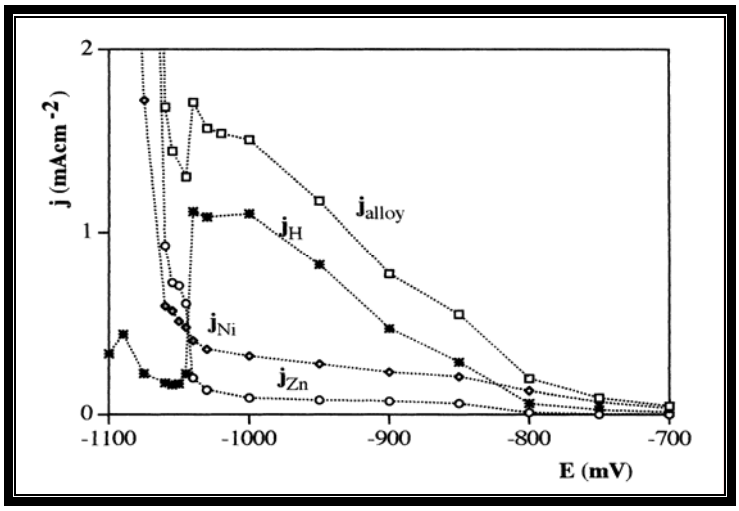

Figure (2.16) Effect of the deposition potential on the partial current densities for the Zn-Ni alloy(□),zinc(O),nickel(◊) and hydrogen(*) [108].

The variations of interreticular spacing can be explained by substitution of zinc atoms by nickel atoms. In fact, the electronic cloud of the Ni atom is not distorted, and its atomic radius is less than the atomic radius of Zn($r_{Ni=}$1.25Å,$r_{Zn=}$ 1.37Å).

In these conditions ,one can easily understand that the substitution of Zn by Ni atoms consequently modifies the lattice parameter of the η structure of Zn figure (2.17).

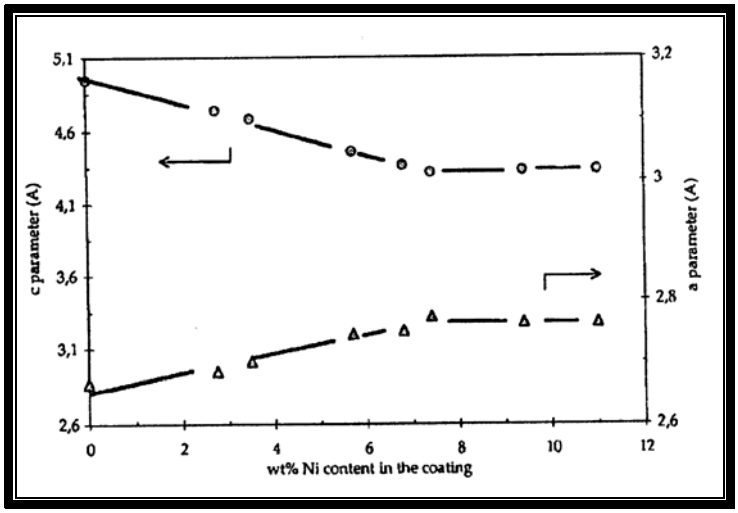

Figure (2.17) Variation of the a and c parameters of the γ structure according to the Ni content in the coating [104].

The c parameter, therefore, decreases rapidly and the a parameter increase slowly as the Ni content increases. Thus, the hcp structure of the η phase returns to the more stable hcp structure at 7.4 wt% of Ni, which has a c/a ratio close to the theoretical hcp 1.633 figure (2.18).

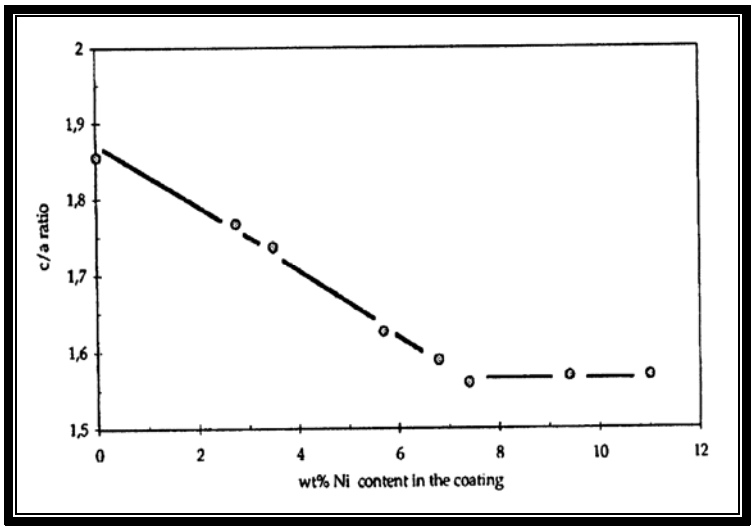

Figure (2.18) Variation of the c/a ratio of the η structure according to the Ni content in coating[104]

The exothermal peak was observed at approximately 281°C and the calorific value was 3.95 kJ/mol . It was considered that this sharp peak corresponded to the transformation from an amorphous Zn-Ni to a crystalline γ -Ni_5 Zn_{21} figure (2.19).

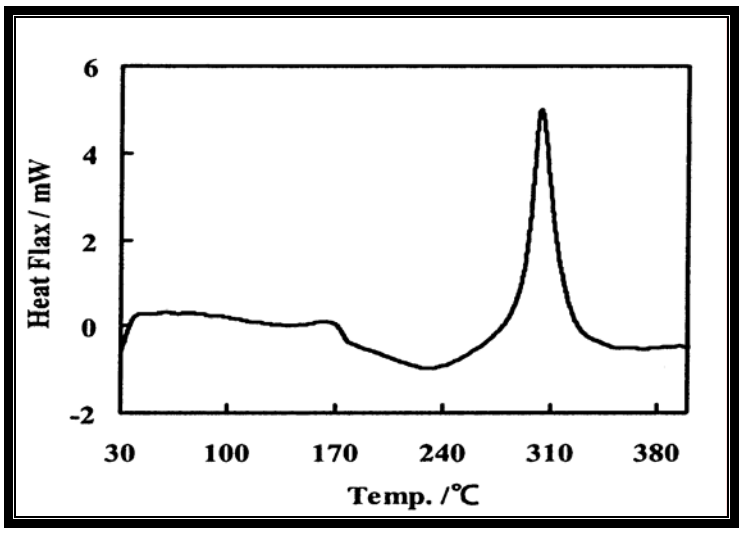

Figure (2.19) DSC curve for Zn-Ni electrodeposit (Ni content:40.6 at %)[112]
scan rate : 15°C/min ,Atmosphere: Ar

2.2.7 Types of Zinc-Nickel Plating System

A large number of electroplating bath have been successfully employed to deposit Zn-Ni , for example : chloride baths[113] sulfate baths[114] ,methanol baths[115],ammonium baths[116],sulfate-chloride baths[117],and cyanide baths[118].

The main Zn-Ni alloy process are based on two types of electrolyte systems as shown in Table (2.2).

One acid type uses zinc and nickel salts(sulfate or chloride) as the main source of metal ions in solution.

The acid electrolyte contains buffering agents, such as boric acid or acetic acid ,to stabilize the pH during plating. Some electrolytes also contain a brightener ,such as strontium sulfate[119],and leveling agent such as phenolic derivative.

The alkaline electrolyte consist of zinc oxide and nickel salt as a major source of zinc and nickel ions. The electrolyte contains sodium or potassium hydroxide[120].

Table(2.2) Types of electrodeposited Zn-Ni alloy[121].

Electrolyte Constituents Concentration,g/L	Operating Conditions	Remarks
Acidic bath 1		
$ZnSO_4$ $7H_2O$ 260 $NiCl_2$ $6H_2O$ 240 CH_3COOH 3%v/v	Nickel strike bath prior to Alloy plating. pH 1.5 to 3.5,50°C Current Density 30 A/dm^2	Acid-type bath:Coatings contain 15% Ni Application to continuous Strip plating
Acidic bath 2		
$ZnCl_2$ 83.3 $NiCl_2$ $6H_2O$ 1-40 KCl 210 H_3BO_3 25	25 & 30°C,pH 5.5 Current Density 1-4 A/dm^2	The optimum corrosion resistance of Zn-Ni alloy. Current efficiency is 95%.
Acidic bath 3		
$ZnCl_2$ 50 $NiCl_2$ $6H_2O$ 15-100 NaCl 200 NH_4Cl 30	40°C,pH 4.5 Current Density 3 A/dm^2	Average coating for rack & barrel plating are 9 and 6.5 µm respectively.
Alkaline bath		
Zinc oxide 6-12 NaOH 100-120 $NiCl_2$ $6H_2O$ 0.7-1.5 Zn:Ni 6-7:1	21-32°C pH above 12 Current Density 1-4.5 A/dm^2	Zn-Ni alkaline plating bath.Application are rack & barrel plating. Plating efficiency ranges from 60-80%

2.2.8 The factor presence for coating layer

2.2.8.1 Influence Concentration of ions

The polarization resistances were estimated as a function of the Zn ions in the bath , the potential was scanned 10mV above and below the mixed potential after initiating the deposition process. The addition of Zn ions in the bath increases

the polarization resistance figure (2.20),thereby suggesting that the zinc ions inhibit the deposition process.

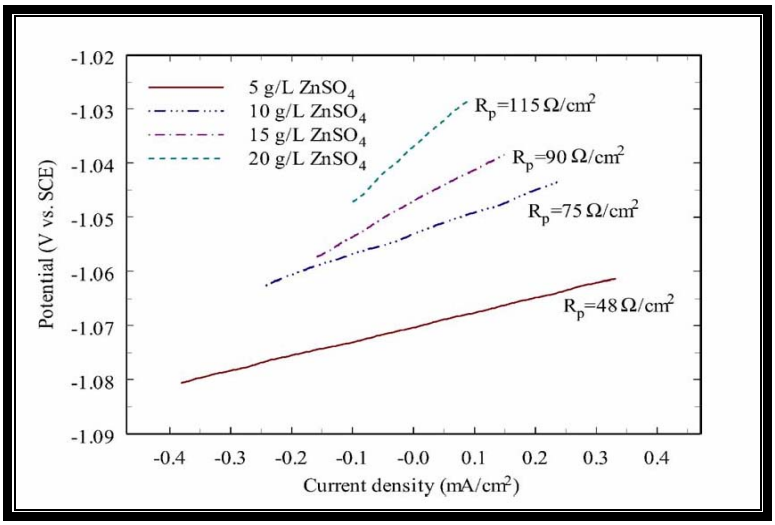

Figure (2.20) Liner polarization during the deposition process as a function of $ZnSO_4$ concentration in the bath[122].

2.2.8.2 Influence of pH

Material balances coupled various equilibrium relations and electroneutrality conditions were used to plot the pH-concentration diagram figure (2.21) .

The equilibrium concentration of different electroactive species as a function of bath pH ,the concentration of the zinc and nickel complexes varies with increase of pH above 9.0.

The nickel to zinc complex concentration ratio increases with increasing pH .This variation in the concentration of nickel and zinc complexes is expected to favor the nickel deposition from alkaline electrolytes.

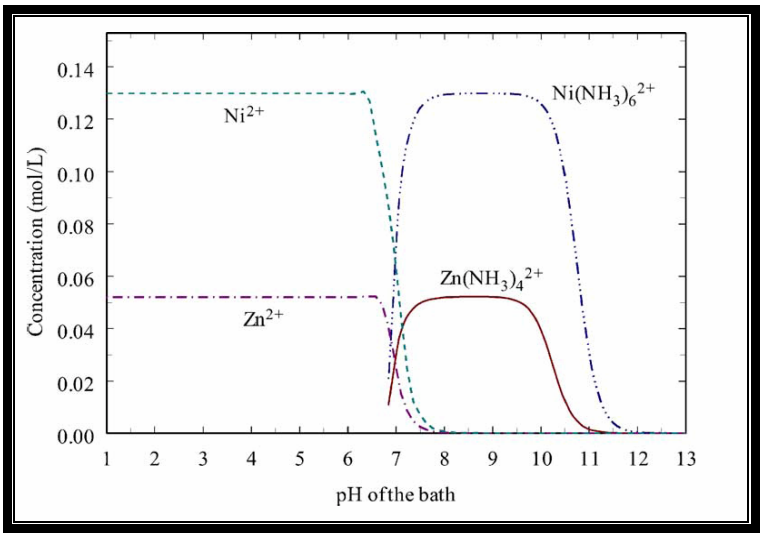

Figure (2.21) Variation in equilibrium concentrations of complex Zn and Ni species as a function of bath pH[122].

2.2.8.3 Influence of distance from the electrode

Dimensionless concentration profiles for each of the reacting species near the electrode surface are different. The concentration of the hydrogen ions at the electrode surface drops to zero, suggesting that the diffusion process controls the hydrogen evolution reaction.

This can be expected due to a very low concentration of H^+ ions in the electrolyte at pH 10.5.The Other reactions are controlled by the charge transfer reactions at the electrode/electrolyte interface figure (2.22).

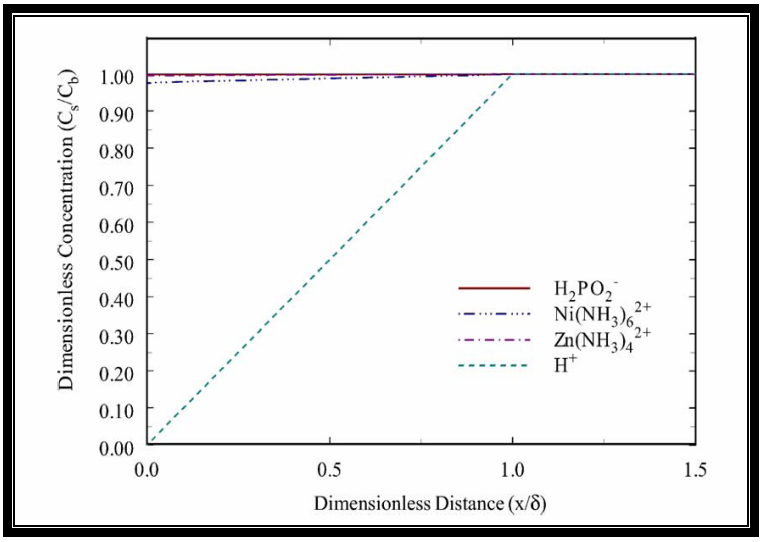

Figure (2.22) Dimensionless concentration profiles for the various reactants as a function of distance from the electrode surface[122].

2.2.8.4 Influence of current density

Nickel content of zinc-nickel coating significantly changes as the deposition current density changes figure (2.23).The coatings deposited at the current density of 50mA/cm² have about 17% Ni in the deposit .

As the current density increases to the range of 200 to 500 mA/cm² , the nickel content in the deposit drops to 13 to 15%.Further increase of the current density up to 1200mA/cm² results in a dramatic increase of nickel content up to 42%.

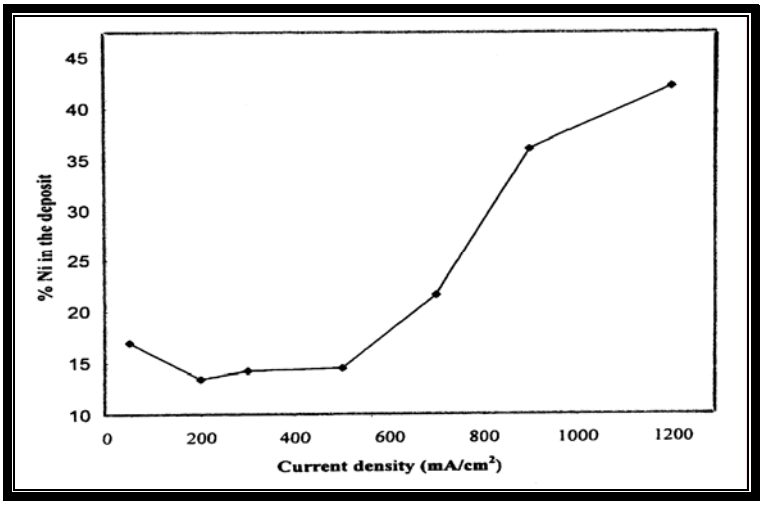

Figure (2.23) Correlation between current density and percent of nickel in the Zinc-Nickel electrodeposited coatings [123].

2.2.8.5 Influence of bath temperature

Operating temperature of the bath plays a significant role in the deposition Zn-Ni alloy ,because the polarization resistance of the coating deposited at various bath temperatures. The polarization resistance for the deposit prepared at a room temperature was 300Ωcm^2.Deposits prepared at 75°C show polarization resistance value of 1432 Ω cm^2 figure (2.24).

Higher temperature could increase cathode hydrogen evolution, as well as making evaporation of plating solution faster than before, as a result ,cathode current efficiency and deposition speed decreased respectively, this will increase the internal stress of the plating layer increased [124].

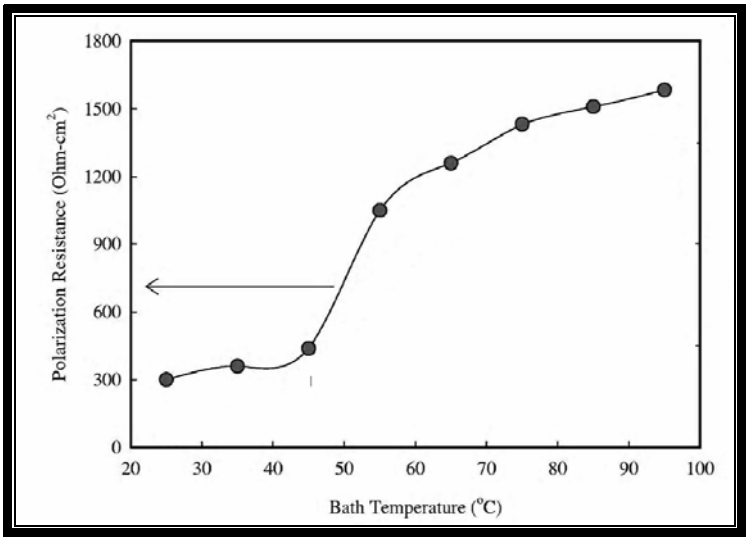

Figure (2.24) Average polarization resistance of the deposits as a function of operating bath temperature(125).

2.2.8.6 Influence of the speed rotational

Under stationary conditions, current efficiencies are lower than with electrode rotation and coatings are richer in Zn because of the blocking effect of the hydrogen bubbles on the electrode surface figure (2.25) (126).

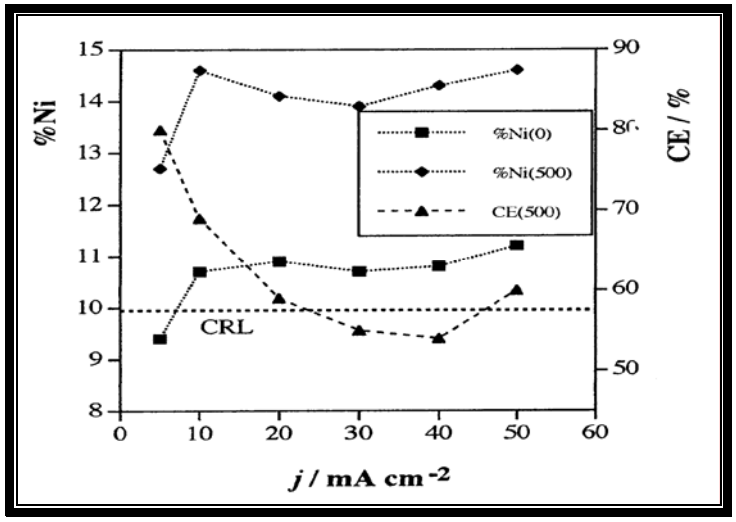

Figure (2.25) Dependence of nickel content and current efficiency on the current density at the rotation speeds indicated(126).(CRL: composition reference line)

2.2.9 Ternary Alloy Coatings

To develop an electrodeposition process for plating of Zn-Ni-X (X=Cd,Cu,P) ternary or quaternary alloys, which will induce barrier properties to the sacrificial Zn-Ni alloy thereby extending the life of the coating .By introducing a new element in the Zn-Ni alloy one can expect to decrease the Zn-Ni ratio in the alloy and this process offers a unique way of controlling the Zinc-Nickel ratio and consequently to decrease the Zn-Ni alloy corrosion potential from -1.14 Vvs. SCE to even lower values of corrosion potential ,but it is more negative than the Fe corrosion potential.

Introducing a third element in the alloy could modify the rate of hydrogen evolution reaction, by the recombination and adsorption kinetics hydrogen proton at the surface and to impede completely the proton penetration in the alloy, and by the way to eliminate the hydrogen embrittlement[127].

2.2.10 The Uniform of Thickness Distribution

Leaving unplated or recessed areas that will be subjected to oxidation and rusting after plating for the acid bath system comparing with alkaline bath. In addition, the deposite from the acid solution tends to have a poor thickness distribution and significant alloy variation from high to low current density area.

The alkaline bath is more uniform in terms of both thickness of deposit and alloy composition[61].

2.2.11 Mechanism of Preferential Deposition of Zn

Nickel deposition is strongly inhibited in the presence of Zn^{2+} ion and therefore the deposited Zn layer in the underpotential region is considered to play a role in the inhibition of Ni deposition ,although the Zn deposition takes place only in the monolayer.

Figure(2.26) indicates a schematic model for the preferential deposition of Zn from based upon of the monolayer formation for Zn deposition in the potential region from .0.8 to .1.0V .In this potential region the Zn deposition takes place only in the level of monolayer figure (2.26A) ; however, the Ni deposition can grow to relatively large thickness through the nucleation-nucleous growth figure (2.26B).

It is thus suggested that the presence of Zn^{+2} ion in the Zn-Ni codeposition strongly prevents the nucleus growth of the Ni nuclei, because the thin layer of Zn deposition , which may be a monolayer level ,covers on the almost electrode surface figure (2.26C),this picture describes the case of the initial thin layer during the preferential deposition of Zn in the Zn-Ni electroplating .The model may be expanded into the case of thick layer formation in the Zn-Ni electroplating[128].

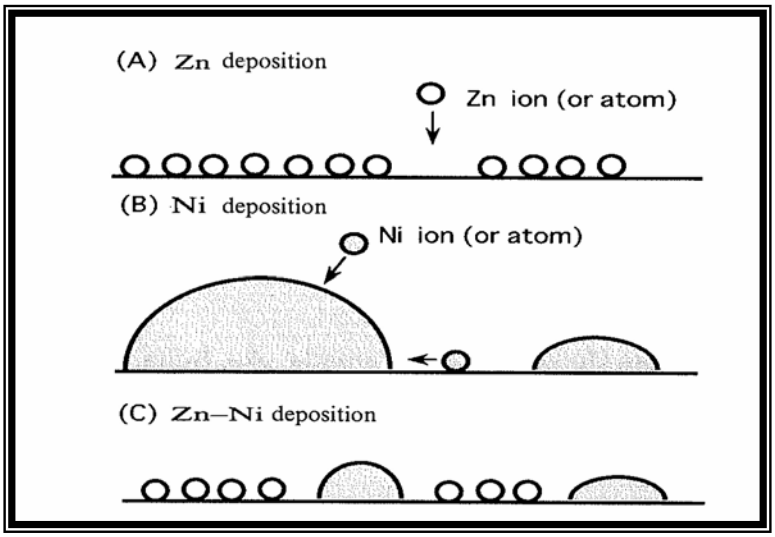

Figure (2.26) Schematic model of the initial process of the thin layer formation for (A) Zn,(B) Ni, and (C) Zn-Ni deposition [128].

2.2.12 Sacrificial Zinc layers

Performance enhancing properties of surface coating continue to meet the demands of many industrial metals based application, because they allow the bulk properties of one metal to be combined with the surface properties of another .

Surface coatings extend in-service component life through improved corrosion protection, enhanced aesthetic appeal and greater wear resistance. The zinc coating works by separating from its surroundings, helping to delay the formation of surface oxidation, which is the basis of rusting process. Zinc offers galvanic protection, because it is electrochemically anodic to steel and will sacrifice itself in the act of protection.

In the presence of corrosive condition zinc layers are more active than steel so corrode anodically , steel substrate remains cathodic and is protected .Zinc will corrode

preferentially to the steel, even when the surface coating layer is damaged, and the steel substrate does not corrode until virtually all the surrounding zinc has been consumed[129] figure (2.27).

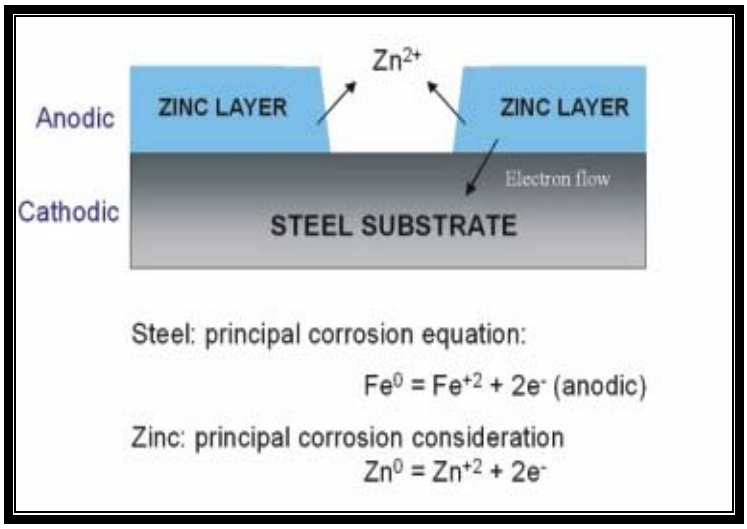

Figure (2.27) Zinc sacrificial protection[129]

2.2.13 Modulated Zn-Ni Multilayer

In the present study, a novel potentiostatic electroplating process has been developed for the deposition of compositionally modulated Zn-Ni multilayer on steel substrate .

For example Acidic plating bath [130] was used for the deposition process, DC voltage varying between -0.85 and -1.30Vvs saturated calomel electrode (SCE) was applied for the deposition process. In the first deposition experiment ,the deposition was carried out initially at -1.3Vvs SCE for 5 minuets and then changed to -1.25V in the second step.

This was continued until the voltage reaches -0.85V with a difference of 5mV in each step. Total of 10 different steps,5

minutes each was continuously carried out for the deposition process. As expected, this sequence resulted samples with nickel as high as 35 wt.% since the final potential(-0.85Vvs SCE) favors the nickel deposition.

In the second deposition experiment , the initial potential was kept the same i.e., -1.3 Vvs SCE and the deposition was ended at -0.9 Vvs SCE (9 step of 5.5 minutes each).Totally 10 different potential sequences each ending at -0.85, -0.9, -0.95Vvs SCE and so on were carried out and the individual Zn and Ni wt% were obtained figure (2.28).

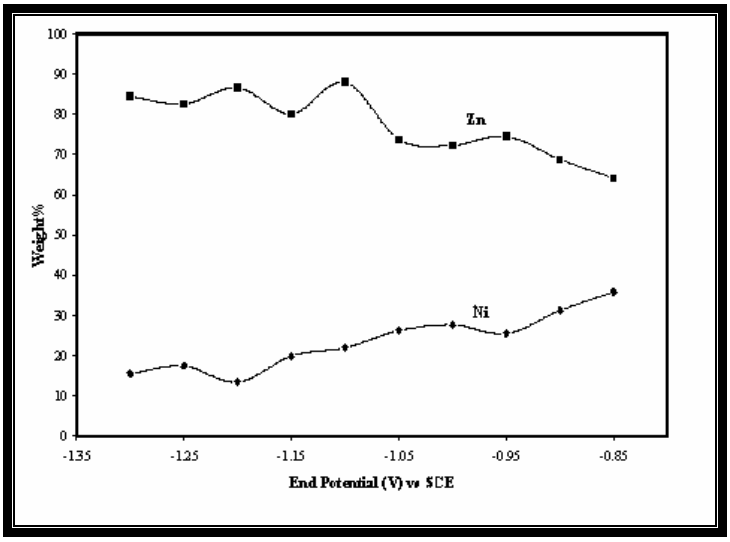

Figure (2.28) Effect of end potential on Zn-Ni composition (starting potential -1.3Vvs SCE) [131]

Cross-sectional analysis was performed by using a thicker deposit (~ 12.5μm) in order to determine the variation in Zn-Ni composition as a function of thickness from the substrate .

It is seen from figure (2.29) that Zn rich phase (~81 wt.%) is observed up to 6μm thickness from the steel substrate [131].

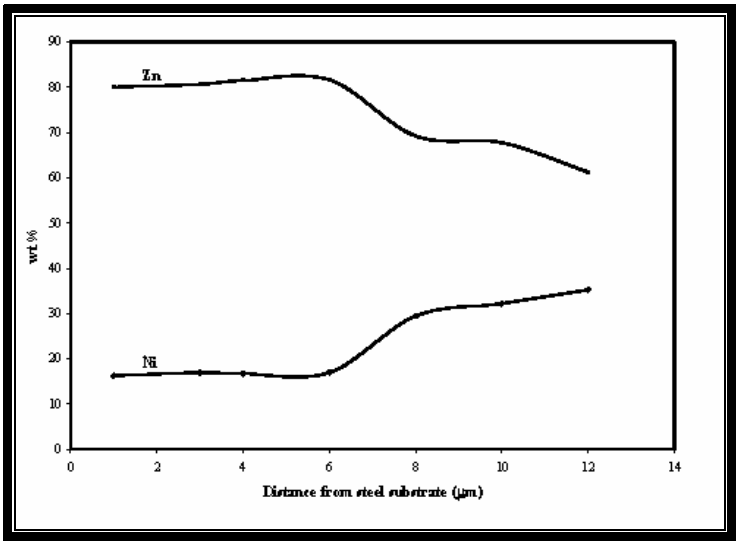

Figure (2.29) Zn-Ni composition through the thickness of sample prepared using potential sequence 1 [131].

2.2.14 Corrosion behavior of Zinc-Nickel coating

Any metal or alloy exposed to the environment will corrode to some extent. The corrosion products usually form a surface layer on the metal. Depending on the type of material and the corrosive environment, the composition and protective characteristics of the corrosion products will vary.

The rate at which a metal corrodes is defined as the amount of metal that is oxidized per unit area in a given time, i.e. the mass loss of the metal per unit area in that given time.

The corrosion products will dissolve to some extent and be released from the surface. The metal release rate (or run off rate) is the amount of metal that is released per unit area in a given time.

The corrosion process occurs at the interface between the metal and the corrosion products whereas the metal release process takes place at the interface between the corrosion products and the atmosphere[132,133].

The difference is schematically illustrated in figure (2.30).

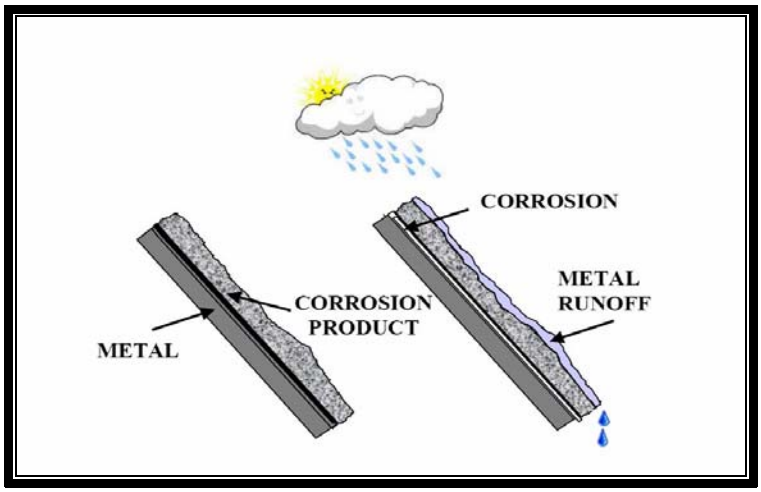

Figure (2.30) The difference between the corrosion and the metal release process[132].

When the thickness of the corrosion product layer increases , the corrosion rate will usually decrease as a result of the protective properties of corrosion products formed, i.e. the corrosion products layer reduces the possibility for corrosion species to diffuse towards the metal surface[134].

Corrosion and metal release rate are generally ruled by different physical, chemical and electrochemical processes, and are note necessarily equal or even proportional[135].

Corrosion rates are characterized by initially high rates decreasing with time. Metal release rates show lower and more time-independent values, at least over long time periods, on a time scale of years. With time, the rates might become equal

when steady state conditions are reached with a constant thickness of the corrosion product layer[136].

The various corrosion behaviors of the Zinc-Nickel coating produced at different deposition conditions. The change of corrosion current as a function of nickel content in the deposit as shown in figure (2.31).

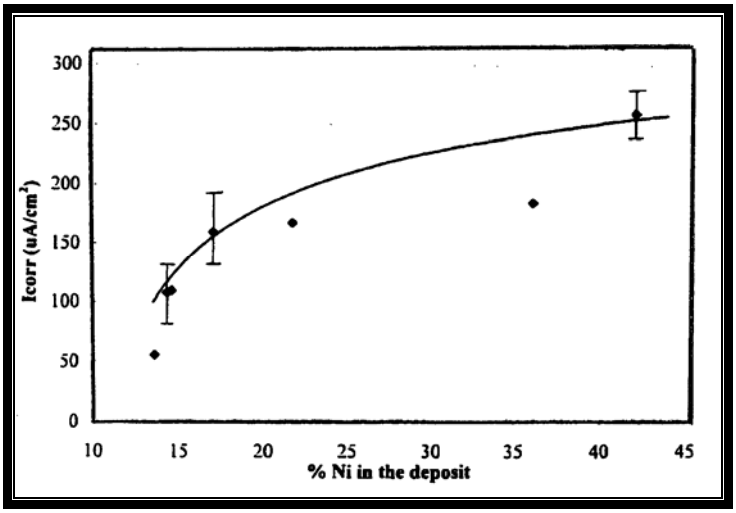

Figure (2.31) Correlation between nickel content in the deposit and corrosion current of zinc-nickel electrodeposited coatings[123].

The coatings that have a low(~ 13%) nickel content show the lowest corrosion current ,whereas coatings with nickel content higher than 15% show a high corrosion current .At this point, the contribution of phase transformation to the corrosion behavior should also be considered, since the γ phase starts to form at a nickel content above 15%,where the coatings have the η+γ dual phase at about 15% of nickel, the dual phase is responsible for sudden increase of corrosion current at this nickel percent range .The coating with a higher nickel content (above 20%) shows poor corrosion resistance .

Numerous other studies, leading to the general conclusion that Zn-Ni alloys containing between 9-17% Ni are better corrosion protection of steel [137].

It was found that corrosion resistance was descended in relation with coating morphologies:

Whisker > nodular > pyramid > dendritic growth figure (2.32) [138]

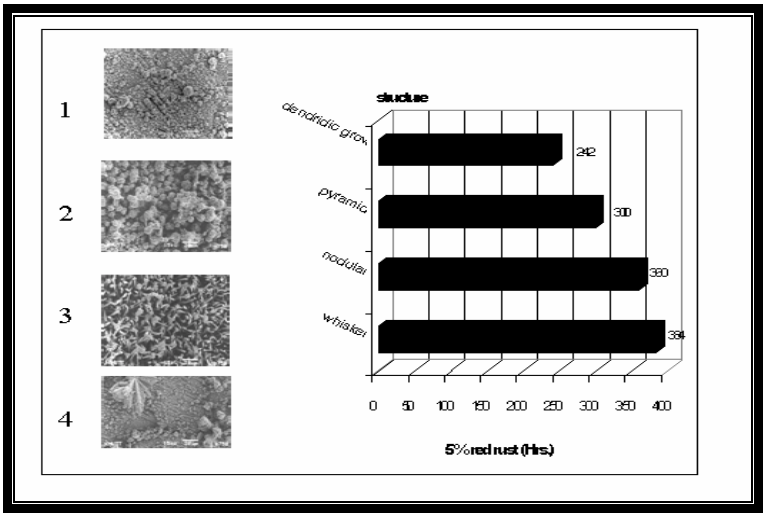

Figure (2.32) Relationships between morphologies of coating (wt%) and corrosion resistance (hours of 5% red rust) [138].

1: dendritic growth structure ,242 hrs
2: pyramid structure,300 hrs
3: nodular structure,360 hrs
4: whisker structure,384 hrs

The surface covered in red rust is measured as a function of exposure time figure (2.33) and figure(2.34).

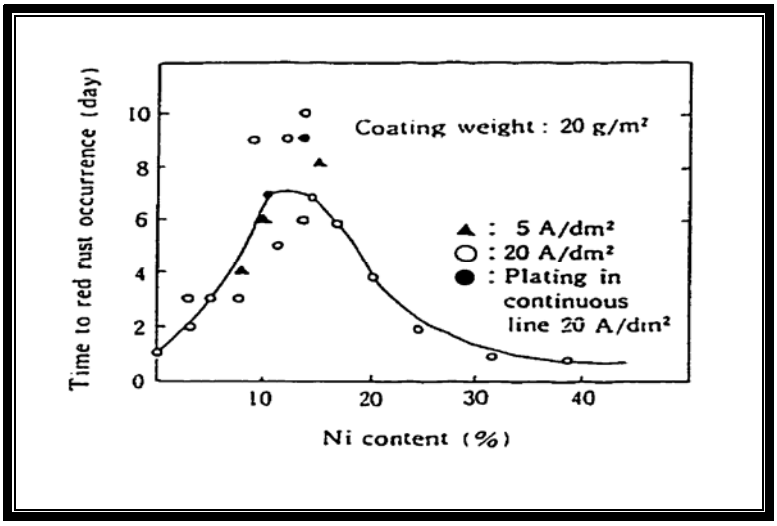

Figure (2.33) Change of time to red rust appearance with nickel content[139].

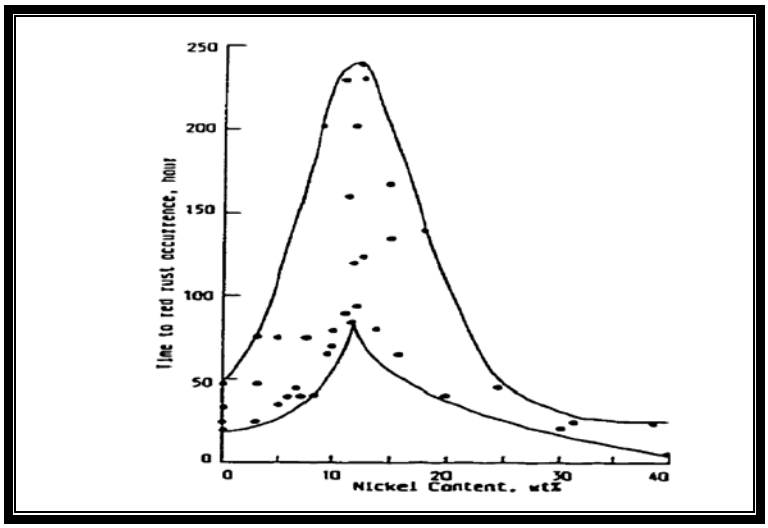

Figure (2.34) Change of time to red rust appearance with nickel content [140].

Zn-Ni surface was dull in appearance and the terrace stepped structure was observed for the Zn-Ni sample. It possessed a nodular fine-grained morphology figure(2.35a),with the grain size in the order of 1-2 μm.

Surface morphology evolution during sample immersion in a $HC\bar{O}_3$ containing NaCl solution was examined by ex situ AFM figure (2.35 b,c,d).

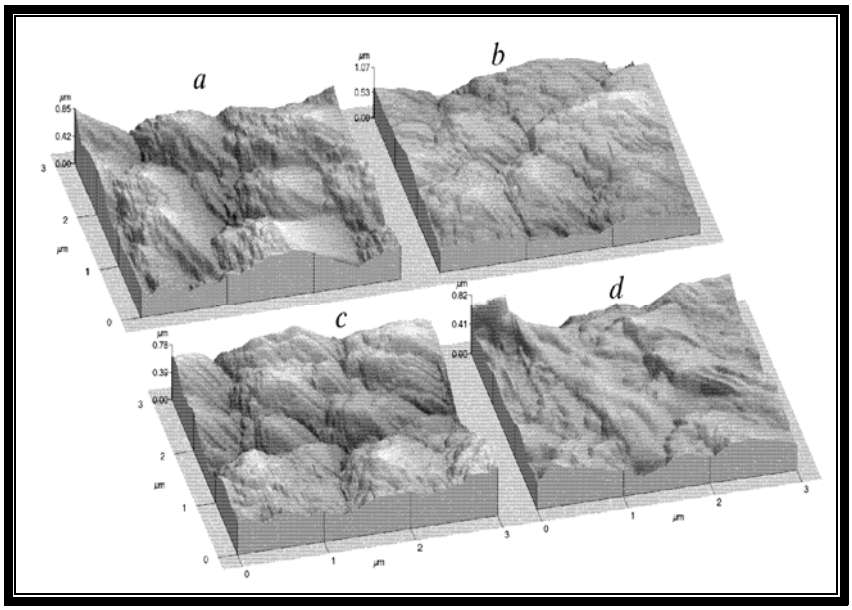

Figure (2.35) AFM images of Zn-Ni surface: a-initial after electrodepostion , b-after 0.5 h of corrosion attack with corrosion products, c- after 0.5 h of corrosion attack without corrosion products, d-after 8 h of corrosion attack, without corrosion products [141].

Some damages along the crystal boundaries for Zn-Ni coating were presented after corrosion attack figure (2.35c).

The surface of the Zn-Ni coating was irregular but smooth, with round shaped features arising from the electrodeposition process figure (2.36a,b) and a network of hair-like cracks, arising from internal stress of the coating[142].

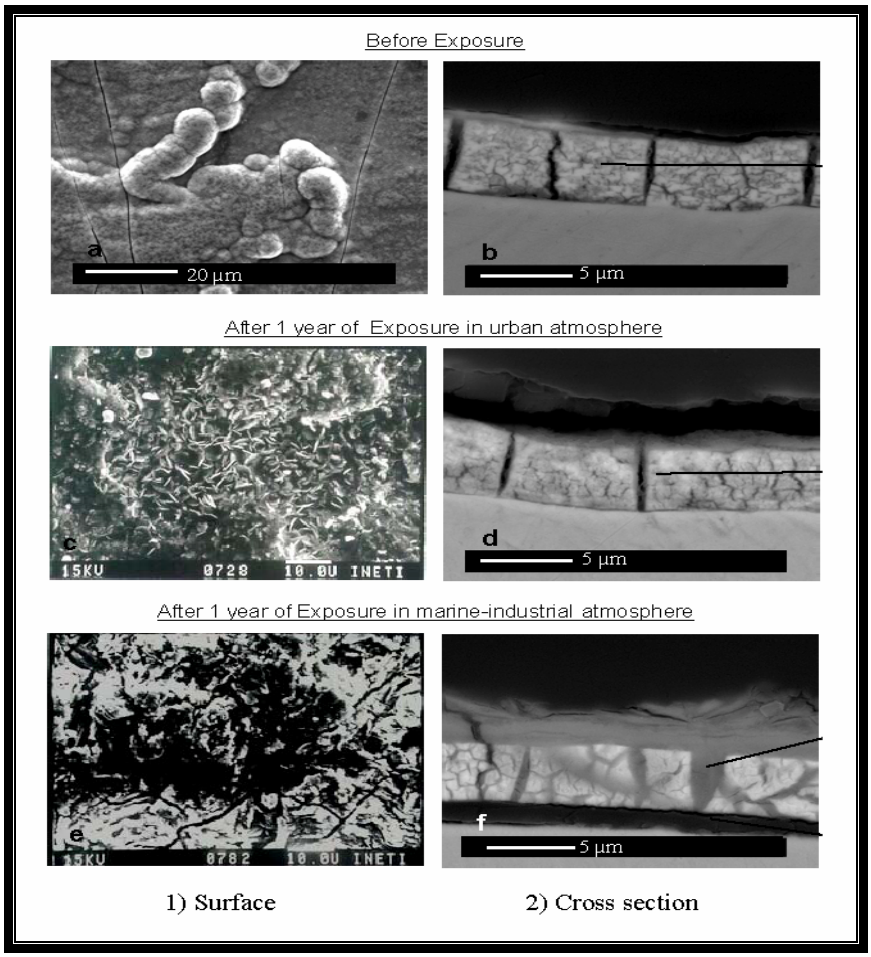

Figure (2.36) Zinc-Nickel to exposure(a),(b); after 1 year of exposure in urban site (c),(d);and in marine-industrial site(e),(f), (for surface1 and cross section 2),respectively. Micrographs form back-scattered electrons[143].

During exposure both the vertical cracks and the smaller microcracks expanded, as a consequence of the selective oxidation of zinc , and a thick layer of corrosion products accumulated at the coating /electrolyte interface.

For the marine-industrial atmosphere the layer of corrosion products become nearly as thick as the coating itself ,a thin layer of corrosion products at the coating /substrate interface appeared , and extensive desagregation of the coating occurred [143].

2.2.15 Silicadizing

Silica is a white, crystalline solid with tetrahedral crystalline structure and a melting point of 1710°C.Due to its inert nature, Silica is widely used for preventing corrosion in aggressive environments in chemical reactors. Silicadizing is a process that has been explored to protect the surface of metals from corrosion.

However, the formation of silica coating for preventing corrosion on steel surfaces remains a challenge and is being actively explored(144).

A cross-sectional SEM analysis of silicate coating indicated the silicate layer is not more than 1μm thick figure(2.37),and maximum thickness to be limited to 3μm(145).

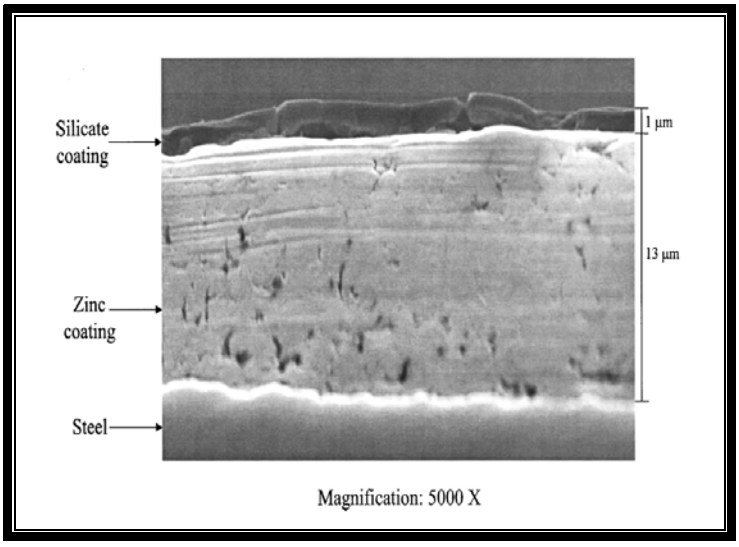

Figure (2.37) Cross section of SiO_2 formed on Zn coating (145).

A post –treatment drying process was found to increase the Si content in the coating and improve the corrosion characteristics of the silicate layer figure (2.38).

Deposition parameters like concentration of the bath, applied voltage and deposition time have been optimized by using corrosion characteristics and surface morphology.

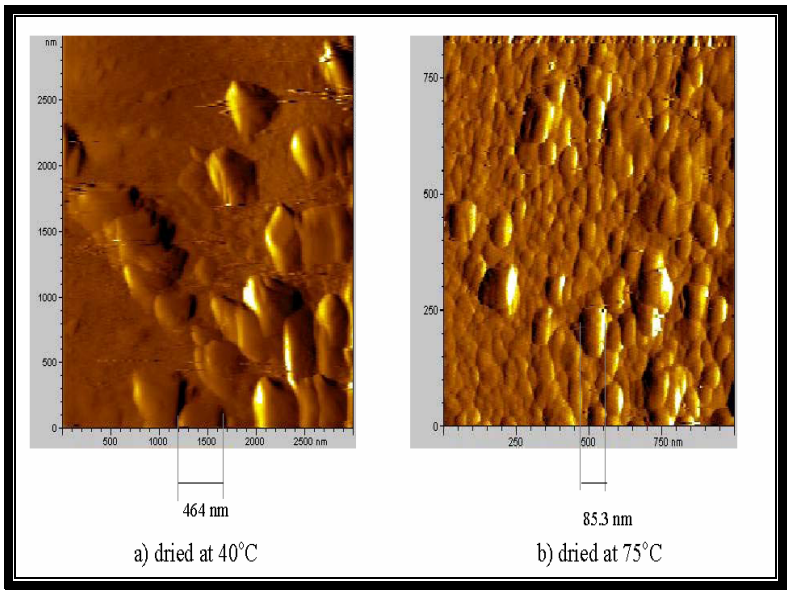

Figure (2.38) Change in particle size of the coatings with drying temperature as determined by AFM analysis[144].

Stability of the coating has been improved by varying the drying temperature and the particle size decreases from 0.5μm to the order of 5nm when the drying temperature is changed from 40 to 200°C figure (2.39).

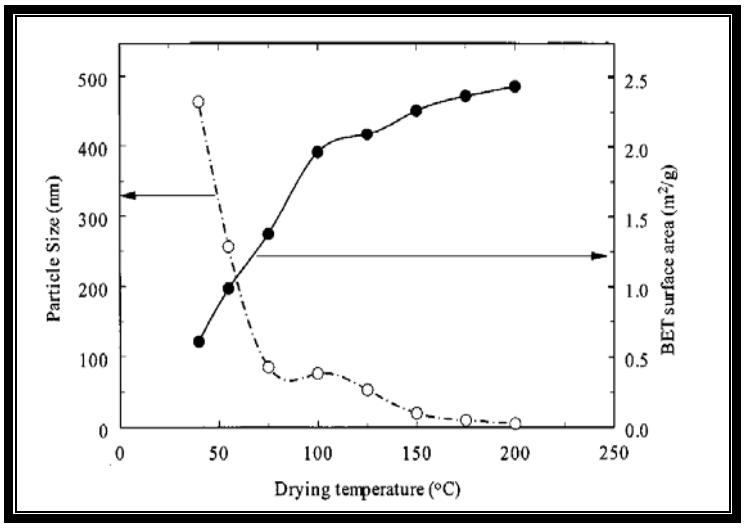

Figure (2.39) Variation in particle size and surface area of the coatings as a function of drying temperature as determined by AFM and BET analysis[145].

The reason for increased stability with heating temperature is due to the decrease in the size and number of cracks on the surface figure (2.40).

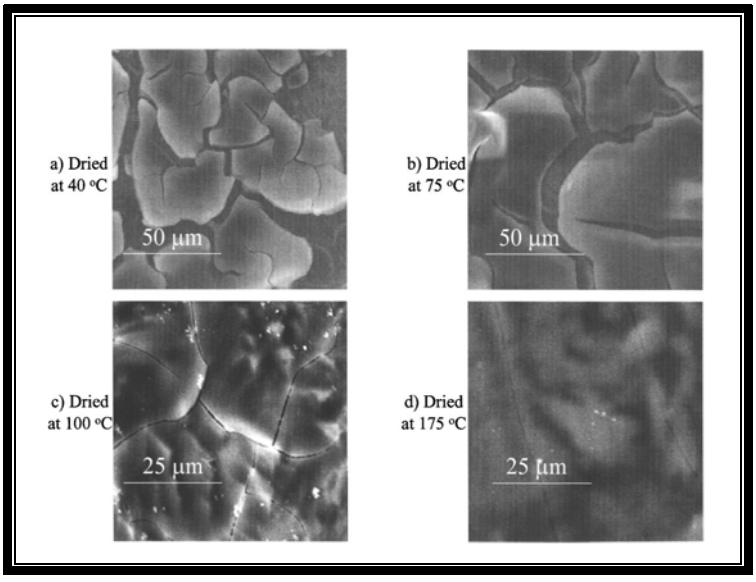

Figure (2.40) Variation in the surface crack structure as a function of drying temperature[145].

The crack size decreases from 10μm in case of samples heated at 40°C to 0.25μm in the case of samples heated at 175°C.

The decrease in the crack opining helps in decreasing the entry of water through them and hence the observed increase in stability. This result indicates that drying plays an important role in determing the microstructure of silicate coating.

The technique for the formation of zinc silicate schematically diagram in figure (2.41).

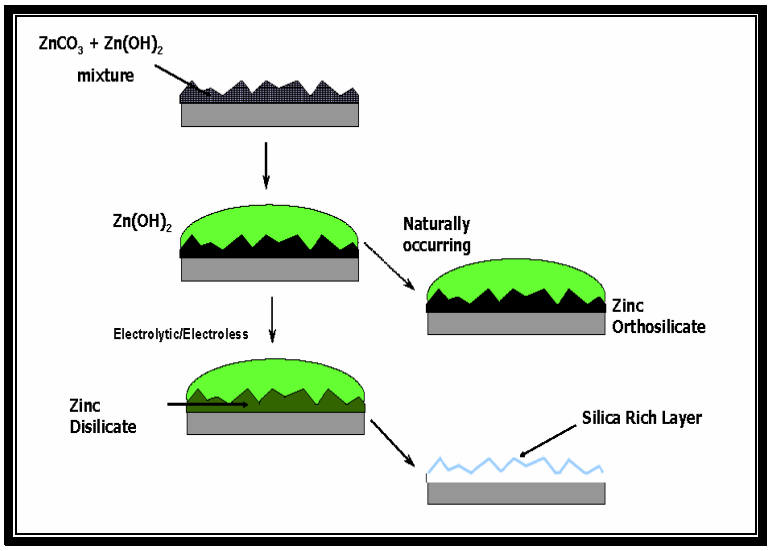

Figure (2.41) Schematic diagram showing the formation of Zinc Silicate[144].

Chapter Three

EXPERIMENTAL WORK

Chapter Three

Experimental Work

3.1 Samples Preparation

The substrate metal used in this study was low carbon steel. The limiting chemical composition of base metal is shown in Table(3.1),was checked by X-Ray fluorescence (XRF-1800 SEQUENTIAL SHIMADZU Japan 2005) and Carbon/Sulfur Analyzer (HORIBA EMIA-22V Japan 2005) .

Table (3.1) Chemical composition of base metal

Al	Cu	Cr	Mn	Mo	Ni
0.0910%	0.0692%	0.0386%	0.5351%	0.0000%	0.0250%
P	Si	V	S	C	Fe
0.0284%	0.3458%	0.0026%	0.01081%	0.18283%	Rem

The substrate samples were cut into circular cross sectional shape with dimensions (12 mm dia.,1.5 mm thickness) and total surface area of 113.04 mm^2.

These samples were cut from a solid rod perpendicular to the rolling direction. All surface, including the edges were wet ground using 120,220,320,600,1000, and 1200 grit silicon carbide papers, then these samples were rinsed in distilled water followed polished by alumina powder to get a bright mirror finish for the

final step using (Grinder and Polisher by BUEHLER METASERV UK).

Next, these samples degreased with acetone and then ultrasonically cleaned (by Ultra Sonic Cleaner Type TK52 Leitz Wetzlar) , for 2minutes using ethanol as a medium figure (3.1). After drying, these samples expection surface by optical Microscope (WRAYMER Optical Microscope Focus 50-500), to insure free from any defect figure (3.2).

After that the process for etching by hydrochloric acid concentration 5.4% for period 2minutes then in ethanol 2minutes and acetone 2minutes followed all these step washing in distilled water and dryer ,after all these process stored in the desiccators.

Microstructure for base metal was examined using the same light optical microscopy(LOM),after being etched by a dipping 1% Nital. For this purpose optical microscopy fitted by a digital camera type (Nikon with 5.8-17.4 Mega pixels resolution) was used.

Figure (3.1) Ultrasonic bath

Figure (3.2) Light optical microscope

3.2 Equipments for Electroplating Process

The experimental apparatus used for the electrode position was made up of double – layered cylindrical glass container from (SCHOTT) , with a capacity of 300ml of electrolyte solution. A stirrer was used to agitate the electrolyte solution at 800 rpm. Electrochemical measurement were carried out by using a three-electrode cell , figure (3.3).

The working electrode (WE) was a coated sample situated in special Teflon holder figure (3.4) and figure(3.5) ,for the exposed surface area, one face of the sample is prone to the solution and the other face is masking by Teflon holder. Ni sheet purity (99.79%) , (1.5 cm X 1.5 cm) from (NAS JAPAN) or Zn sheet purity (99.79%) (1.5cmx1.5cm) from (NAS JAPAN) and another surface with all edge were masked by a wax. This electrode was used as a counter – electrode with a surface area considerably greater than that of the

working electrode , was polished before each run with 1.00 and 0.25 mm diamond compound before rinsed and finally held in an ultrasonic bath for 2 minutes.

The distance between the working and counter electrode was maintained at constant value of 3 cm.

Reference electrode was Vs.Ag/AgCl/$KCl_{(sat)}$ from (Metrohm) mounted in luggin capillary .The electrodeposition was performed by using a potentiostatic (POTENIONSTAT GALVANOSTAT AUTOLAB PGSTAT 30 Netherland) interfaced to personal computer .The potential scan rate was set at $5mVS^{-1}$, step potential $25mVS^{-1}$ and covered the potential range from -2000mV to -900mV Vs.Ag/AgCl/$KCl_{(sat)}$ figure (3.6) and confirmed the area of sample figure (3.7).This process deposition of compositionally is a multilayer on steel substrate figure (3.8).

Nitrogen purity (99.99%) was purged through out the experiment in order to remove dissolved oxygen from the electrolytes , and all experiment at ambient temperature (28° C).

After electrodepostion , the coating were held in an ultrasonic bath for 2minutes in order to remove loosely adsorbed particles from the surface.

All samples were held overnight in glass desiccator in order to eliminate any defect of humidity on the sample weight determination.

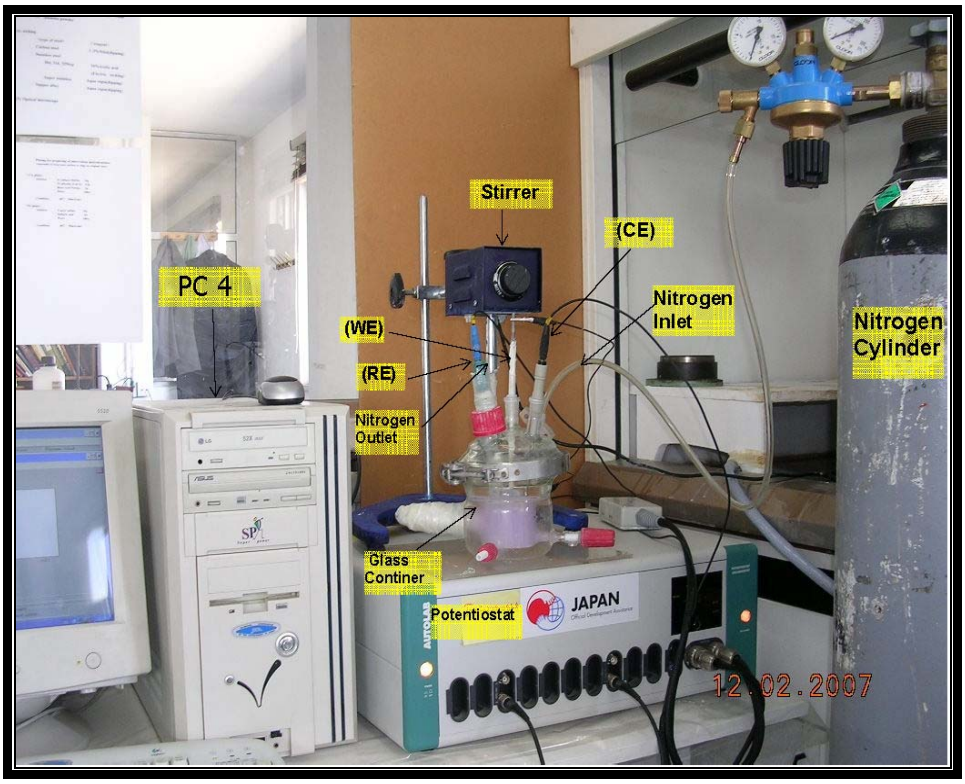

Figure (3.3) Electroplating equipment

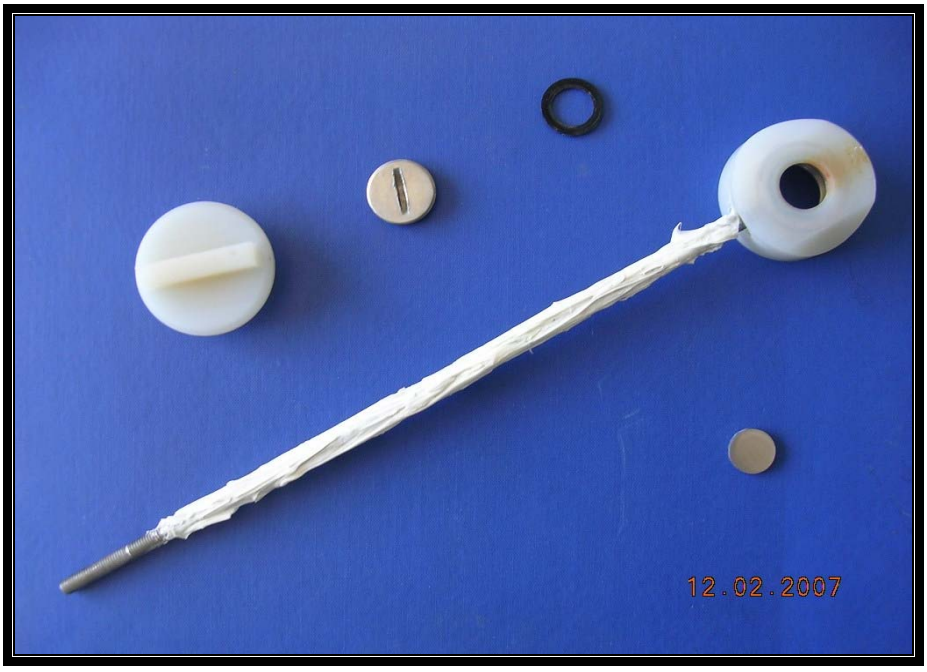

Figure (3.4) Special Teflon holder

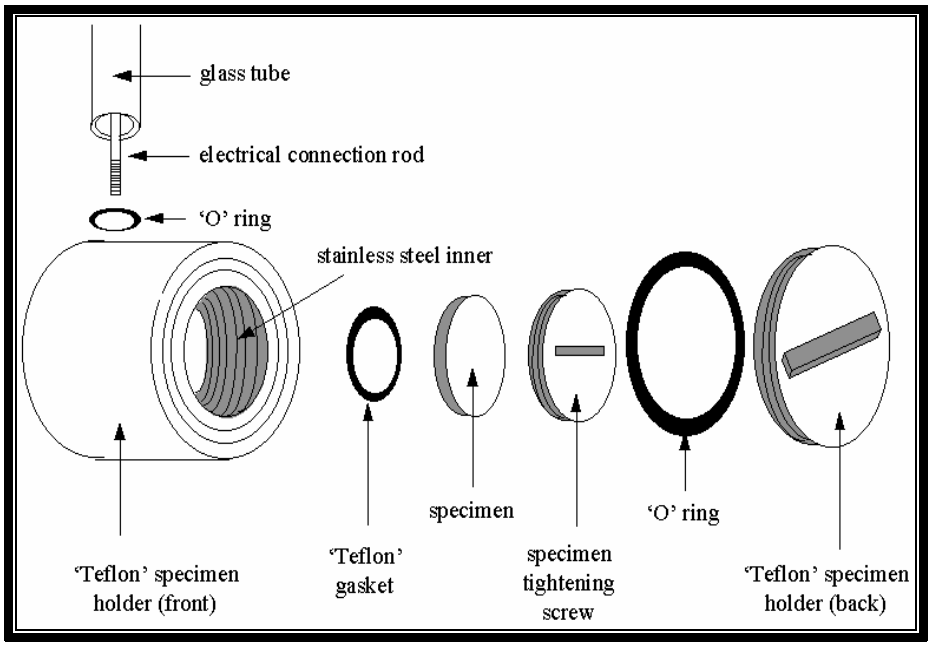

Figure (3.5) Schematic diagram for special Teflon holder

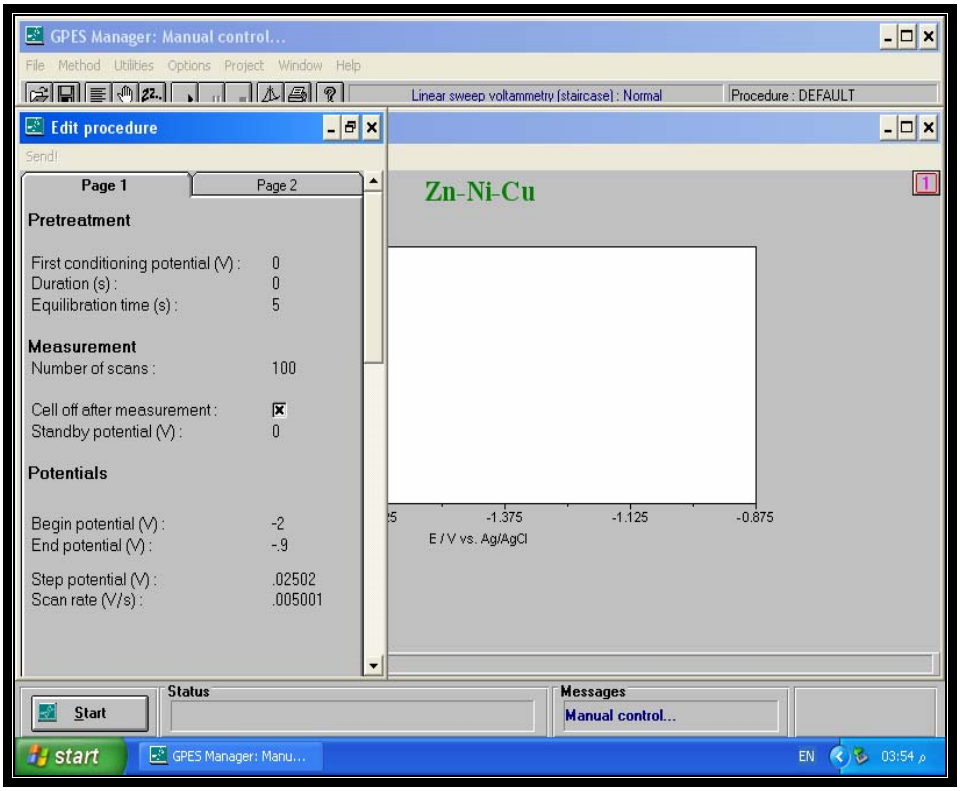

Figure (3.6) Confirm begin potential, end potential, step potential and scan rate

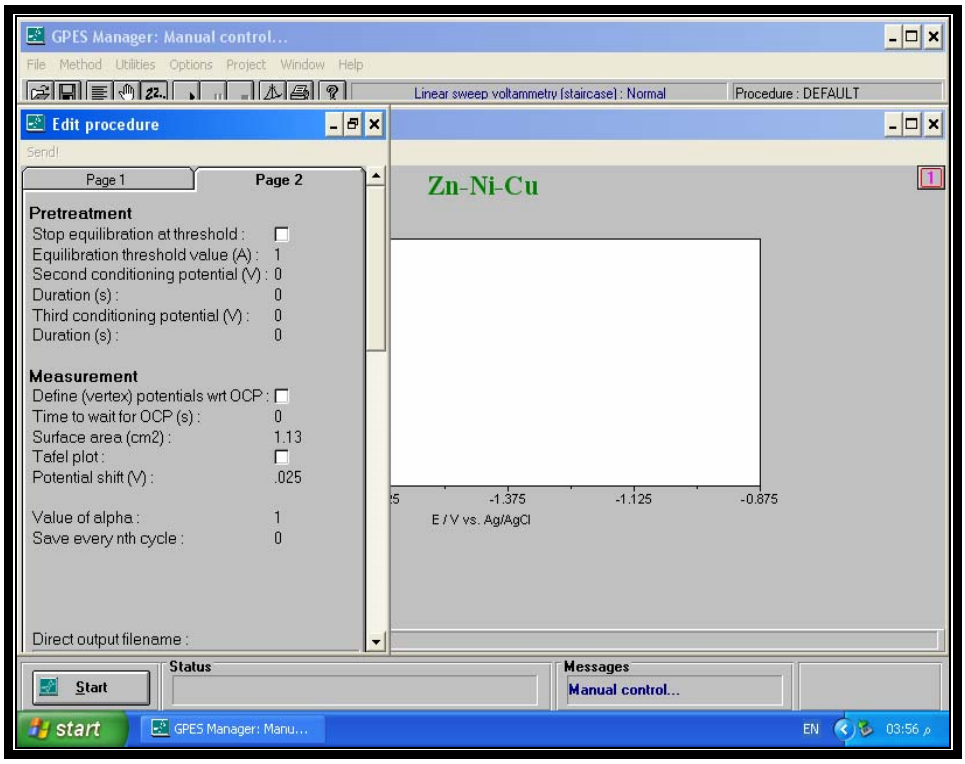

Figure (3.7) Confirm surface area

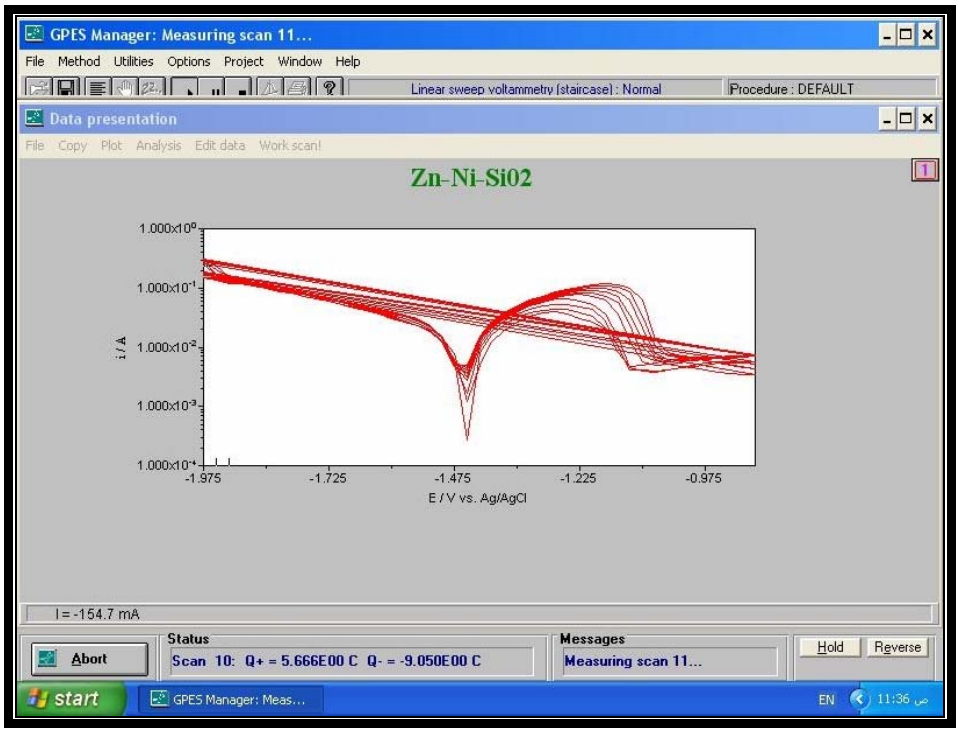

Figure (3.8) Multilayer scan for electroplating

3.3 Composition of the bath

Many experimental works were carried out to investigate the feasibility of simultaneous Zn-Ni, Zn-Ni-Cu and Zn-Ni-SiO_2 by electroplating process to reach demand percentage for the first layer coated .

All solutions were prepared with analytical-grade regents and distilled water ,chemical dissolution occurs under alkaline conditions.

Three baths were prepared for coating Zn-Ni, Zn-Ni-Cu and Zn-Ni-SiO_2 .The following details of all bath represent the optimum performance coating that could be obtained in this study Table (3.2).

Table (3.2) Composition bath

Bath	***Chemical Composition***	***Depositing Conditions***
Zn-Ni	ZnO(Scharlau Spain) 20 g/l $NiSO_4.6H_2O$(CODEX Spain) 2g/l NaOH (Scharlau Spain) 150 g/l $C_4 H_{13}N_3$ Diethylentriamin(Riedel-deHaen AG Germany) 3.33ml/l (Chelating Agent)	Anode plate:Zn (99.79%) pH:12.5 Bath Temp:Room temp.(28°C) Plating time: 60 min 17 run Dull Appearance
Zn-Ni-Cu	ZnO(Scharlau Spain) 20g/l $NiSO_4.6H_2O$(CODEX Spain) 1g/l Cu $SO_4.5$ H_2O (BDH England)0.66g/l $C_4 H_{13}N_3$ Diethylentriamin (Riedel-deHaen AG Germany) 3.33 ml/l (Chelating Agent)	Anode plate: Ni(99.79%) pH: 12.5 Bath Temp.:Room temp.(28°C) Plating time 60 min 17 run Dull Appearance
Zn-Ni-SiO_2	ZnO(Scharlau Spain) 20g/L $NiSO_4.6H_2O$ (CODEX Spain) 2g/l NaOH(Scharlau Spain) 150g/l $C_4 H_{13}N_3$ Diethylentriamin (Riedel-deHaen AG Germany)3-33 ml/l (Chelating Agent) SiO_2 (High Dispersed)(Scharlau Spain) 33.33 g/l Particle size for SiO_2<10μm	Anode plate:Zn(99.79%) pH:12.5 Bath Temp.:Room temp(28°C) Plating time 60 min 17 run Dull Appearance

All electrolytes were stirring by stirrer 2000 rpm for period two hours before the starting electroplating process and prepared new electrolytes every new sample coating to insure stability of throughing power for electrolyte and without any loosely from solution through the process of electroplating . After plating, the deposits were immediately rinsed in tap water , dried with hot air,and all samples were held overnight in glass desiccators in order to eliminate any effect of humidity on the sample weight determination.

3.4 Measurement Of Coating Thickness

For this work that has been carried out the measurement was done by two ways, the first one is by coating thickness gauge (elcometer 256 FN T9 Germany) used euddy current method figure (3.9),and the second way is by a digital Micrometer (Mitutoyo) (by measurement thickness sample before and after coating).

The two ways were measured in three places to provide averaged sample thickness. Many experimental works were carried out to investigate. The thickness coating approximately 10μm controlled by the period of electrodeposition time.

Figure (3.9) Coating thickness gauge

3.5 X-Ray Flourescence(XRF)

The film composition was determined by X-ray fluorescence spectrometer(XRF-1800 SEQUENTIAL SHIMADZU Japan 2005) figure (3.10). The chemical composition of the coating material under scrutiny is represented by the average of at least four measurements at different point in each sample by followed a quantitative method.

The XRF analysis was carried out at chemical production department –RSS/Amman.

Figure (3.10) X-ray fluorescence

3.6 Energy Dispersive X-Ray (EDX)

Energy Dispersive X-ray model (super scan SS-550 SHIMDZU Japan) figure (3.11), as an analytical method was used to determine the concentrations for base metal and layer coated for Zn-Ni, Zn-Ni-Cu, and Zn-Ni-SiO_2.

The (EDX) analysis was combined with SEM apparatus,was carried out at the Mechanical Department –RSS-Amman.

Figure (3.11) Energy Dispersive X-ray

3.7 Scanning Electron Microscopy (SEM)

The morphology of surface deposits were observed by a scanning electron microscopy model (Superscan SS-550 SHIMADZU-Japan 2005) figure(3.12).Were carried out electroplating magnification layer for X100, X500,X2000,X8000,X10000,andX20000 and magnification after corrosion for X150 and X300 also after thermal shock for X700,X800 and X1500.The SEM analysis was carried out at the Mechanical Department –RSS-Amman.

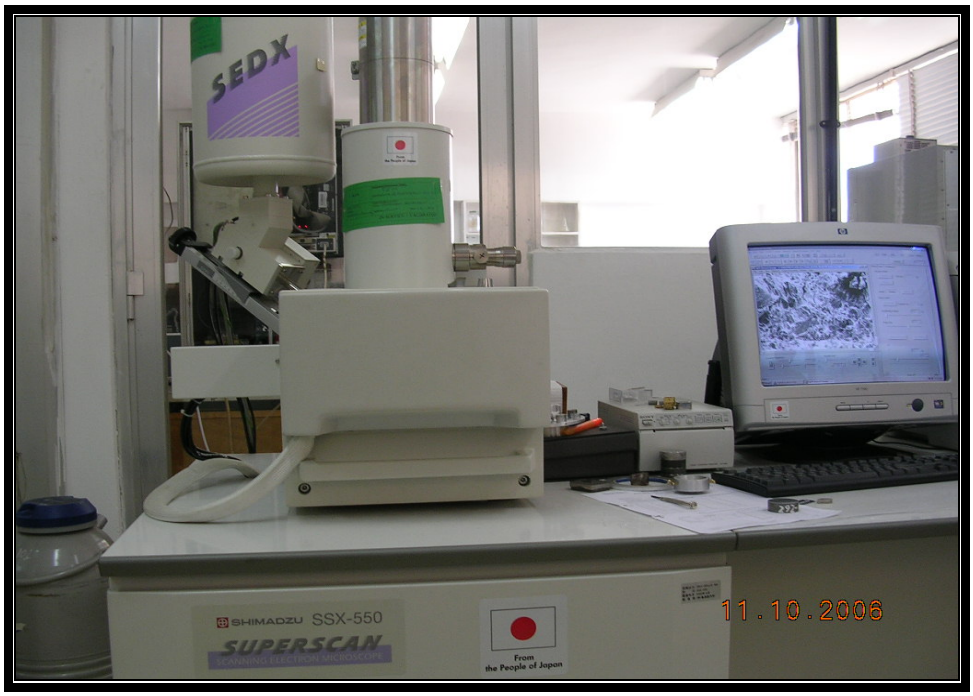

Figure (3.12) Scanning electron microscopy

3.8 Heat Treatment

Heat treatments were carried out in a programmable furnace (memmert Germany) figure (3.13), in the temperature 200°C in air at one atmospheric pressure . Each heating cycle includes heating in the furnace for 1 hr at the test temperature and cooling in still air.

Figure (3.13) programmable furnace

3.9 Microhardness Measurement

Microhardness Vikeres tester type (HMV Micro Hardness Tester SHIMDZU Japan 2005) figure (3.14), was used to measure hardness distribution at coated layer for Zn-Ni,Zn-Ni-Cu,Zn-Ni-SiO_2 and base metal before and after heat treatment, with 10g load and holding time of 26 seconds combined with optical microscopy to measure the diagonal length of Vicker's impression.

The Vicker's microhardness (H.V) is defined as follows:

$$HV = 1.845\ P/d^2$$

Where P= applied load, = 10g

d = average length of diagonal, mm

Three readings were recorded for each sample coated and one at the substrate. The Microhardness Vickers test was carried out at the Mechanical Department-RSS -Amman.

Figure (3.14) Microhardness Vikeres Tester

3.10 Salt Spray Chamber

The salt spray chamber is available for accelerated corrosion testing of sample specimens. Standard tests like salt spray (DIN 50021),condensed water (DIN 50017).

In addition, programmable tests with parameters different from the standard testing are carried out to review the relevance of testing conditions such as temperature, humidity, exposure time periods or the ratio between different test phases for the delamination and corrosion behavior of various test specimens.

The apparatus for testing(Salt spray WEISS TECHNIK weiss Umwelttechnik GmbH Simulationsanlagen Messtechnik Germany 2006) figures (3.15,3.16 ,3.17 and 3.18) , consists of a closed testing chamber, where a salted solution (mainly,a solution of sodium chloride 5%) is sprayed by means of a nozzle.

The equipment under test (EUT) is placed in the chamber. It is suspended at the same height as the top of the salt fog delivery tubes, but tipped at a 15 degree angle so condensation will run off instead of pooling figure (3.19).

The salt solution is atomized by mixing it with humid pressurized air in the nozzle and delivered to the salt fog chamber figure (3.20) .

It may be necessary to preheat the incoming air to avoid a reduction in saturation due to heat loss during vaporization.

This produces a corroding environment in the chamber and thus, parts in it are attacked under this severe corroding atmosphere.

The experiment condition for salt spray test was as following:

Salt spray flow capacity :	0.4 ± 0.1 L/(h.m^3)
Drop diameter :	5~20 µm
Test chamber volume:	450 Liter
Pressure :	1 bar
Brine reservoir capacity:	180 Liter (5% NaCl-Solution)
Temperature :	35°C
Humidity:	50%
Experiment time :	24 hrs

The experiment condition for humidity test was as following:

Temperature :	35°C, 45°C, 55°C
Humidity :	50%
Pressure :	1 bar
Experiment Time:	24 hrs

The correspondence of coating weight with salt spray and humidity for corrosion resistance can carried out by weight loss before and after test by (Sensitive Balance LIBROR AEG-120 SHIMADZU). The salt spray test carried out before and after heat treatment for all samples Zn-Ni,Zn-Ni-Cu,Zn-Ni-SiO_2 and base metal. The salt spray chamber test was carried out at the Mechanical Department –RSS-Amman.

Figure (3.15) Salt spray chamber

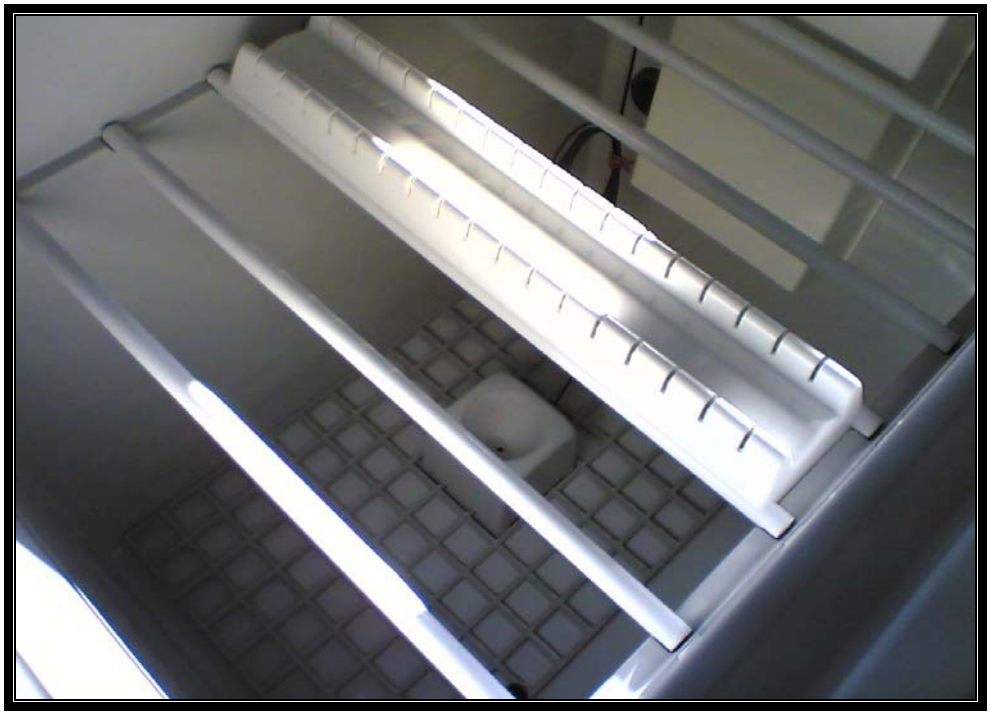

Figure (3.16) Salt spray chamber from inside

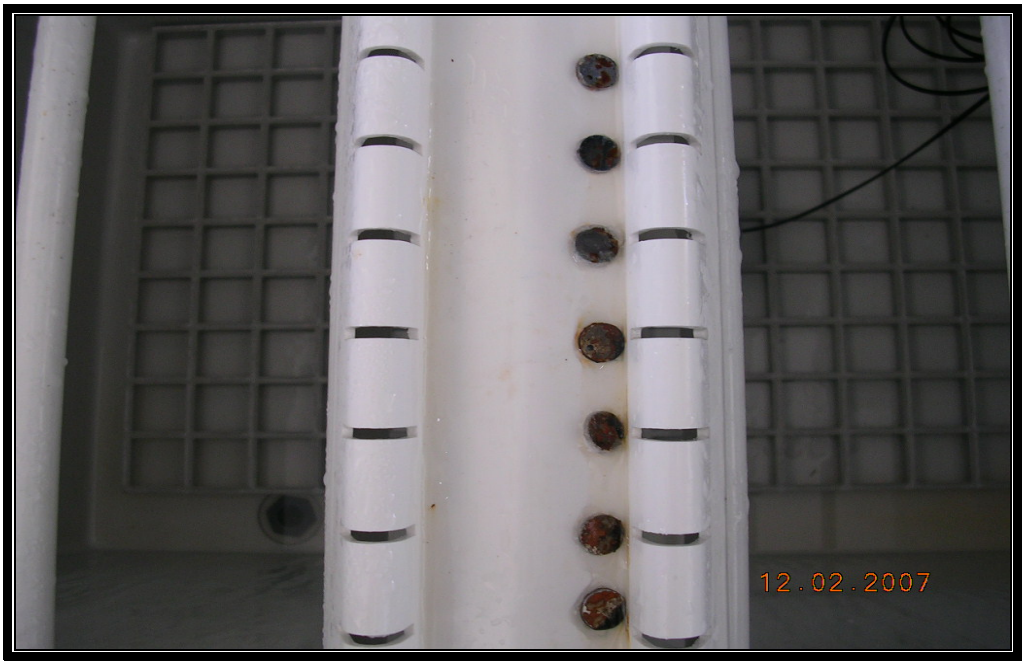

Figure (3.17) Samples after salt spray test

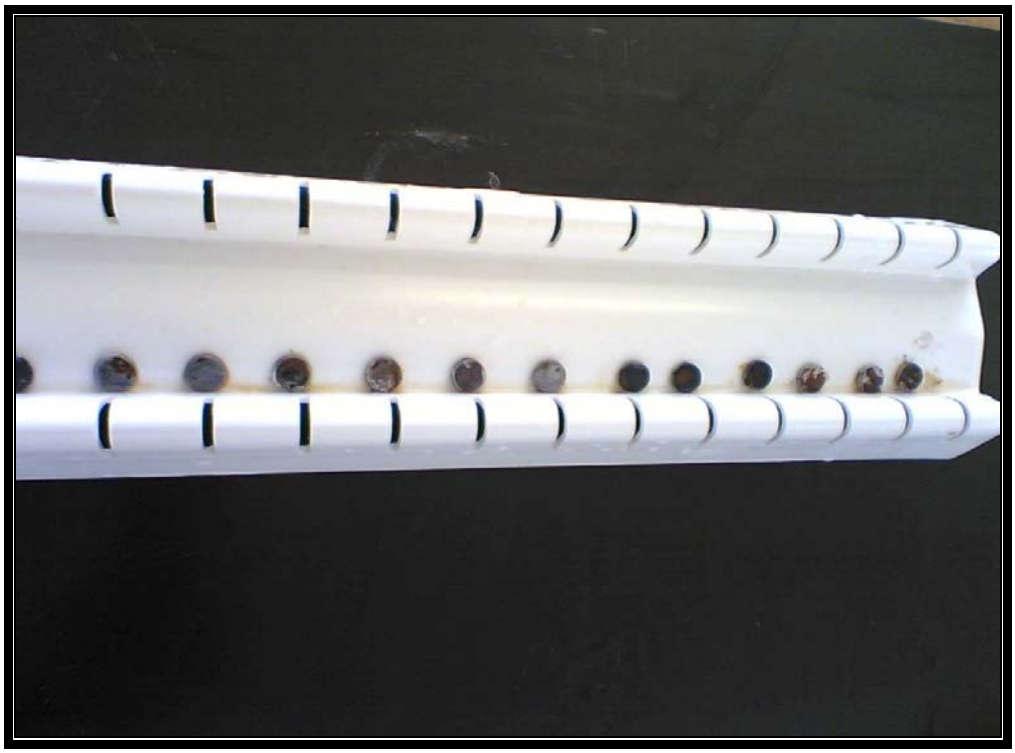

Figure (3.18) Samples after salt spray test

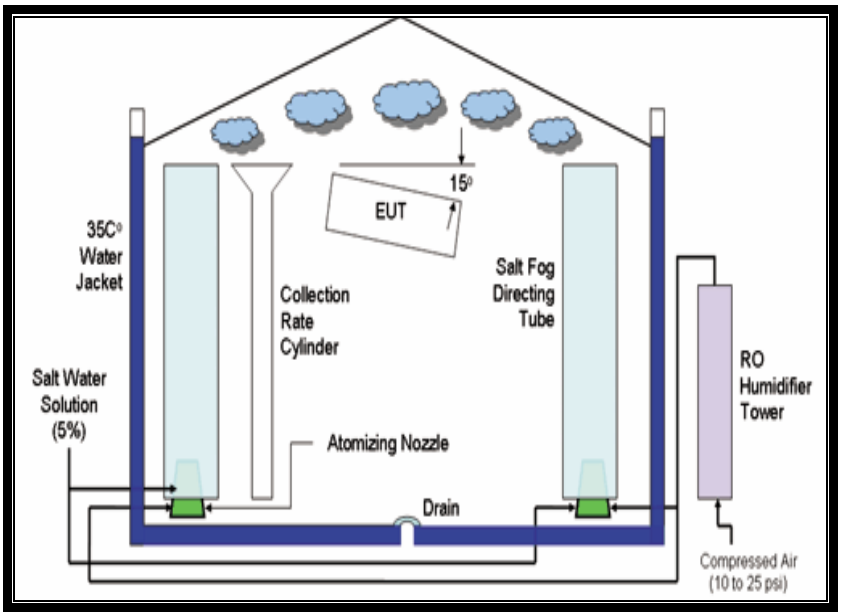

Figure (3.19) Schematic diagram for salt spray chamber

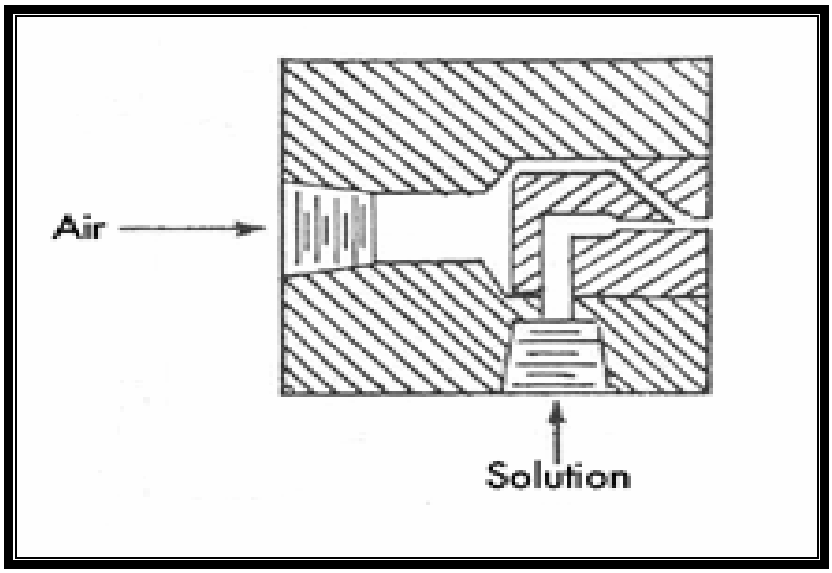

Figure (3.20) Typical spray nozzle

3.11 Free E_{corr}

The experimental apparatus used a cylindrical glass container,with a capacity of 500ml of electrolyte solution(distilled water with 5% NaCl).Samples were hanged by cupper wire(masked by a wax in all point contact with solution) through perforated stainless steel stand.Electrochemical measurement were carried out by using a colamel electrode Vs $Ag/AgCl/KCl_{(sat)}$ as a reference electrode with a sample (Base Metal, Zn-Ni ,Zn-Ni-Cu and Zn-Ni-SiO_2) to measure accurate free E_{corr} .

This circuit connected to voltimeter type (Fluke 175 TRUE RMS MULTIMETER) and begin reading free E_{corr} until step this reading after average one hours.

3.12 Tafel Method

The Tafel method is a technique to determine the corrosion rate of a specimen by analyzing the cathodic or anodic polarization curves.

A Tafel plot is performed on a metal specimen by polarizing the specimen to about 500 mV anodically and cathodically from the free corrosion potential,E_{corr}.

The potential is scanned with a scan rate of 0.1 ~ 1 m V/Sec. The corrosion current, I_{corr},is directly related to the corrosion rate and obtained from a Tafel plot by extrapolating computerize the linear portion of the curve to E_{corr}.

In this work , corrosion tests were conducted in deacrated 5% NaCl and 1% H_2So_4 solution at 35°C using a potentiostat (POTENIOSTAT GALVANOSTAT AUTOLAB PGSTAT 30

Netherland) figure (3.21),interfaced to personal computer, a standard corrosion cell kit containing the working electrode, two graphite counter electrodes and a saturated calomel reference electrode (SCE) as described by ASTM standard G3-89.

Schematic diagrams of the corrosion cell and the electrode arrangement are illustrated in figure (3.22). The corrosion test monitors both the galvanic current between the anode (the working electrode) and the cathode (the counter electrode) and the potential between the anode and the reference electrode.

The volume of electrolyte for each test was 500 ml and the solution was stirred at 800 rpm.

Potentiodynamic scanning was conducted by stepping the potential at a scan rate of 1mV/sec from -1.250 VS Ag /AgCl / $KCl_{(sat)}$ to 0 VS Ag/AgCl /$KCl_{(sat)}$. From the automatic data acquisition system,the polarization curves were plotted and the corrosion current and potential were calculated by the Tafel computerize extrapolation method figure (3.23).

Figure (3.21) Tafel cell interface with computer

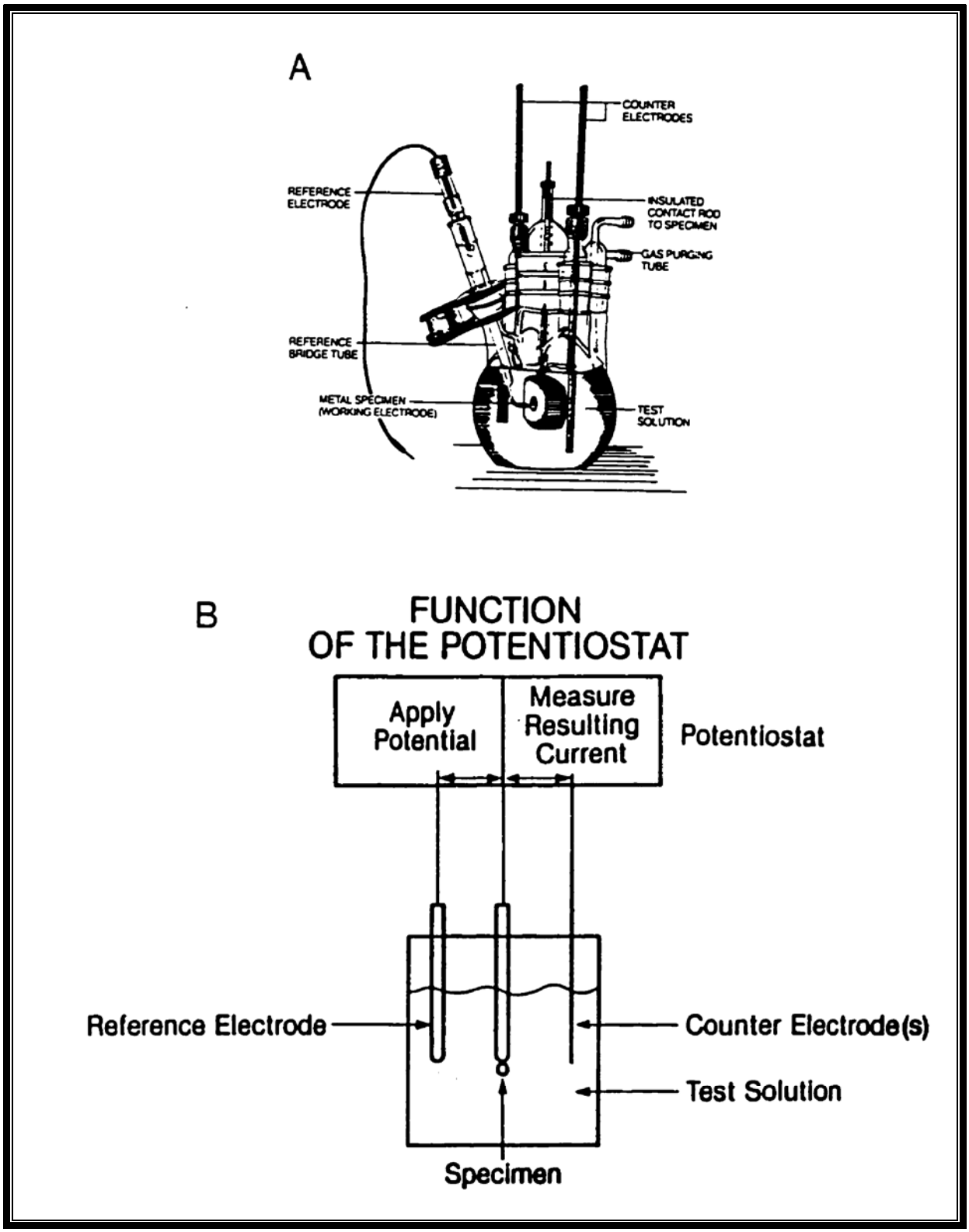

Figure (3.22) Schematic diagrams of Tafel cell

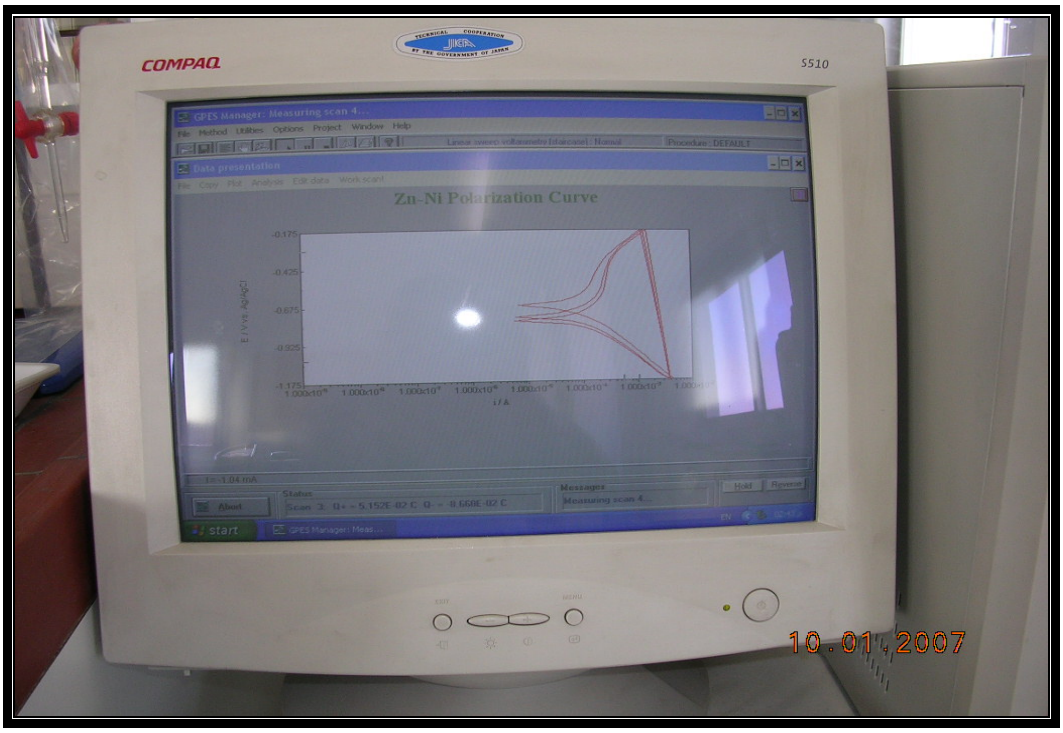

Figure (3.23) Polarization curves were plotted.

3.13 Acid Test

This test were carried out to insure stability of coated samples in sever condition .In this work ,corrosion tests were conducted deacrated in 1% HCl at 35°C,45°C and 55°C,the samples were measured weighted first ,then placed on the solution for a period 24 hrs. figure (3.24).

After testing the samples they were cleaned in an ultrasonic bath, first in distilled water and then in ethanol, they were then weighed on a digital balance to determine the change in weight .

Figure (3.24) Samples immersed in acid

3.14 Surface Roughness Test

Surface roughness gauges type (FEDERAL) figure (3.25), was used to determine the value of R_a (Roughness Average).This value is related as the arithmetic average deviation of the surface valleys and peaks as irregularities measured form a mean line within the evaluation length (L) expressed in micrometers, figure (3.26) shows surface asperates, equation 1 and equation 2 expressed for analysis surface roughness value.

Figure (3.25) Surface roughness gauges

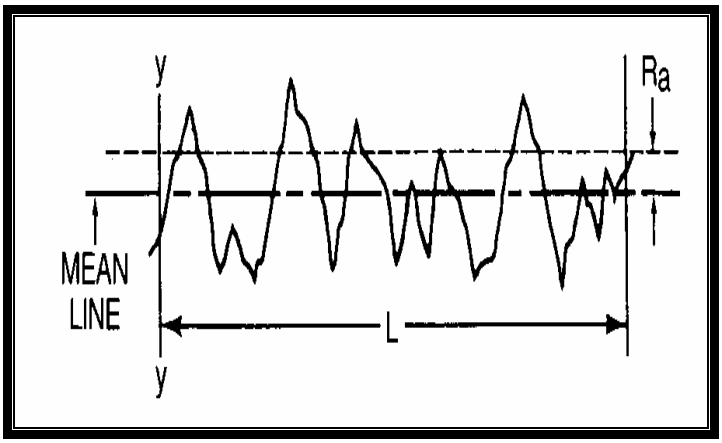

Figure (3.26) Surface asperates

$$Ra = \frac{1}{L}\int_{0}^{L} |y|\,dx \quad \text{……..…… (3.1)}$$

$$Ra\,(approx.) = \frac{y_1 + y_2 + y_3 + \dots y_n}{n} \quad \text{……..(3.2)}$$

Three readings were recorded for each coated sample type. The surface roughness test was carried out at the Mechanical Department-RSS-Amman.

3.15 Reflectivity –Transmissivity Test

This test is carried out by Spectrophotometer type (Macbeth 7000 spectrophotometer USA), figure (3.27).

A spectrophotometer is a device for measuring light intensity as a function of the color and the wavelength of light.

Visible region 400-700 nm spectrophotometry is used and usually take readings every 10 nanometers along the visible region , and produce a spectral reflectance and transmissivity curve.

Three samples measured Zn-Ni,Zn-Ni-Cu and Zn-Ni-SiO_2 for reflectivity and transmissivity test,they were carried out and compare with (standard ceramic black) and standard white (as a barium sulfate powder) .

The Reflectivity –Transmissivity test was carried out at the Chemical Department-RSS-Amman.

Figure (3.27) Spectrophotometer

Chapter FOUR

RESULTS & DISCUSSION

Chapter Four

Results and Discussion

4.1 Introduction

The chemical reaction between a metal and its environment which leads to a change of the characteristics of the metal and its alloy in sever environments constitutes a limitation to the development of more efficient energy conversion devices. The five principal degradation problems are corrosion, oxidation, wear, fatigue and metal dusting.

Electroplating technique has been used in these environments, but its corrosion resistance needs to be improved by surface modifications. Among the various surface modification methods, electroplating Zn-Ni has been applied during the last 15 years to enrich zinc or nickel at the alloy surface. However, Zn-Ni deposition is known to be an anomalous electrodepostion process and yet poorly understood[146]. It has an industrial importance and outstanding properties ,such as ductility, wear resistance and adhesion. In electroplating Zn-Ni for carbon steel substrate, the resulting depletion of alloy coating from its surface is problematic, especially for materials used in corrosion environments.

In addition, carbon steel has poor salt spray and humidification resistance at sever condition. Therefore, to alleviate this difficulty, simultaneous deposition of alloys by electroplating is very effective in protecting substrate from sever corrosion environments.

In this study, zinc and nickel with and without cupper or silicon dioxide are simultaneously deposited by electroplating into carbon steel substrates using potenionstat technique.

Figure (4.1) shows carbon steel sample as a polished and with coating Zn-Ni, Zn-Ni-Cu and Zn-Ni-SiO_2 by electroplating technique coating used in this study. The as-coated surface is smooth with a matt metallic appearance. No pack particles could be observed in surface layer.

This chapter will discuss the results that are obtained from the corrosion of as received carbon steel and its coated systems (Zinc-Nickel, Zinc-Nickel-Cupper, Zinc-Nickel-Silicon Dioxide) in corrosion environments (salt water, salt spray, humidity, hydrochloric and sulfuric acid) in the temperatures range (35,45,55°C) and humidity 50% with and without post heat treatment at 200°C for a period 1 hr .

Effects of the above environment on corrosion kinetics and scale formed morphologies are studied. In addition, this chapter will review and discuss results and data obtained from Tafel plot by potentionstat technique in salt water (5% NaCl) and (1% sulfuric acid) with and without heat treatment at 200°C for period 1hr.,also microhardness, surface roughness and transmissivity experiments are described in chapter three.

The role of silicon dioxide in improving corrosion resistance, microhardness and reflectivity will be explained.

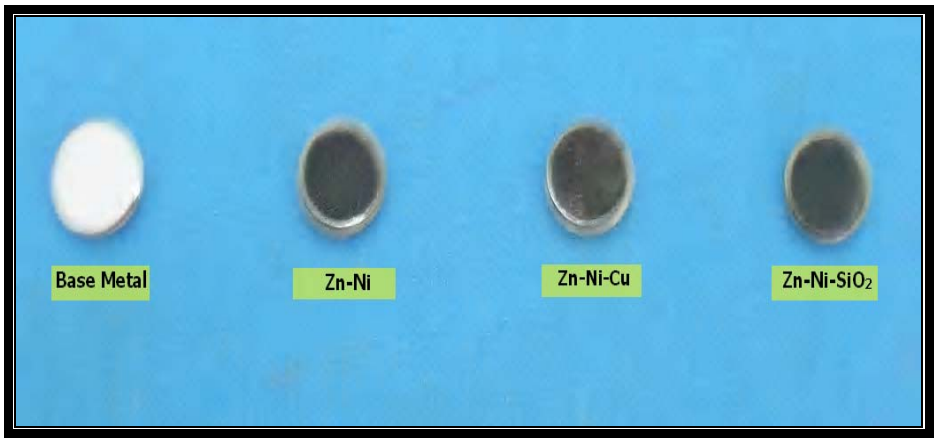

Figure (4.1) Carbon steel sample
-as a polished
-in the as coated Zn-Ni
- in the as coated Zn-Ni-Cu
- in the as coated Zn-Ni-SiO_2

4.2 Microstructure of Base Metal

The initial microstructure was characterized using light optical microscopy (LOM).As shown in figure(4.2),the grain structure of the uncoated carbon steel surface is homogenous over the sample surface. It is clear that the structure is ferrite and pearlite (α+ p). The microstructures of carbon steel surface was observed after being etched for approximately 1 min. in an etchant containing 1% Nital.

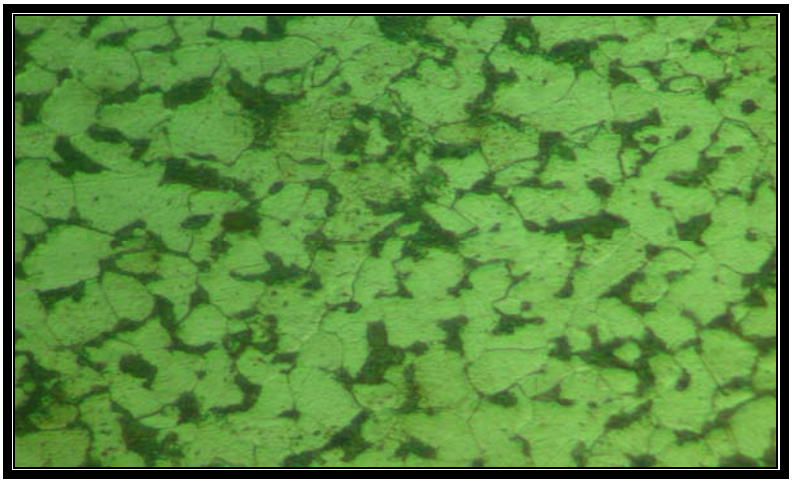

Figure.(4.2) The microstructure of carbon steel after etched in 1% Nital X500

Energy Dispersive X-ray Spectroscopy (EDX) figure (4.3) examination of the as received carbon steel shows that only two main peaks are presented in the limited scope of 0-14 [kev].This peak is related mainly to Fe.

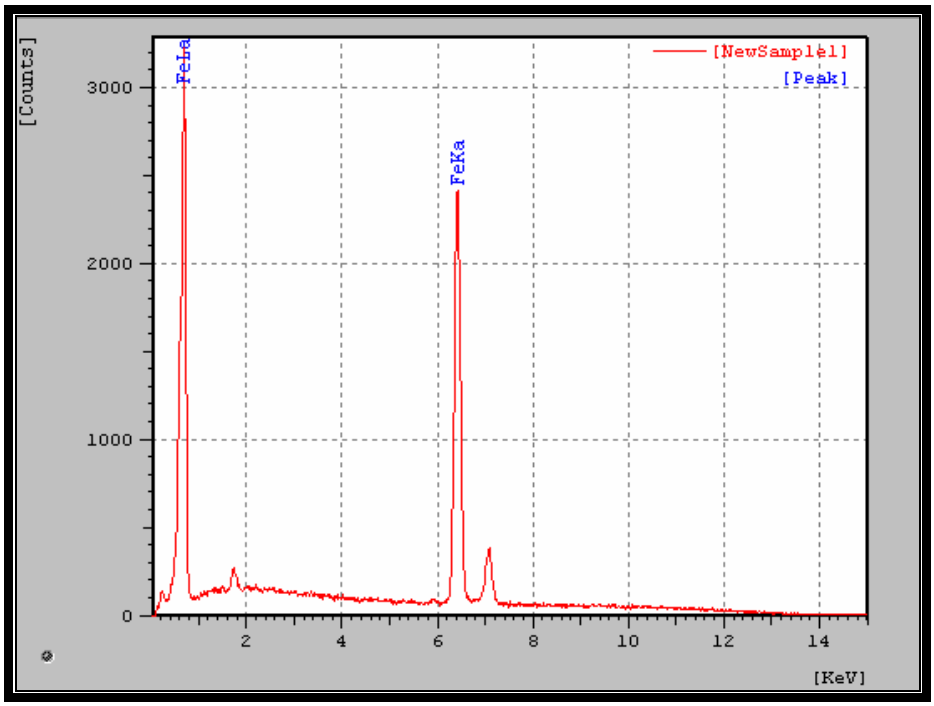

Figure (4.3) EDX for carbon steel

4.3 Deposition Mechanism

The codepostion of Zn-Ni process is however, anomalous electrodepostion and much of it mechanism is not well understood [146] and when additive are employed during the electrodepostion of Zn-Ni alloy some unexpected effect occur. Therefore, controlling the process is a big job.

The standard electrode potential of Zn (- 0.76 Vvs SHE) is far less than that of Ni (- 0.25V vs.SHE) . Therefore, when plating from a bath containing a significant number of both Zn and Ni ions ,one would

expect to obtain an electrodeposit of nearly pure Ni as a result of its strong thermodynamic nobility. This is not the case , however, as Zn has often been observed to codeposit readily with Ni .Furthermore, under most practical conditions, the ratio of the less noble metal Zn to the more noble metal Ni in the deposit is larger than in the bath this is due to the composition difference.

Figure (4.4) shows the polarization curves for potentiostatic electrodeposion Zn-Ni carried out at 28°C.The measurement carried out for i/A and E/V vs Ag/AgCl/$kCl_{(sat)}$,this curve is automatically plotted to describe the deposition process confirmed at Appendix C1.

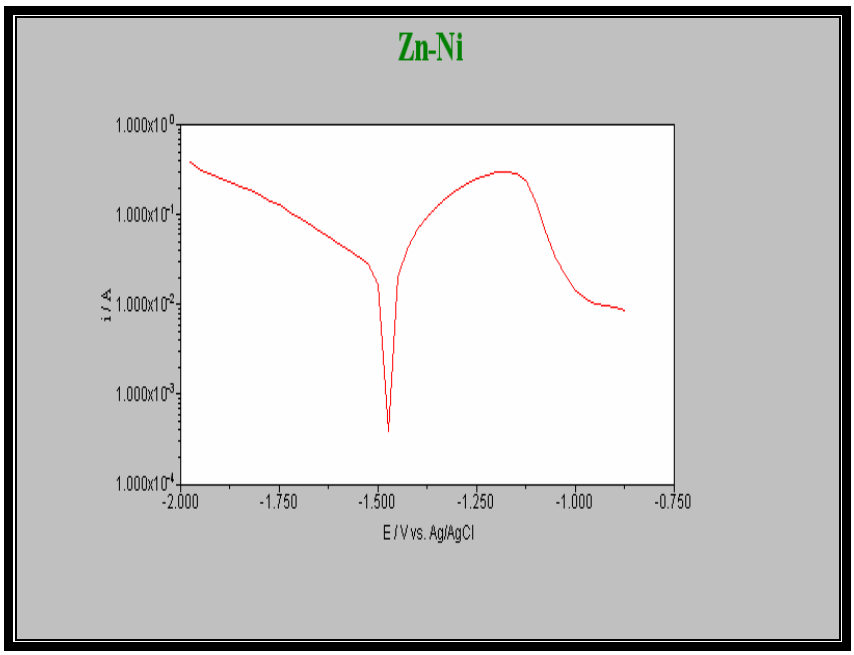

Figure (4.4) Polarization curve during alloy deposition Zn-Ni

Results obtained from early experiments showed that the presented Ni was higher than the expected values. Several changes of the composition was made later on, to modify the deposition.

As shown in figure(4.4) the polarity is reversed at -1.485V,therefore this magnitude its different from potential of zinc or nickel because now

its an alloys. If zinc deposited from bath containing only zinc ions starts at about -1000 mV. At higher potentials however cathode surface analysis did not reveal the presence of zinc, indicating that the current is due to hydrogen discharge. Alloy deposition is strongly inhibited of pure nickel, but it is enhanced by comparing it with a pure zinc deposition at potentials above -1000 mV [61].

These results show that zinc can be codeposited with nickel at potentials where it dose not deposit in pure form. These results can be explained by the formation at low cathodic polarization ,of a mixed intermediate which catalyses one by the induced codeposition, where a given element can be codeposited to form an alloy. Two different mechanisms depending on the potential have been hypothesized available else where [147].

1- At low polarization, the production of Zn-Ni alloys is due to the underpotential discharge of Zn, driven by nickel ion reduction, in the potential range from -700 to about -900 mV/SCE, the iZn/iNi ratio changes only slightly and does not depend on the bath composition.
2- At potential more negative than -900 mV/SCE , corresponding to the equilibrium potential of zinc rich phase deposition, zinc and nickel reduction can occure separately, according to their respective exchange current densities.

But it can not be deposited in a pure form. However, interactions between the components in the deposit may shift the deposition potential of the less noble metal [148].

It is found in this work that when increasing the nickel bath concentration, the changes in composition of the deposits become gradually less dependent on the applied potential.

When the deposition potential decreases, the slope of the curves increases because zinc can be more codeposited with nickel and anomalous deposition is often obtained.

Fig.(4.5) shows the polarization curves for potentiostatic electrodepostion Zn-Ni-Cu carried out at 28°C,the measurement carried out for i/A and E/V vs Ag/Ag Cl/$kCl_{(sat)}$ confirmed at Appendix C2.

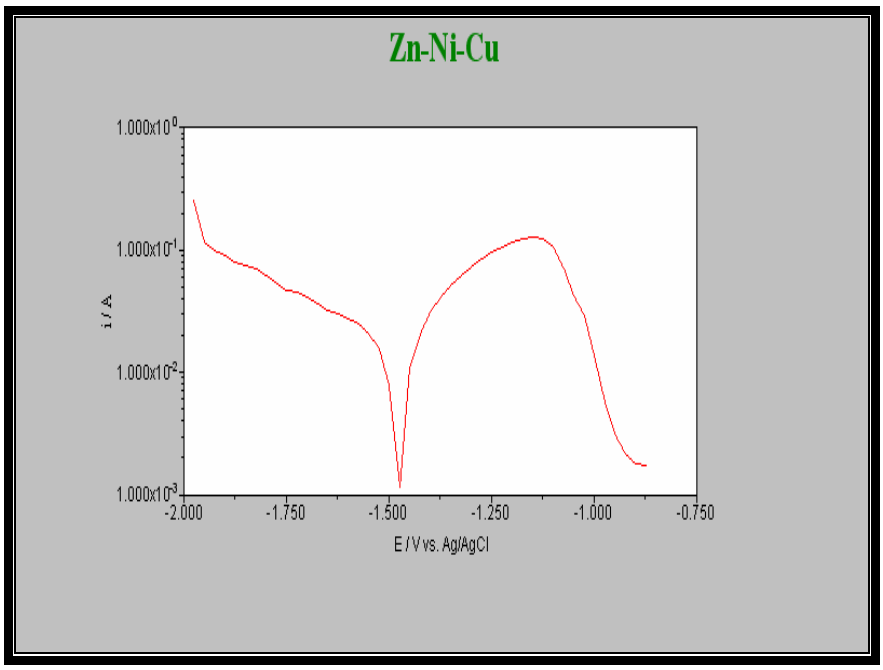

Figure (4.5) Polarization curve during alloy deposition Zn-Ni-Cu

When electrolyte solution contain Zn,Ni,Cu ions were observed current efficiency for polarization curve increases, because the partial current depending on the alloy composition according to the Butler-

Volmer equation[61] under potentiostatic mode with the case study of Zn-Ni alloy anomalous deposition.

Cupper, which is the more noble metal, can be deposited firstly on the electrode surface and then catalyze nickel deposition and the final stage zinc deposition .

At the potential during this work, several values of applied practical was used less negative than the equilibrium potential of zinc, zinc deposition is induced by nickel .When the potential is more negative than the equilibrium potential of zinc, zinc can be deposited with the faster rate after nickel deposition. However, as well as the study of alloy composition with time, cupper and nickel can be deposited firstly on the electrode layer and reduced with time. In addition, the electrode layer has the strong effect on the initial stage of deposition .

Fig.(4.6) shows the polarization curve for potentiostatic electrodeposition Zn-Ni-SiO_2 carried out at 28°C,the measurement carried out for i/A and E/V vs Ag/AgCl/$kCl_{(sat)}$ confirmed at appendix C3

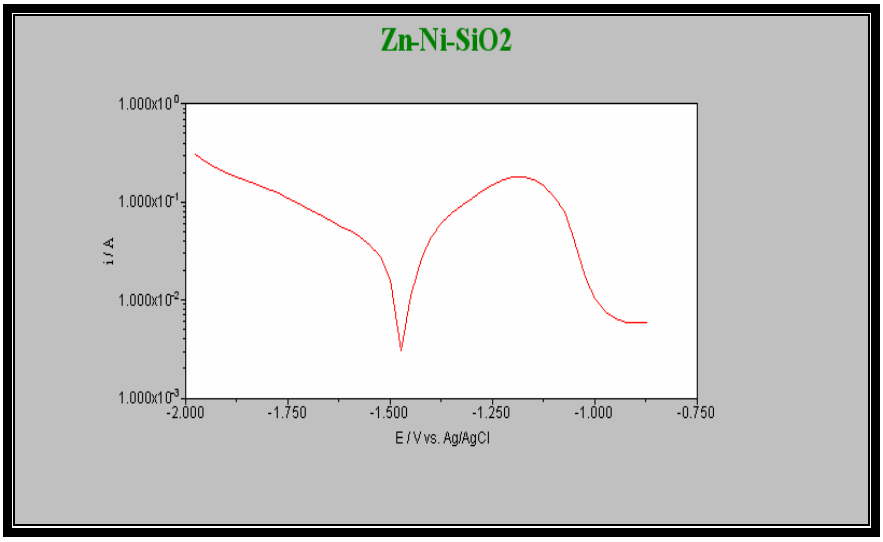

Figure (4.6) Polarization curve during alloy deposition Zn-Ni-SiO_2

According to the experimental results of the Zn-Ni-SiO_2 average polarization curve was indicated for increasing current when additive silicon dioxide in the bath was compared with the average polarization curve for Zn-Ni and Zn-Ni-Cu because get a rich layer from SiO_2 on the top of the surface was got. Similar behavior was observed SiO_2 deposited directly on steel[149].

4.4 Surface of Coated Systems

As mentioned in the previous chapter, simultaneous electroplating Zn-Ni, Zn-Ni-Cu and Zn-Ni-SiO_2 for carbon steel base metal was carried out using alkaline bath.

Figure (4.7) and figure (4.8) illustrate the homogenous topography of coated surface while figure (4.9) shows morphology rich SiO_2 particle of coated layer. In general, the morphology and structure of the coating is complex, this is attributed to the structure of Zn-Ni coated layer and multiple alloying additions, i.e. Cu and SiO_2.

The major alloying on the surface is zinc as indicated by X-Ray fluorescence Table (4.1).

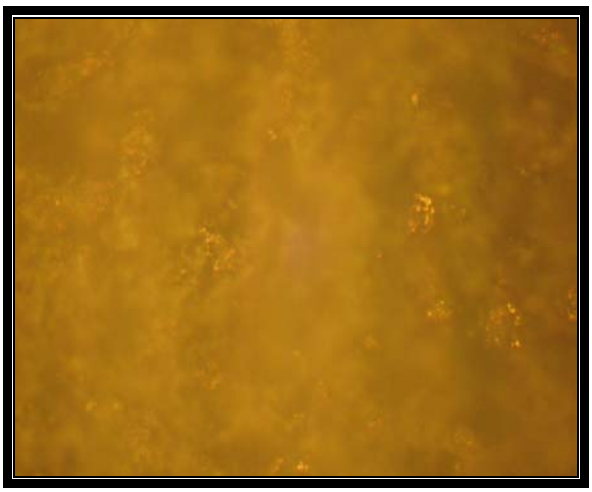

Figure (4.7) LOM images of carbon steel with electroplating Zn-Ni X500

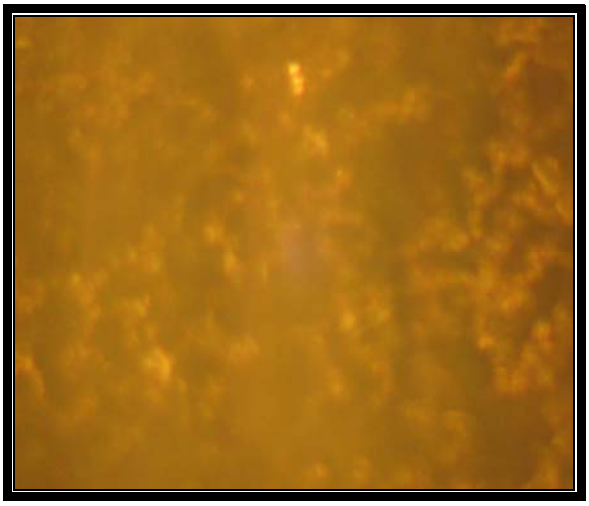

Figure (4.8) LOM images of carbon steel with electroplating Zn-Ni-Cu X500

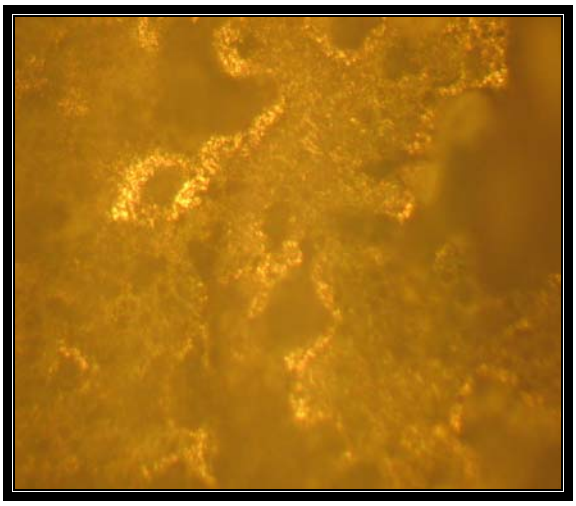

Figure (4.9) LOM images of carbon steel with electroplating Zn-Ni-SiO_2 X500

Table (4.1) X-Ray fluorescence for a) Zn-Ni b) Zn-Ni-Cu c) Zn-Ni-SiO_2

System	Composition element for first layer	Weight percentage for first layer
a) Zinc-Nickel	Zn	85.6578%
	Ni	14.3422%
b) Zinc-Nickel-Cupper	Zn	81.0505%
	Ni	15.3172%
	Cu	3.6323%
c) Zinc-Nickel-Silicon	Zn	81.1490%
	Ni	13.8370%
	SiO_2	5.0140%

Several attempts were made to obtain a composition in such away that it situated in the single phase in the phase diagram.

On the other hand the results of Energy Dispersive Spectroscopy (EDX) test for Zn-Ni is shown in figure (4.10) which shows the main peak for zinc metal.

Figures (4.11) and (4.12) show the appearance of cupper profiles and silicon dioxide respectively.

During electroplating processing, zinc and nickel diffuses into the substrate and the results in a phase transformation are shown in figure (2.9).The coating surface is finally composed mainly of ɣ phase. Ni content of the coating layer is nearly from 14%,other worker

mentioned such layers exhibited a top specification is obtained when the deposited alloy contains about 12-15% Ni [150,151].

In order to form an optimum coating layer, the cupper activity in the coating layer needs to be high enough to induce the ɣ to phase transformation, as in figure (4.13). These alloy were targeted as a replacement for Cd deposition and can inhibit corrosion and completely eliminate hydrogen induced cracking.

Silicon dioxide of Zn-Ni coating was achieved by a rich layer on the surface coating based on thin silicate layer formation with the help of a novel electrocatalytic process to form different phase for Zn-Ni and Zn- Ni-Cu coated.

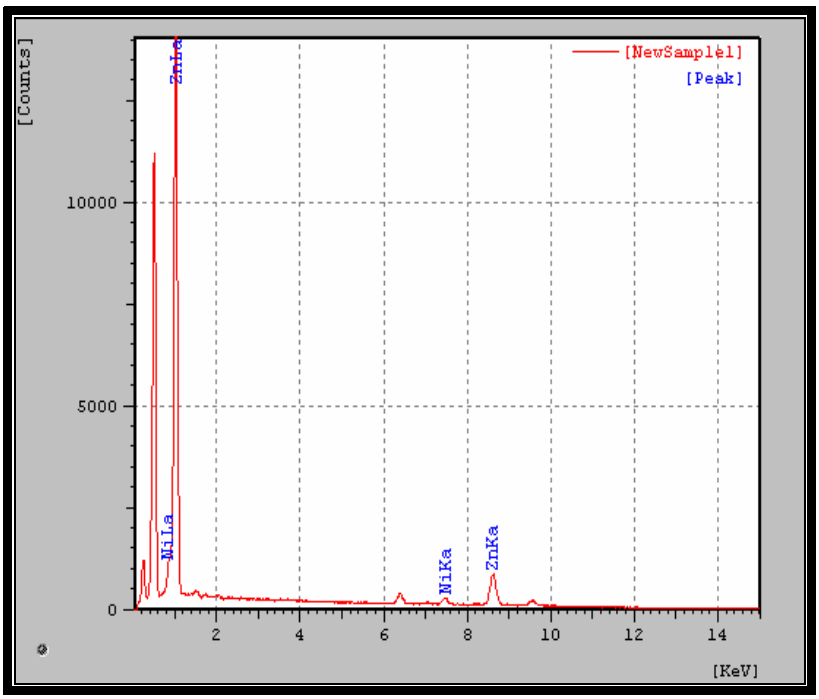

Figure (4.10) EDX for Zn-Ni coating

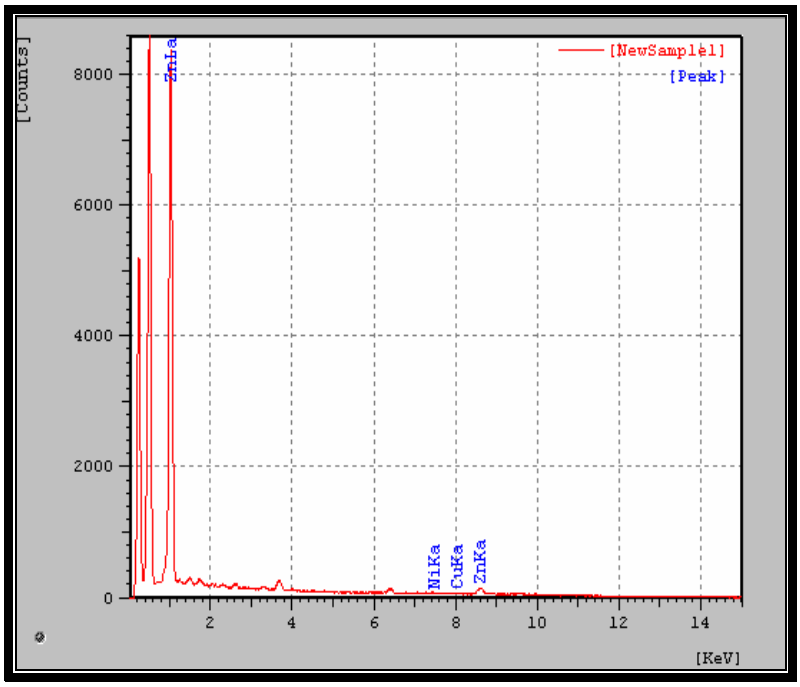

Figure (4.11) EDX for Zn-Ni-Cu coating

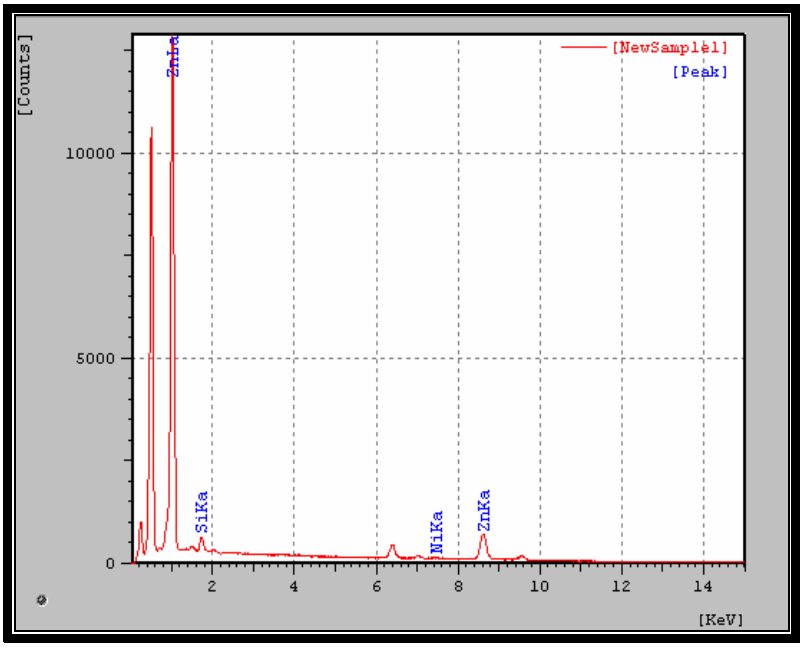

Figure (4.12) EDX for Zn-Ni-SiO_2 coating

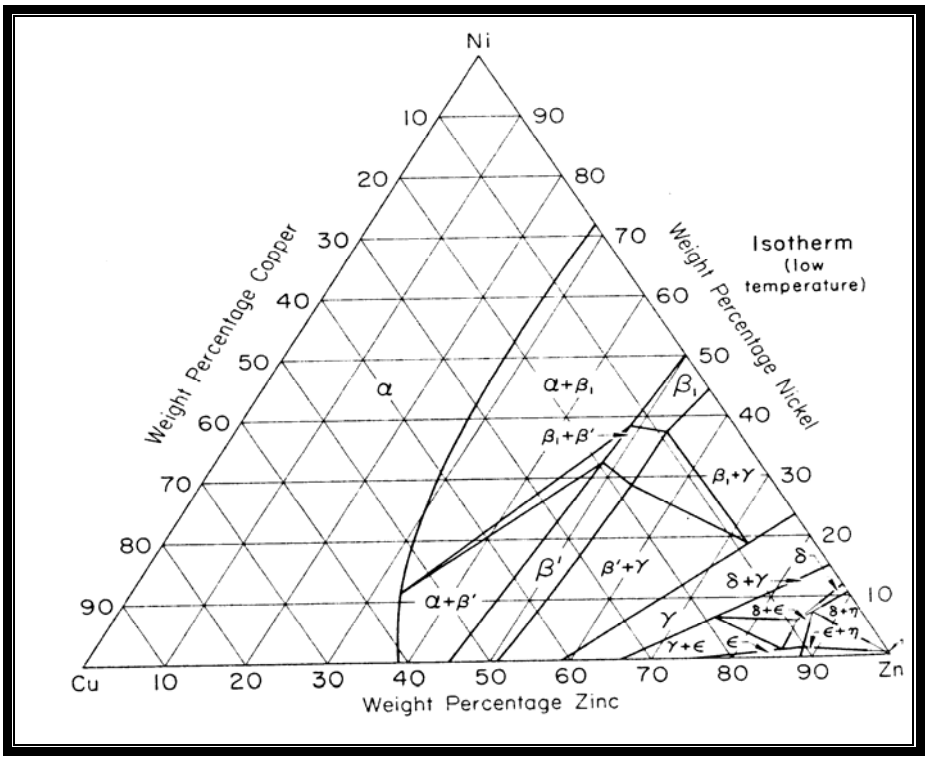

Figure (4.13) Phase diagram Zn-Ni-Cu [152]

Figure(4.14) shows the scanning electron microscopy topography for Zn-Ni coating for a) X100, b) X500, c) X2000, d) X8000,e) X10000 and f) X20000.The inner layer of coating is expected to be in a direct contact with the substrate which had all the typical features of a diffusion zone . Irregularly shaped, Kirkendall voids are usually formed between the diffusion zone and the boundary for zinc and nickel particles.

The SEM picture (figure 4.14f) shows the rough sponge-like structure of Zn-Ni.

The thickness of the coating layer is 10 microns.

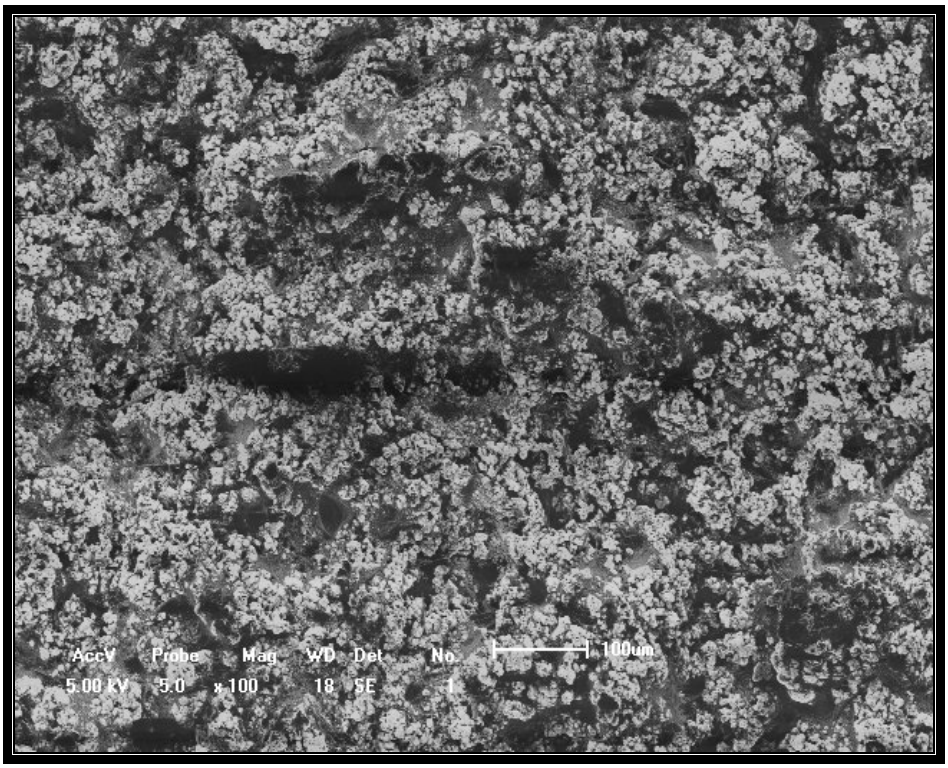

Figure (4.14 a) SEM Zn-Ni coated X100

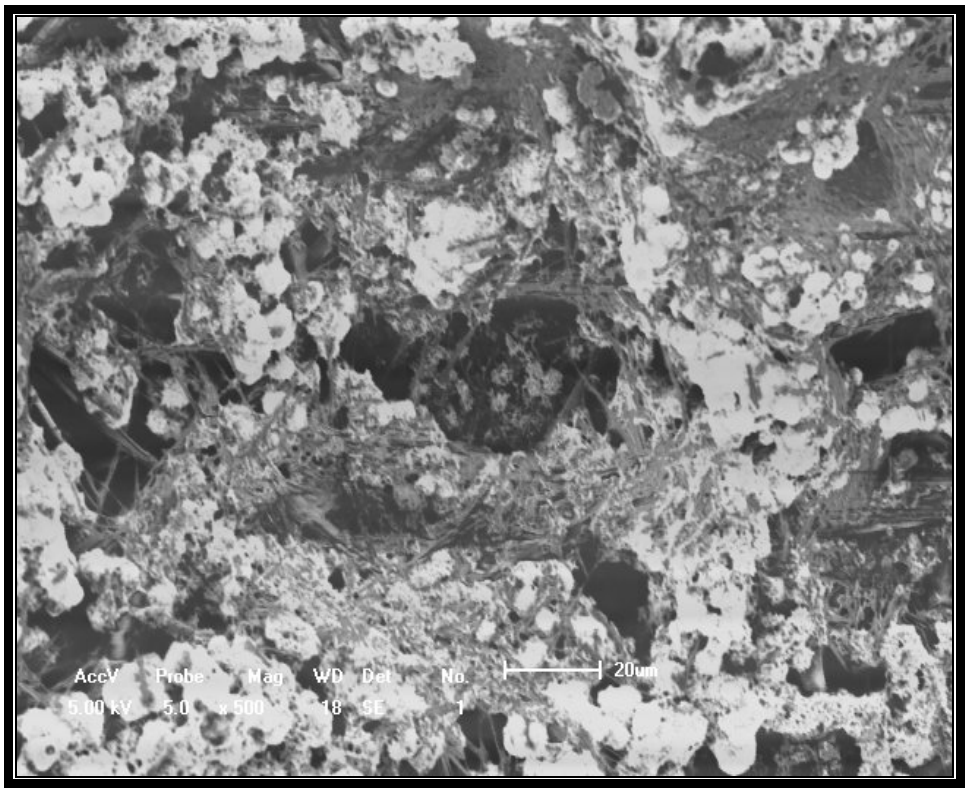

Figure (4.14 b) SEM Zn-Ni coated X500

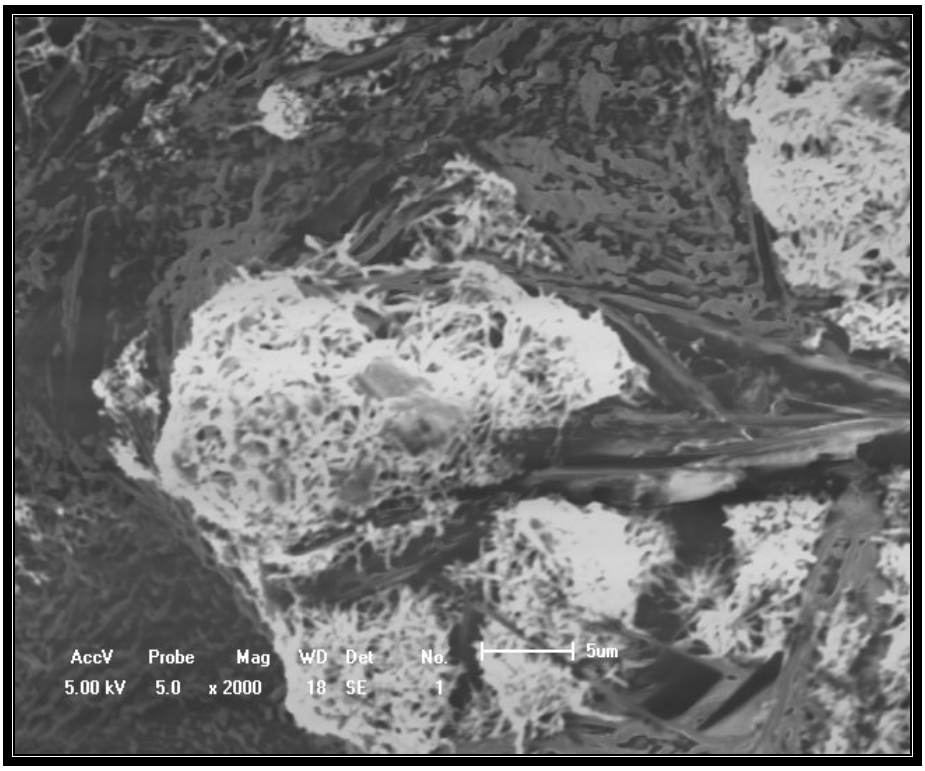

Figure (4.14 c) SEM Zn-Ni coated X2000

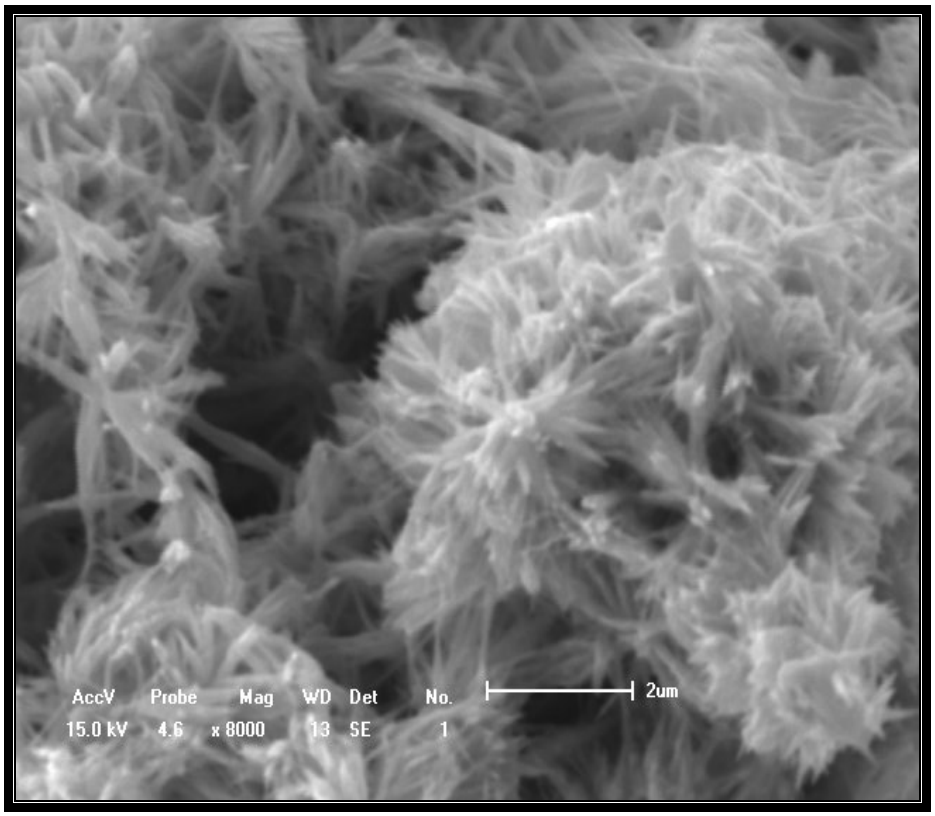

Figure (4.14 d) SEM Zn-Ni coated X8000

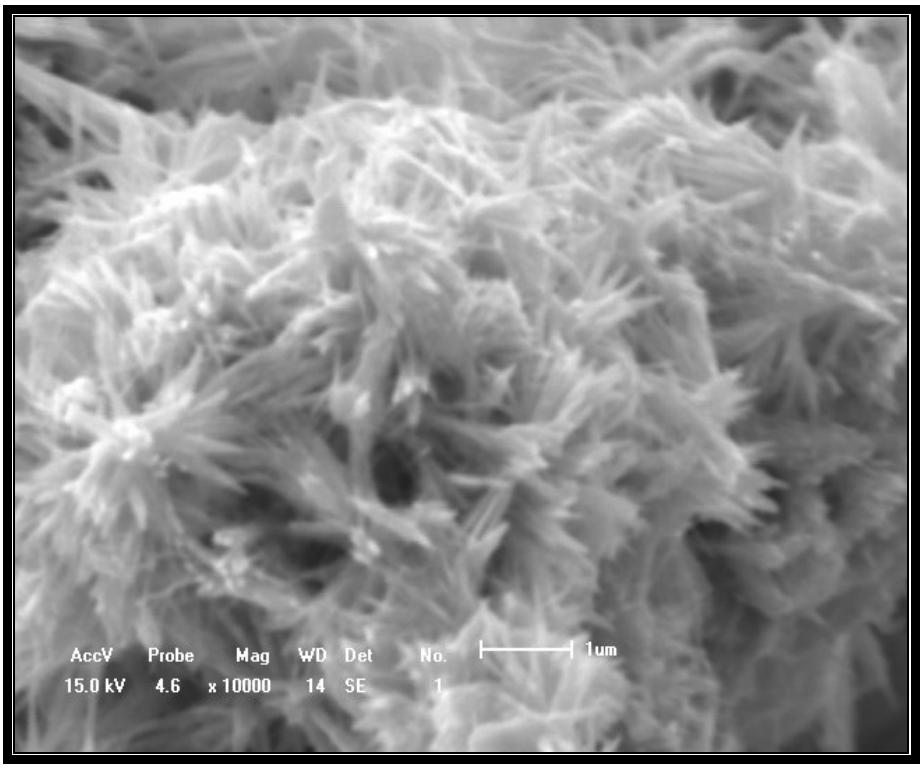

Figure (4.14 e) SEM Zn-Ni coated X10000

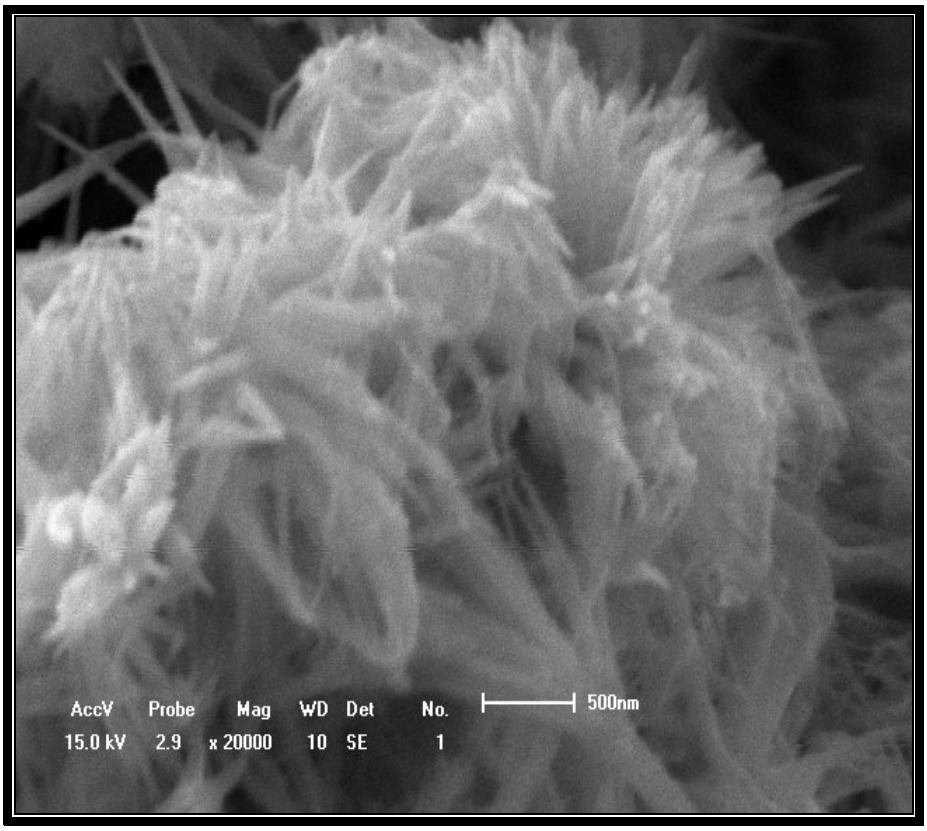

Figure (4.14 f) SEM Zn-Ni coated X20000

Fig.(4.15) shows the scanning electron microscopy topography for Zn-Ni-Cu coating for X100, X500, X2000, X8000, X10000 and X20000. kirkendall voids may also formed but less than those observed in the Zn-Ni coating, due to inward diffusion flux of Zn,Ni and Cu, Since coating elements they were fully compensated.

The coating surface is covered by a number of submicron sized grains conglomerated together to form the "cauliflower-like" structure (figure 4.15 f).

The thickness of coating layer is also 10 microns.

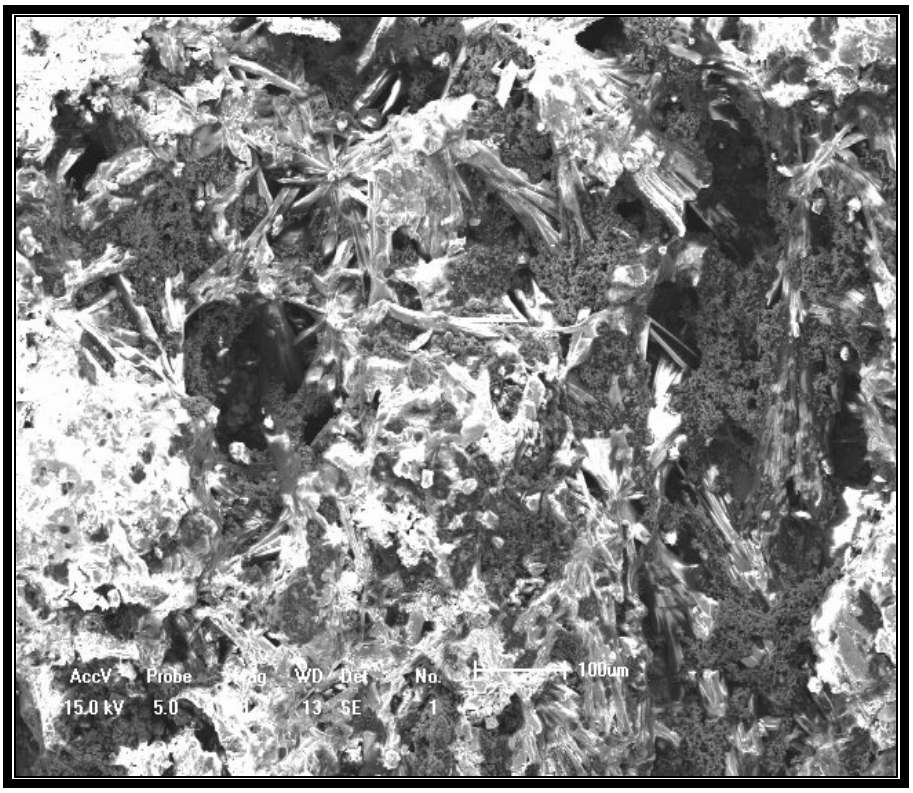

Figure (4.15 a) SEM Zn-Ni-Cu coated X100

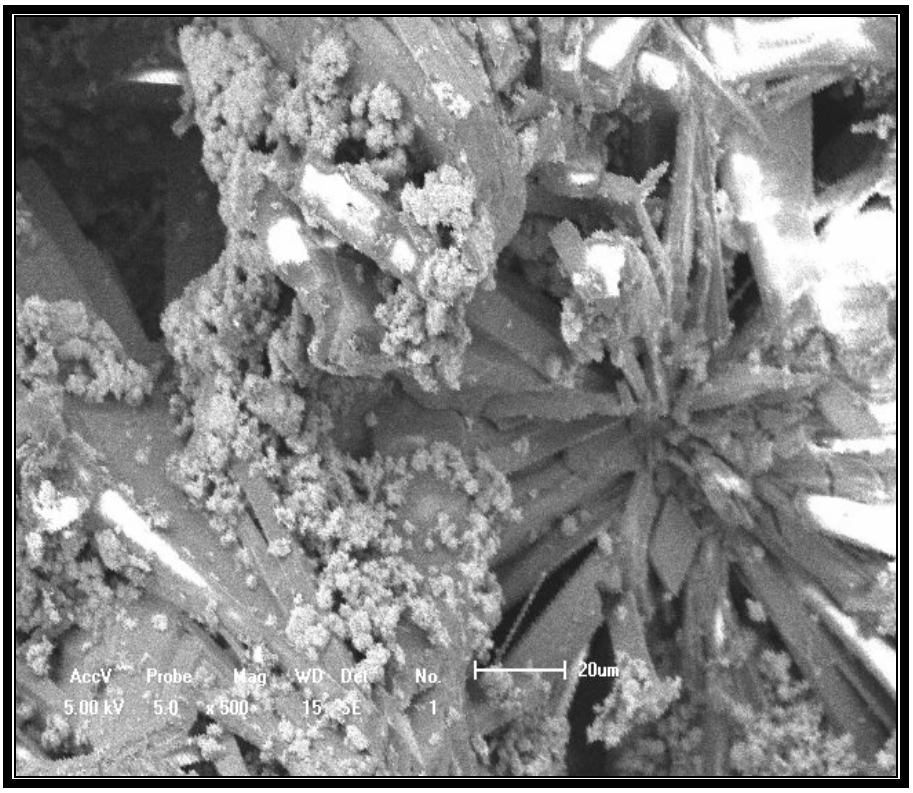

Figure (4.15 b) SEM Zn-Ni-Cu coated X500

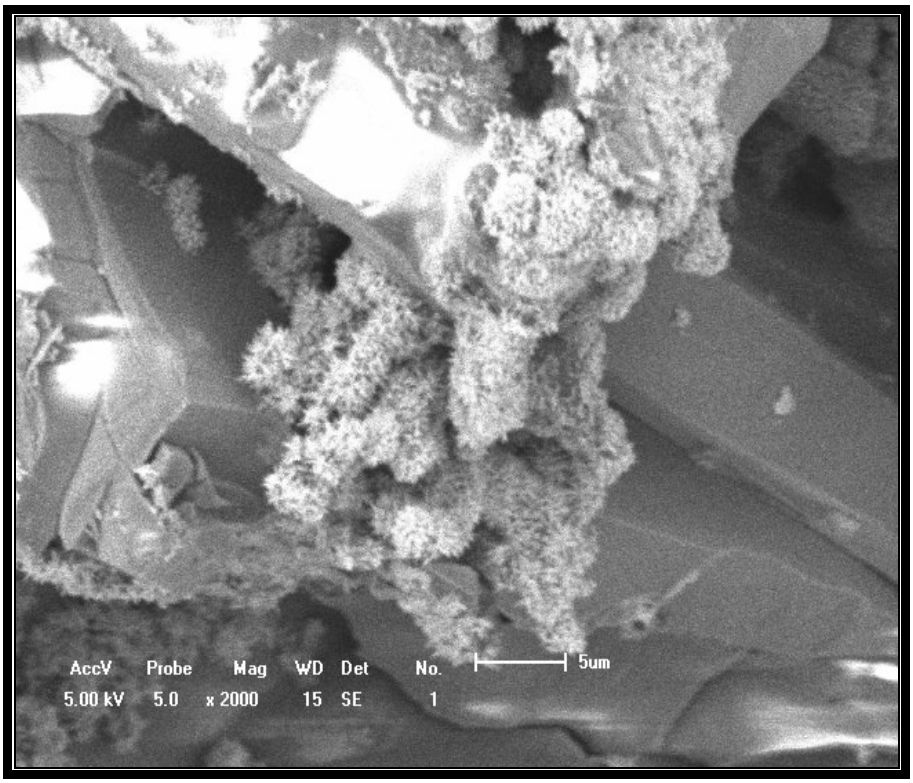

Figure (4.15 c) SEM Zn-Ni-Cu coated X2000

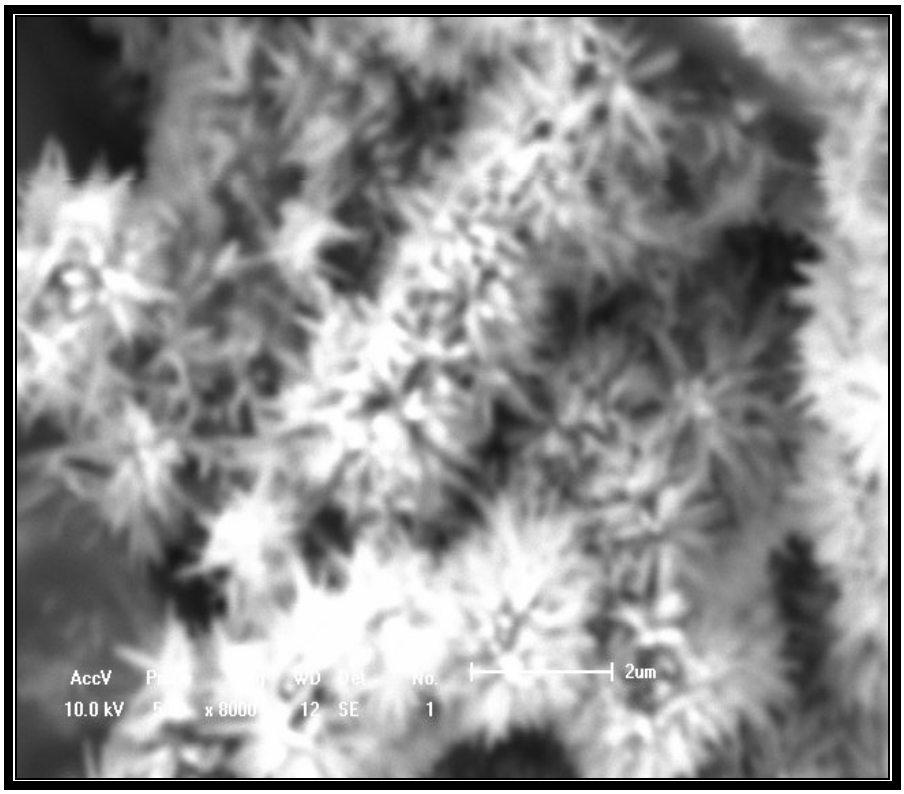

Figure (4.15 d) SEM Zn-Ni-Cu coated X8000

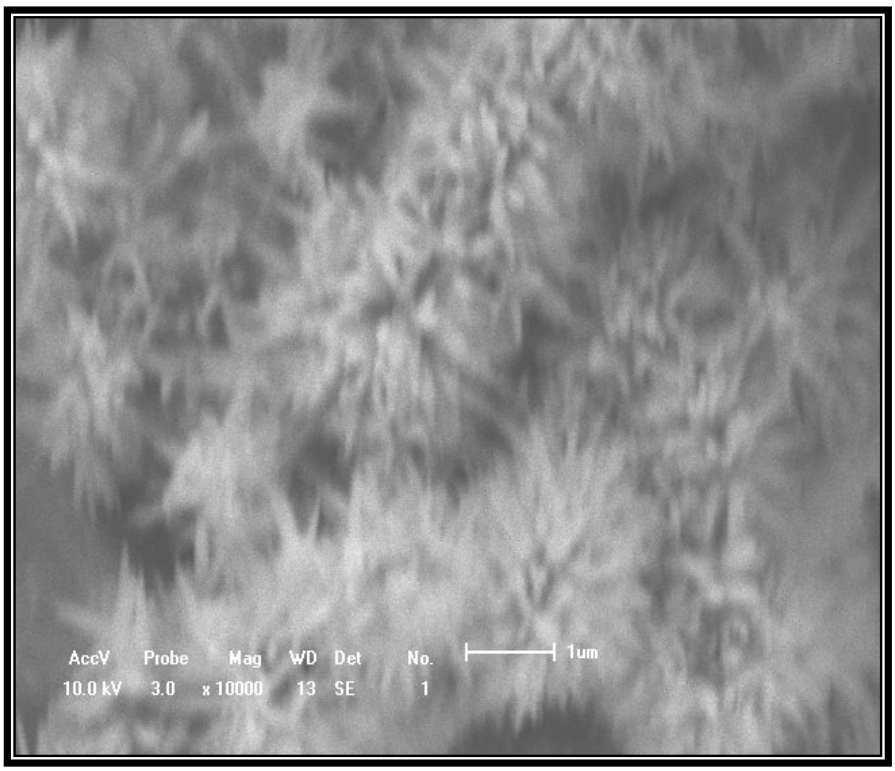

Figure (4.15 e) SEM Zn-Ni-Cu coated X10000

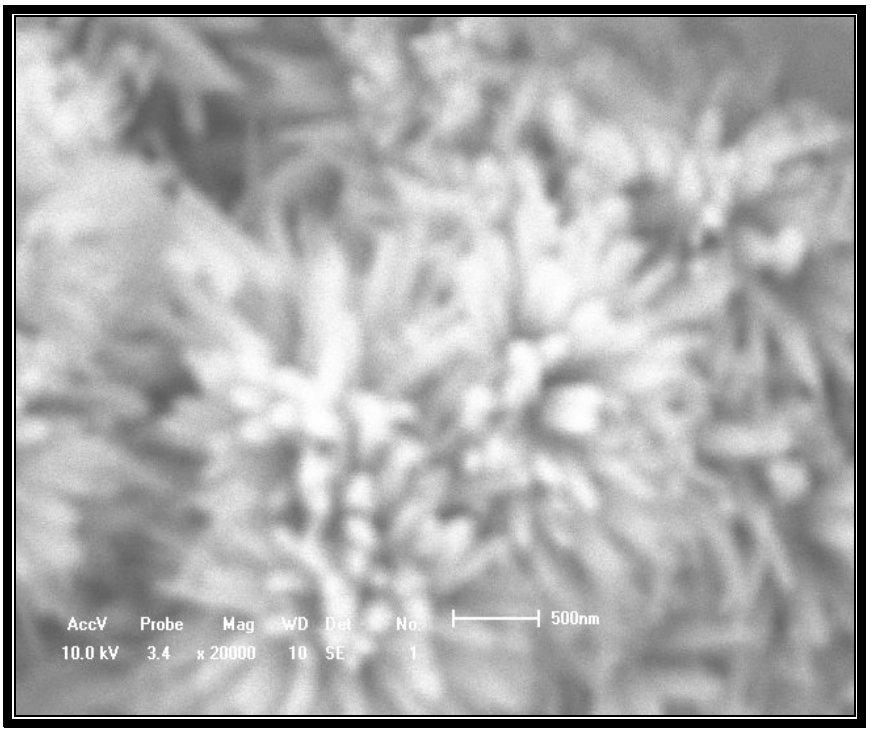

Figure (4.15 f) SEM Zn-Ni-Cu coated X20000

It can be concluded that the addition ~3.6% cupper to Zn-Ni alloy is probably modified the nucleation or growth mechanism.

Figure (4.16) shows the scanning electron microscopy topography for Zn-Ni-SiO_2 coating for X100, X500, X2000, X8000, X10000, X20000 and a cross section X800, from X20000 Significant change in topography of the coating layer is observed. A more homogenous well distribution and less porous is clearly seen. A similar modification effect is also observed by the addition of ~ 5% SiO_2.This effect ,however, produces a more homogenous layer.

Figure(4.16f) revealed that the coating mainly consisted of well-flattened SiO_2 particles.

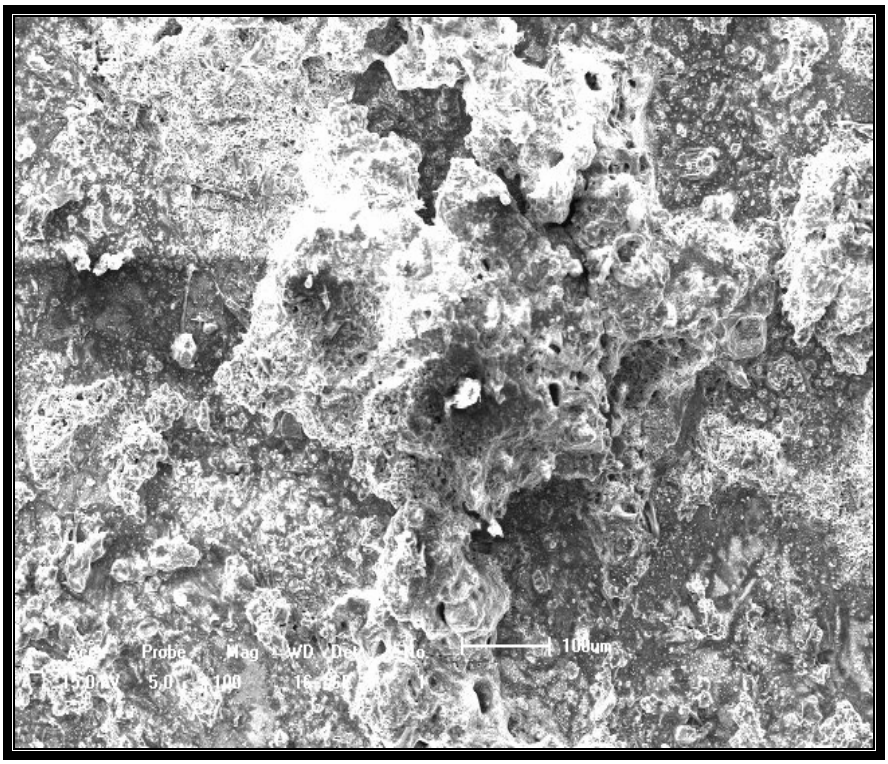

Figure (4.16 a) SEM Zn-Ni-SiO_2 coated X100

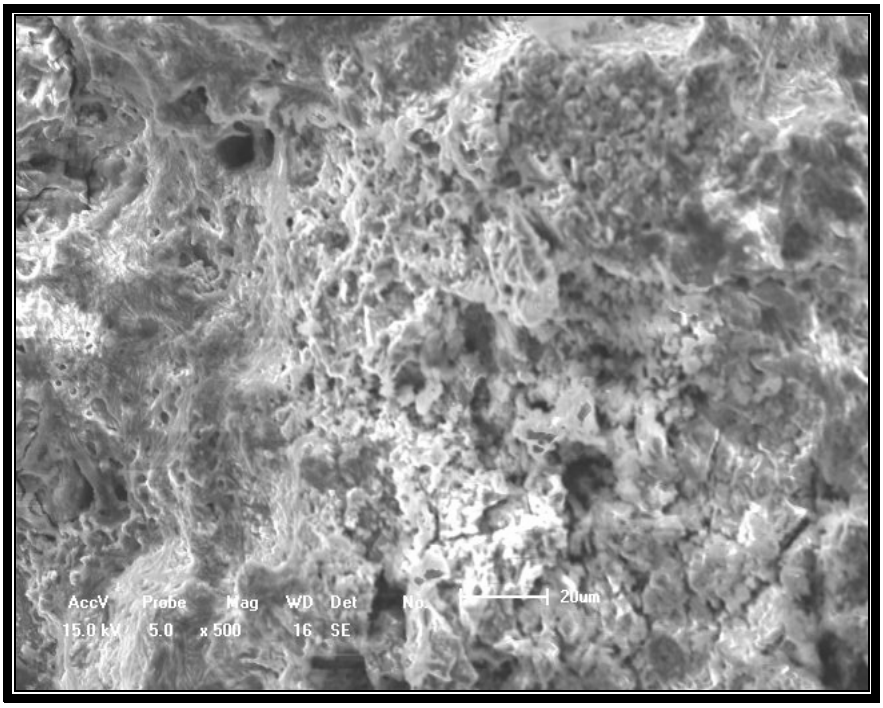

Figure (4.16 b) SEM Zn-Ni-SiO_2 coated X500

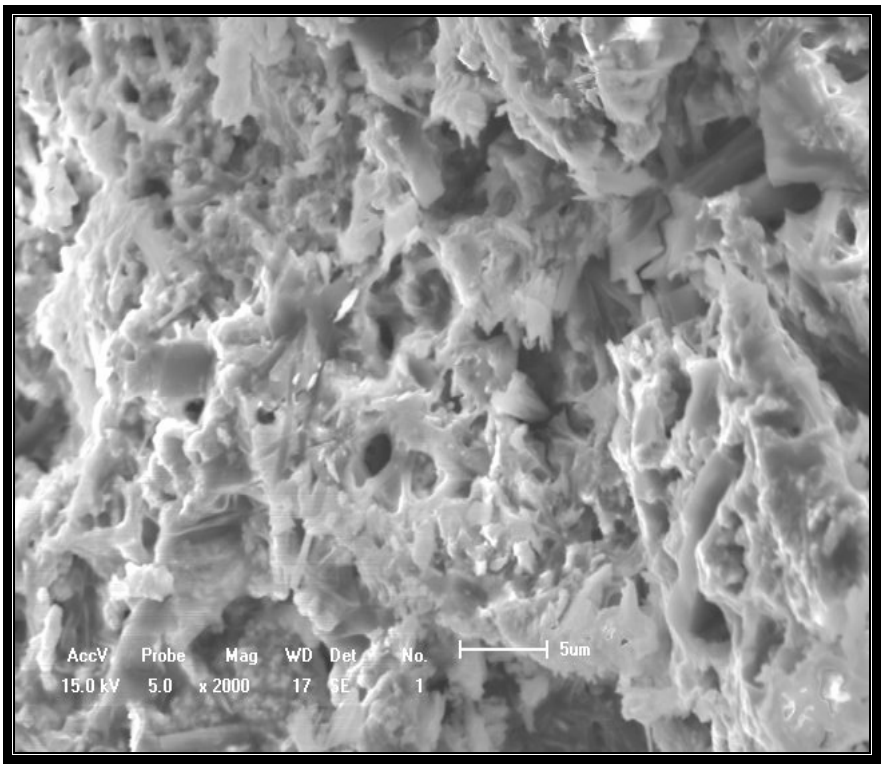

Figure (4.16 c) SEM Zn-Ni-SiO_2 coated X2000

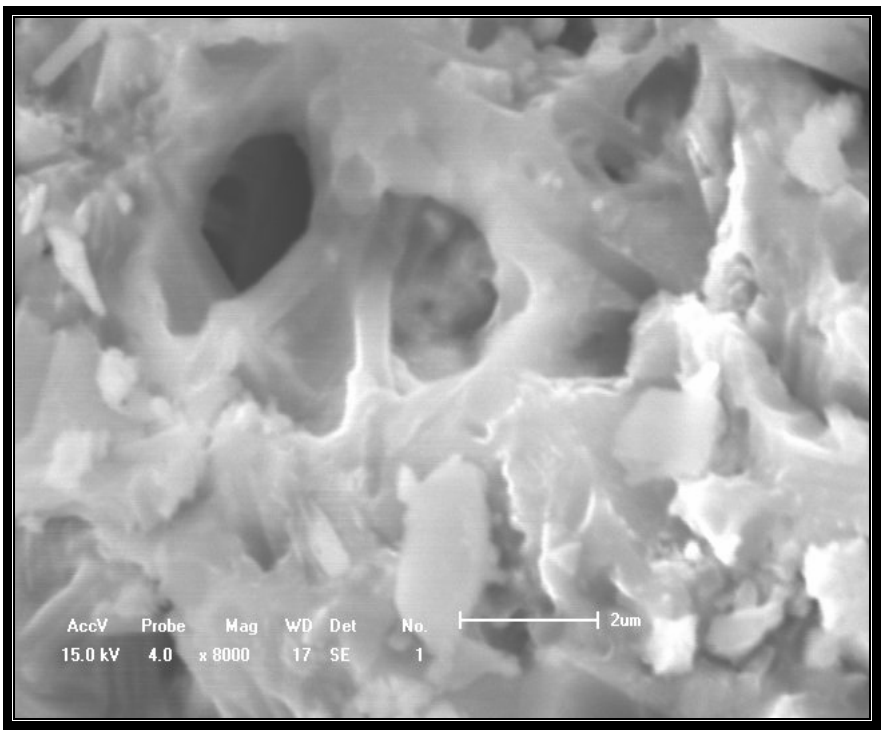

Figure (4.16 d) SEM Zn-Ni-SiO_2 coated X8000

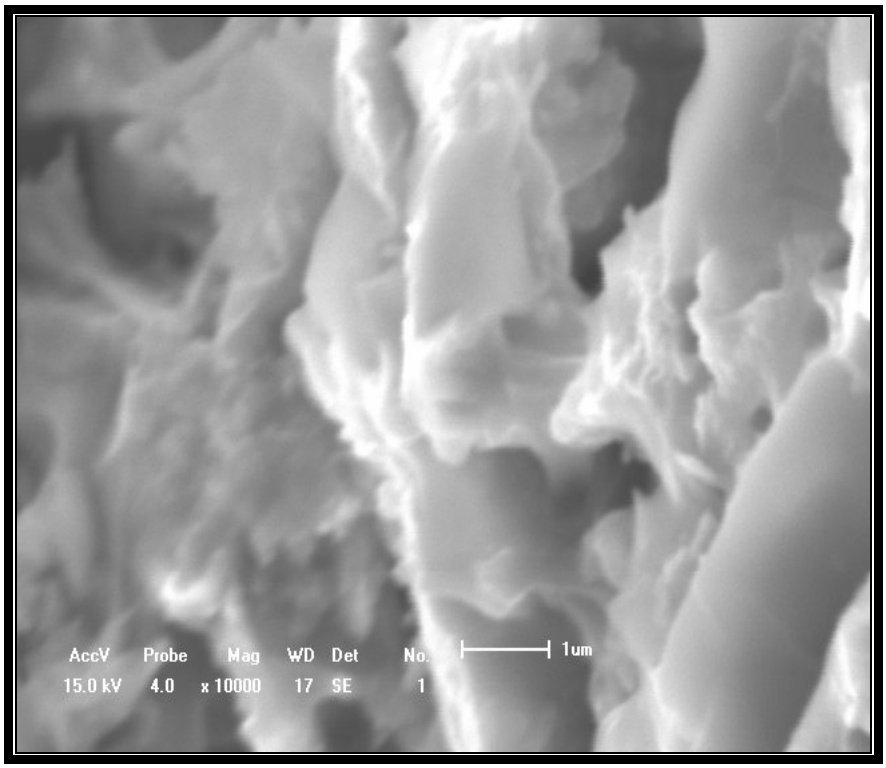

Figure (4.16 e) SEM Zn-Ni-SiO_2 coated X10000

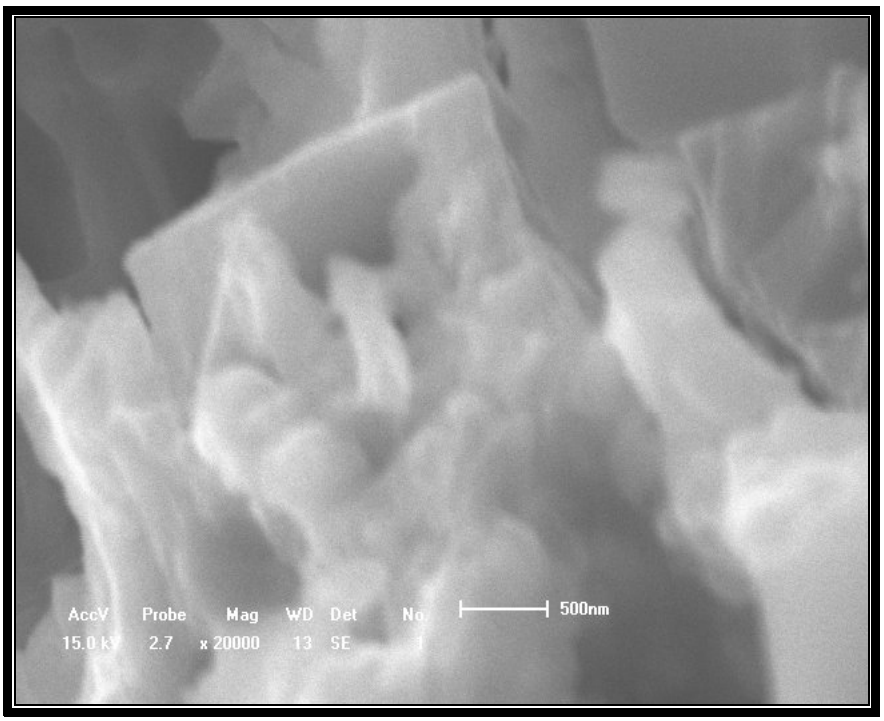

Figure (4.16 f) SEM Zn-Ni-SiO_2 coated X20000

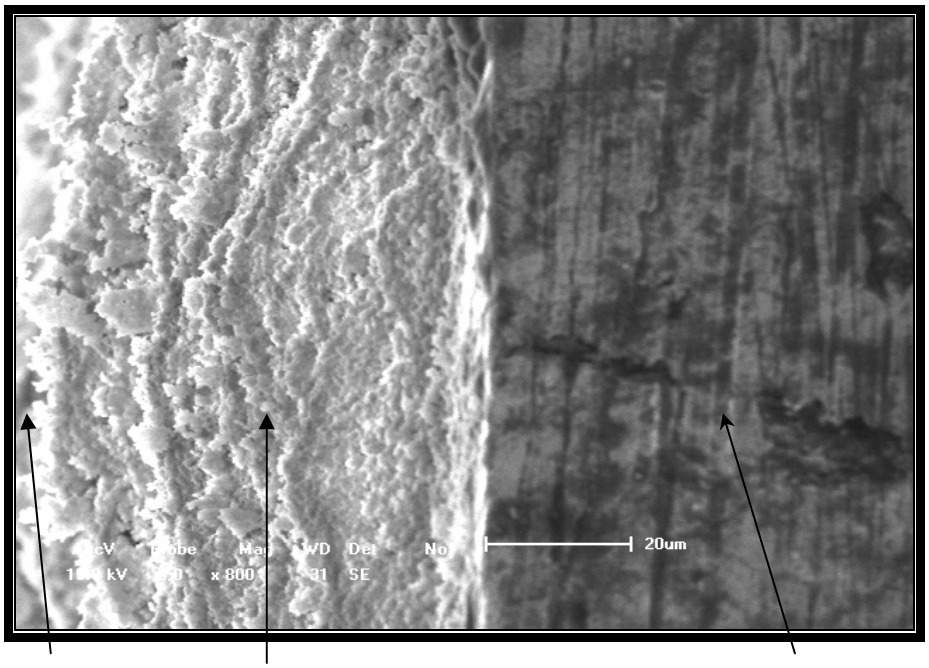

Figure (4.16 g) SEM Cross Section Zn-Ni- SiO_2 coated X800

Figure (4.16g) shows a scanning electron microscopy micrograph for a cross section of Zn-Ni-SiO_2 coating at X800 .This figure explains where homogeneously rich SiO_2 throughout the samples occurs without local aggregation .

It appears clearly that a homogenous adhesive layer of Zn-Ni finally deposited on the surface of the base metal. No voids ,cavities ,or detachment is observed at the interface.

In addition ,a homogenous ,non-pours, adhesive ,and this outer layer of SiO_2 is also formed on the surface of Zn-Ni coating.

The mechanism of deposition is available elsewhere[145,149]. From this cross section and the sharp interface between Zn-Ni layer and the outer layer there is a clear evidence that an outer passive layer of SiO_2 is formed. The high corrosion resistance is attributed to this layer proved by many tests in this study.

4.5 Microhardness Result

4.5.1 As Deposited

The mechanical properties of base metal and Zn-Ni, Zn-Ni-Cu and Zn-Ni-SiO_2 coatings produced in this work were investigated by using microhardness testing. All 16 samples synthesized were hardness tested and the results of this study are presented in Table (4.2) .

Table (4.2) Hardness testing results

Item	Type of layer	Run	Vickers Hardness
1-	Base Metal	1_1	251
2-	Zn-Ni	2_1	423
		2_2	412
		2_3	427
		2_4	420
		2_5	420
3-	Zn-Ni-Cu	3_1	477
		3_2	482
		3_3	481
		3_4	482
		3_5	488
4-	Zn-Ni-SiO_2	4_1	634
		4_2	640
		4_3	645
		4_4	633
		4_5	640

Figure (4.17) presents these average results as a function of different alloy composition .It is evident that the hardness of the coatings is strongly dependent upon the element material type that has been codeposited along with zinc.

The average value of Zn-Ni 420 VHN and a slightly sharper increase in hardness is then observed when cupper is added in the composition.

At the average values of Zn-Ni-Cu of 482 VHN ,and increasing sharply when composition contains silicon dioxide to 638.4 VHN.

The compositional dependence of hardness becomes very significant when grain size of the electrodeposits is taken into account. Generally, the hardness of a material is known to depend, in part, upon its grain size ,mathematically expressed via the well-known Hall-Petch relationship [153,154] :

$H_v = H_o + Kd^{-1/2}$ …….. (4.1)

Where H_v is the hardness of the material with a reduced grain size d, H_o is the hardness of the material with a conventional polycrystalline grain size and K is a constant .It should be noted that K, the slope of the hardness when plotted as a function of $d^{-1/2}$, is material dependent.

Employing the Hall-petch equation, one would expect that materials of an ultra-fine microstructure would always exhibit higher hardness values than coarser-grained specimens of the same solid .

Indeed , confidence in the validity of the Hall-Petch relationship is one of the prime reason why materials with ultrafine grain sizes are considered to be desirable.

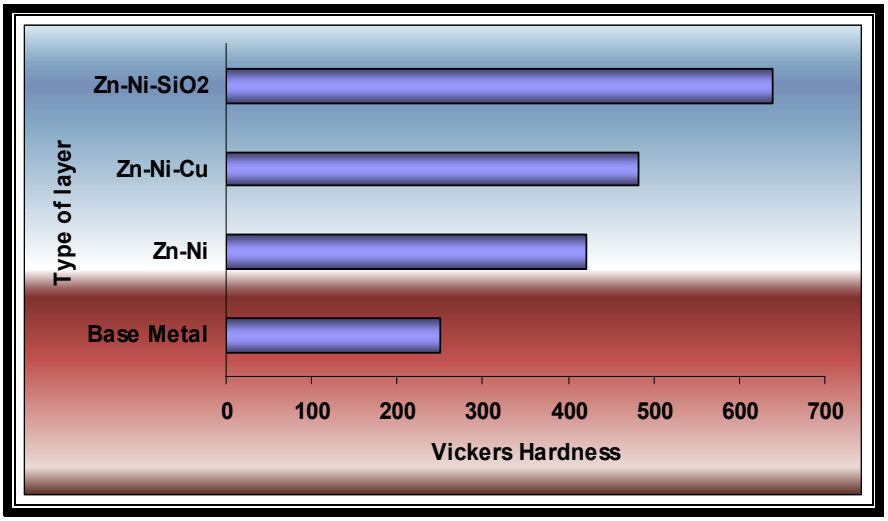

Figure (4.17) Average Vickers hardness for Base metal, Zn-Ni , Zn-Ni-Cu and Zn-Ni-SiO_2

The addition of SiO_2 becomes more effective when its ability to produce dispersive harding and inhibits grain growth. A possibility of obstracting dislocation movement or grain boundary sliding is also existd.

4.5.2 As Heat Treated

All hardness tests for 15 samples were carried out after heat treatment at 200°C 1hr and the result of this study is presented in Table (4.3).

Table (4.3) Hardness testing result after heat treatment at 200° C 1hr

item	Type of layer	Run	Vickers Hardness
1-	Zn-Ni	1_1	435
		1_2	440
		1_3	431
		1_4	433
		1_5	439
2-	Zn-Ni-Cu	2_1	481
		2_2	487
		2_3	492
		2_4	495
		2_5	487
3-	Zn-Ni-SiO_2	3_1	679
		3_2	682
		3_3	680
		3_4	689
		3_5	682

Figure (4.18) presents the average values of hardness after heat treatment. A slight change in hardness of Zn-Ni and Zn-Ni-Cu coating is observed.

However ,a significant increase in Zn-Ni-SiO_2 layer occurs. This is due to enhancing stability of the coating as been improved by drying temperature and the decrease of particles. A possibility of decreasing the particle size which may leave it within the nano size [144].

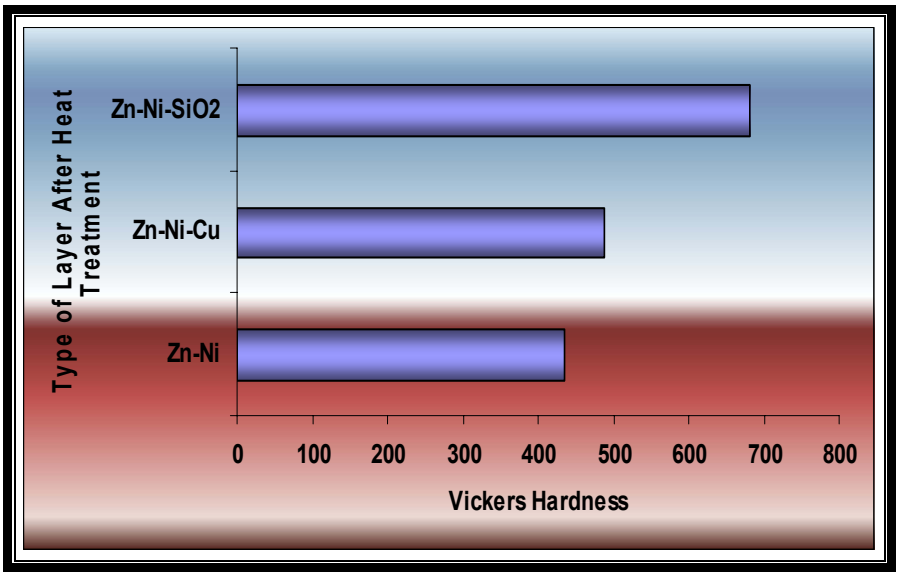

Figure (4.18) Average Vickers hardness for Zn-Ni, Zn-Ni-Cu and Zn-Ni-SiO_2 after heat treatment at 200°C 1hr

4.6 Corrosion Properties of Coated Samples

This section demonstrates the change of corrosion properties of Base Metal , Zn-Ni, Zn-Ni-Cu and Zn-Ni-SiO_2 carried out by electroplating technique .The base metal was tested ,to provide a standard control to be compared with corrosion resistance for coated system .The role of Cu and SiO_2 in improving corrosion resistance will be explained by linking literatures to the corrosion mechanisms of alloys containing additives to the data collected in this study.

It is expected that scale layer should be pore-free, crack-free, and stress-free at operation temperatures, resistance to spalling and damage during cooling or heating.

In addition, the oxygen and metal ions hopefully have low diffusion coefficients through the scale, and the recession rate of the original surface is low enough during the desired surface life.

Unfortunately for practical service conditions, it is nearly impossible to set up such an ideal protective layer. However, it is proposed in this work to optimize the self-healing layer by changing the coated layer compositions and operating conditions.

Compositional change is also associated with phase transformation which, in turn , also influences the corrosion behavior of the coatings. It has been reported that corrosion resistance is also depended upon the alloy content of zinc based coatings[147,155,156,157].

In this section the growth kinetics and morphologies of scales in aggressive environments (salt spray, humidity, acidic media) and corrosion conditions due to the effect of NaCl and H_2SO_4 for Tafel method will be illustrated and discussed .The results are given in terms of

1- Specific weight change .

2- Polarization curve.

3- Metallographic investigations.

4.6.1 Salt Spray Result

Salt spray test is an accelerated corrosion test that produces a corrosive attack to the coated samples in order to predict its suitability in use as a protective finish.

The corrosion resistance of Zn-Ni alloy is related to Ni content of the alloy. Considered as having a barrier role for the corrosion factors, the growth of the Ni content induces a growth of the corrosion resistance. Nevertheless corrosion resistance of the Zn-Ni alloys is related to their anodic potential versus steel (sacrifice protection),which is controlled by the Ni content. The growth of the Ni content switches the corrosion potential towards less electronegative values, making it to become cathodic versus steel. It means that there is an optimum range of the Ni concentration in alloy to obtain the maximum corrosion resistance ranged between 8-14% Ni[157].

The corrosion kinetics of Base metal, Zn-Ni, Zn-Ni-Cu and Zn-Ni-SiO_2 with 5% NaCl in salt spray chamber at 35°C 24 hrs are plotted of weight loss change before and after heat treatment at 200°C 1 hr as shown in figure(4-19) and figure(4.20).This test is an evident that SiO_2 improved the corrosion resistance of Zn-Ni system .

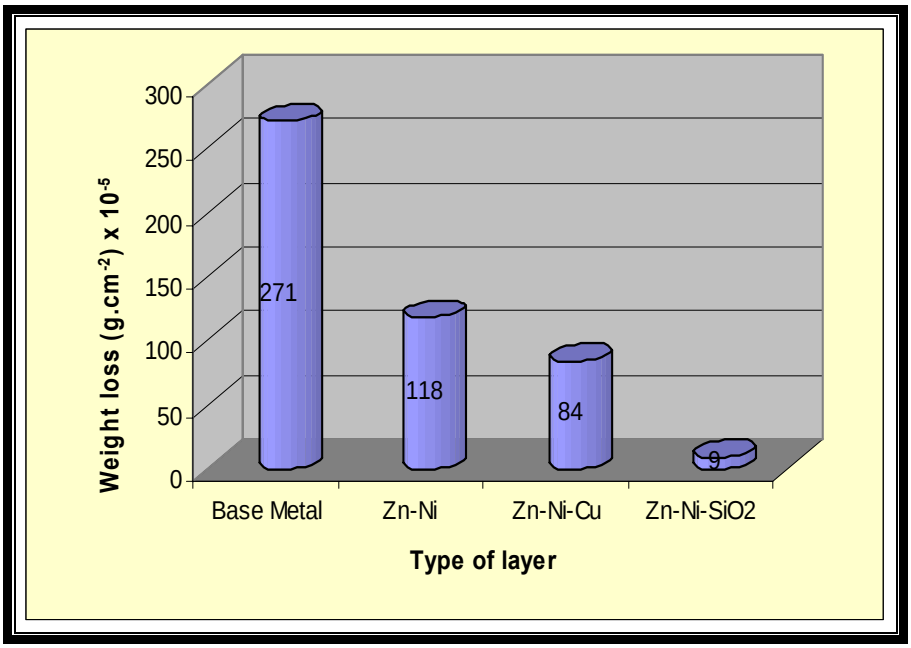

Figure(4.19) Influence of exposed Base Metal ,Zn-Ni, Zn-Ni-Cu and Zn-Ni-SiO_2 in salt spray chamber after 24 hrs at 35°C 50% humidity.

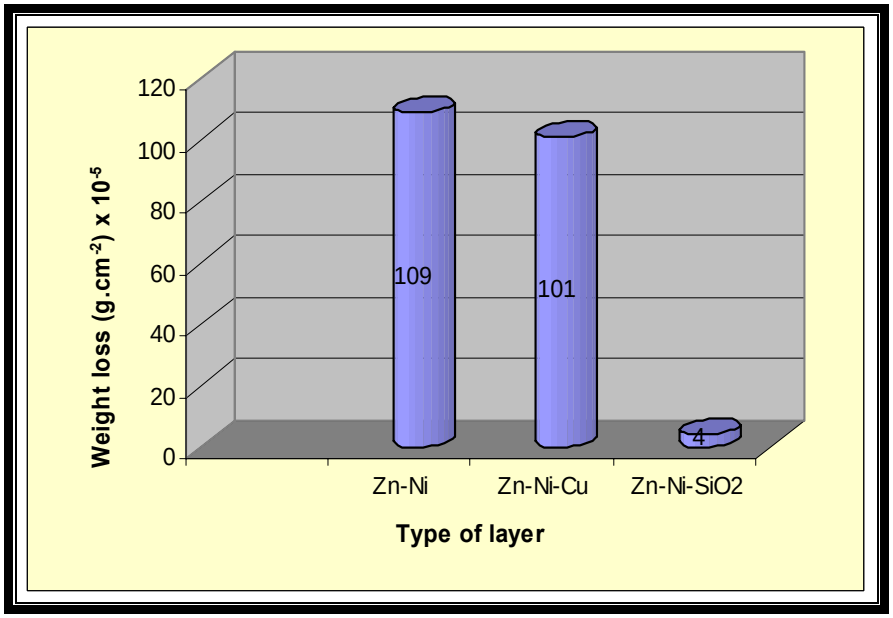

Figure (4.20) Influence of exposed Zn-Ni,Zn-Ni-Cu and Zn-Ni-SiO_2 (heat treated) in salt spray chamber after 24 hrs at 35°C 50% humidity

Figure (4.19) and figure(4.20) explain the corrosion resistance when rich layer by SiO_2, because it acts as a good barrier layer between metals and environment. Also evident the role of heat treatment for SiO_2 to improve corrosion resistant, due to improving corrosion resistance characteristics of SiO_2 coatings which will then effectively acts as diffusion barrier.

The experimental data results of the three average samples were calculated as gmd,mm/y and mpy ,Table (4.4) and Table (4.5) (See Appendix D).

Table (4.4) Corrosion rate after exposed in salt spray chamber at 35°C,50% humidity 24 hrs.

Metal	Base Metal	Zn-Ni	Zn-Ni-Cu	Zn-Ni-SiO_2
Δg (g)	$271x10^{-5}$	$118x10^{-5}$	$84x10^{-5}$	$9x10^{-5}$
gmd	23.9823	10.4424	7..4336	0.7964
mm/y	1.2258	0.5337	0.3799	0.0407
mpy	48.2598	21.0118	14.9566	1.6023
ί(μA/cm^2)	81.9402	35.6787	25.3984	2.7212

If the weight loss of each sample after 24 hrs is regarded as a measure of corrosion resistance then:

The weight loss of Zn-Ni ,Zn-Ni-Cu and Zn-Ni-SiO_2 coatings are only (43%, 30%,and 3%) respectively with respect to the corresponding value of the base metal, the superiority of SiO_2 layer it is obvious.

Table (4.5) Corrosion rate after exposed in salt spray chamber (after heat treated) at 35°C,50% humidity 24 hrs.

Metal	Zn-Ni	Zn-Ni-Cu	Zn-Ni-SiO_2
Δg (g)	$109x10^{-5}$	$101x10^{-5}$	$4x10^{-5}$
gmd	9.6460	8.9380	0.3539
mm/y	0.4930	0.4568	0.0180
mpy	19.4094	17.9842	0.7086
į(μA/cm²)	32.9575	30.5386	1.2094

After heat treatment ,however ,at 200°C one hours these results becomes (40%,37% and 1%) respectively.

These results ,one again ,show the sharpen increase in corrosion resistance of SiO_2 and the enhancement of heat treatment. Similar great improvement are also observed in other items (gmd, mm/y, mpy, į(μA/cm²) in Tables (4.4 and 4.5).

Exposure to spray of aggressive medium i.e. (salt solution) certainly , creates damages on surfaces of the exposed samples. Extended a criteria for corrosion evaluation in this work, Can be seen from figures (4.21,4.22,4.23,and 4.24) the SiO_2 layer exhibits less damage and most damage was observed on the samples of base metal.

Figure (4.21) LOM images of surface damage on Base metal after exposed in salt spray test 24 hrs ,35°C,50% humidity.

Figure (4.22) LOM images of surface damage on Zn-Ni after exposed in salt spray test 24 hrs ,35°C,50% humidity.

Figure (4.23) LOM images of surface damage on Zn-Ni-Cu after exposed in salt spray test 24 hrs ,35°C,50% humidity.

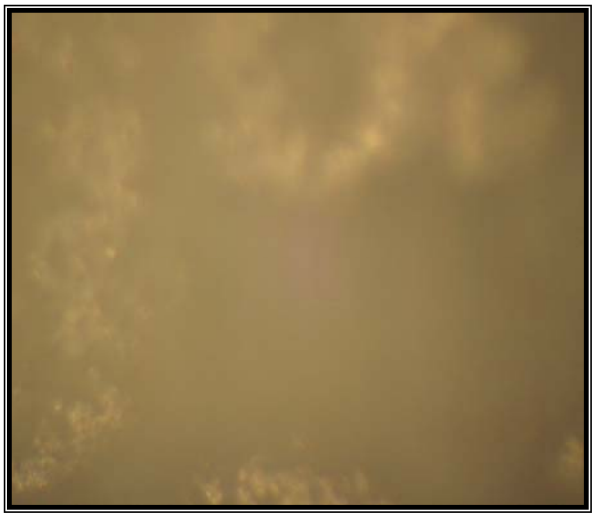

Figure (4.24) LOM images of surface damage on Zn-Ni-SiO_2 after exposed in salt spray test 24 hrs ,35°C,50% humidity.

Others samples ,figures (4.25,4.26 and 4.27) can be seen from the topography of the samples which are expected to form corrosion products of Zn-rich .

However , it seems difficult to identify the difference in behavior by using the optical microscopy only.

The remaining surface is , therefore , enriched with Ni , this conclusion is almost similar to that of other workers[136].

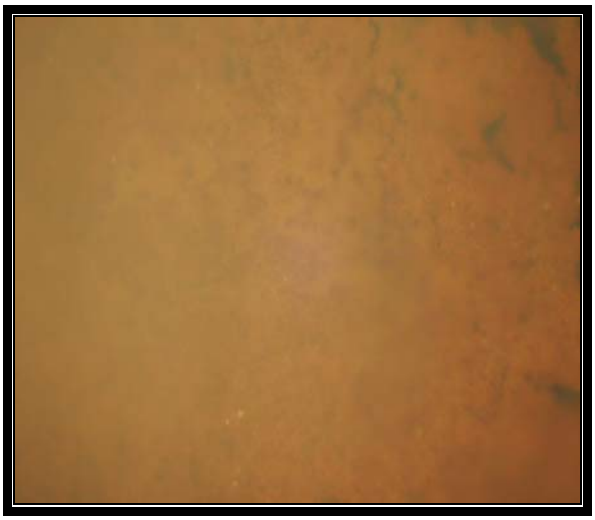

Figure (4.25) LOM images of surface damage on Zn-Ni (Heat Treated) after exposed in salt spray test 24 hrs,35°C,50% humidity.

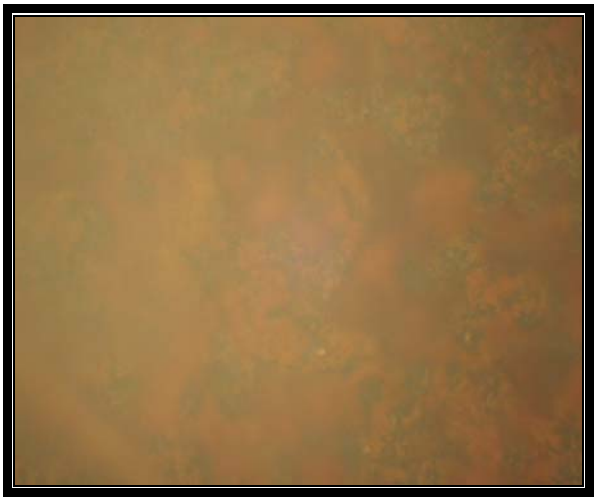

Figure (4.26) LOM images of surface damage on Zn-Ni-Cu (Heat Treated) after exposed in salt spray test 24 hrs,35°C,50% humidity.

Figure (4.27) LOM images of surface damage on Zn-Ni-SiO_2 (Heat Treated) after exposed in salt spray test 24 hrs,35°C,50% humidity.

When SEM is used ,the topography of the base metal is shown in figures (4.28 a,b and c).

Corrosion products of the metal in air ,water, or vapor are available elsewhere[25,29,27].These products are known to be porse , thick and of poor adhesion .Therefore ,a great damage is expected to occur when exposed to such hostile environment (i.e. salt spray).

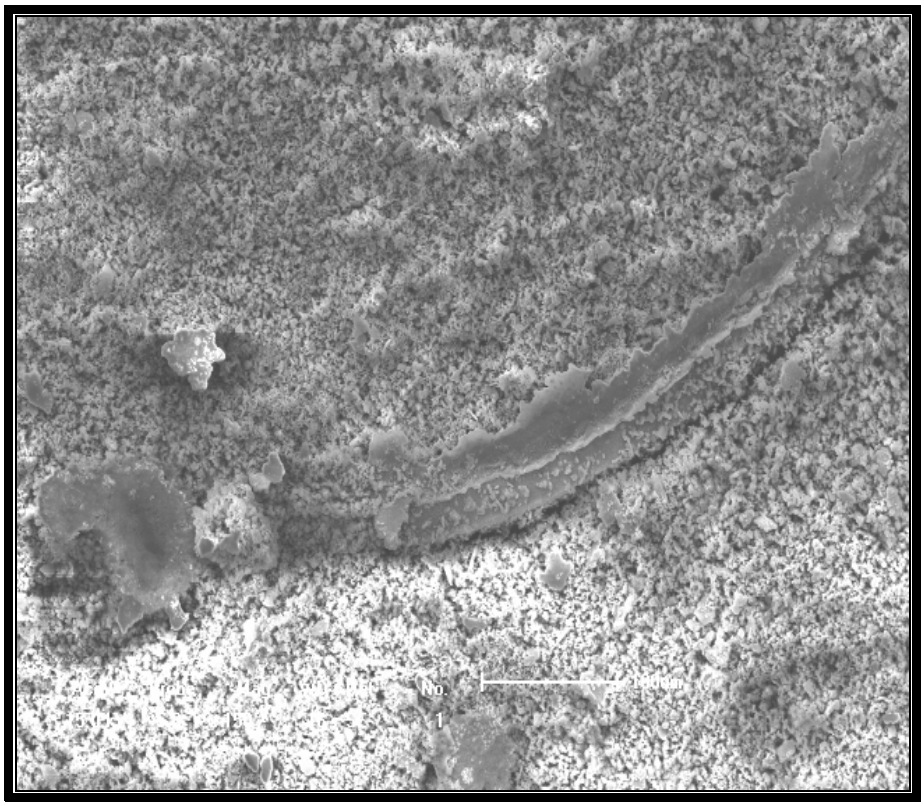

Figure (4.28 a) SEM micrographs X150 of Base metal after exposed in salt spray chamber at 35°C 50% humidity for 24 hrs

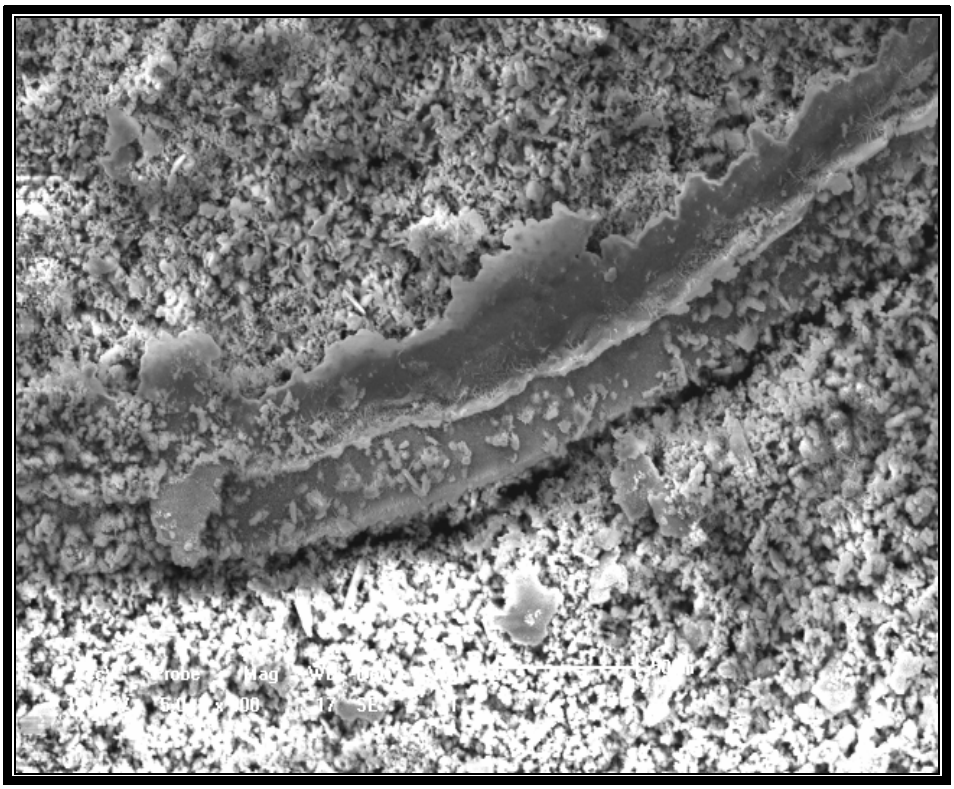

Figure (4.28 b) SEM micrographs X300 of Base metal after exposed in salt spray chamber at 35°C 50% humidity for 24 hrs

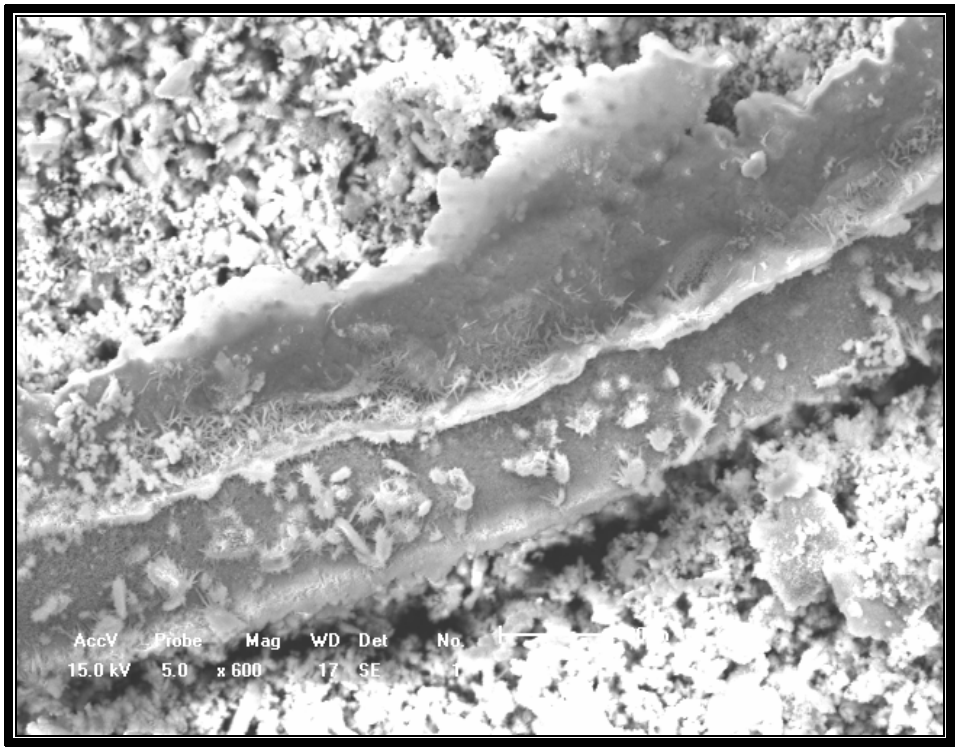

Figure (4.28 c) SEM micrographs X600 of Base metal after exposed in salt spray chamber at 35°C 50% humidity for 24 hrs

When samples coated with Zn-Ni layer were exposed to salt spray for 24 hrs at 35°C and 50% humidity ,figures (4.29 a and b),It is obvious that these samples are also subjected to a certain degree of damage. The measured weight loss is this Zn-Ni layer is significantly less than the corresponding values in the case of the base metal.

Spalling of the corrosion products is clear ,the origin of the damage is of chemical and mechanical causes. The nature of these products determines the size of the damage. There is possibility of forming , zinc carbonates, $Zn(CO_3)_2(OH)_6$, after a longer time of exposure as mentioned by other researcher[132].

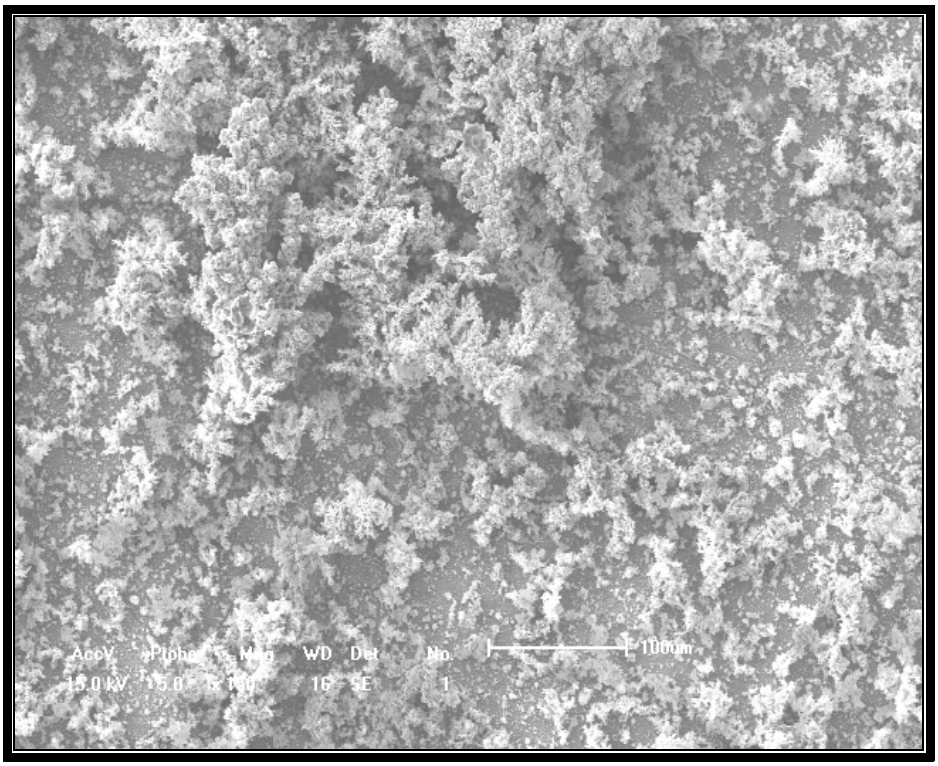

Figure (4.29 a) SEM micrographs of X150 Zn-Ni after exposed in salt spray chamber at 35°C 50% humidity for 24 hrs

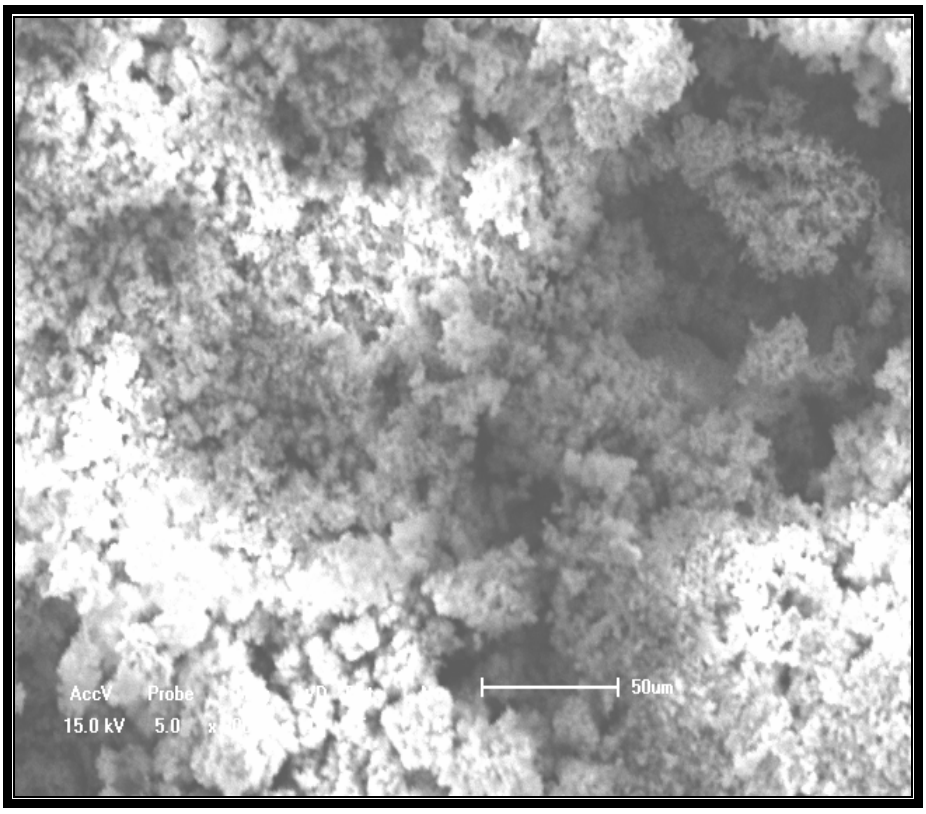

Figure (4.29 b) SEM micrographs of X300 Zn-Ni after exposed in salt spray chamber at 35°C 50% humidity for 24 hrs

It is clear from figures(4.30 a and b) that a change in the topography of the surface occurs. In addition an improvement in the corrosion results is also happened in terms of a decrease in the weight loss. It is expected that a certain degree of cracking and spalling occurs. However, the corrosion products seem to be more particles than that of Zn-Ni only.

The protective corrosion products probably fill up the cracks that are formed in the coating , preventing a decrease in corrosion resistance due to crack formation.

The figure (4.30 a and b) illustrate the appearance of Zn-Ni-Cu after exposing in a salt spray chamber at 35°C,50% humidity for 24 hrs.

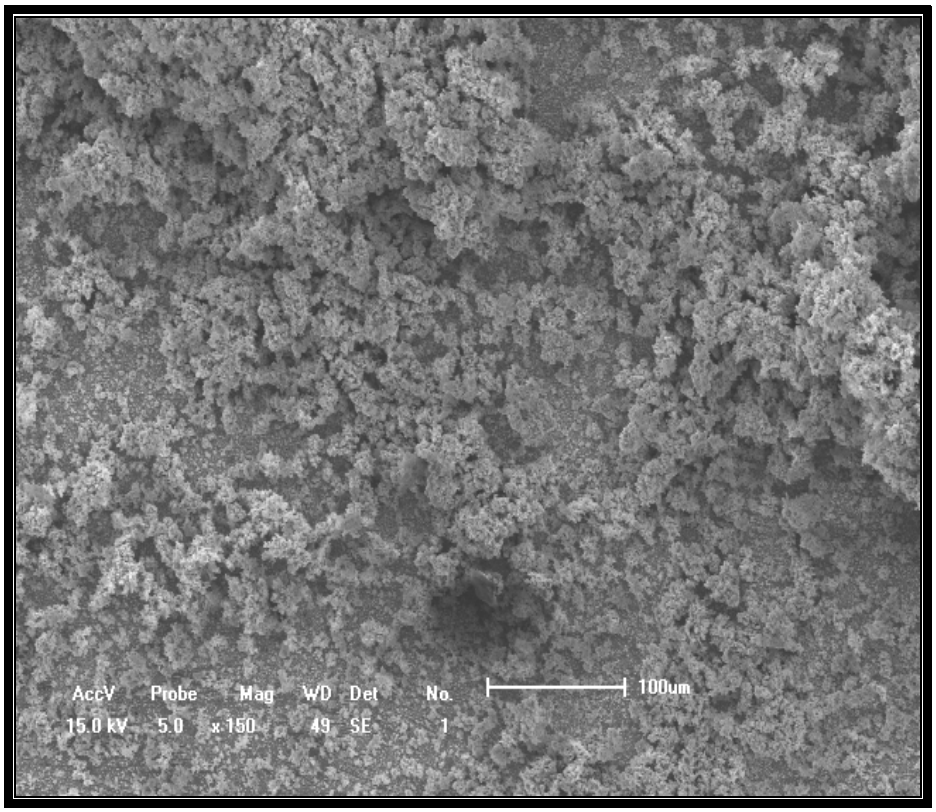

Figure (4.30 a) SEM micrographs of X150 Zn-Ni-Cu after exposed in salt spray chamber at 35°C 50% humidity for 24 hrs

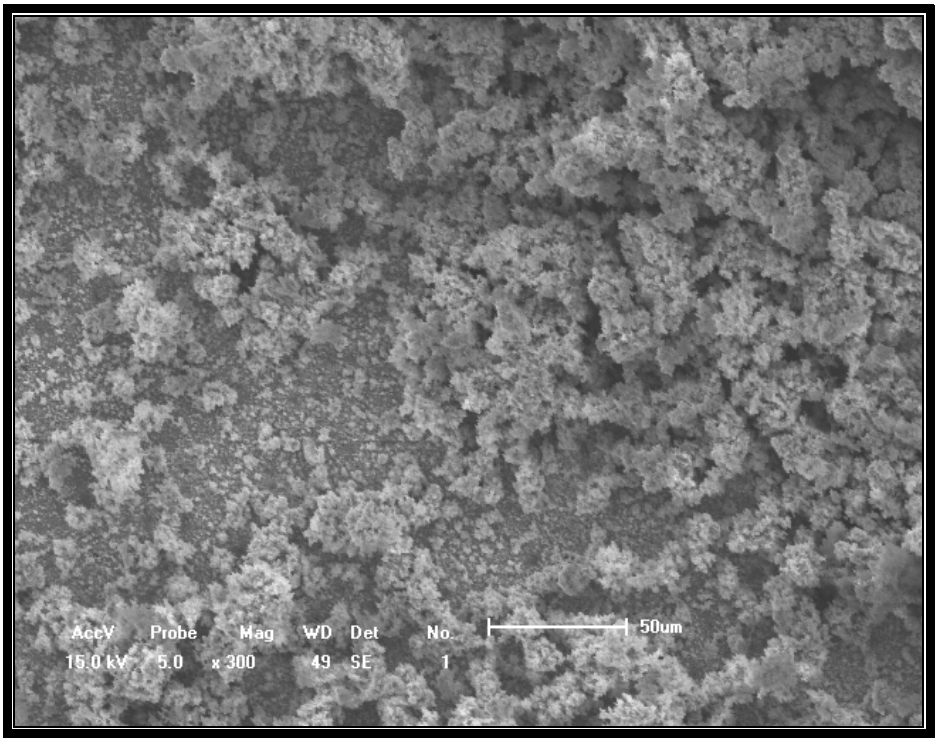

Figure (4.30 b) SEM micrographs of X300 Zn-Ni-Cu after exposed in salt spray chamber at 35°C 50% humidity for 24hrs

Figures (4.31 a and b) describe the additive effect of SiO_2 rich layer to have a good barrier layer for corrosion resistance .

These figures explain the material alloy surface for Zn-Ni-SiO_2 in salt spray chamber after exposure at 35°C,50% humidity ,24hrs.These tests showed clearly a change in the topography of the outer layer, see figures (4.29,4.30 and 4.31).The characteristic appearance of the surface is completely changed, and a smooth surface is observed.

The layer is enriched in SiO_2 particle forming a diffusion barrier and preventing further reaction,as in figures (4.31a and b).

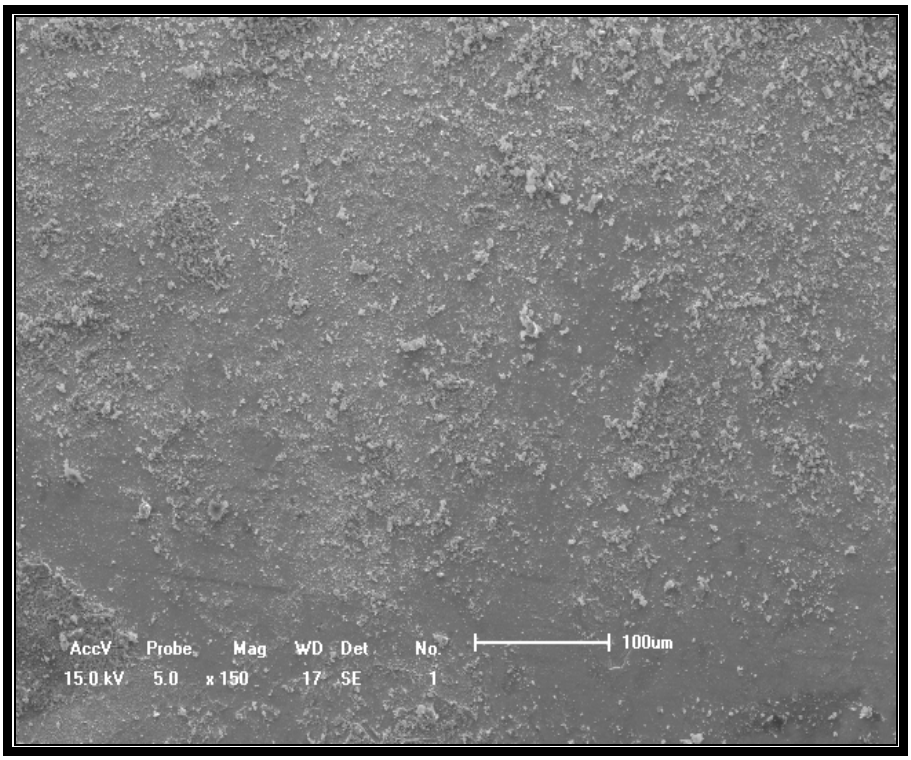

Figure (4.31 a) SEM micrographs of X150 Zn-Ni-SiO_2 after exposed in salt spray chamber at 35°C 50% humidity for 24hrs

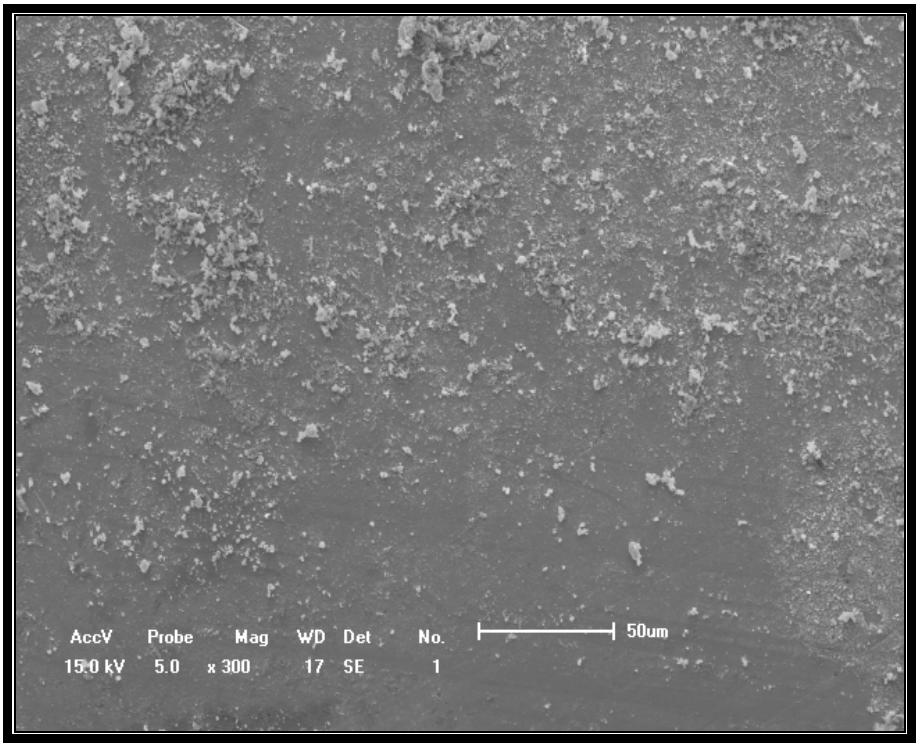

Figure (4.31 b) SEM micrographs of X300 Zn-Ni-SiO_2 after exposed in salt spray chamber at 35°C 50% humidity for 24 hrs

The effect of heat treatment on the morphology and corrosion resistance is shown in figures (4.32,4.33 and 4.34),and Table (4.20).

A change in the morphology of the surface is clear in addition to a slight improvement in the corrosion resistance, in the case of Zn-Ni and Zn-Ni-Cu. However ,a significant change in both morphology and corrosion resistance of Zn-Ni-SiO_2 occurs,as in figures (4.34a and b) and figure (4.20).

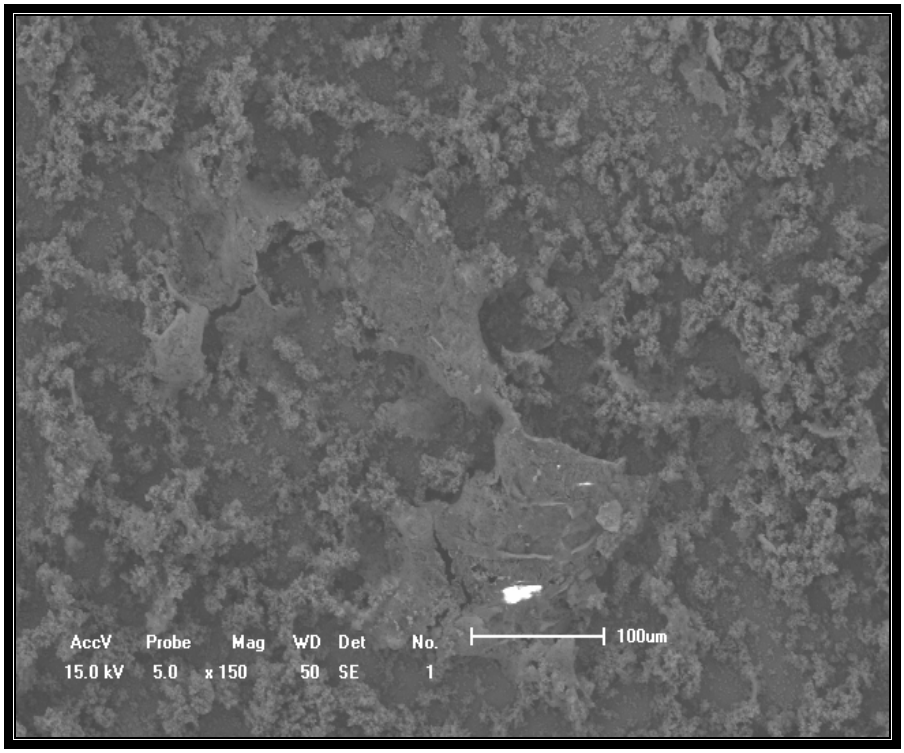

Figure (4.32 a) SEM micrographs of X150 Zn-Ni after heat treated exposed in salt spray chamber at 35°C 50% humidity for 24 hrs.

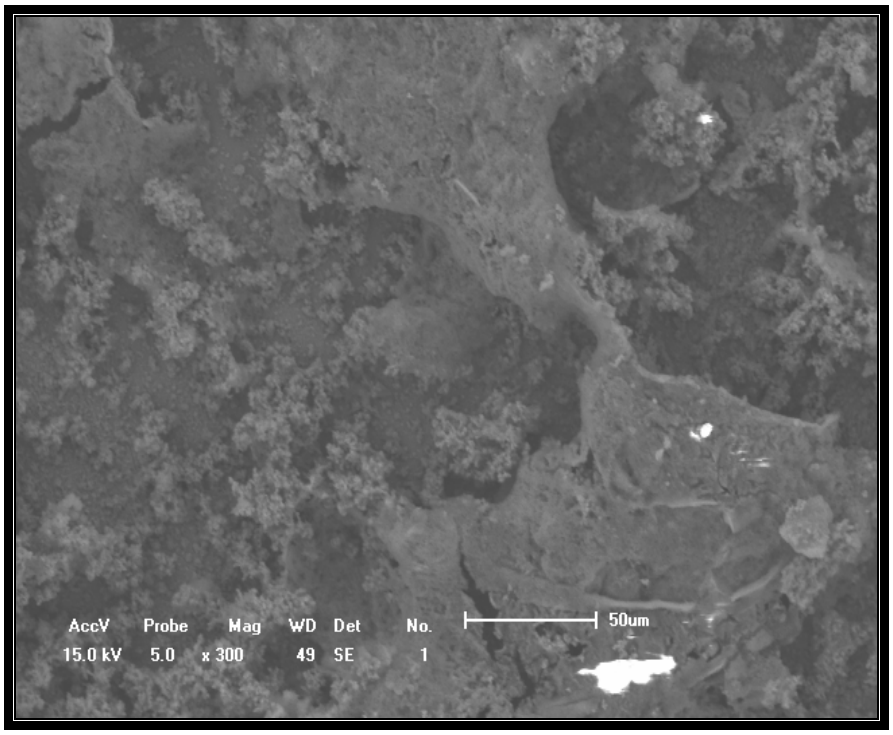

Figure (4.32 b) SEM micrographs of X300 Zn-Ni after heat treated exposed in salt spray chamber at 35°C 50% humidity for 24 hrs.

Figures (4.32 a and b) show a morphology consisting of some areas covered by oxides, and another areas uncovered.

It will be shown that the nickel is not presented to a significant extent in the corrosion products of a zinc-nickel coating. It is probable that, similar to the case of pure zinc or nickel, some sort of oxide , hydroxide or carbonate is quickly formed on the surface of zinc-nickel alloy[136].

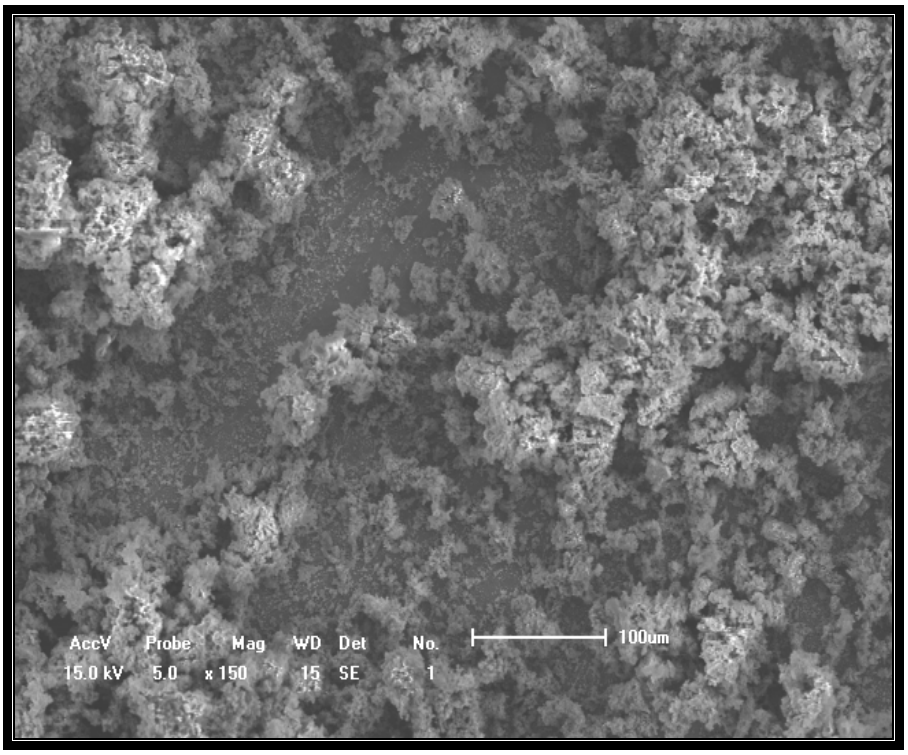

Figure (4.33 a) SEM micrographs of X150 Zn-Ni-Cu after heat treated exposed in salt spray chamber at 35°C 50% humidity for 24 hrs.

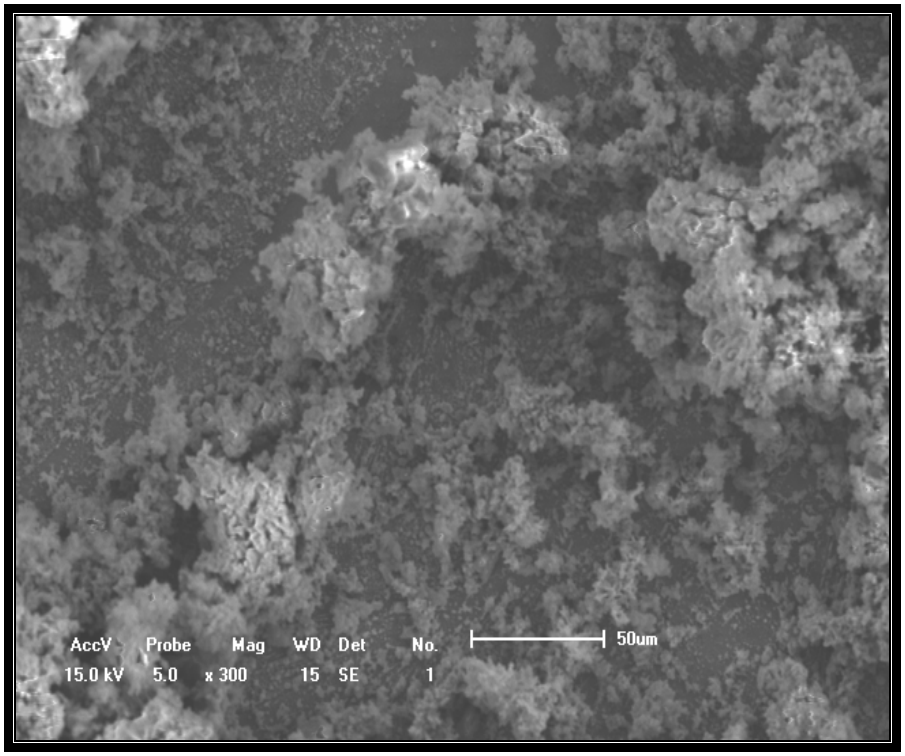

Figure (4.33 b) SEM micrographs of X300Zn-Ni-Cu after heat treated exposed in salt spray chamber at 35°C 50% humidity for 24 hrs.

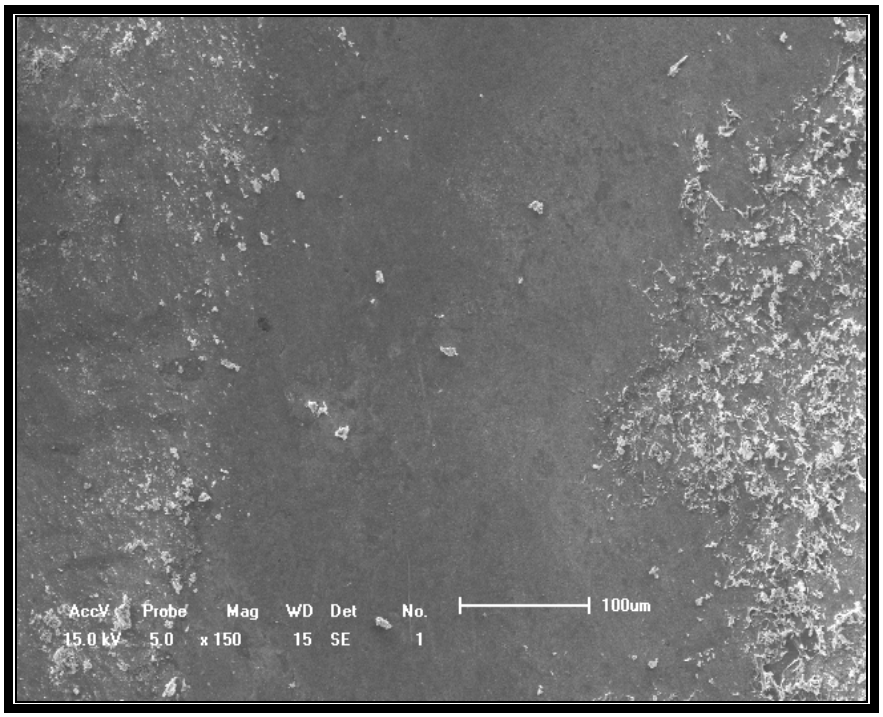

Figure (4.34 a) SEM micrographs of X150 Zn-Ni-SiO2 after heat treated exposed in salt spray chamber at 35°C 50% humidity for 24 hrs.

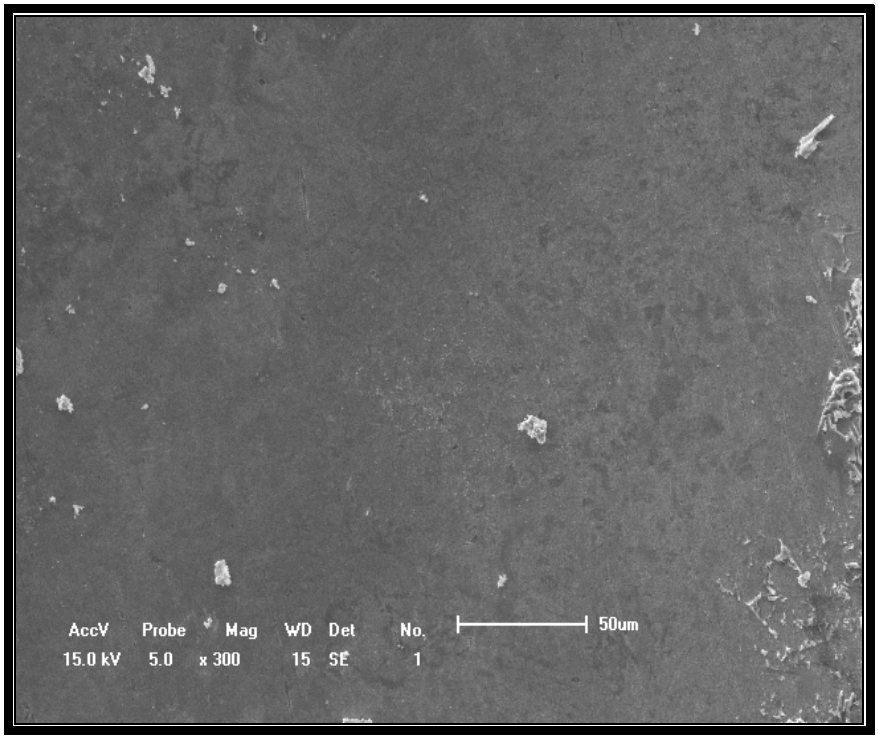

Figure (4,34 b) SEM micrographs of X300 Zn-Ni-SiO2 after heat treated exposed in salt spray chamber at 35°C 50% humidity for 24 hrs.

4.6.2 Tafel Test:

4.6.2.1 Polarization Curve (Tafel Slope) 5% NaCl

The range of the used voltage E-free corrosion was (-550 mV) determined automatically by immersing the reference electrode and examined a sample in the solution after the stability of the magnitude. Therefore, the limits were chosen in such away (0-1250 mV) higher and lower, E-free corrosion is considered the shape of polarization curve.

In this study ,the corrosion current and the corrosion potential were measured on the polarization curves by using computerize Tafel extrapolation method.

The Tafel calculation gives access to the corrosion current regularly presented at the surface of a metal which is in contact with a corroding solution .

The exchange current density ,$i_{\circ}$,and the Tafel slope a and b, are both dependent on the material of the electrode. According to the equation (1.15) the performance of an electrode can be accomplished by either increasing the exchange current density, $i_{\circ}$ or by decreasing the Tafel constant a and b, or both if possible.

A voltammetric curve i=f (Vg) having a zero current potential can be processed according to the Tafel method.

The Tafel method gives also access to other corrosion parameters such as the zero current potential (corrosion potential) , the corrosion current and the polarization resistance of the sample under study .The Tafel calculation is a complete tool to study the corrosion process at a metal surface at different environments.

Figures (4.35 a and b) show the corrosion behavior for base metal and confirmed that $I_{corr.}$ $1.139x10^{-4}A/cm^2$,$E_{corr.}$-0.541 V, b_c 0.282 V/dec

and b_a 0.714 V/dec, all computerize data for polarization curve confirmed at appendix (E).

This result indicated a poor corrosion resistance of the base metal (carbon steel) as expected. Ripple on the polarization curve indicated evolution of hydrogen.

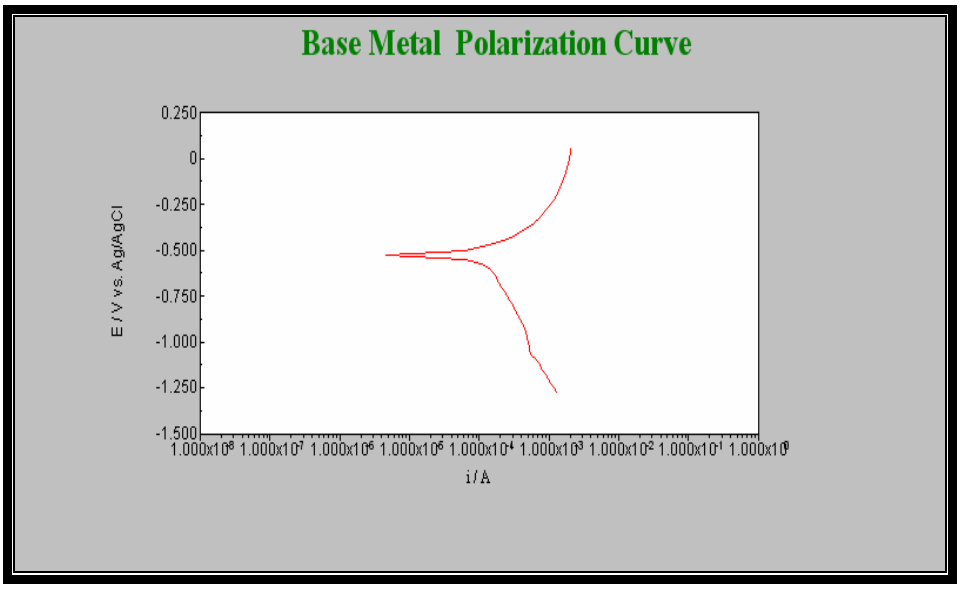

Figure (4.35 a) Polarization curve (Tafel Slope)for Base Metal in 5% NaCl

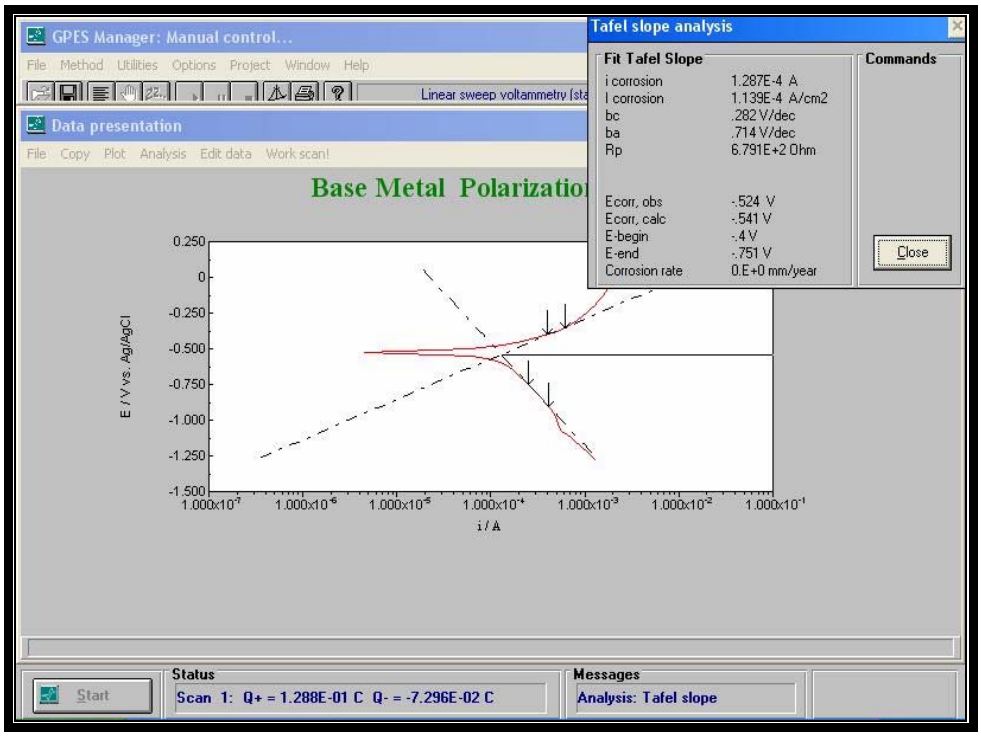

Figure (4.35 b) Tafel slope analysis for Base Metal

From figures (4.36 a and b) show the corrosion behavior for Zn-Ni coating. The observed values are I_{corr} to $6.928x10^{-5}$ A/cm^2, E_{corr} – 0.308 V, b_c 0.344 V/dec and b_a 0.382 V/dec.

As can be seen from these values ,a significant decrease in the corrosion current is observed ,i.e. a decrease of a value 60% occurred, This result is in agreement with the salt spray tests, when coated by Zn-Ni increase corrosion resistance.

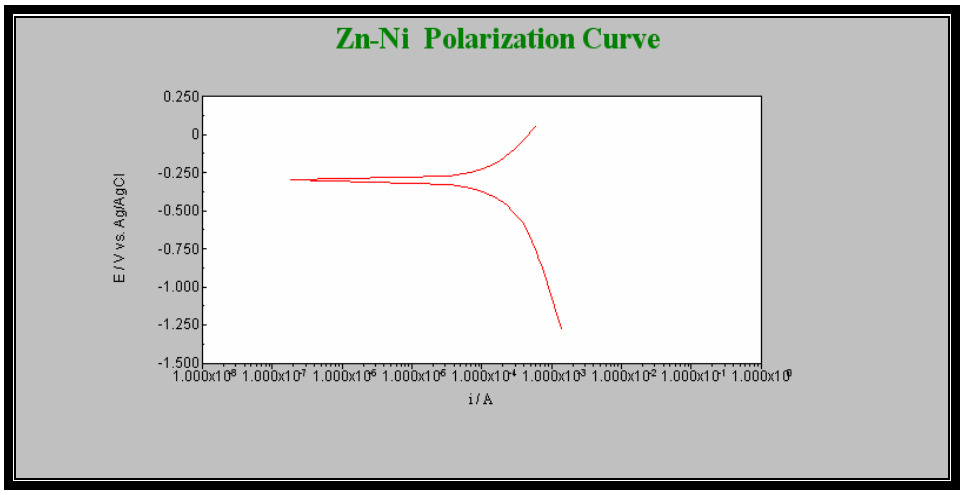

Figure (4.36 a) Polarization curve (Tafel slop) for Zn-Ni in 5% NaCl .

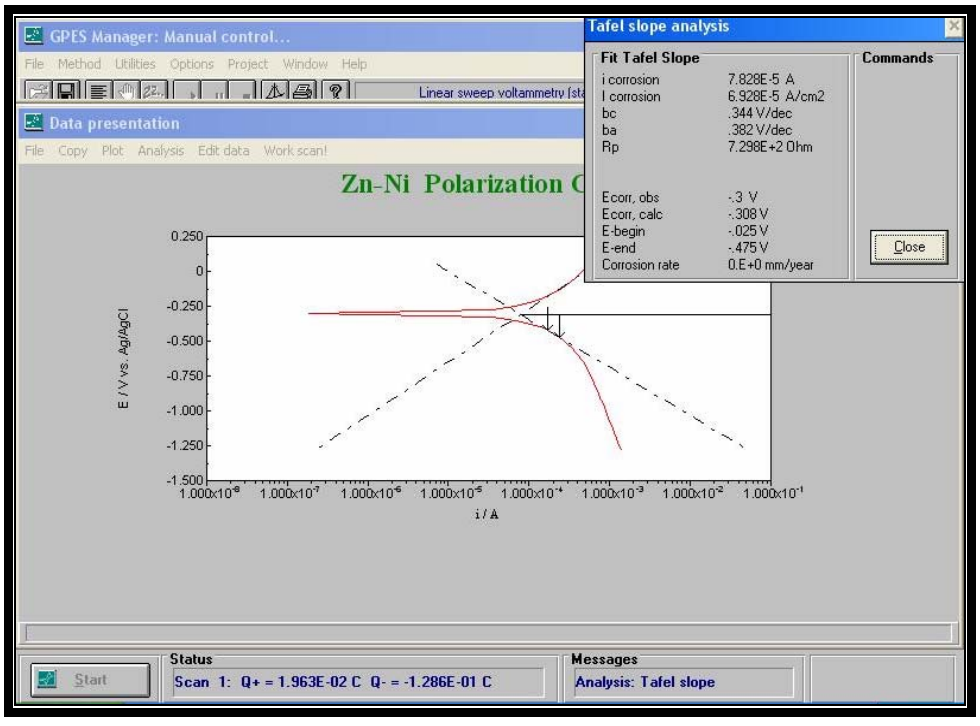

Figure (4.36 b) Tafel slope analysis for Zn-Ni

When cupper is added to Zn-Ni coating the Tafel results are shown in figure (4.37 a and b) to observe the values I_{corr}. $5.83x10^{-5}$ A/cm², E_{corr} – 0.739 V, b_c 0.298 V/dec and b_a 0.28 V/dec.

The corrosion current is only 51% when compared with the corresponding value of base metal and 84% to the Zn-Ni coating.

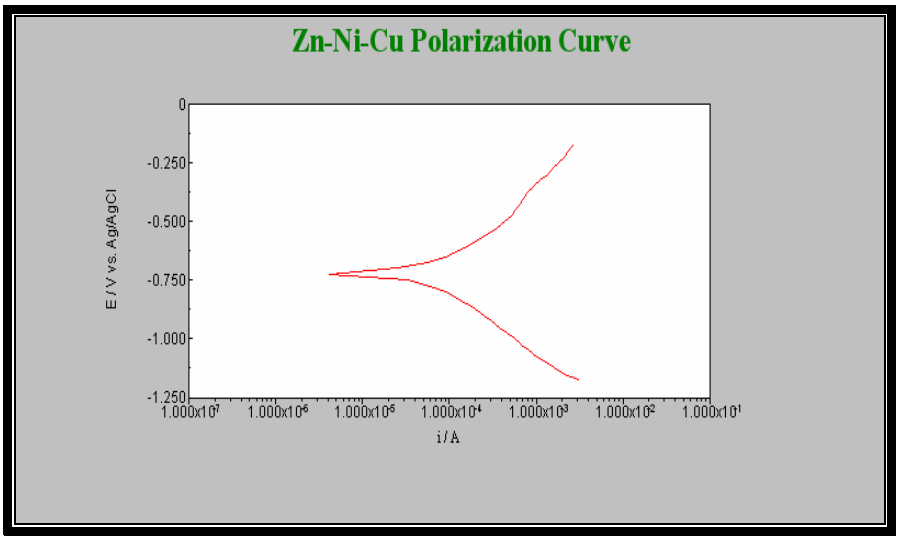

Figure (4.37 a) Polarization curve (Tafel Slope) for Zn-Ni-Cu in 5% NaCl.

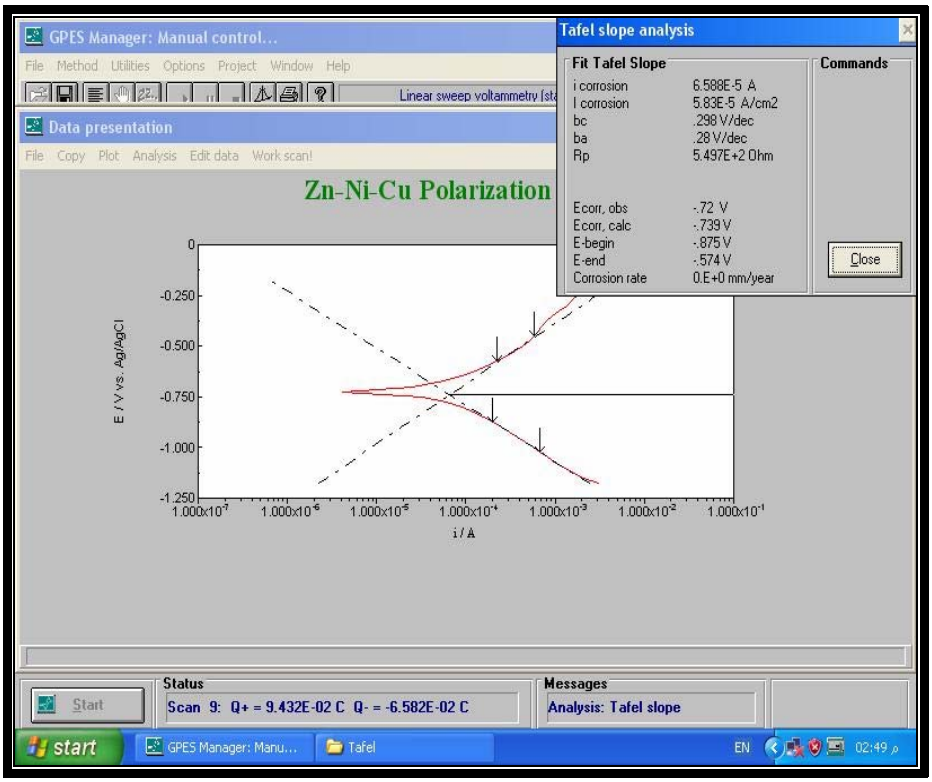

Figure (4.37 b) Tafel slope analysis for Zn-Ni-Cu

When cupper is replaced by SiO_2 the corrosion current becomes only 0.8% when corresponded to the base metal and 13% to the Zn-Ni and 16% to Zn-Ni-Cu coating.

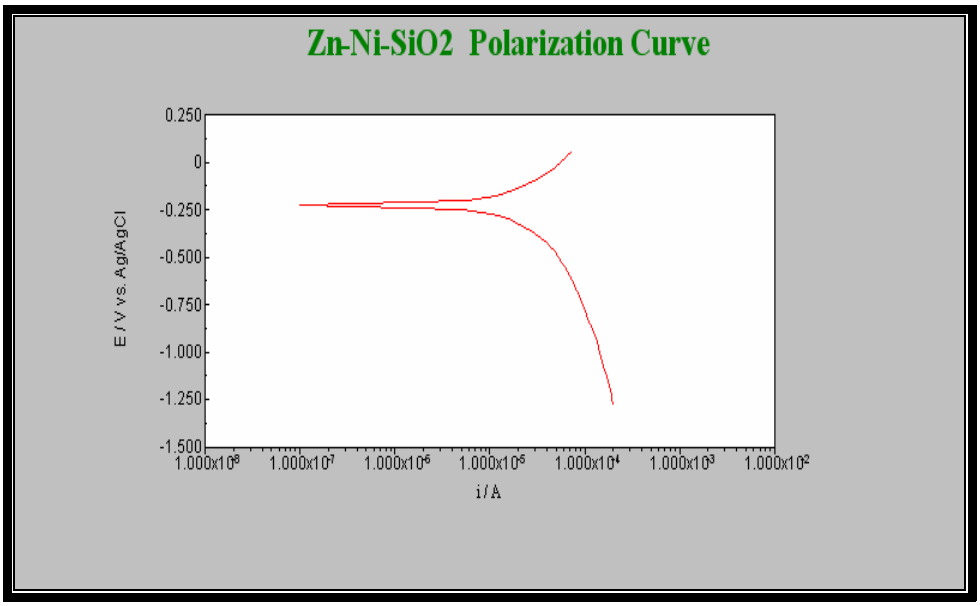

Figure (4.38 a) Polarization curve (Tafel Slope) for Zn-Ni-SiO_2 in 5% NaCl.

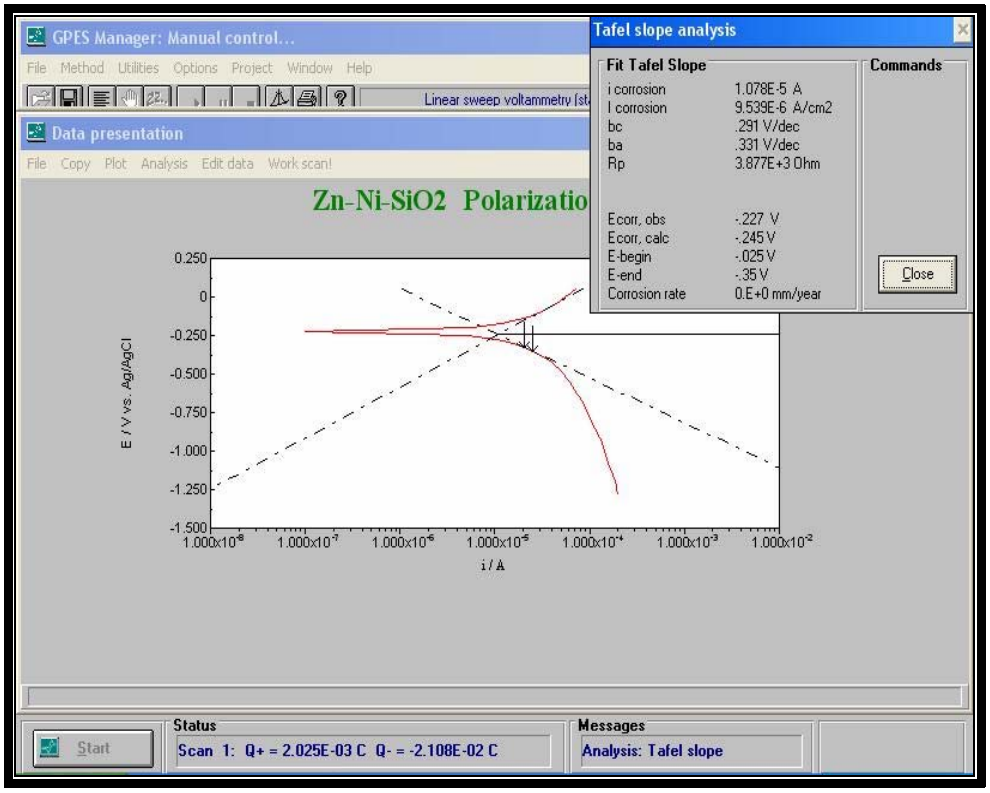

Figure (4.38 b) Tafel slope analysis for Zn-Ni-SiO_2

When heat treatment is applied to the coating then the results are shown in figures (4.39,4.40 and 4.41).A slight change in the corrosion current is observed ,this is only again is in a good agreement with the salt spray tests.

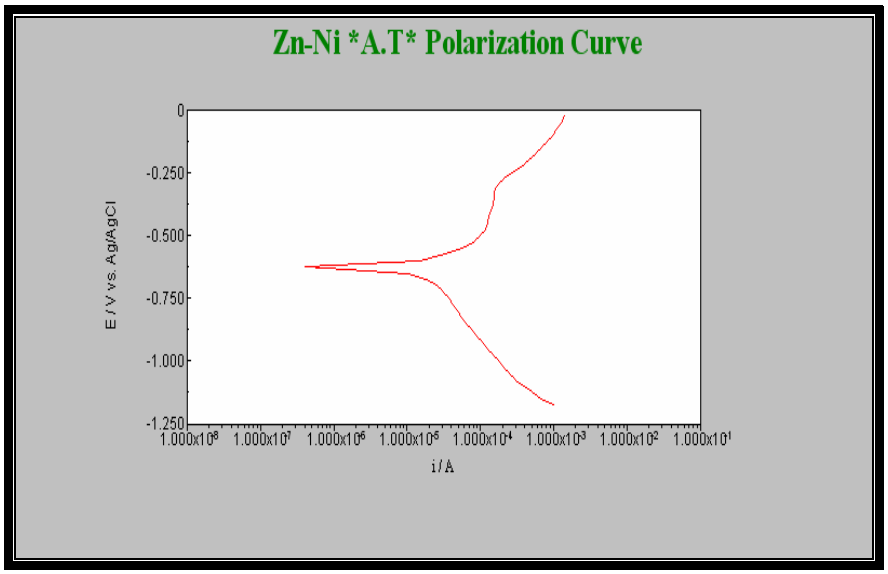

Figure (4.39a) Polarization curve (Tafel Slope) for Zn-Ni(Heat Treated) in 5% NaCl.

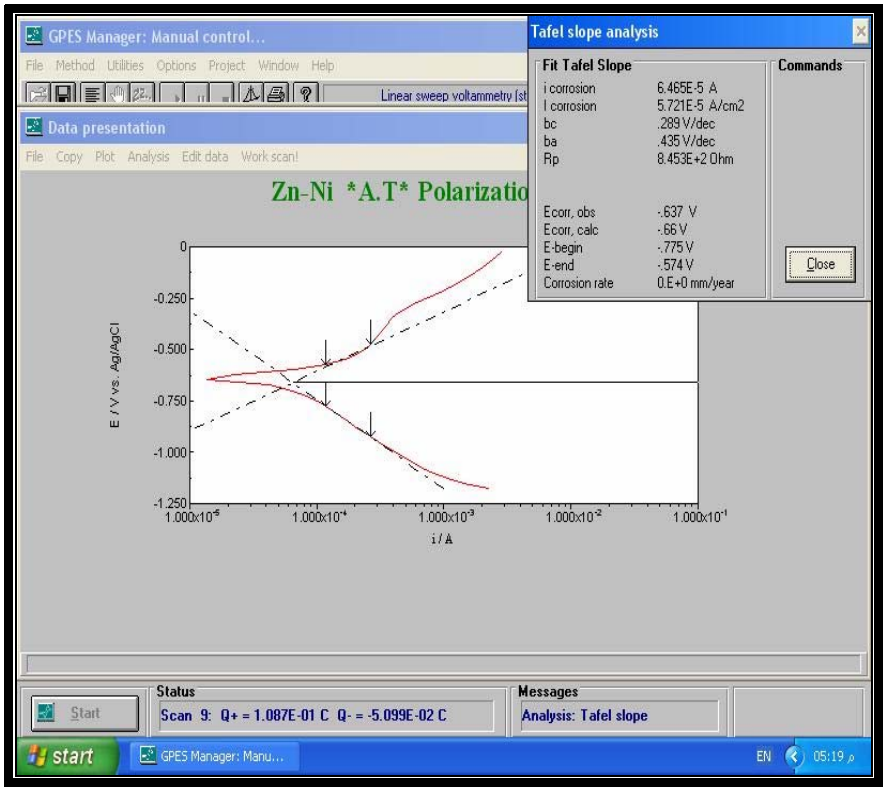

Figure (3.39b) Tafel slope analysis for Zn-Ni (Heat Treated).

For figures (4.40 a and b) polarization curve Zn-Ni-Cu indicated this result for $I_{corr.}$ more than I_{corr} without heat treatment.

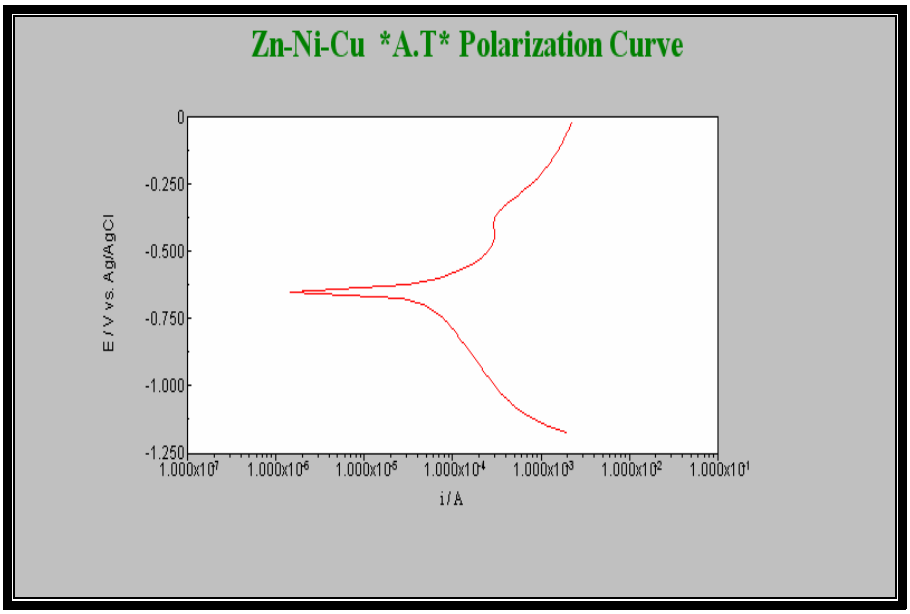

Figure (4.40 a) Polarization curve (Tafel Slope) for Zn-Ni-Cu (Heat Treated) in 5% NaCl.

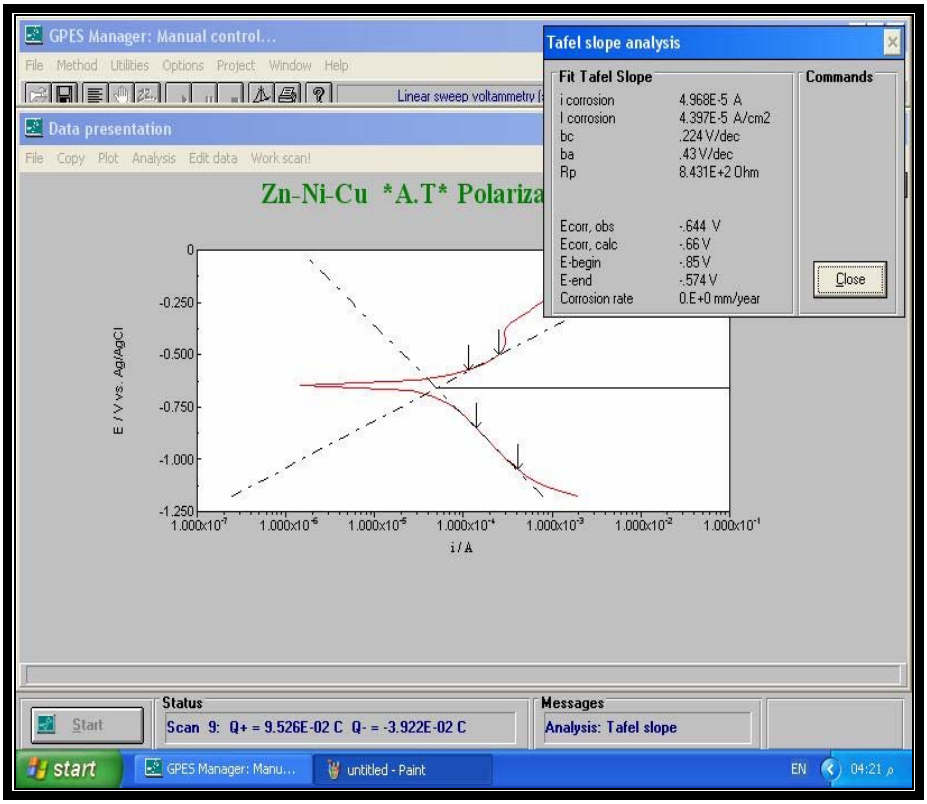

Figure (4.40 b) Tafel slope analysis for Zn-Ni (Heat Treated).

A second time Zn-Ni-SiO_2 proved superiority compared with other kind of coatings when heat treatment is carried out at 200°C and 1hr and to be better than Zn-Ni-SiO_2 before heat treatment.

From figures (4.41 a and b) $I_{corr.}$ $4.149x10^{-6}A/cm^2$,$E_{corr.}$ – 0.273 V,b_c 0.374 V/dec and b_a 0.557 V/dec ,these results indicated an improvement in resistance to corrosion which is attributed to the a passive layer which prevents contact between metals and solution, and acts as a diffusion barrier, this result is in agreement with other researcher(159).

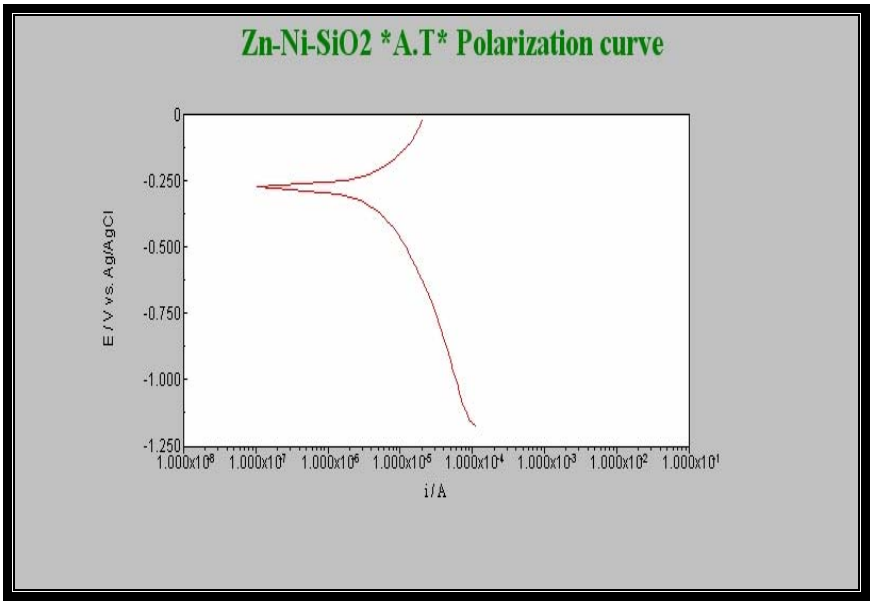

Figure (4.41a) Polarization curve (Tafel Slope) for Zn-Ni-SiO_2 (Heat Treated) in 5% NaCl.

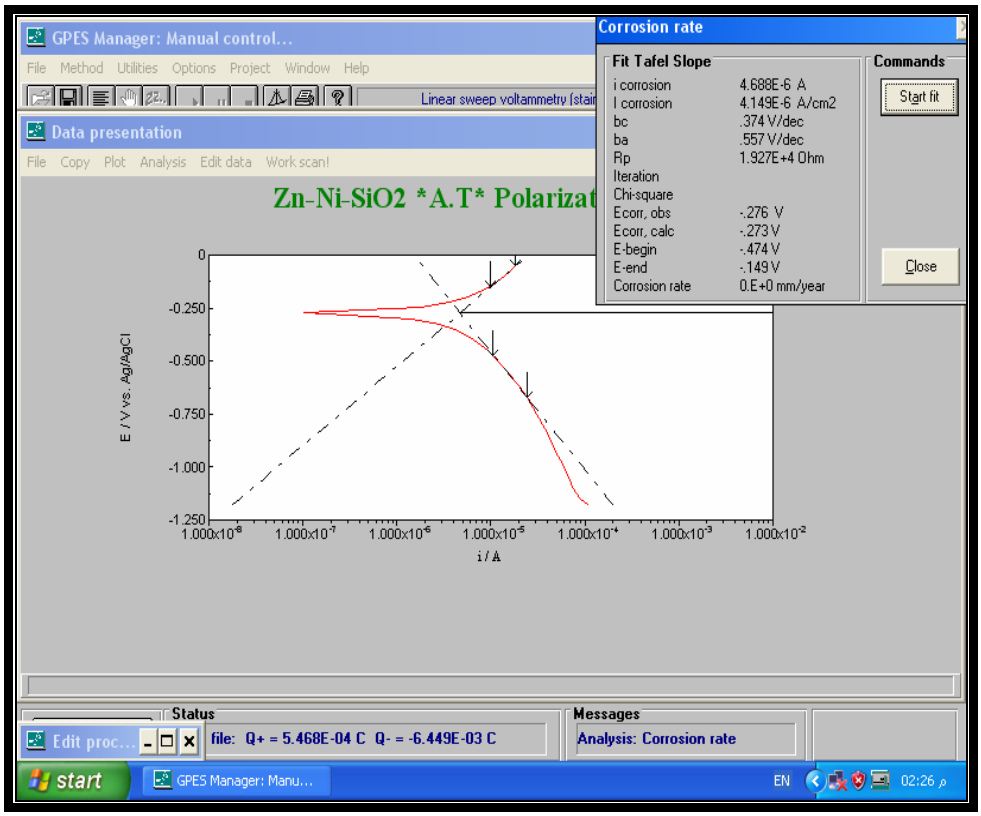

Figure (4.41b) Tafel slope analysis for Zn-Ni-SiO_2 (Heat Treated).

4.6.2.2 Polarization Curve (Tafel Slope)1% Sulfuric Acid:

Most sulfuric acid is formed in the atmosphere from sulfur dioxide released by either the burning of fossil fuels or smelting of high sulfide metaiores ,which observed the dangerous transformation to Acid rain (See Appendix F). This test was carried out at 35°C 1hr to insure stability coating layer for Zn-Ni, Zn-Ni-Cu and Zn-Ni-SiO_2,before and after heat treatment at 200 °C.

In 1% sulfuric acid the corrosion current is shown in figures (4.42,4.43 and 4.44),these values $I_{corr.}$ are $1.078x10^{-2}A/cm^2$,2.533 $x10^{3}A/cm^2$,2.466 $x10^{-3}A/cm^2$ and 5.773 $x10^{-4}A/cm^2$ for the base metal, Zn-Ni, Zn-Ni-Cu and Zn-Ni-SiO_2 respectively, all computerize data for polarization curve were confirmed at (Appendix G).

These values only 23%, 22% and 5% corresponding Zn-Ni, Zn-Ni-Cu ,Zn-Ni-SiO_2 with the base metal.

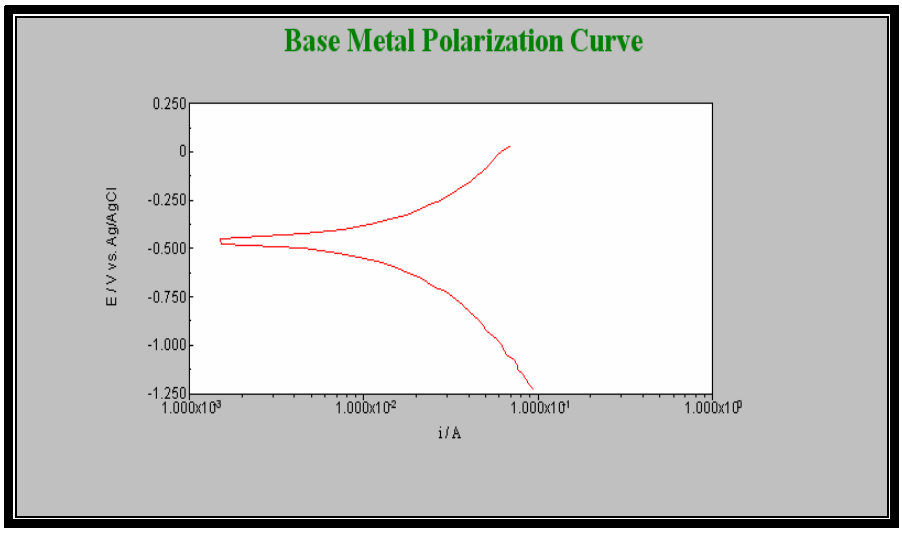

Figure (4.42a) Polarization curve (Tafel Slope) for Base Metal in 1% Sulfuric Acid.

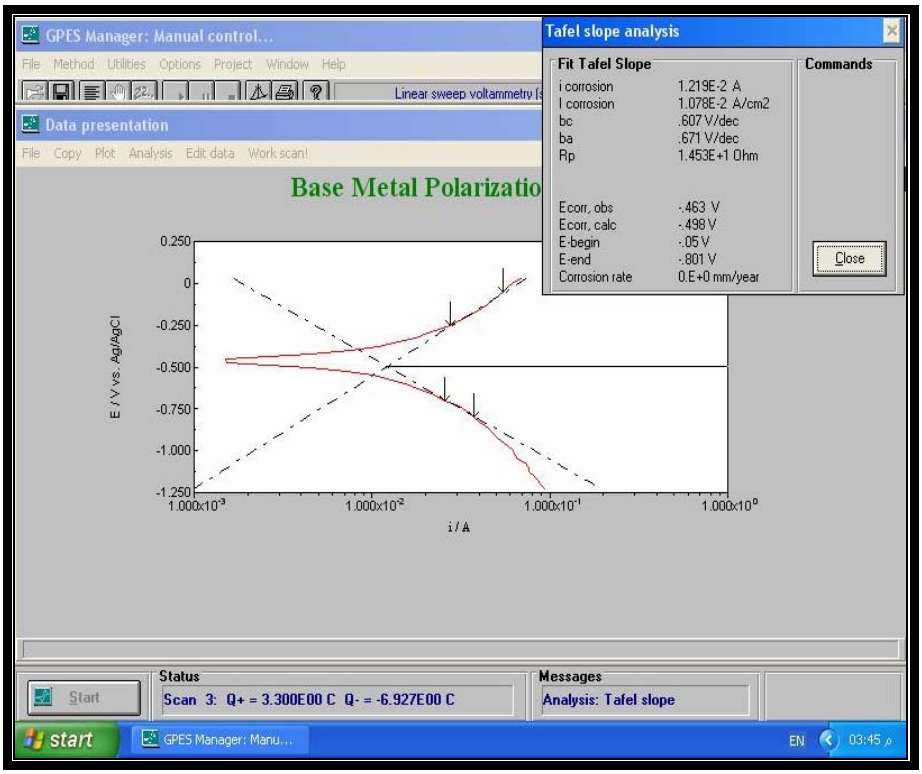

Figure (4.42b) Tafel slope analysis for Base Metal in 1% Sulfuric Acid.

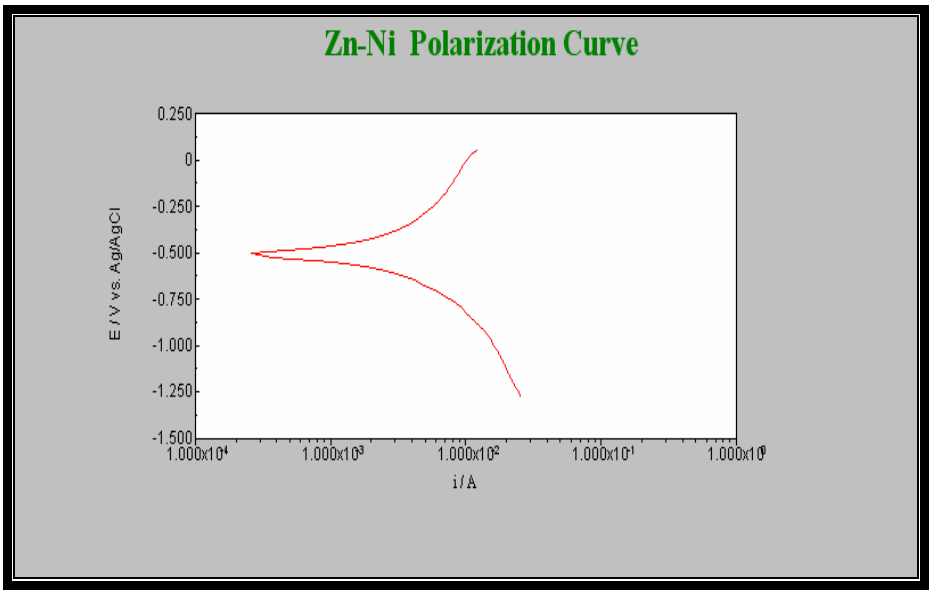

Figure (4.43a) Polarization Curve (Tafel Slope) for Zn-Ni in 1% Sulfuric Acid..

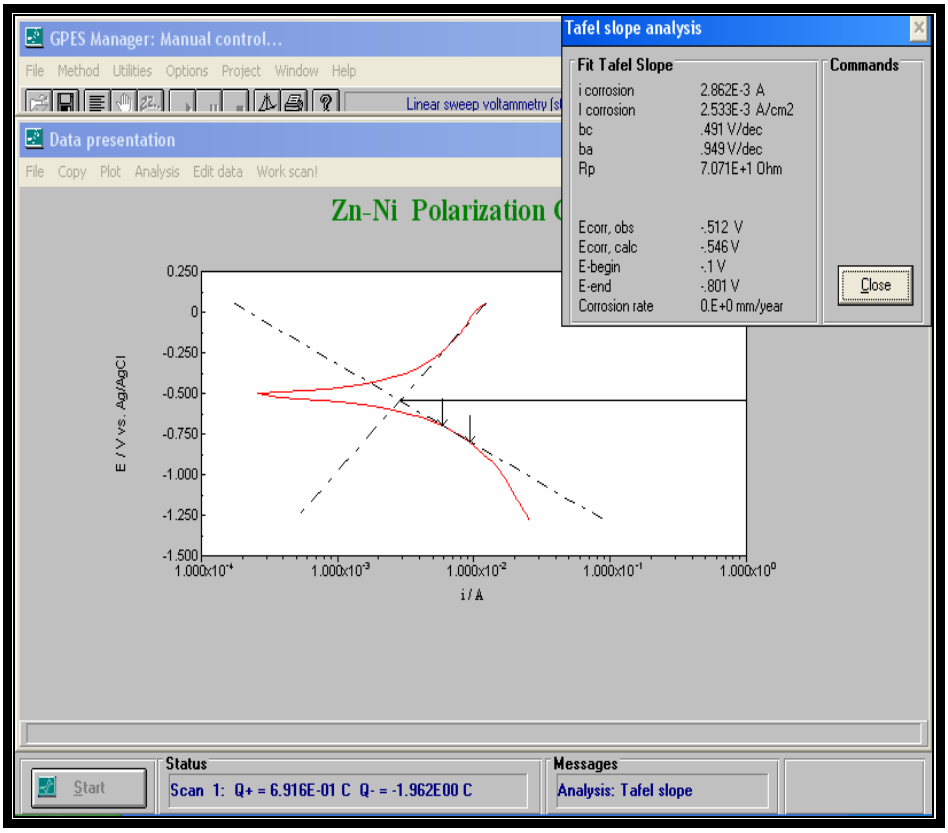

Figure (4.43b) Tafel slope analysis for Zn-Ni in 1% Sulfuric Acid.

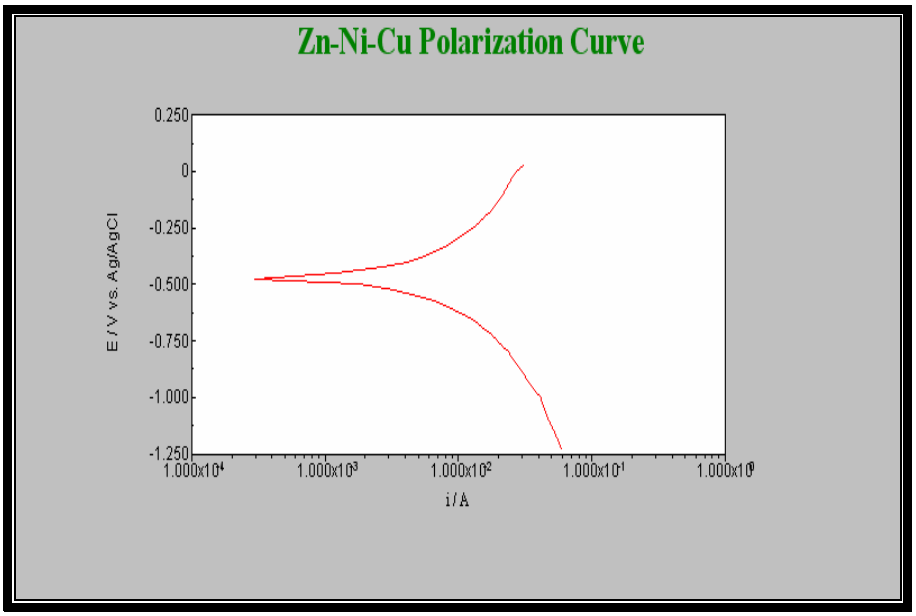

Figure (4.44 a) Polarization Curve (Tafel Slope) for Zn-Ni-Cu in 1% Sulfuric Acid.

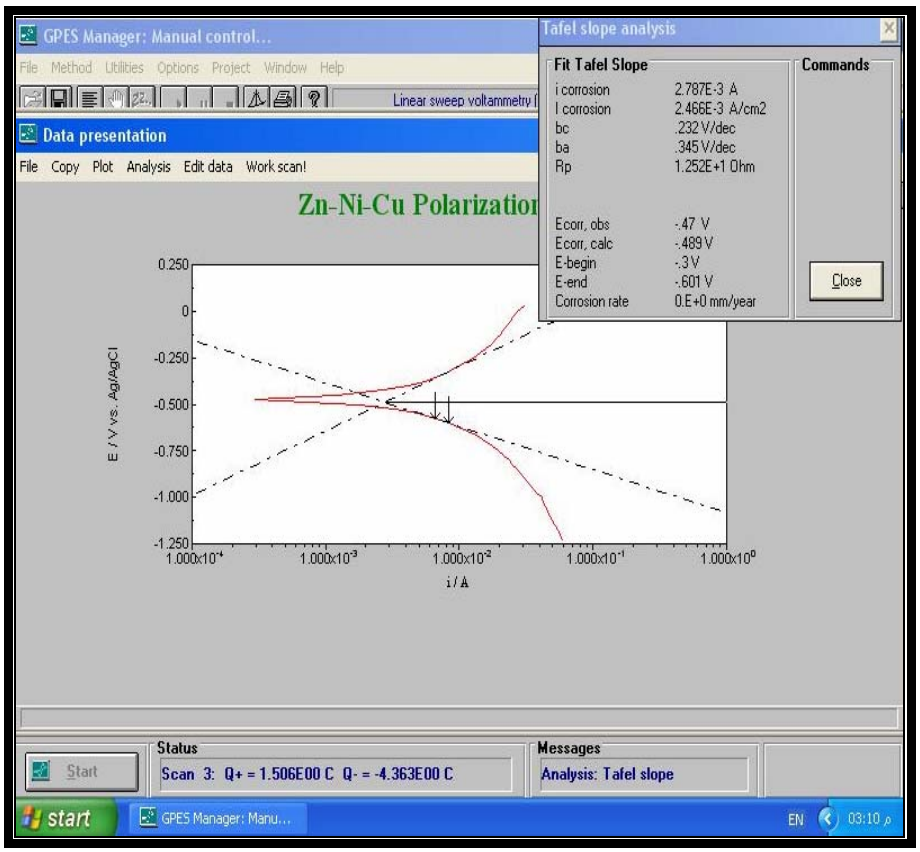

Figure (4.44b) Tafel slope analysis for Zn-Ni-Cu in 1% Sulfuric Acid.

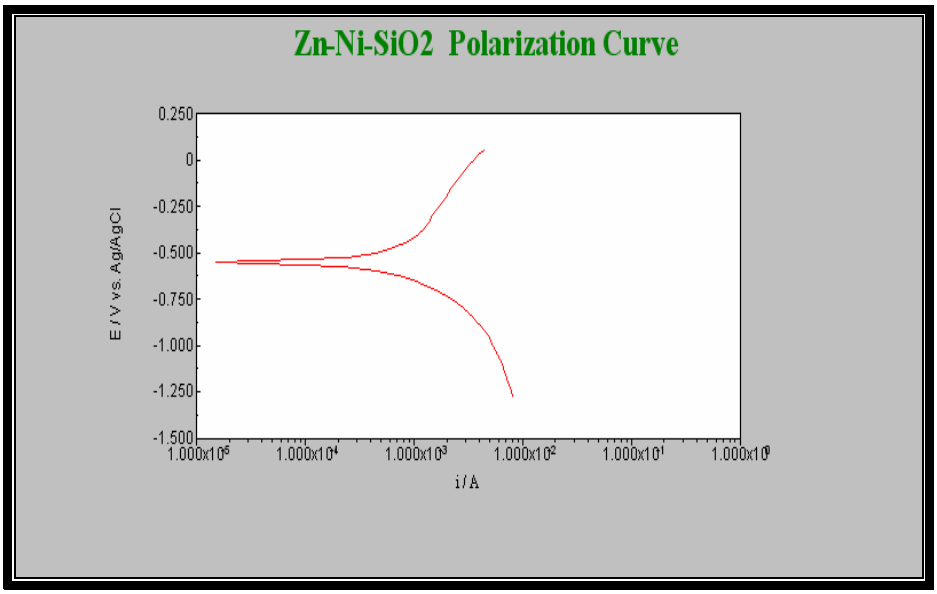

Figure (4.45 a) Polarization Curve (Tafel Slope) for Zn-Ni-SiO_2 in 1% Sulfuric Acid.

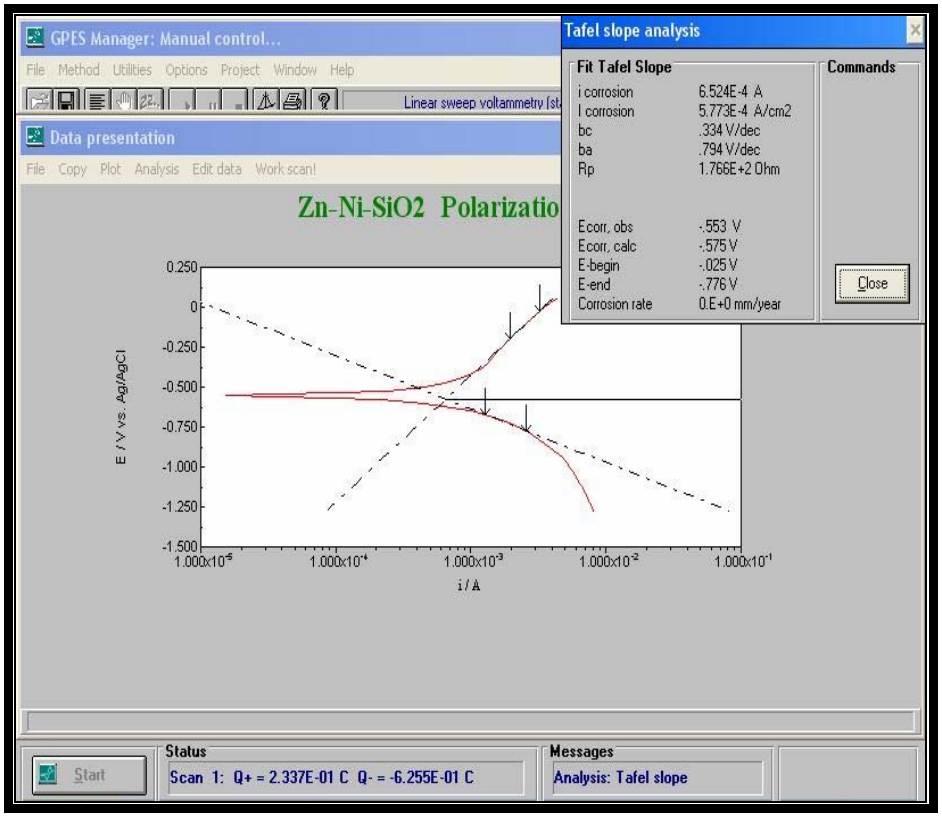

Figure (4.45 b) Tafel slope analysis for Zn-Ni-SiO_2 in 1% Sulfuric Acid.

After heat treatment ,however the values of corrosion current are presented in figures (4.46,4.47 and 4.48).These values for $I_{corr.}$ are $2.461x10^{-3}A/cm^2$,1.2 $x10^{-3}A/cm^2$,and 2.27 $x10^{-4}A/cm^2$ for Zn-Ni, Zn-Ni-Cu and Zn-Ni-SiO_2 respectively.

Once again the value of the corrosion current are 22%,11% and 2% corresponding Zn-Ni, Zn-Ni-Cu and Zn-Ni-SiO_2 (after heat treated) with the base metal.

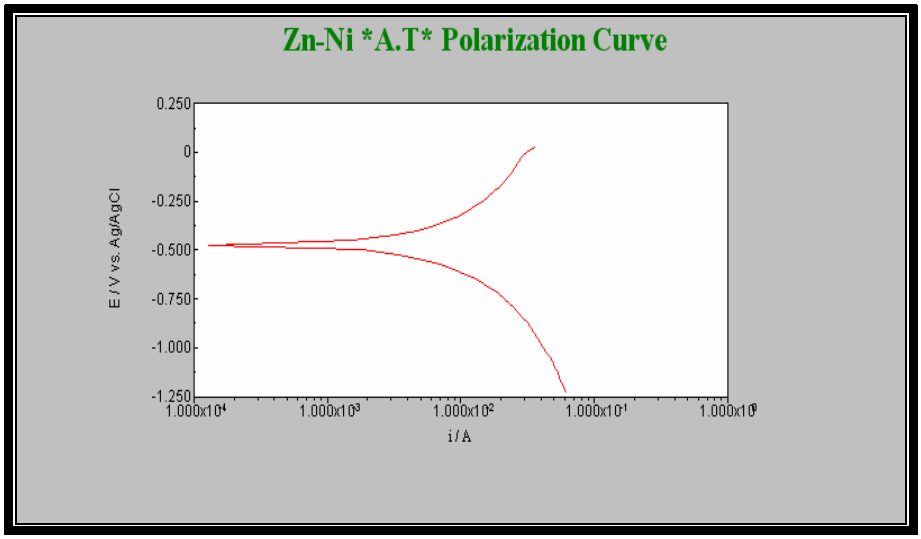

Figure (4.46 a) Polarization Curve (Tafel Slope) for Zn-Ni (Heat Treated) in 1% Sulfuric Acid.

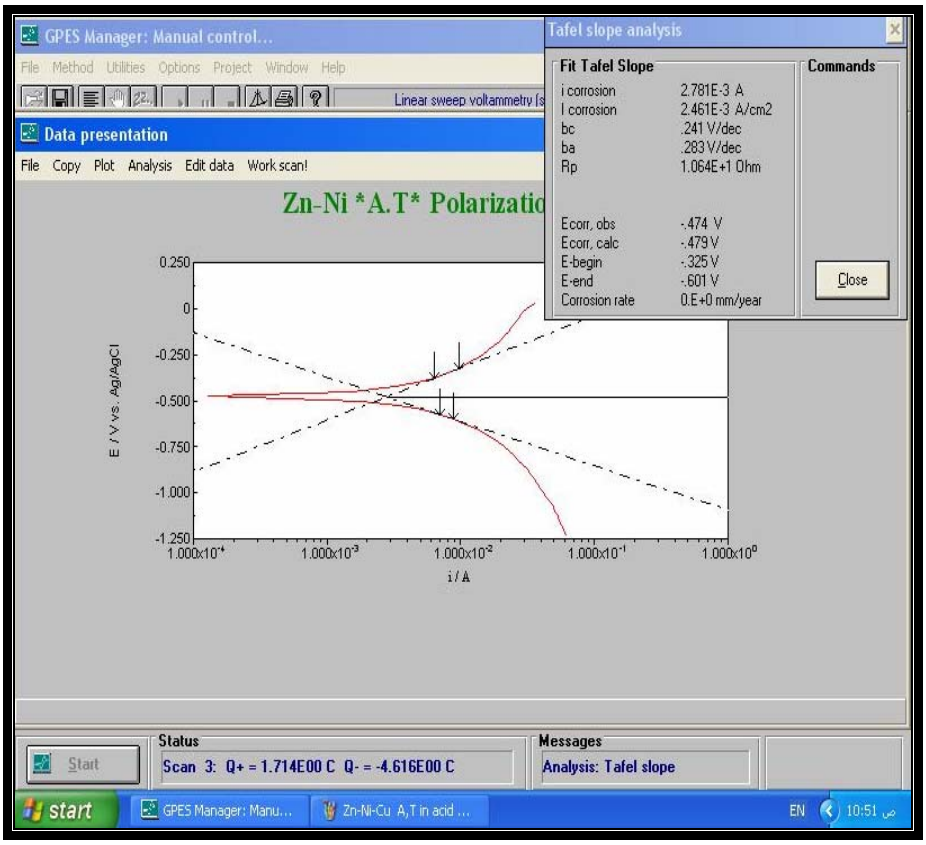

Figure (4.46 b) Tafel slope analysis for Zn-Ni (Heat Treated) in 1% Sulfuric Acid.

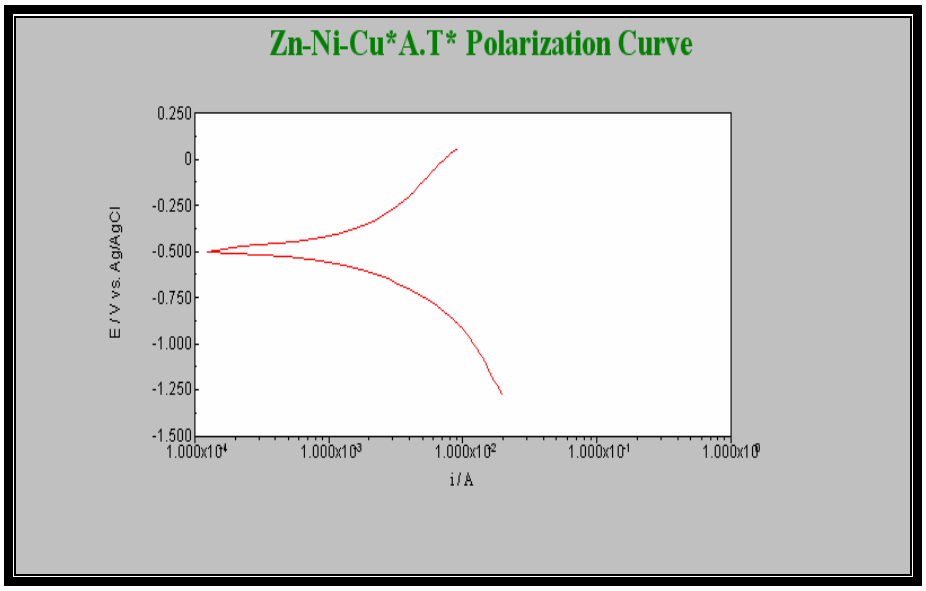

Figure (4.47 a) Polarization Curve (Tafel Slope) for Zn-Ni-Cu (Heat Treated) in 1% Sulfuric Acid.

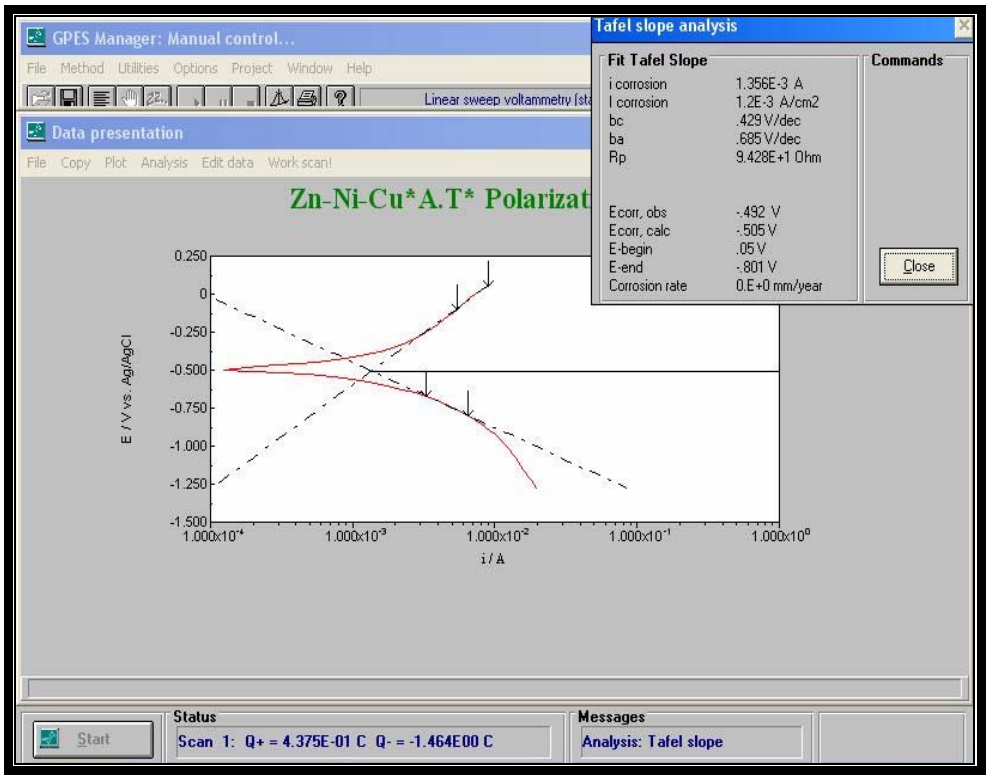

Figure (4.47 b) Tafel slope analysis for Zn-Ni-Cu (Heat Treated) in 1% Sulfuric Acid.

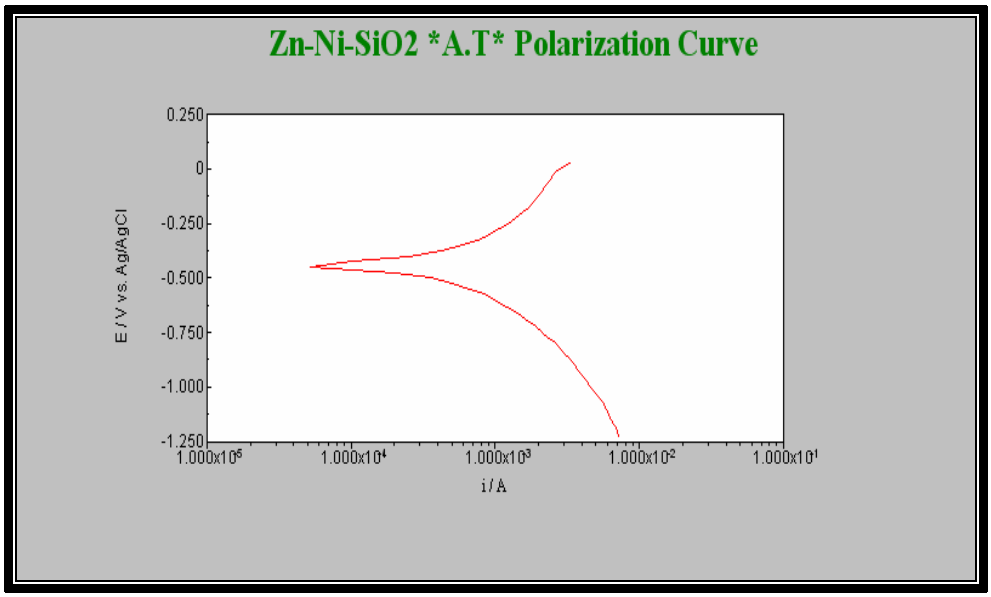

Figure (4.48 a) Polarization Curve (Tafel Slope) for Zn-Ni-SiO_2 (Heat Treated) in 1% Sulfuric Acid.

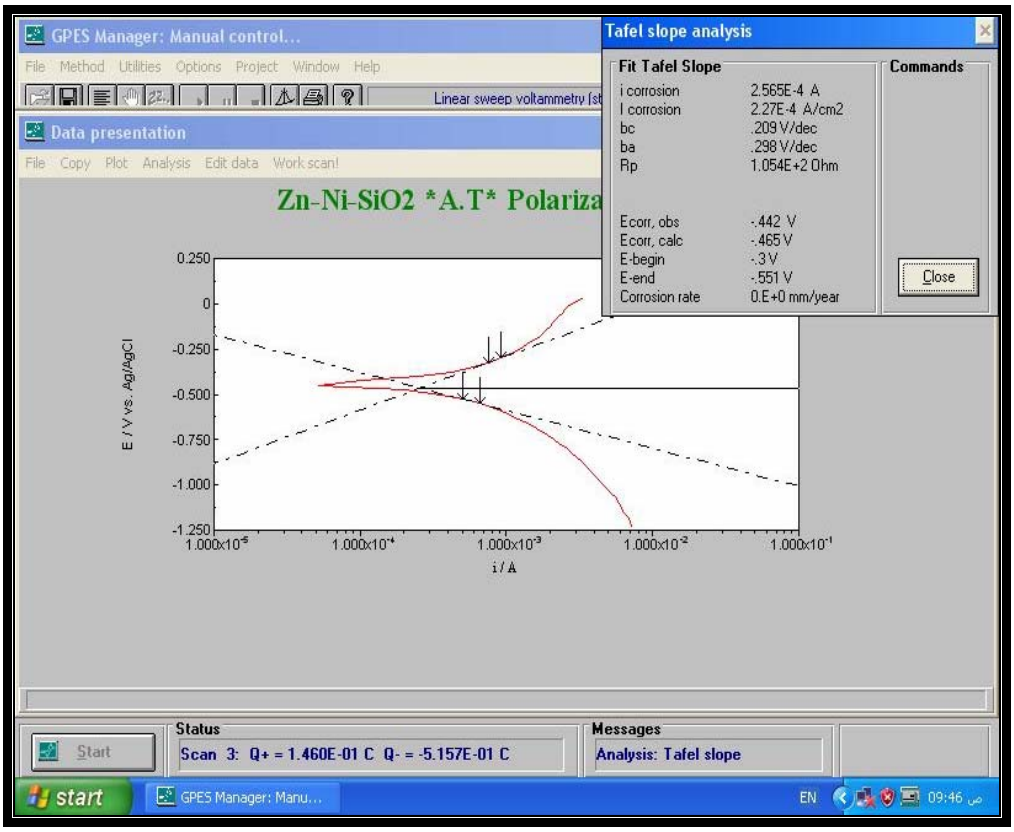

Figure (4.48 b) Tafel slope analysis for Zn-Ni-SiO_2 (Heat Treated) in 1% Sulfuric Acid.

Materials with indistinguishable to values but with different Tafel values will have different activities therefore, these activities are changed in the polarization curve (See Appendix H).

4.6.3 Corrosion in Hydrochloric Acid Solution:

This test is carried out by using 1% HCl at ambient temperature,35°C,45°C and 55°C for Base Metal, Zn-Ni, Zn-Ni-Cu and Zn-Ni-SiO_2.

Figures (4.49,4.50,4.51 and 4.52) show the weight change of the samples at this environment.

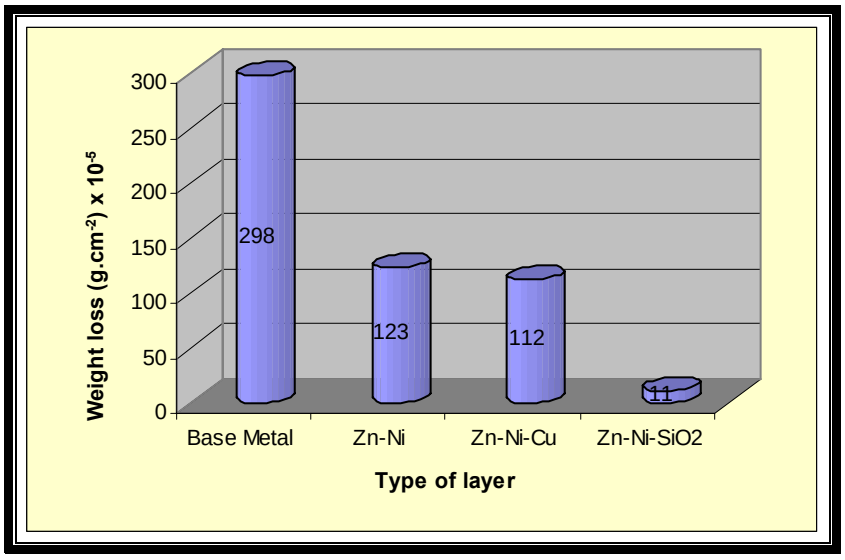

Figure (4.49) Influence of exposed Base Metal,Zn-Ni,Zn-Ni-Cu and Zn-Ni-SiO_2 in 1% HCl at ambient Temp. 15°C 24 hrs.

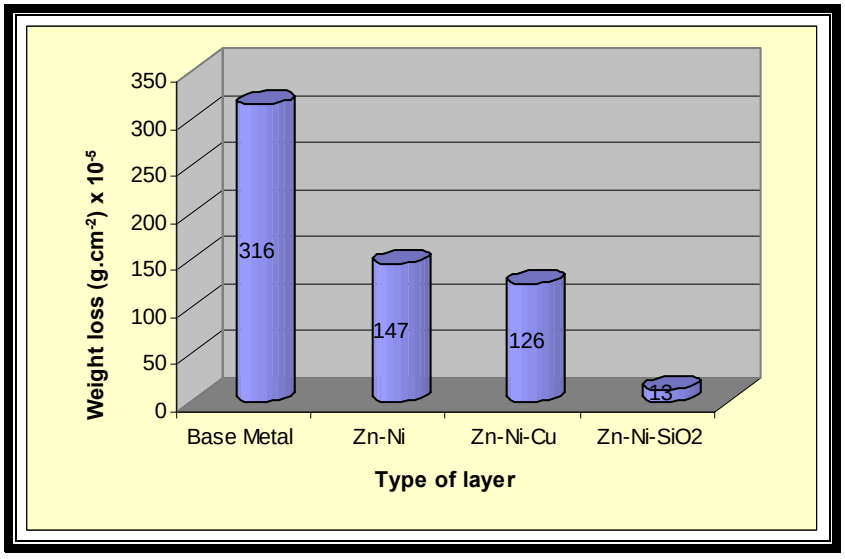

Figure (4.50) Influence of exposed Base Metal, Zn-Ni, Zn-Ni-Cu and Zn-Ni-SiO_2 1% HCl at 35°C 24 hrs.

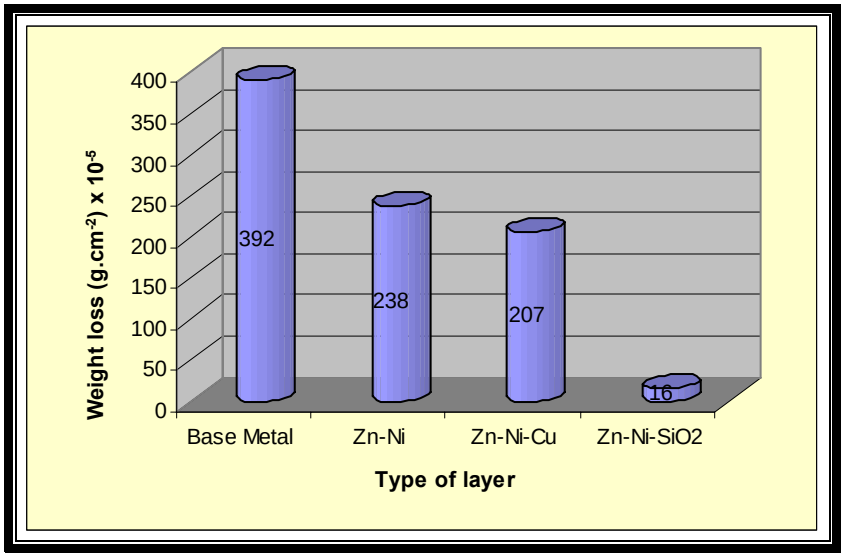

Figure (4.51) Influence of exposed Base Metal,Zn-Ni,Zn-Ni-Cu and Zn-Ni-SiO_2 in 1% HCl at 45°C 24 hrs.

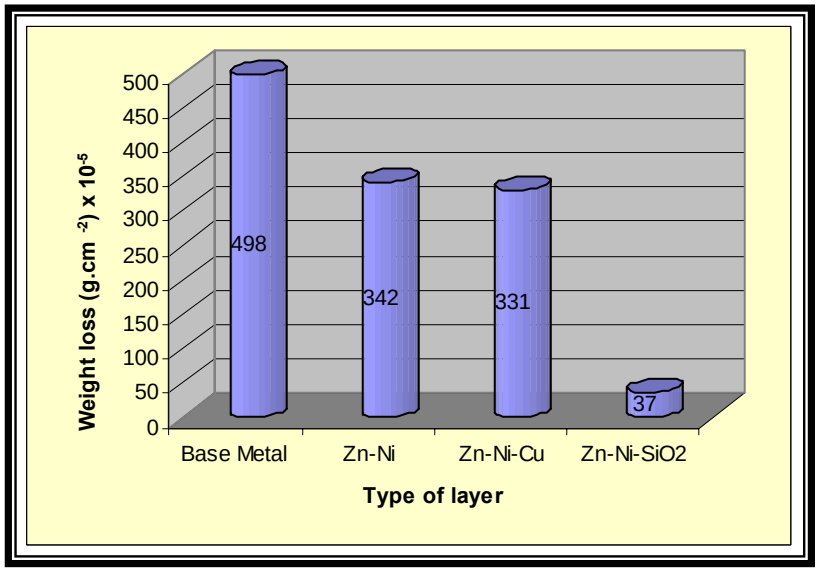

Figure (4.52) Influence of exposed Base Metal,Zn-Ni,Zn-Ni-Cu and Zn-Ni-SiO_2 in 1% HCl at 55°C 24 hrs.

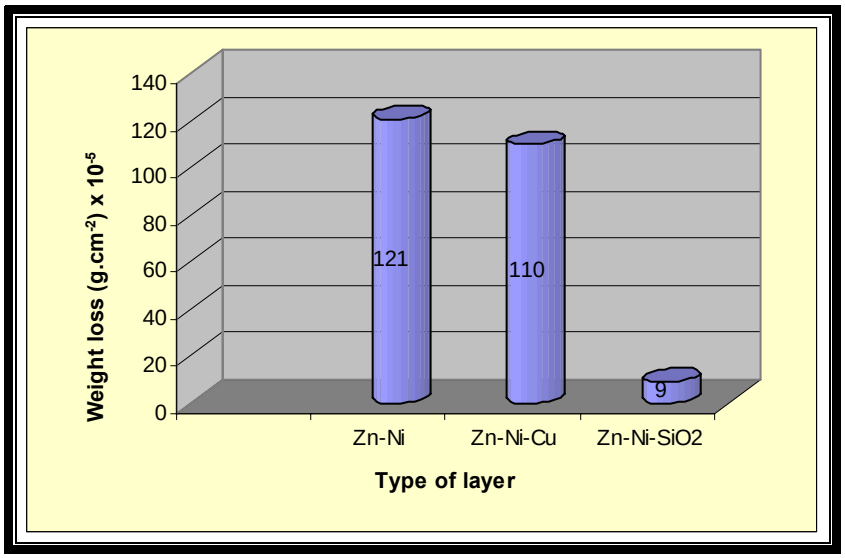

Figure (4.53) Influence of exposed Base Metal,Zn-Ni,Zn-Ni-Cu and Zn-Ni-SiO_2 (Heat Treated) in 1% HCl at ambient Temp.(15°C) 24 hrs.

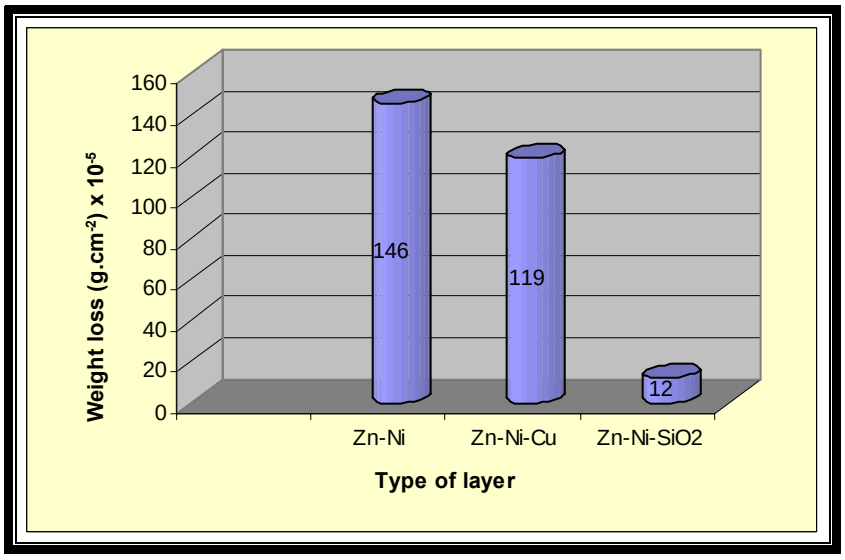

Figure (4.54) Influence of exposed Base Metal,Zn-Ni,Zn-Ni-Cu and Zn-Ni-SiO_2 (Heat Treated) in 1% HCl at 35°C 24 hrs.

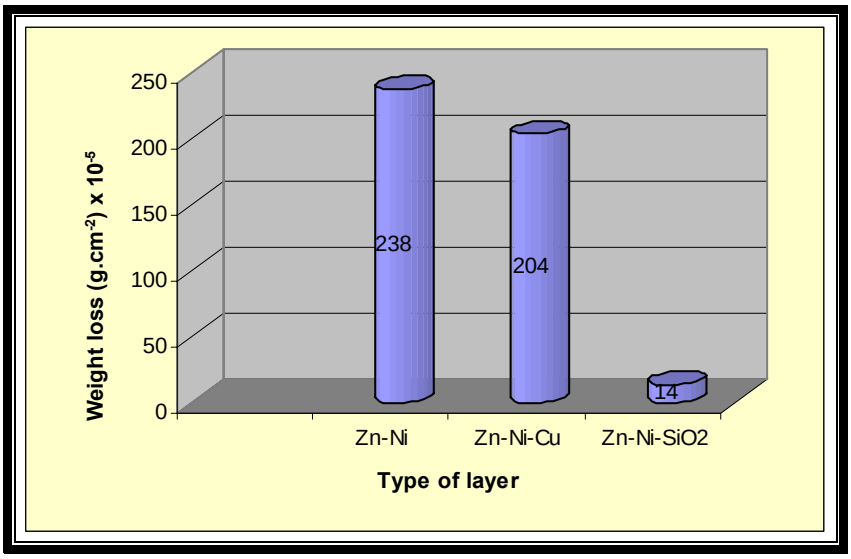

Figure (4.55) Influence of exposed Base Metal,Zn-Ni,Zn-Ni-Cu and Zn-Ni-SiO_2 (Heat Treated) in 1% HCl at 45°C 24 hrs.

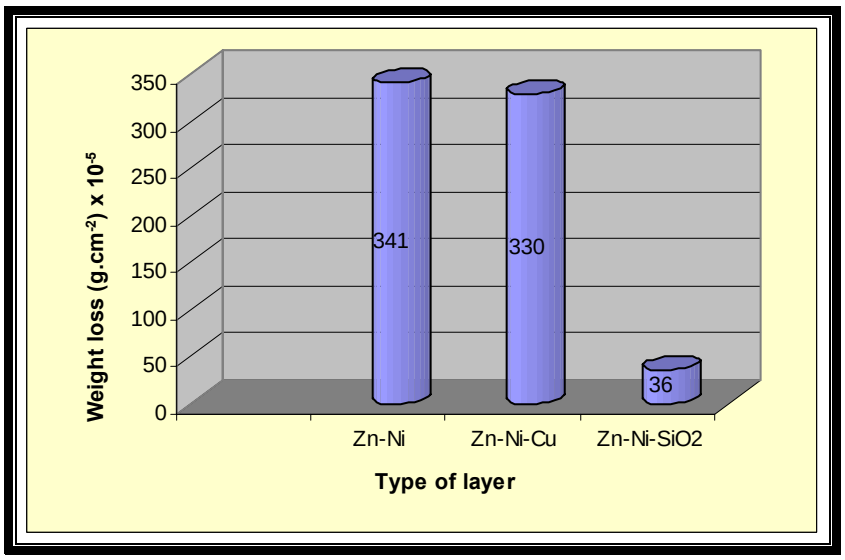

Figure (4.56) Influence of exposed Base Metal,Zn-Ni,Zn-Ni-Cu and Zn-Ni-SiO_2 (Heat Treated) in 1% HCl at 55°C 24 hrs.

It is clear once again from figures (4.49 to 4.56) the superiority of corrosion resistance of the passive layer of SiO_2 .For instance the weight loss of this layer after 24 hrs in 1% hydrochloric acid at 55°C is only

7%,10% and 11% with respect to the corresponding values of the base metal, Zn-Ni and Zn-Ni-Cu .

In spite of the fact that the famous layer of Zn-Ni is sacrificial layer for the base metal,the weight loss of this layer is 68%.This value is greatly higher than the percentage of the passive SiO_2 layer ,i.e. only 7% with respect to the base metal. The heat treatment produces a slight improvement.

Ionization of hydrochloric acid causes hydrogen ions to move towards the immersed electrode. Hydrogen ions play an important part in determing the polarization characteristics .This process is normally controlled by slowest step.

The values of corrosion currents, as gmd, mm/y and mpy are listed in Tables (4.6 to 4.13).

The corrosion currents of SiO_2 layer for instant is only ~ 7% of the corresponding value of the base metal. This value is comparable to that observed in salt spray test when tested is carried out at 35°C. Other values are almost in the same range. Table (4.6 To 4.13) calculated a corrosion rate at ambient Temp.(15 °C),35°C,45°C and 55°C for a period time 24 hrs.

Table (4.6) Corrosion rate after exposed in 1%HCl at ambient Temp. (15°C).

Metal	Base Metal	Zn-Ni	Zn-Ni-Cu	Zn-Ni-SiO_2
Δg (g)	298 $x10^{-5}$	123 $x10^{-5}$	112 $x10^{-5}$	11 $x10^{-5}$
gmd	26.3716	10.8849	9.9115	0.9734
mm/y	1.3479	0.5563	0.5066	0.0497
mpy	53.0669	21.9015	19.9448	1.9566
ί($\mu A/cm^2$)	90.1040	37.1906	33.8646	3.3259

Table (4.7) Corrosion rate after exposed in 1%HCl at 35°C

Metal	Base Metal	Zn-Ni	Zn-Ni-Cu	Zn-Ni-SiO_2
Δg (g)	316 $x10^{-5}$	147 $x10^{-5}$	126 $x10^{-5}$	13 $x10^{-5}$
gmd	27.9646	13.0088	11.1504	1.1504
mm/y	1.4294	0.6649	0.5699	0.0588
mpy	65.2755	26.1771	22.4370	2.3149
ί($\mu A/cm^2$)	95.5465	44.4473	38.0976	3.9307

Table (4.8) Corrosion rate after exposed in 1%HCl at 45°C

Metal	Base Metal	Zn-Ni	Zn-Ni-Cu	Zn-Ni-SiO_2
Δg (g)	392 $x10^{-5}$	238 $x10^{-5}$	207 $x10^{-5}$	16 $x10^{-5}$
gmd	34.6902	21.0619	18.3185	1.4159
mm/y	1.7732	1.0765	0.9363	0.0723
mpy	69.8110	42.3818	36.8622	2.8464
ί($\mu A/cm^2$)	118.5261	71.9623	62.5890	4.8378

Table (4.9) Corrosion rate after exposed in 1%HCl at 55°C

Metal	Base Metal	Zn-Ni	Zn-Ni-Cu	Zn-Ni-SiO_2
Δg (g)	498 $x10^{-5}$	342 $x10^{-5}$	331 $x10^{-5}$	37 $x10^{-5}$
gmd	44.0707	36.2654	29.2920	3.2743
mm/y	2.2526	1.8537	1.4972	0.1673
mpy	88.6850	72.9803	58.9448	6.5866
i(μA/cm^2)	150.5765	103.4080	100.0820	11.1874

Table (4.10) Corrosion rate(Heat Treated after exposed in 1%HCl at ambient Temp.(15°C).

Metal	Zn-Ni	Zn-Ni-Cu	Zn-Ni-SiO_2
Δg (g)	121 $x10^{-5}$	110 $x10^{-5}$	9 $x10^{-5}$
gmd	10.7079	9.7345	0.7964
mm/y	0.5473	0.4975	0.0407
mpy	21.5472	19.5866	1.6023
i(μA/cm^2)	36.5858	33.2598	2.7212

Table (4.11) Corrosion rate(Heat Treated) after exposed in 1%HCl at 35°C.

Metal	Zn-Ni	Zn-Ni-Cu	Zn-Ni-SiO_2
Δg (g)	146 $x10^{-5}$	119 $x10^{-5}$	12 $x10^{-5}$
gmd	12.9203	10.5309	1.0619
mm/y	0.6604	0.5382	0.0542
mpy	26	21.1889	2.1338
i(μA/cm^2)	44.1449	35.9811	3.6283

Table (4.12) Corrosion rate(Heat Treated) after exposed in 1%HCl at 45°C.

Metal	Zn-Ni	Zn-Ni-Cu	Zn-Ni-SiO_2
Δg (g)	238 $x10^{-5}$	204 $x10^{-5}$	14 $x10^{-5}$
gmd	21.0619	18.0530	1.2389
mm/y	1.0765	0.9227	0.0633
mpy	42.3818	36.3267	2.4921
¡(μA/cm^2)	71.9623	61.6819	4.2330

Table (4.13) Corrosion rate(Heat Treated) after exposed in 1%HCl at 55°C.

Metal	Zn-Ni	Zn-Ni-Cu	Zn-Ni-SiO_2
Δg (g)	341 $x10^{-5}$	330 $x10^{-5}$	36 $x10^{-5}$
gmd	30.1769	29.2035	3.1858
mm/y	1.5425	1.4927	0.1628
mpy	60.7283	58.7677	6.4094
¡(μA/cm^2)	103.1056	99.7796	10.8850

Figures (4.57 To 4.63) indicate the corrosion conduct at 45°C in aggressive medium. A sever damage is expected to occur in the base metal as shown in the optical photograph in figure (4.57).A cracking and spalling of the thick layer are clear in the SEM micrographs figures (4.64 a,b and c).

For Zn-Ni coating less damage occurs as shown in the optical photograph figure(4.58) and SEM micrograph figures(4.65 a and b), It is also clear some sort of spalling.

Cracking is clear in Zn-Ni-Cu coating ,especially in SEM micrograph figure (4.66 b).

In the case of SiO_2 a great improvement is observed in SEM micrograph figures (4.67 a and b).No cracking or spalling is observed. This is in accordance with the measured values of weight losses in measured in section (4.6.3).

Cracking and spalling are still observed in certain samples even after heat treatment figures (4.68 and 4.69).

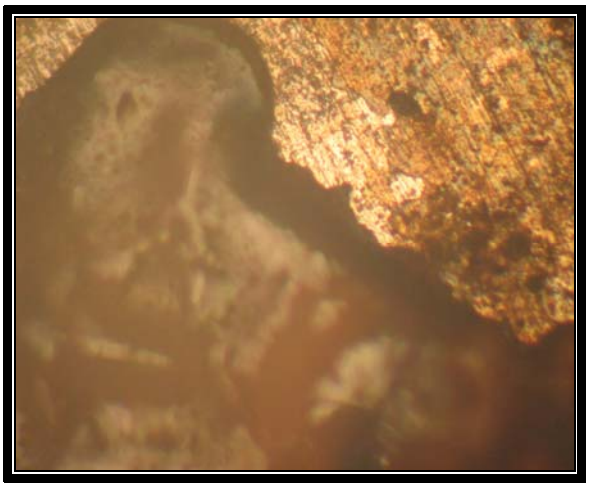

Figure (4.57) LOM images of surface damage on Base Metal after exposed in 1% HCl at 45°C 24 hrs.

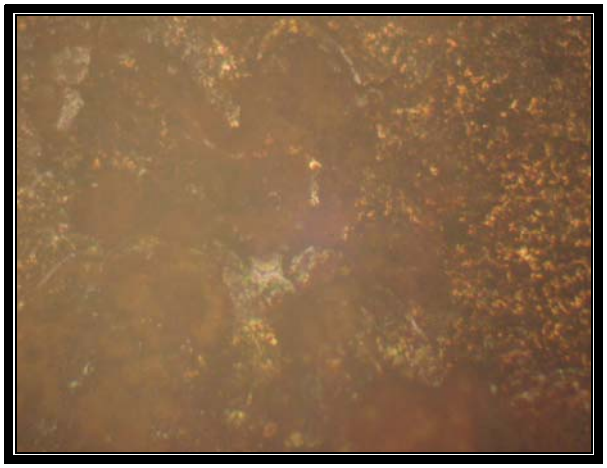

Figure (4.58) LOM images of surface damage on Zn-Ni after exposed in 1% HCl at 45°C 24 hrs.

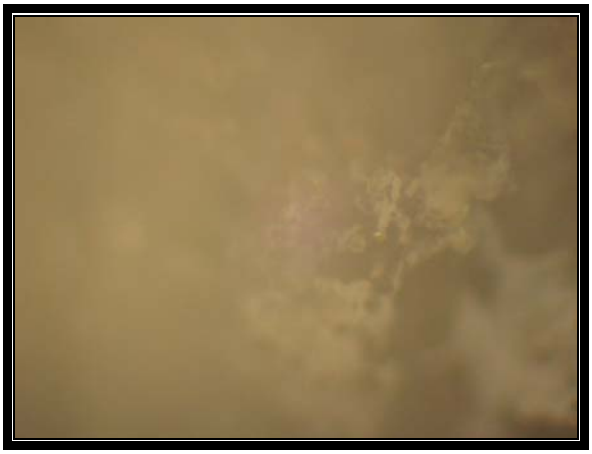

Figure (4.59) LOM images of surface damage on Zn-Ni-Cu after exposed in 1% HCl at 45°C 24 hrs.

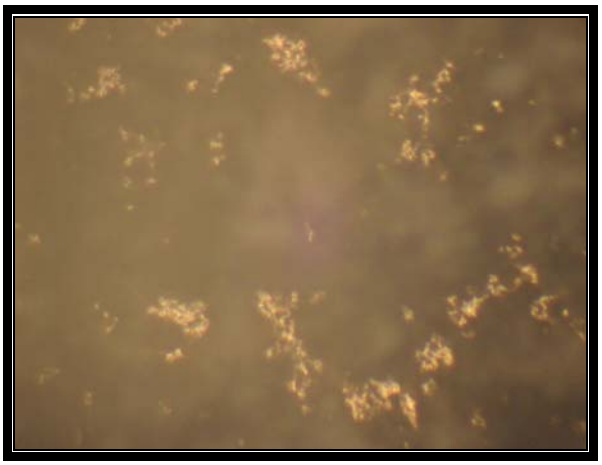

Figure (4.60) LOM images of surface damage on Zn-Ni-SiO_2 after exposed in 1% HCl at 45°C 24 hrs.

Zn-Ni-SiO_2

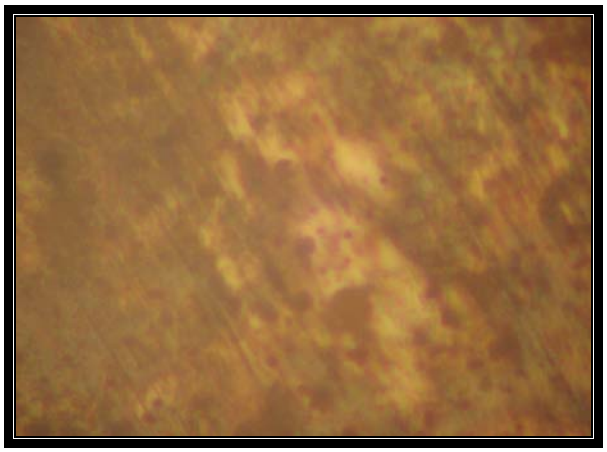

Figure (4.61) LOM images of surface damage on Zn-Ni (Heat Treated) after exposed in 1% HCl at 45°C 24 hrs.

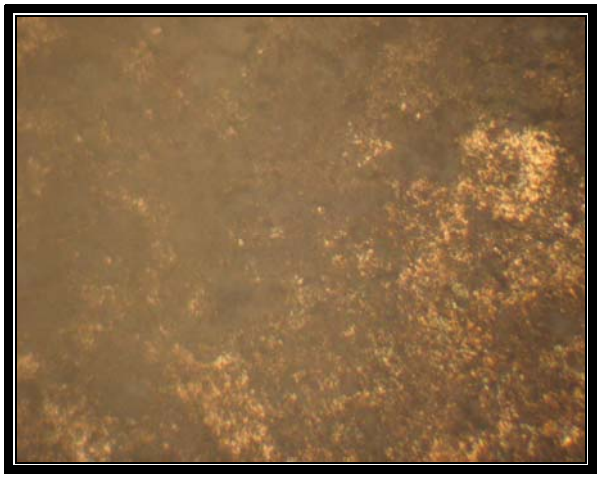

Figure (4.62) LOM images of surface damage on Zn-Ni-Cu (Heat Treated) after exposed in 1% HCl at 45°C 24 hrs.

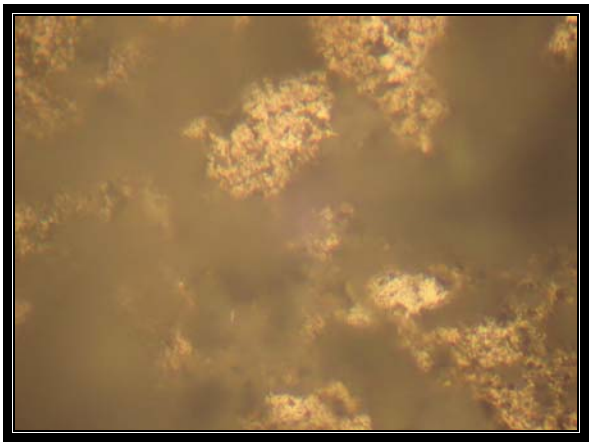

Figure (4.63) LOM images of surface damage on Zn-Ni-SiO_2 (Heat Treated) after exposed in 1% HCl at 45°C 24 hrs.

Figures (4.64 To 4.70) show SEM for Base Metal, Zn-Ni, Zn-Ni-Cu and Zn-Ni-SiO_2 before and after heat treated.

Figure (4.64 a) SEM micrographs of X150 for Base Metal after exposed in 1% HCl at 45°C 24 hrs.

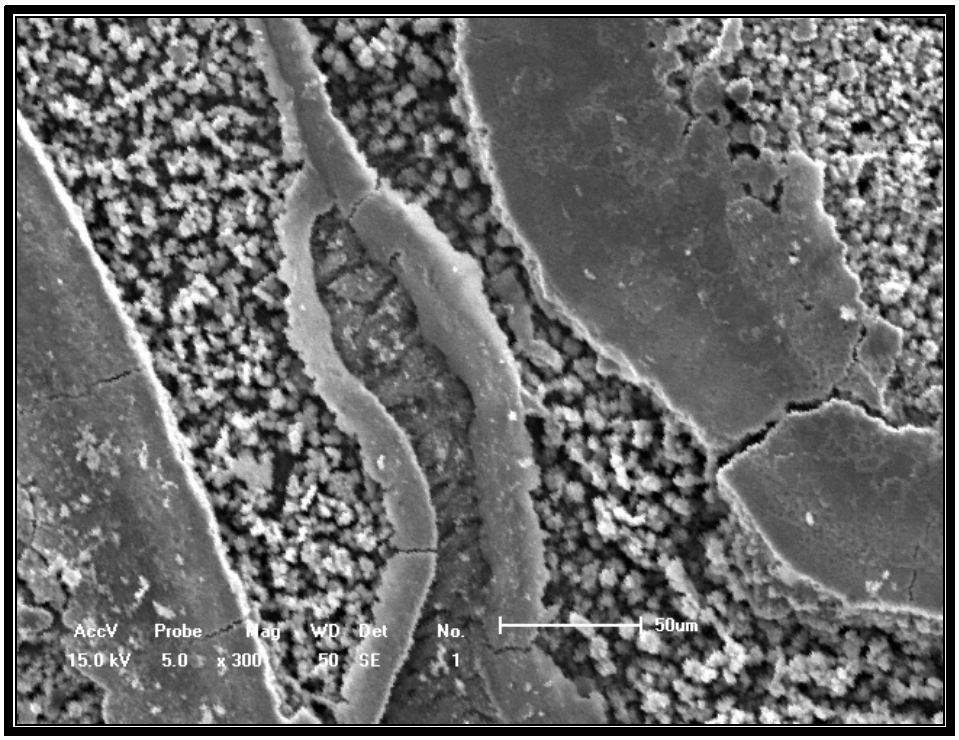

Figure (4.64 b) SEM micrographs of X300 for Base Metal after exposed in 1% HCl at 45°C 24 hrs.

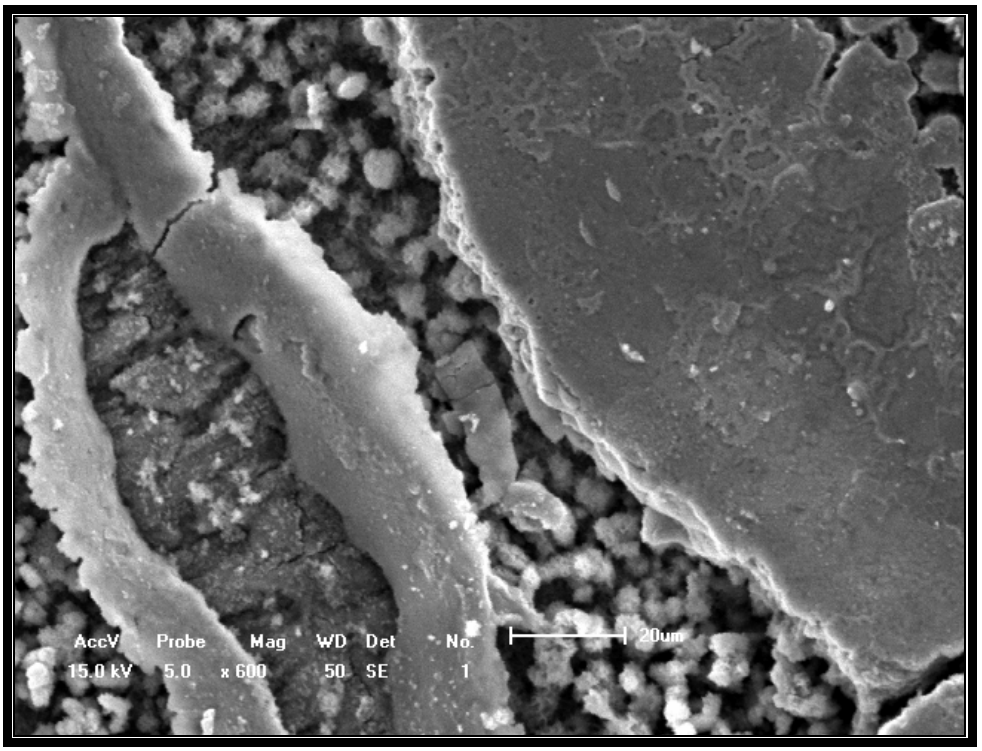

Figure (4.64 c) SEM micrographs of X600 for Base Metal after exposed in 1% HCl at 45°C 24 hrs.

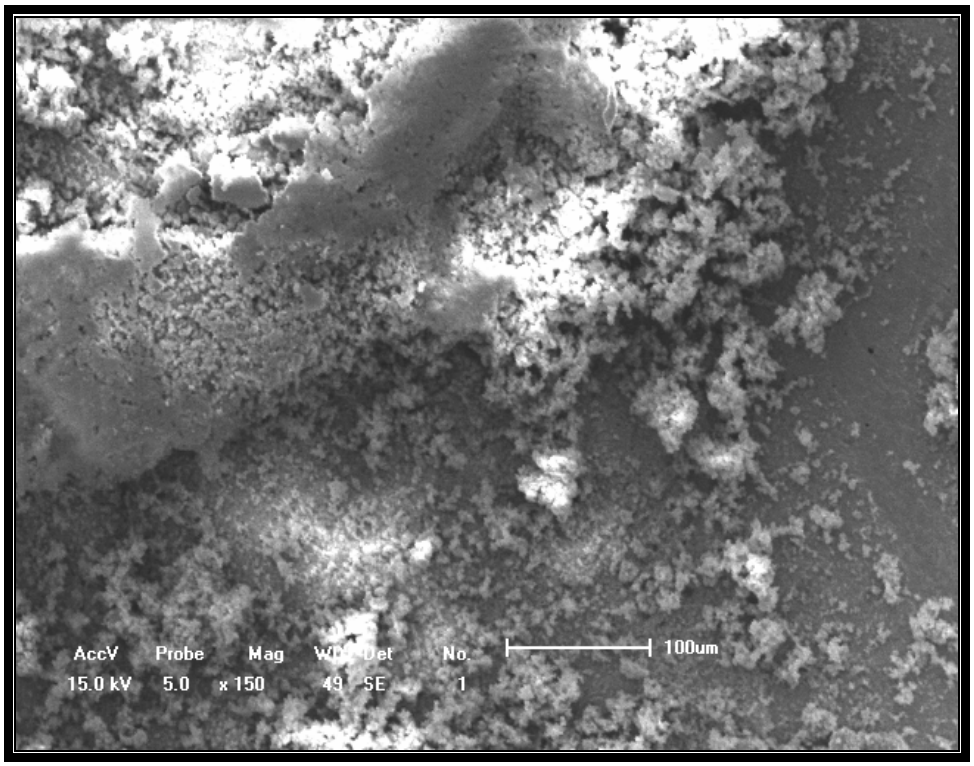

Figure (4.65 a) SEM micrographs of X150 for Zn-Ni after exposed in 1% HCl at 45°C 24 hrs.

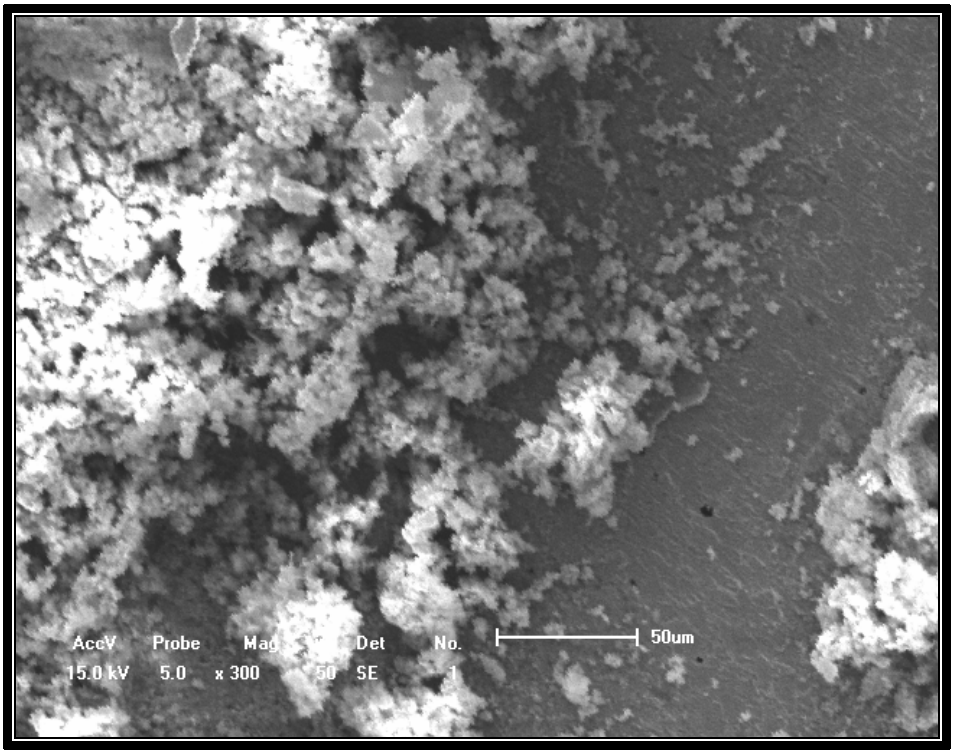

Figure (4.65 b) SEM micrographs of X300 for Zn-Ni after exposed in 1% HCl at 45°C 24 hrs.

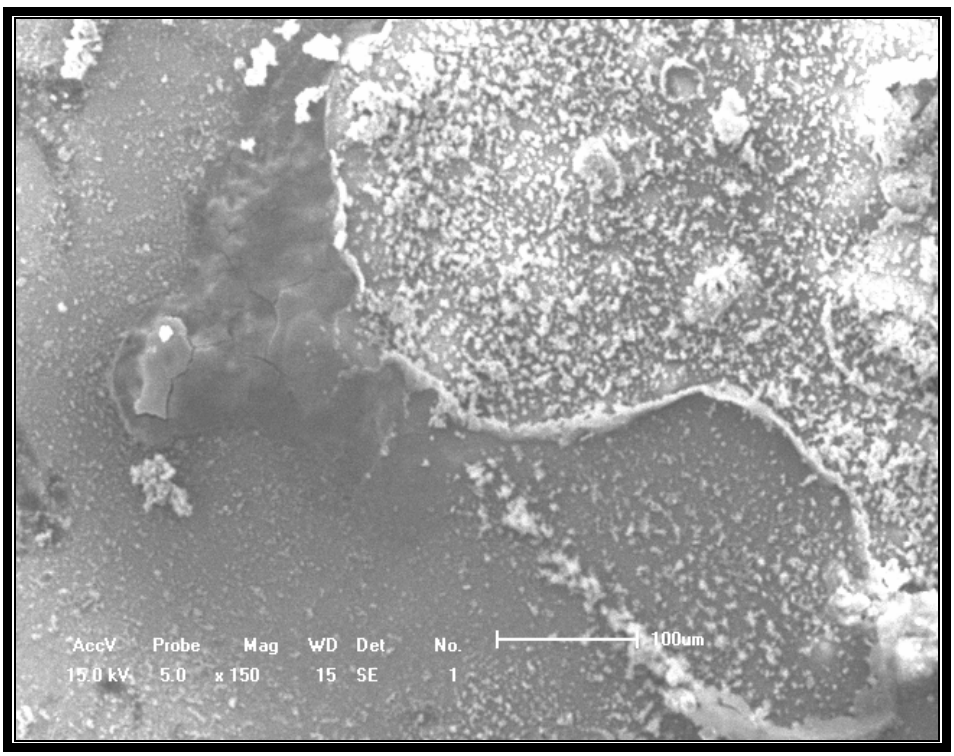

Figure (4.66 a) SEM micrographs of X150 for Zn-Ni-Cu after exposed in 1% HCl at 45°C 24 hrs.

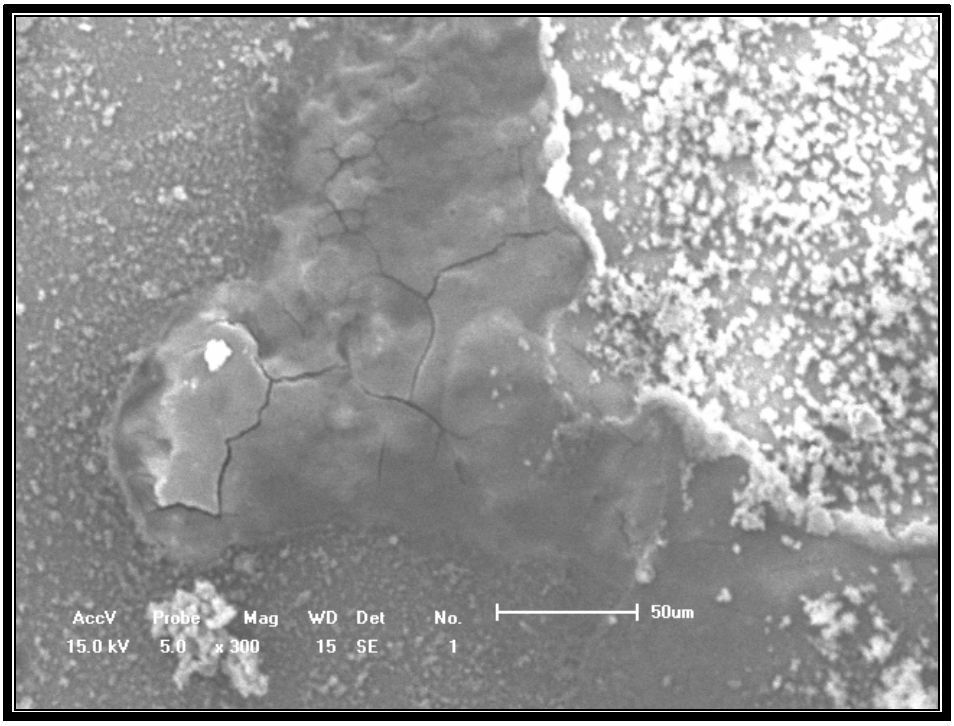

Figure (4.66 b) SEM micrographs of X300 for Zn-Ni-Cu after exposed in 1% HCl at 45°C 24 hrs.

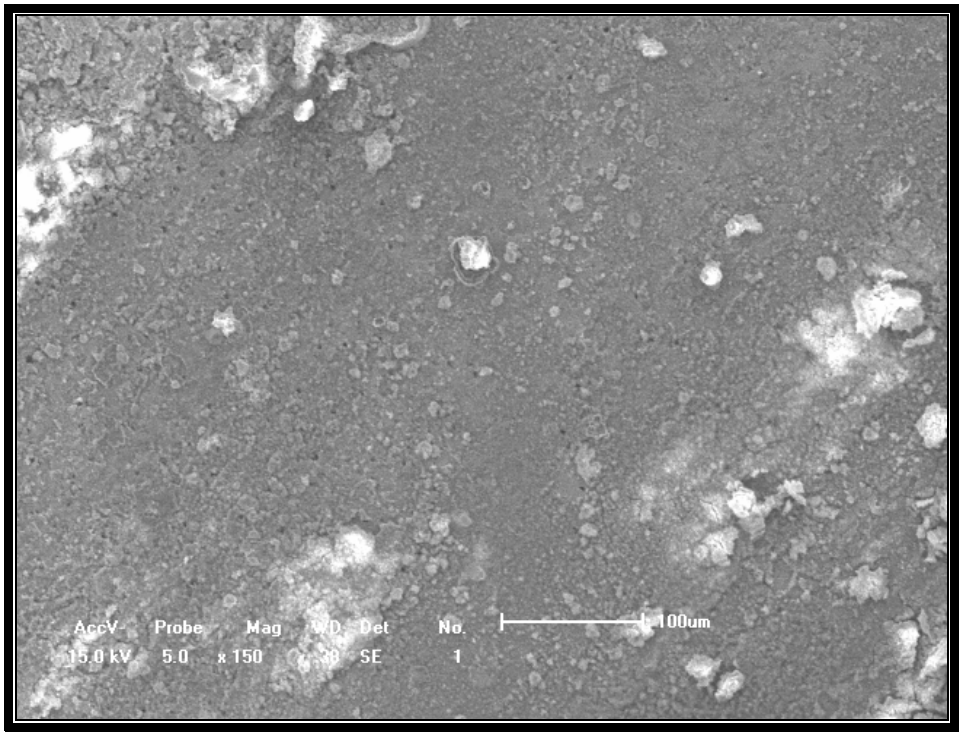

Figure (4.67 a) SEM micrographs of X150 for Zn-Ni-SiO_2 after exposed in 1% HCl at 45°C 24 hrs.

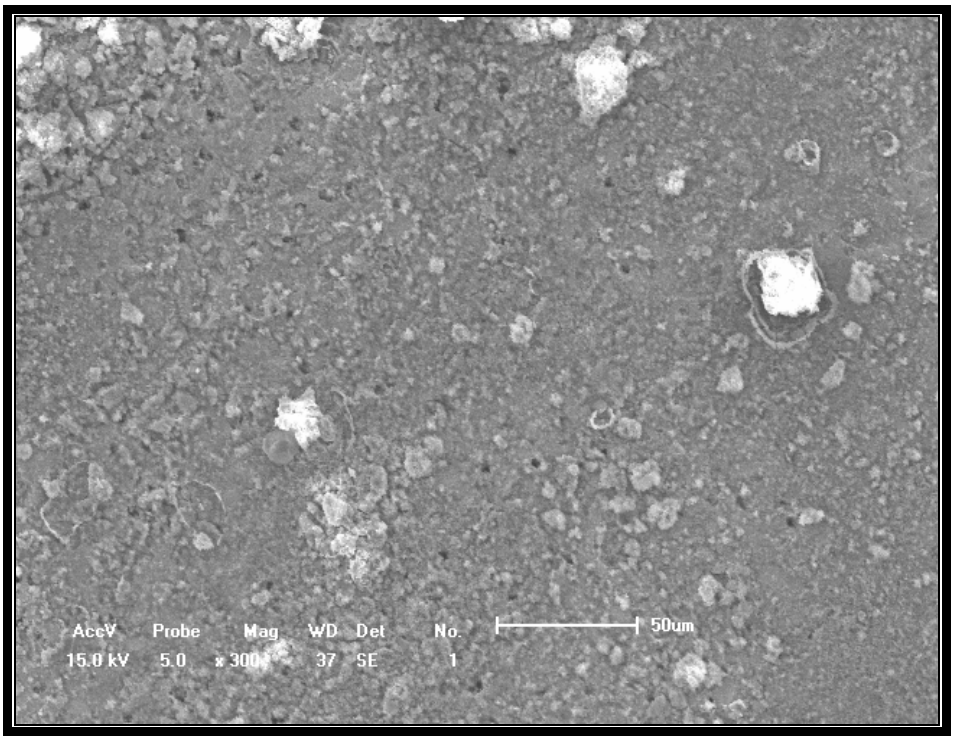

Figure (4.67 b) SEM micrographs of X300 for Zn-Ni-SiO_2 after exposed in 1% HCl at 45°C 24 hrs.

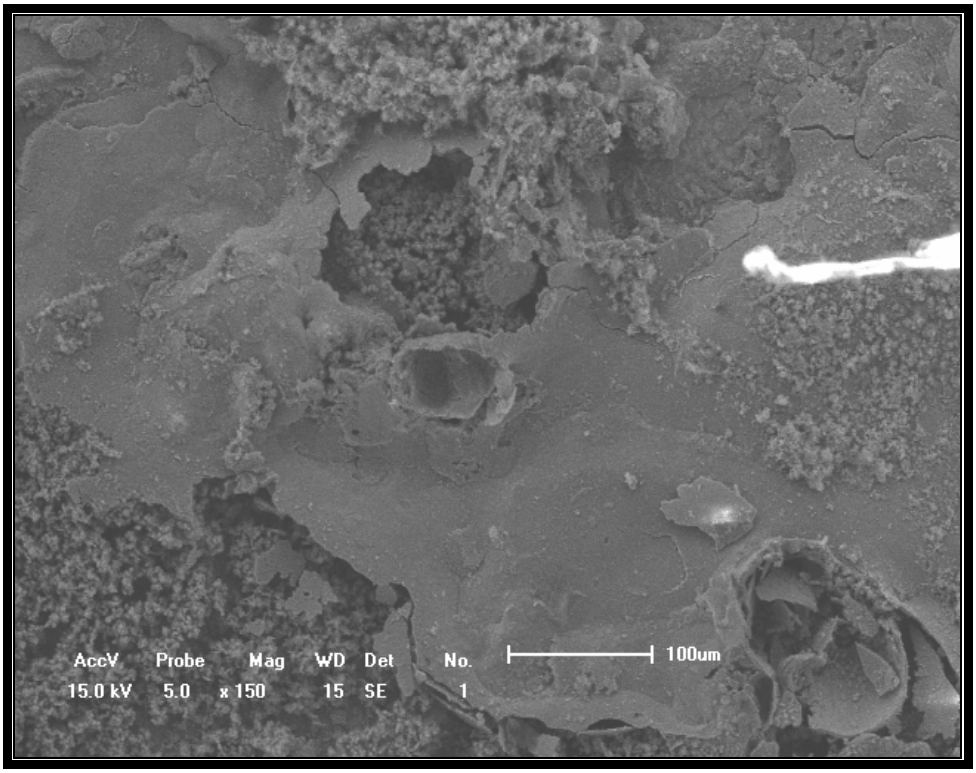

Figure (4.68 a) SEM micrographs of X150 for Zn-Ni (Heat Treated after exposed in 1% HCl at 45°C 24 hrs.

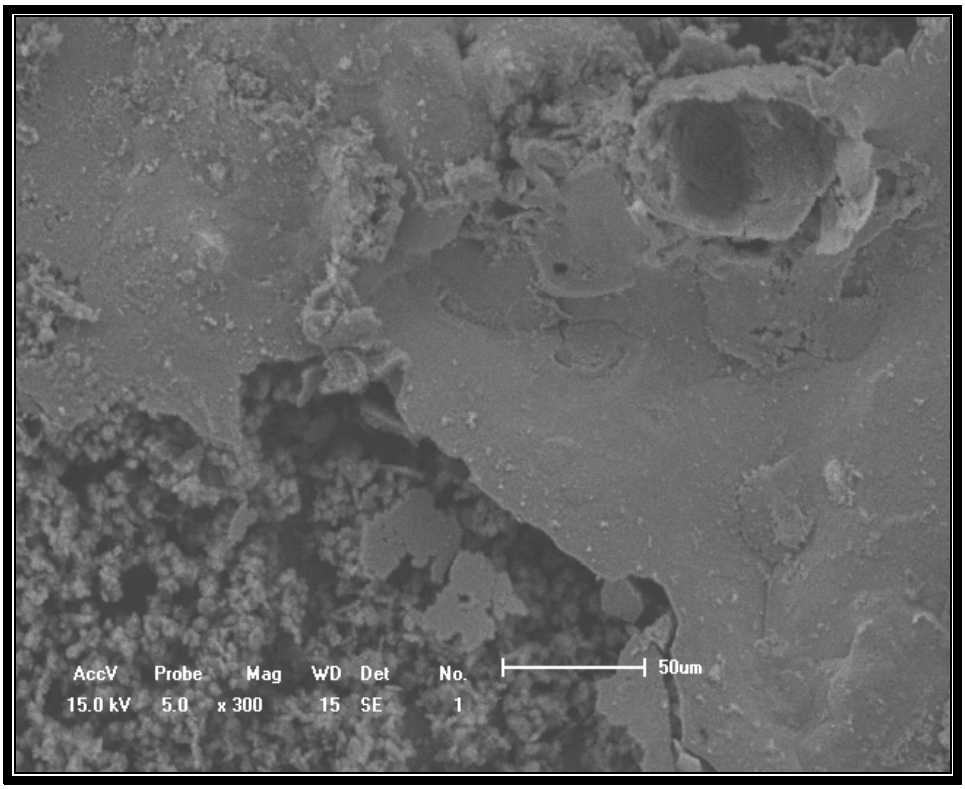

Figure (4.68 b) SEM micrographs of X300 for Zn-Ni (Heat Treated) after exposed in 1% HCl at 45°C 24 hrs.

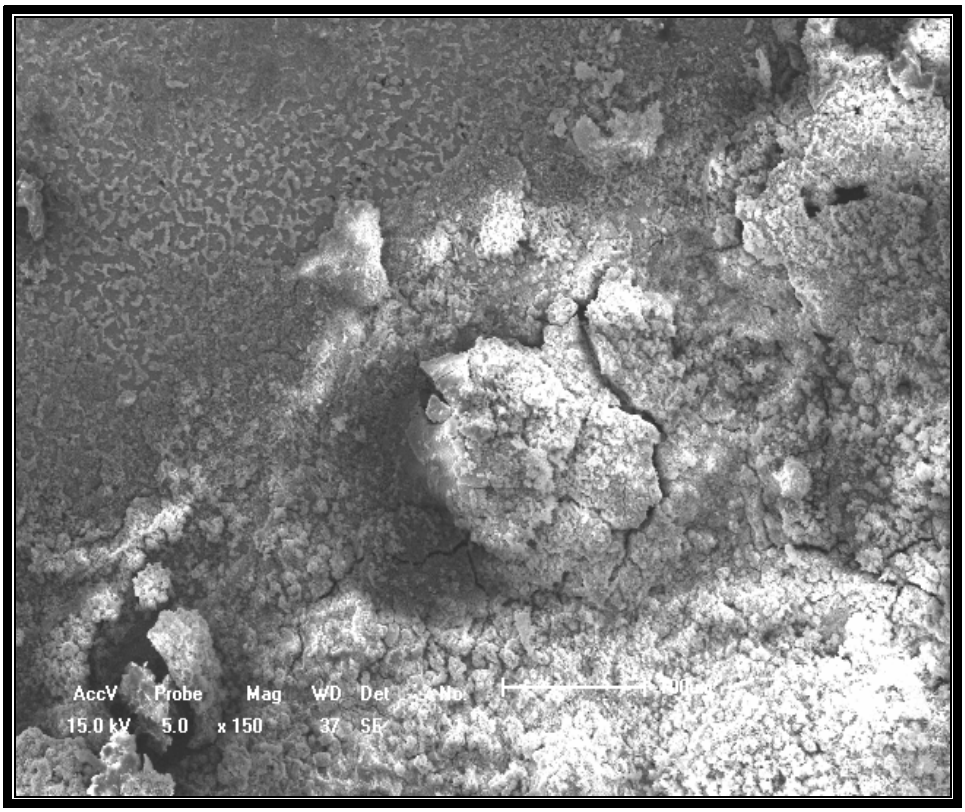

Figure (4.69 a) SEM micrographs of X150 for Zn-Ni-Cu (Heat Treated) after exposed in 1% HCl at 45°C 24 hrs.

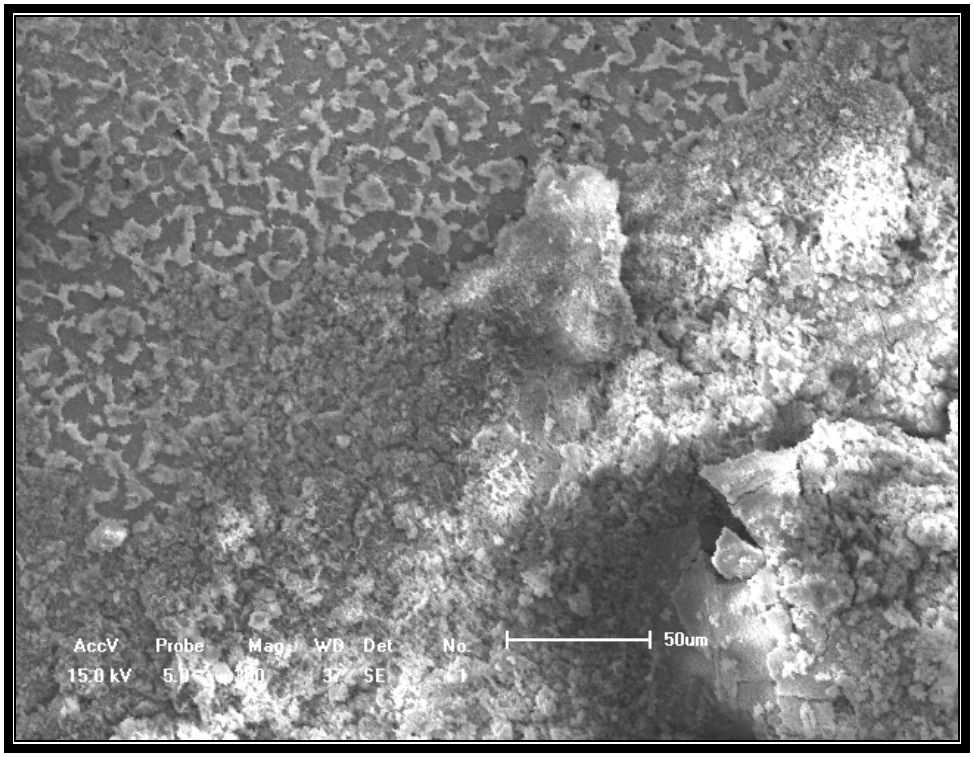

Figure (4.69b) SEM micrographs of X300 for Zn-Ni-Cu (Heat Treated) after exposed in 1% HCl at 45°C 24 hrs.

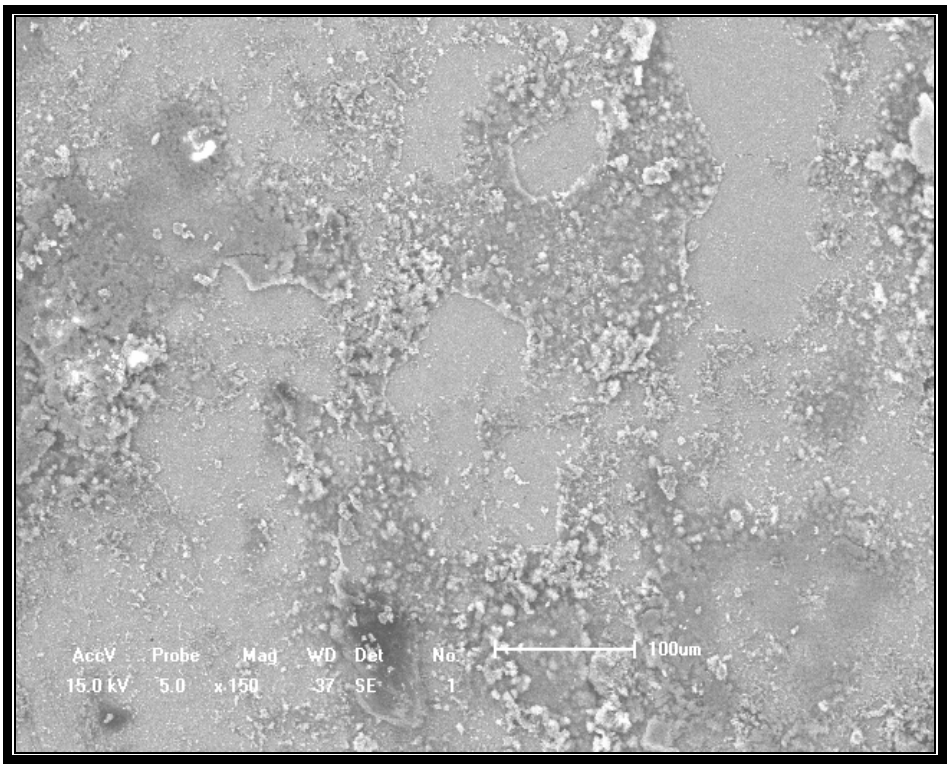

Figure (4.70 a) SEM micrographs of X150 for Zn-Ni-SiO_2 (Heat Treated) after exposed in 1% HCl at 45°C 24 hrs.

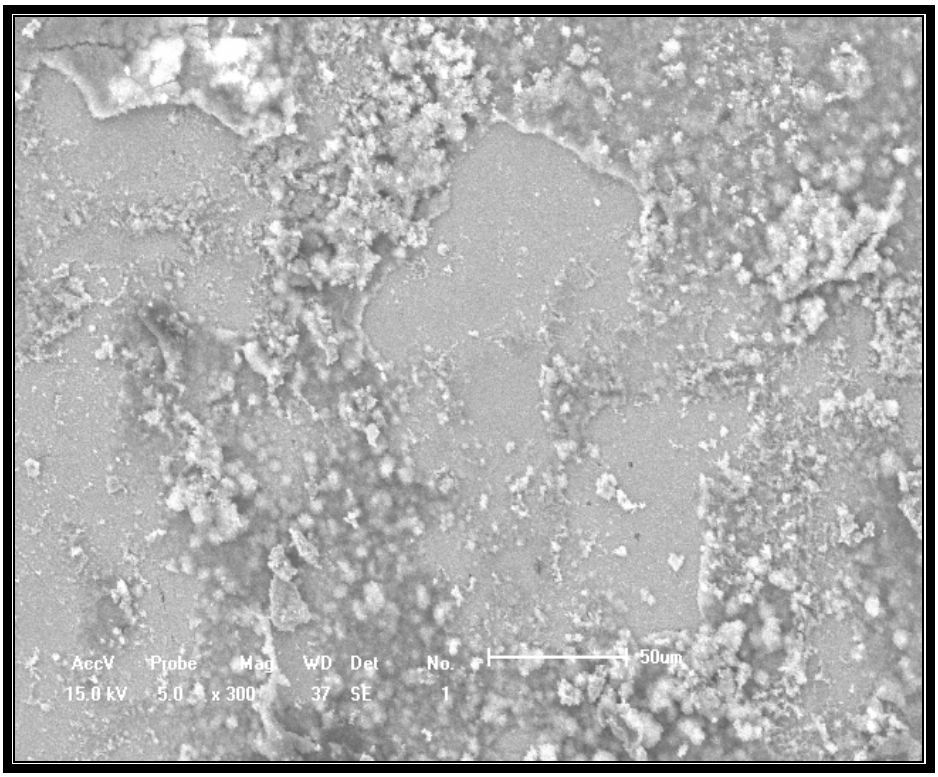

Figure (4.70 b) SEM micrographs of X300 for Zn-Ni-SiO_2 (Heat Treated) after exposed in 1% HCl at 45°C 24 hrs.

4.6.4 Humidity Test

Humidity is the amount of water vapor in the air, causes corrosion for metals.

This test was carried out in the presence of humidity on Base Metal, Zn-Ni, Zn-Ni-Cu and Zn-Ni-SiO_2 before and after heat treatment at 200 °C 1 hr at temperature 35 °C,45°C and 55°C for 50% humidity 24 hrs.

In this test, samples are exposed to a mild corrosion medium similar to natural environment of certain countries. Since, these coatings are used for aerospace industries.

It obvious from figures (4.71 to 4.76) that before and after heat treatment once again a significant corrosion resistance is recorded in the case of Zn-Ni-SiO_2 coatings. For example the weight loss of this layer is

only about (~2%) corresponding to the base metal. In this case of Zn-Ni layer its weight loss was only 27% with respect to the base metal at 55°C.

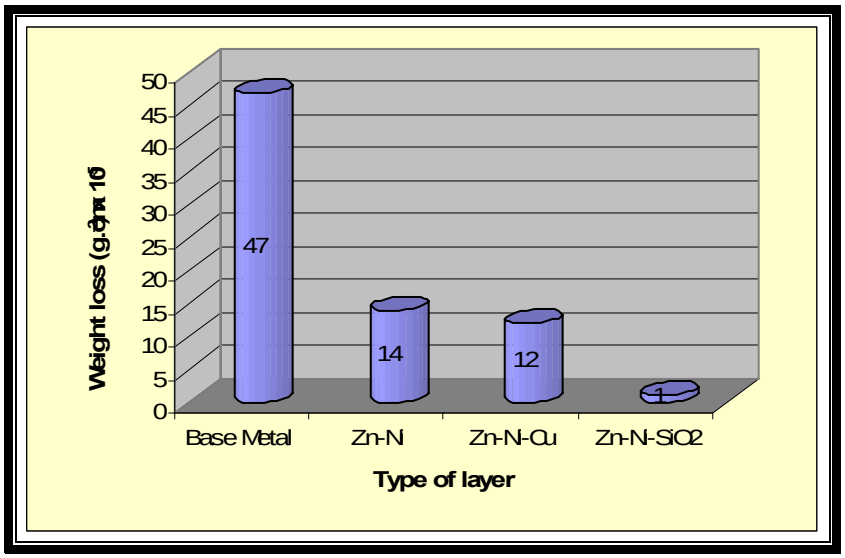

Figure (4.71) Influence of exposed Base Metal, Zn-Ni, Zn-Ni-Cu and Zn-Ni-SiO_2 in humidity chamber after 24 hrs at 35°C , 50% humidity.

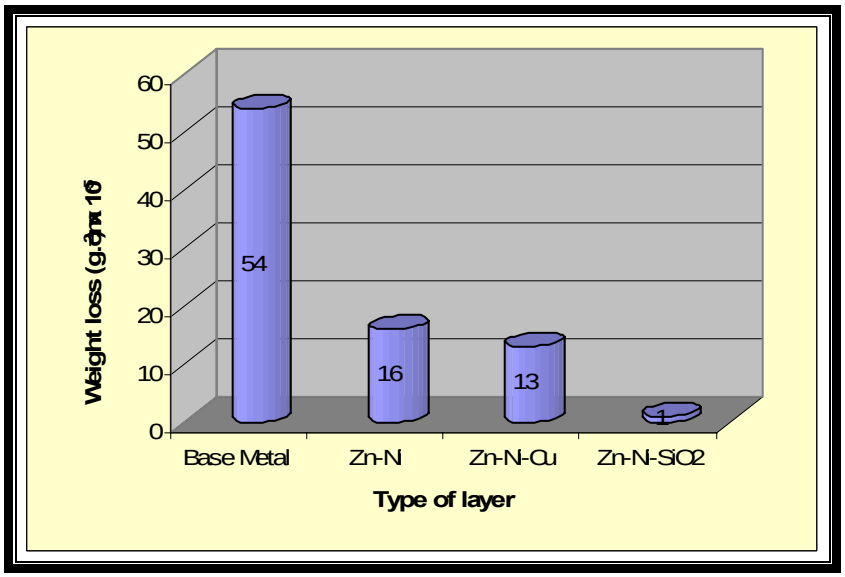

Figure (4.72) Influence of exposed Base Metal, Zn-Ni, Zn-Ni-Cu and Zn-Ni-SiO_2 in humidity chamber after 24 hrs at 45°C , 50% humidity.

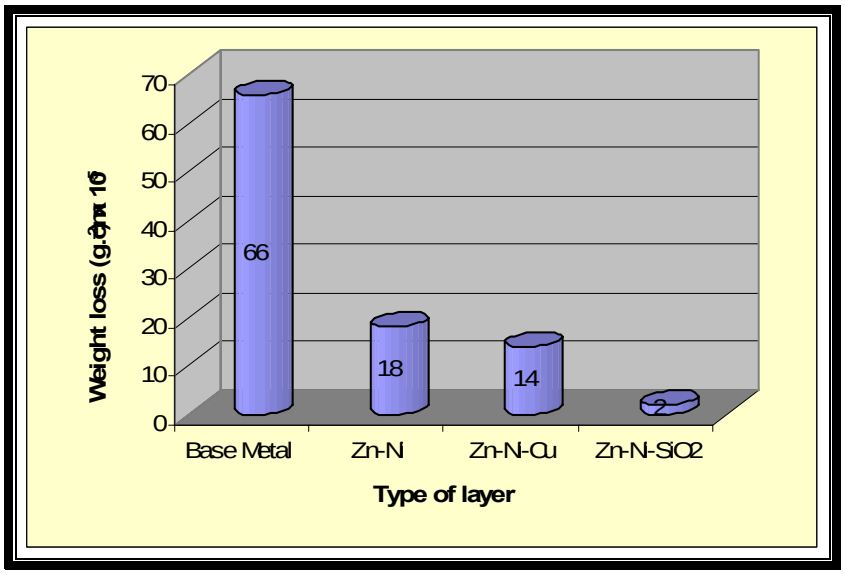

Figure (4.73) Influence of exposed Base Metal, Zn-Ni, Zn-Ni-Cu and Zn-Ni-SiO_2 in humidity chamber after 24 hrs at 55°C , 50% humidity.

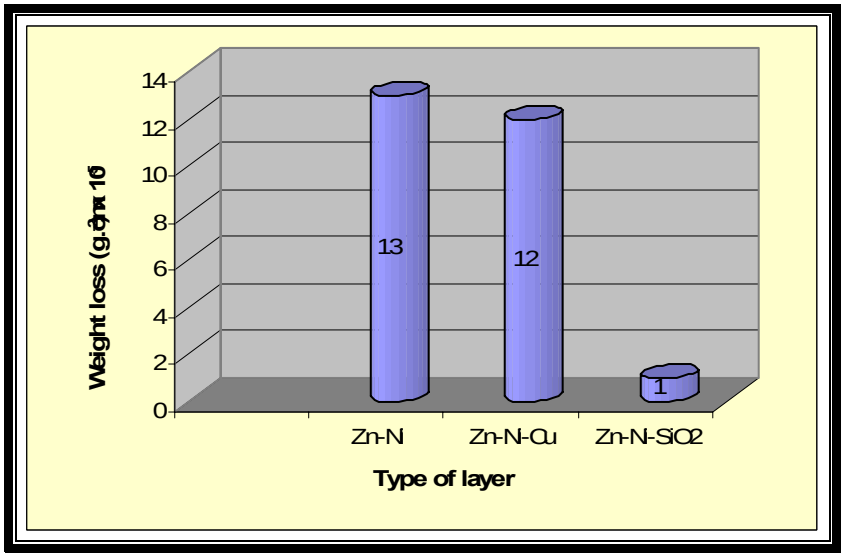

Figure (4.74) Influence of exposed Base Metal, Zn-Ni, Zn-Ni-Cu and Zn-Ni-SiO_2 (Heat Treated) in humidity chamber after 24 hrs at 35°C , 50% humidity.

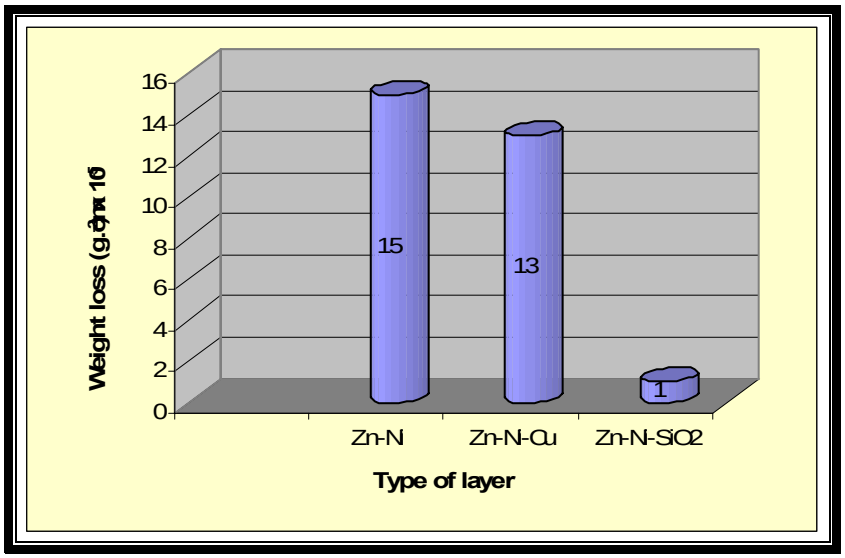

Figure (4.75) Influence of exposed Base Metal, Zn-Ni, Zn-Ni-Cu and Zn-Ni-SiO_2 (Heat Treated) in humidity chamber after 24 hrs at 45°C , 50% humidity.

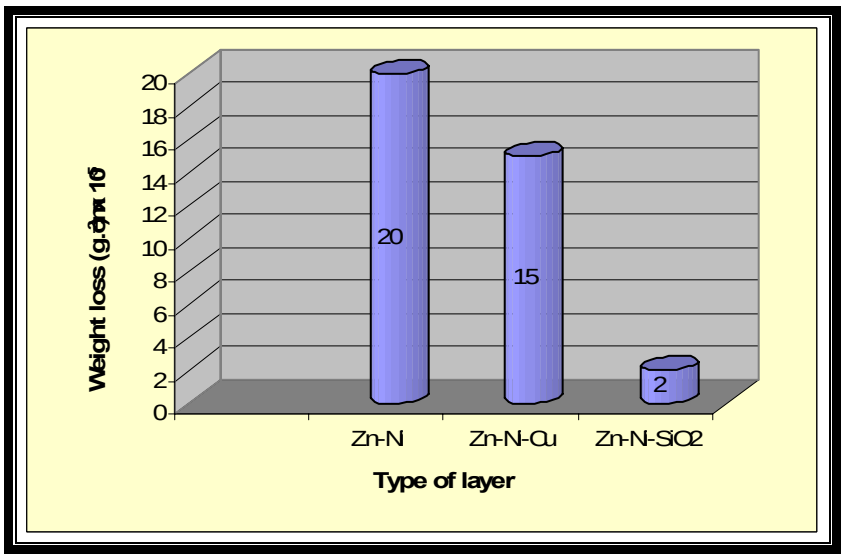

Figure (4.76) Influence of exposed Base Metal, Zn-Ni, Zn-Ni-Cu and Zn-Ni-SiO_2 (Heat Treated) in humidity chamber after 24 hrs at 55°C , 50% humidity.

4.7 Thermal shock test

This test is a measurement of plasticity , adhesive and stability range of the coating layers[160]. This test was carried out at varies temperature ranges (250,300,350,400,450,500 and 550°C) at intervals of 50 °C. Samples were water quenched after 15 min at each temperature, figure (4.77).

It is clear that all coatings exhibits shock resistance at temperature up to 350 °C. After this temperature a great cracking and spalling occurs in Zn-Ni coating figures(4.78 a,b and c) and Zn-Ni-Cu coating figures(4.79a,b and c). However, Zn-Ni-SiO_2 shows an outstanding resistance even at higher degrees as in figures(4.80a and b).

Sudden cooling (quenching) from high temperature induces stresses into the coatings.Zn-Ni-SiO_2 coating appeared to have good plasticity and adhesion with Zn-Ni rich coating.

These coatings seem to have values of thermal expansion matching in such a way to minimize the effects of variation in thermal expansion and hence, the induced stresses. Several mechanisms are proposed for the good adhesion and more likely one is the mechanical keying[161].

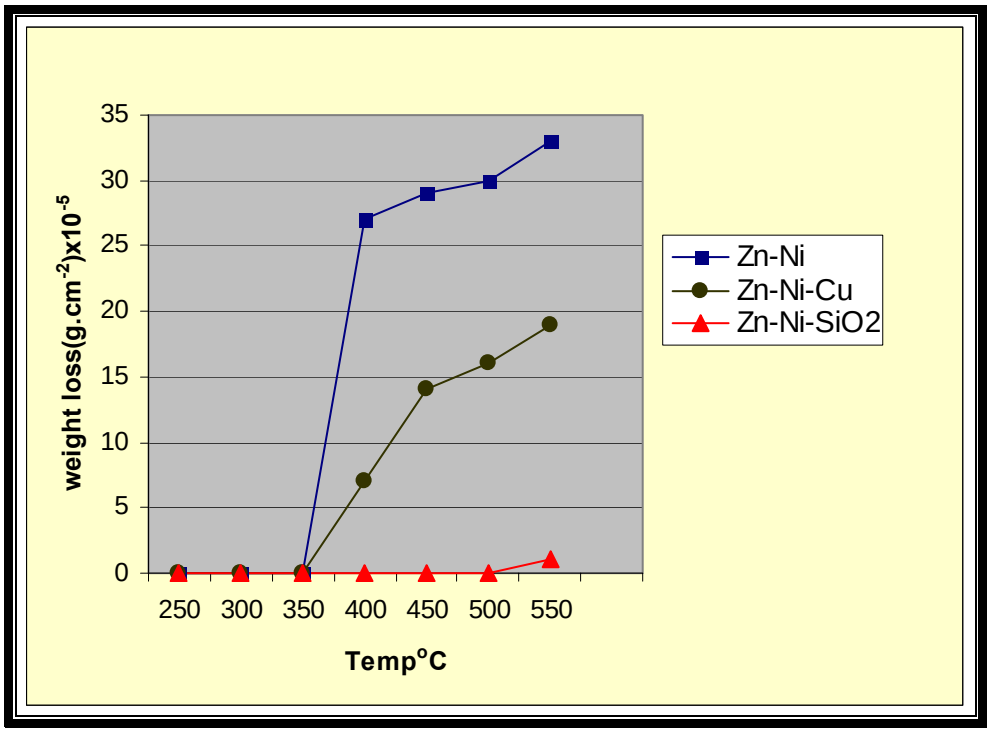

Figure.(4.77) Influence thermal shock on the weight loss

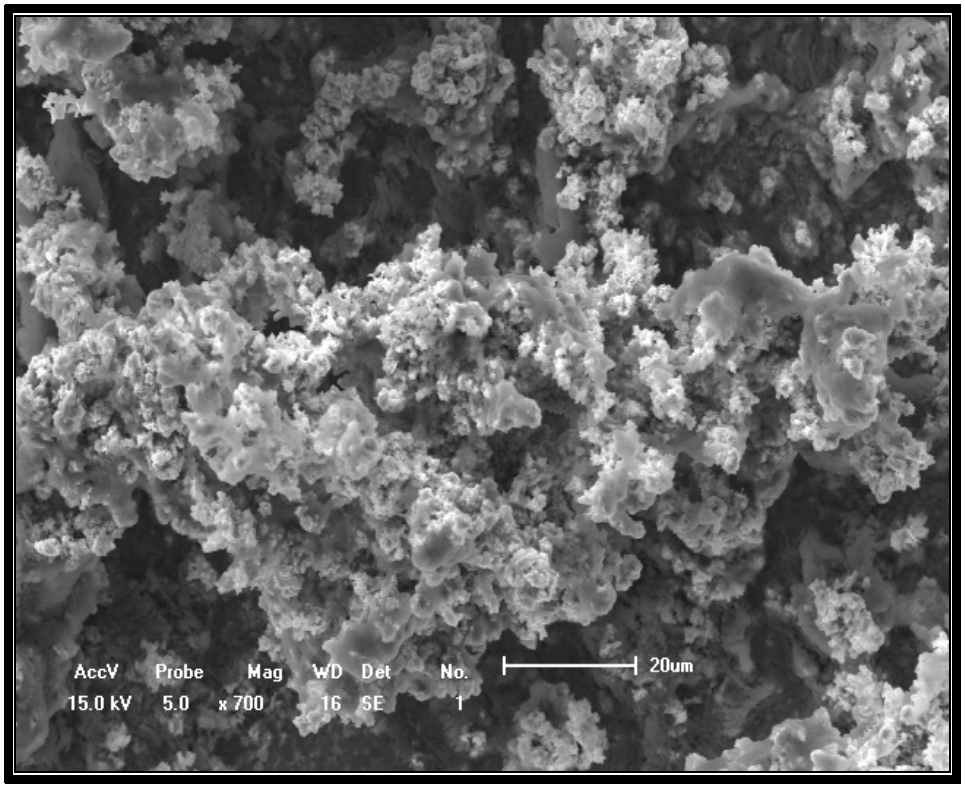

Figure (4.78 a) SEM PictureX700 for Zn-Ni after thermal shock.

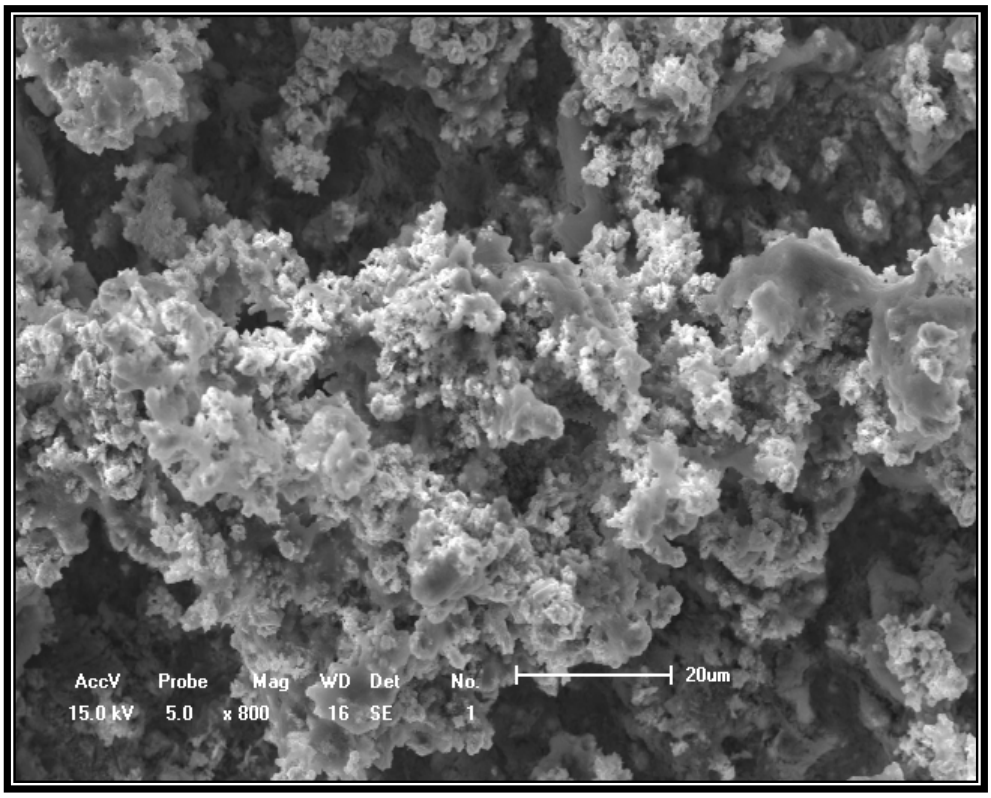

Figure (4.78 b) SEM PictureX800 for Zn-Ni after thermal shock.

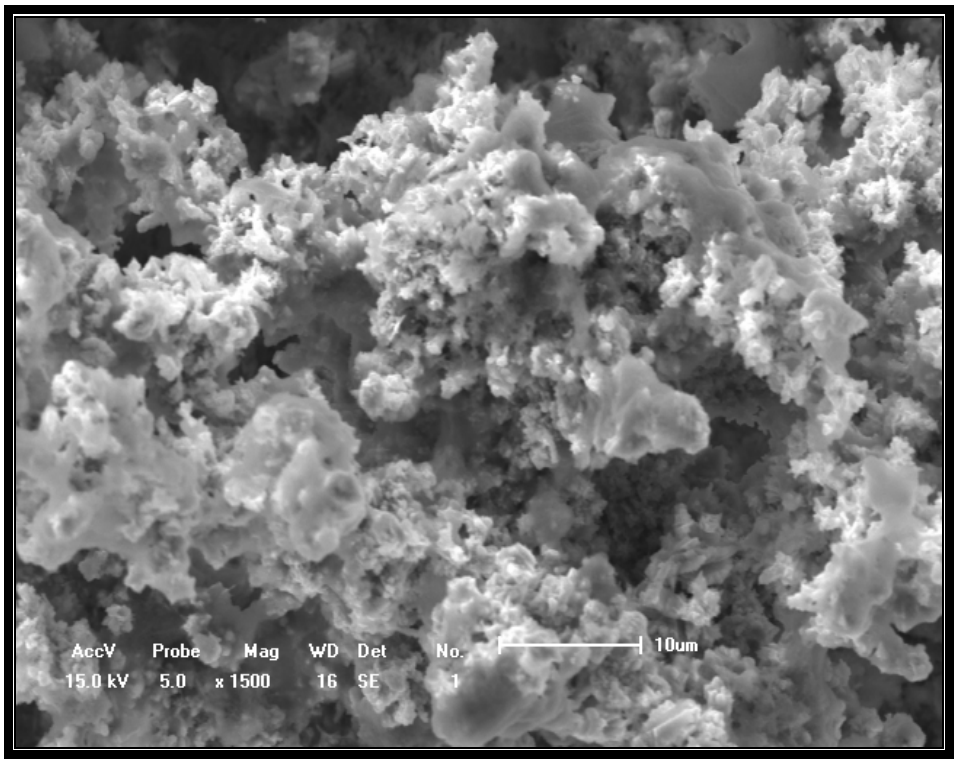

Figure (4.78 c) SEM PictureX1500 for Zn-Ni after thermal shock.

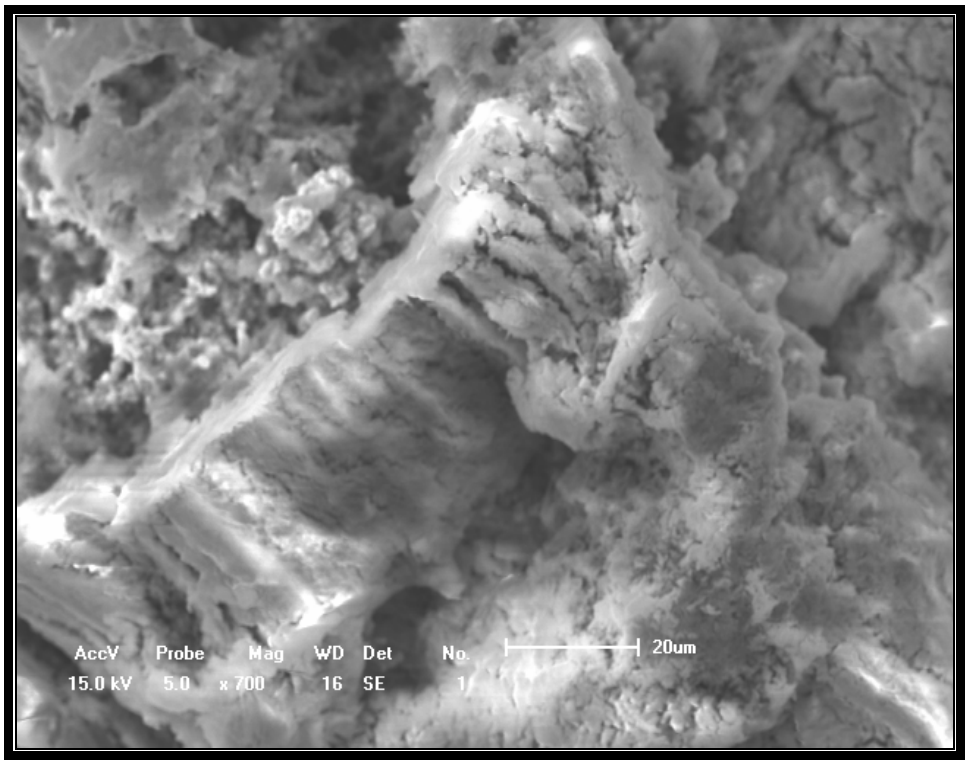

Figure (4.79 a) SEM PictureX700 for Zn-Ni-Cu after thermal shock.

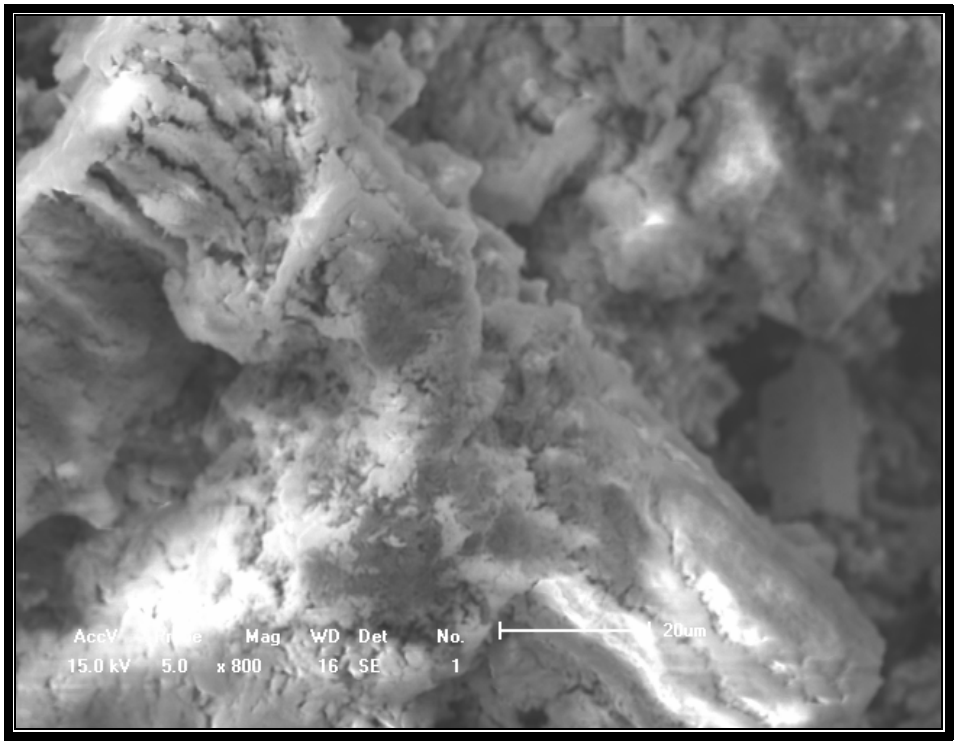

Figure (4.79 b) SEM PictureX800 for Zn-Ni-Cu after thermal shock.

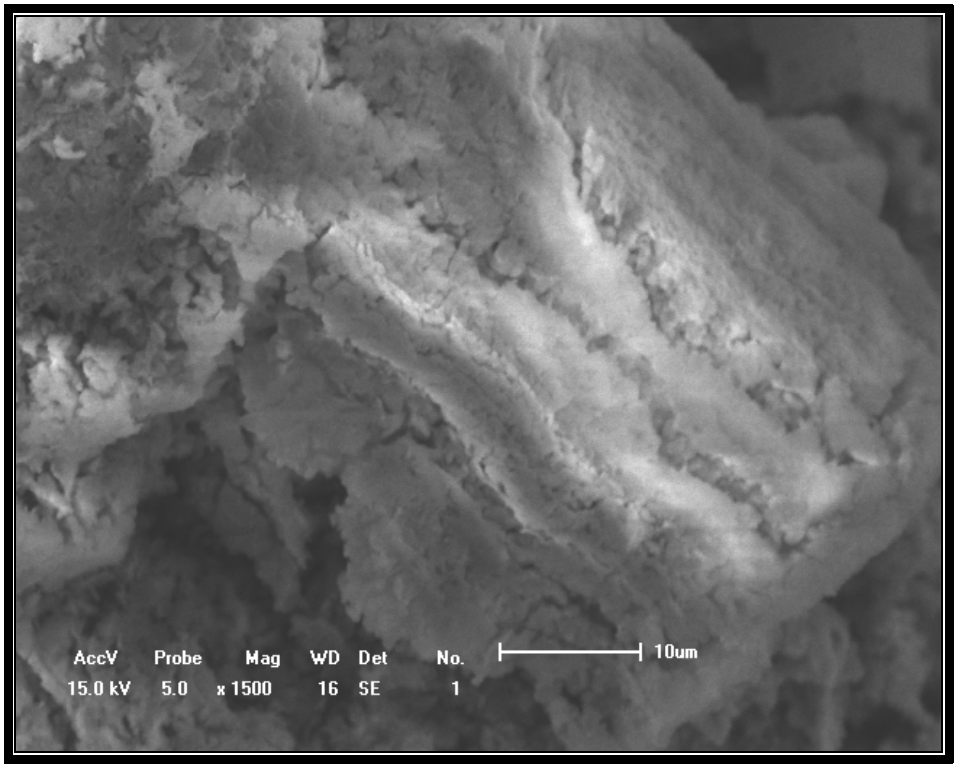

Figure (4.79 c) SEM PictureX1500 for Zn-Ni-Cu after thermal shock.

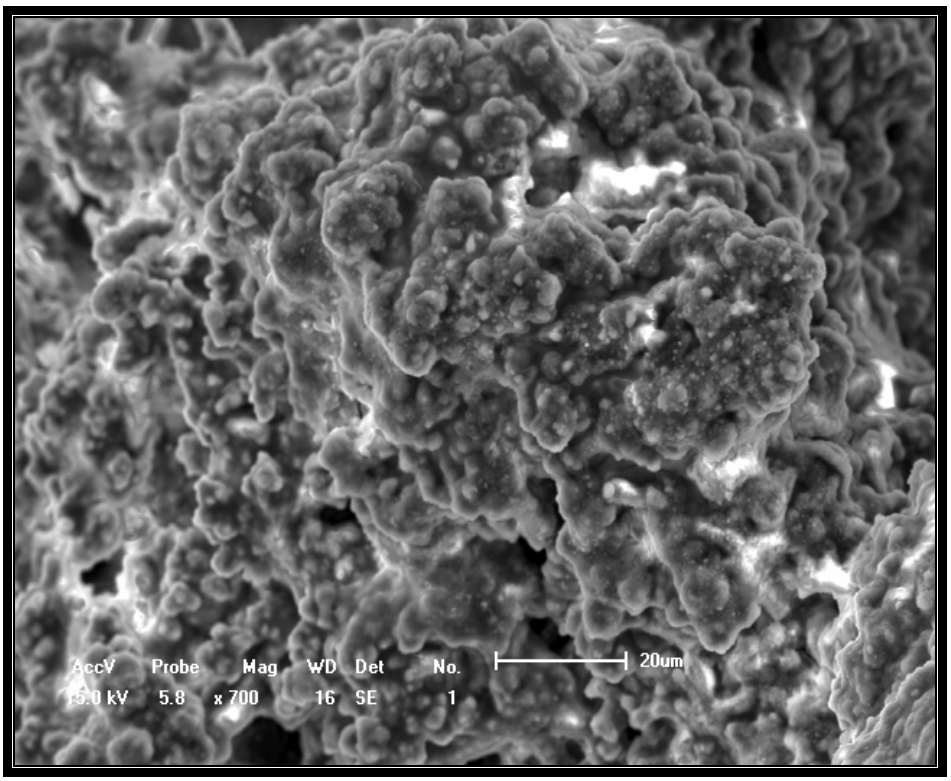

Figure (4.80a) SEM PictureX700 for Zn-Ni-SiO_2 after thermal shock.

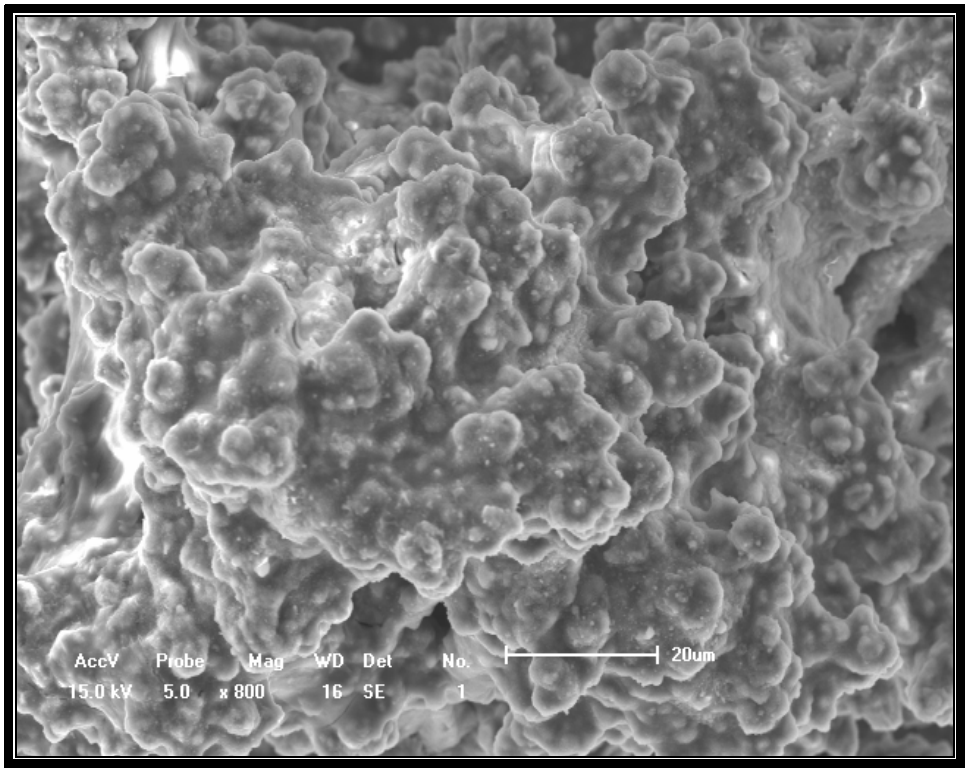

Figure (4.80b) SEM PictureX800 for Zn-Ni-SiO_2 after thermal shock.

4.8 Surface Roughness Test

It is obvious from Table (4.14) that the addition of SiO_2 did not effect the surface roughness of Zn-Ni coating. Surface roughness can effect a components chemical and physical stability. Surfaces that have to stand up to hostile environments (temperature, humidity, or hostile chemicals) must be as smooth as possible in order to present the minimum surface area for attack, and to have as few defects or weak spots as possible.

There are numerous problems caused by surface roughness . Although these problems tend to be application specific, excess light scatter , mechanical malfunction, environmental instability ,and cosmetic acceptability .In optical applications, the primary motivation in

measuring surface roughness is to estimate how much the surface will scatter light at the intended ware length (s) of operation.

Another example of mechanical malfunction can be found in high performance engine machine parts which are required to move or rotate at a high speed without wear. Excess surface roughness can lead to unacceptably high levels of frictional heating, causing damage and even failure.

Table (4.14) Surface roughness results

Type of Coating	Surface Roughness Result(µm)	Average (µm)
Zn-Ni	0.71	0.71
	0.73	
	0.71	
Zn-Ni-Cu	0.80	0.80
	0.80	
	0.82	
Zn-Ni-SiO_2	0.72	0.72
	0.71	
	0.73	

4.9 Reflectivity-Transmissivty Test

This technique used as a measure of absorpitivity and reflectivity spectroscopic to get information for material compound and transmissivity activation depend upon the principle for interface electromagnetic waves [162].

Figures (4.81,4.82 and 4.83) show the reflectivity for Zn-Ni, Zn-Ni-Cu and Zn-Ni-SiO_2 respectively.

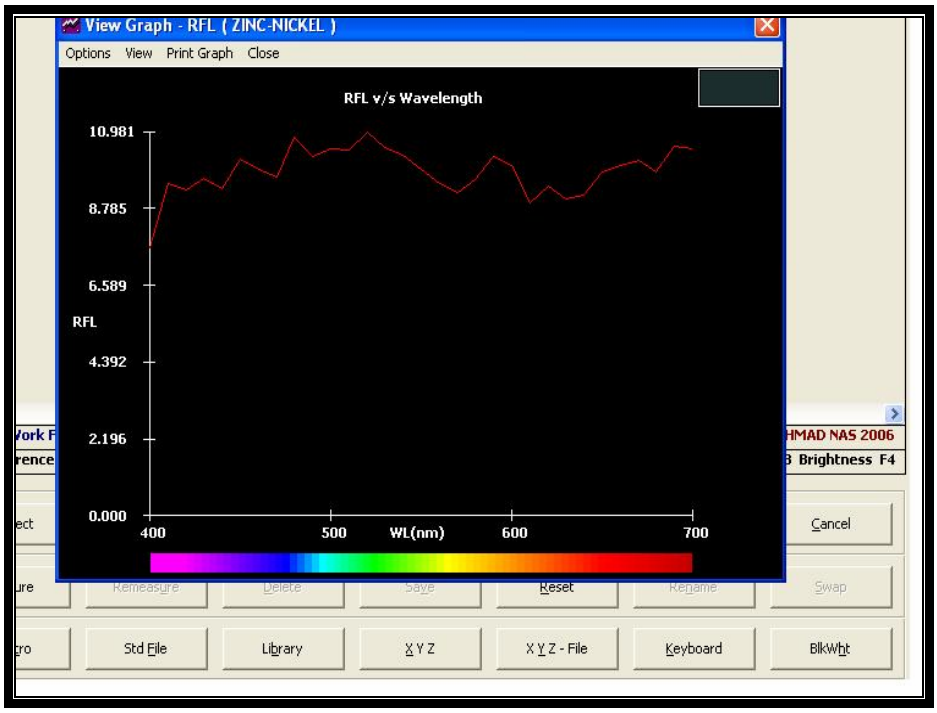

Figure (4.81) Zn-Ni Reflectivity

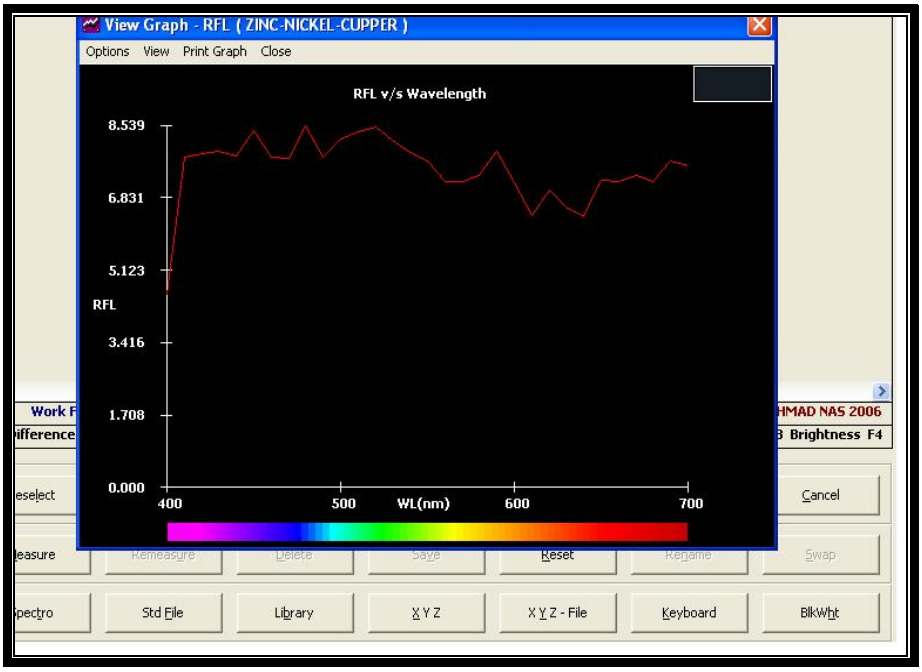

Figure (4.82) Zn-Ni-Cu Reflectivity

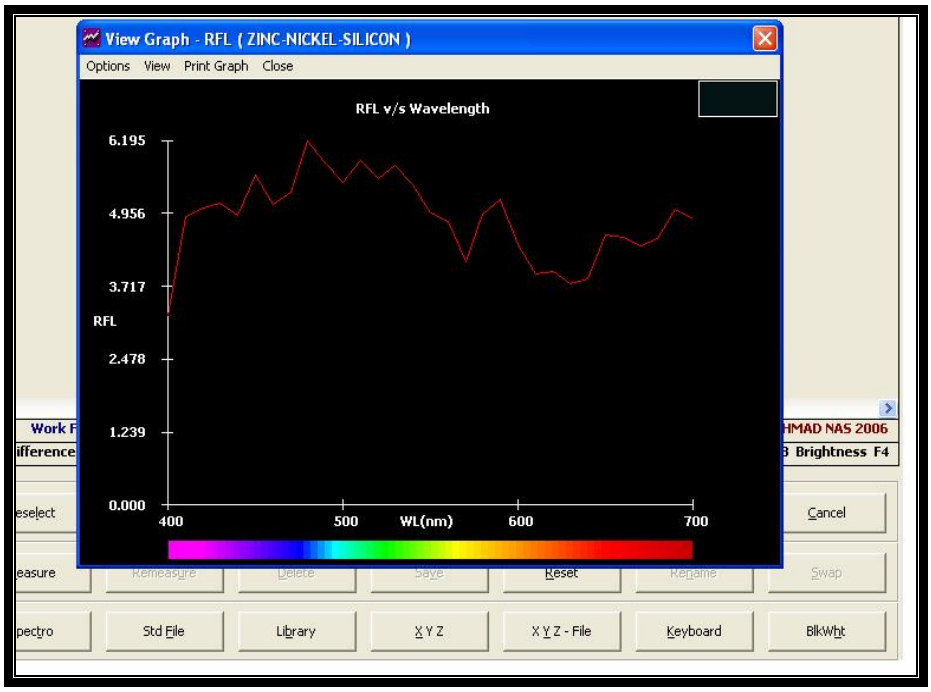

Figure (4.83) Zn-Ni-SiO_2 Reflectivity

From three above figures Zn-Ni-SiO_2 is less than magnitude reflectivity.

Figures (4.84, 4.85 and 4.86) shows comparable all type coating with standard black, all data reflected at (Appendix I).

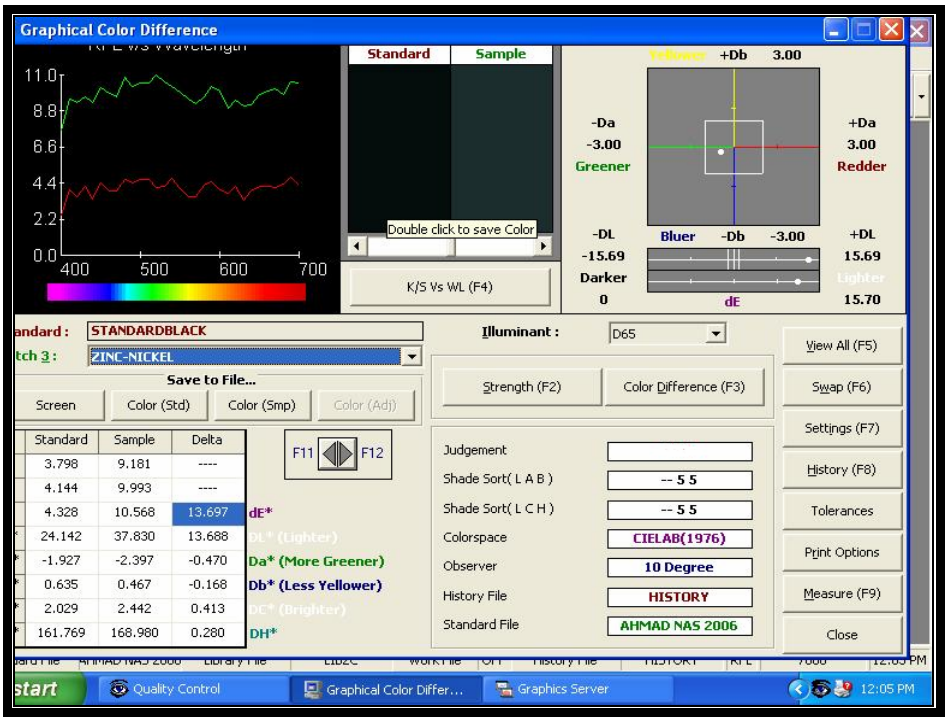

Figure (4.84) Comparable of reflectance Zn-Ni with standard black

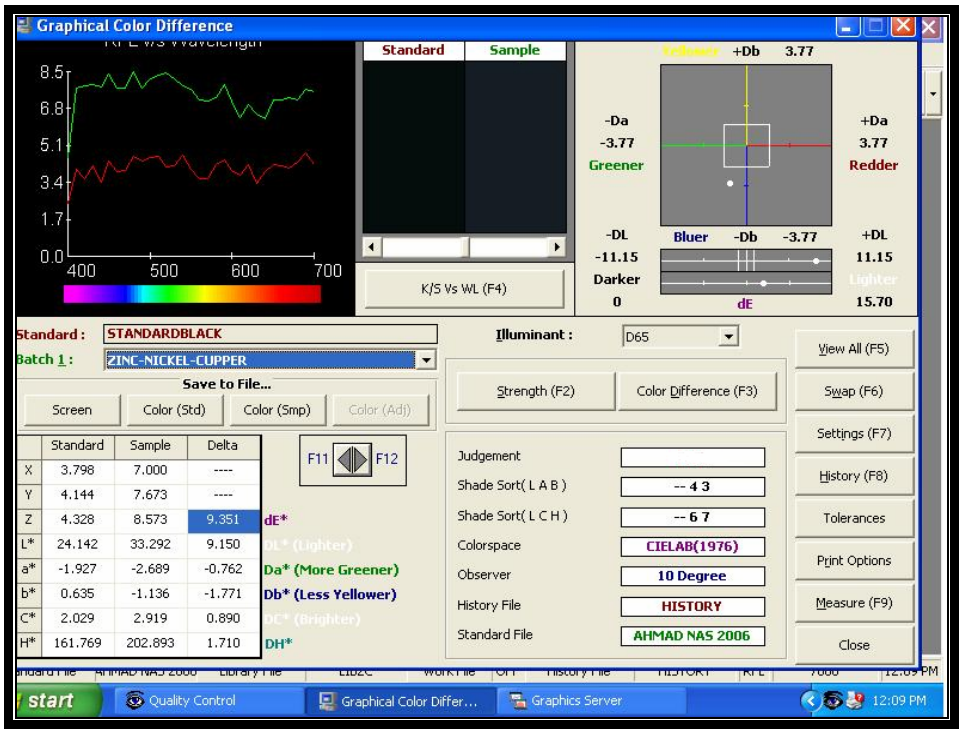

Figure (4.85) Comparable of reflectance Zn-Ni-Cu with standard black

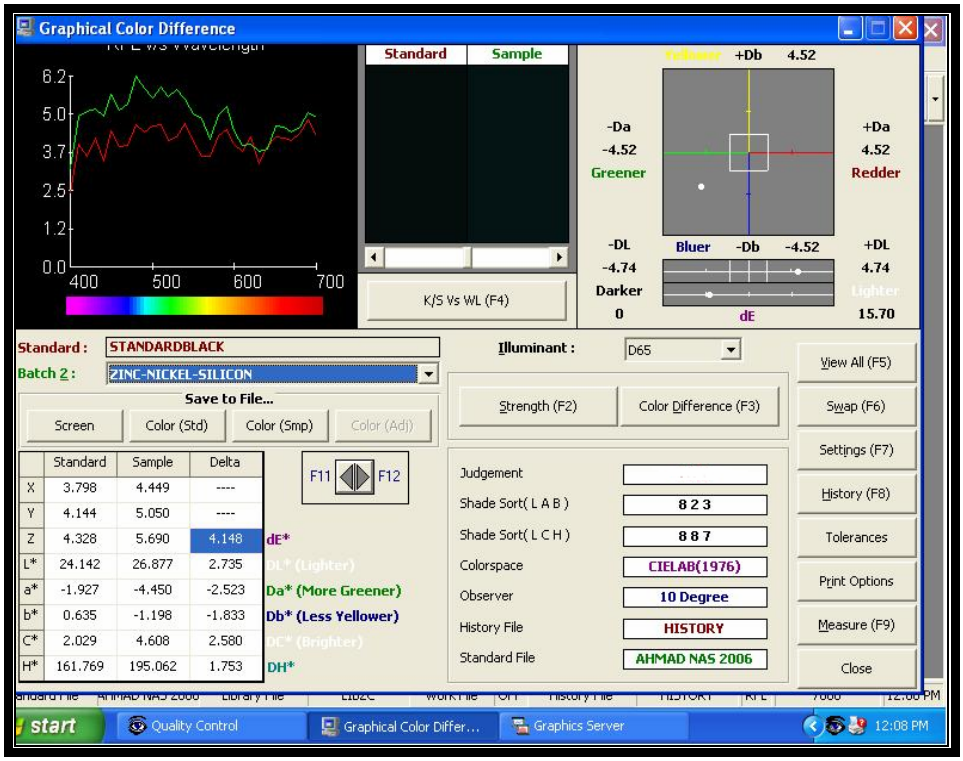

Figure (4.86) Comparable of reflectance Zn-Ni-Cu with standard black

From figures (4.84,4.85 and 4.86) indicated the difference in reflectance magnitudes for Zn-Ni (13.697 dE*),Zn-Ni-Cu (9.351 dE*) and Zn-Ni- SiO_2 (4.148 dE*).

Small reflectance for Zn-Ni-SiO_2 indicates the characteristics of compound to other coatings.

Figuers (4.87,4.88 and 4.89) indicated the transmisivity magnitude for Zn-Ni Cu and Zn-Ni-SiO_2 respectively.

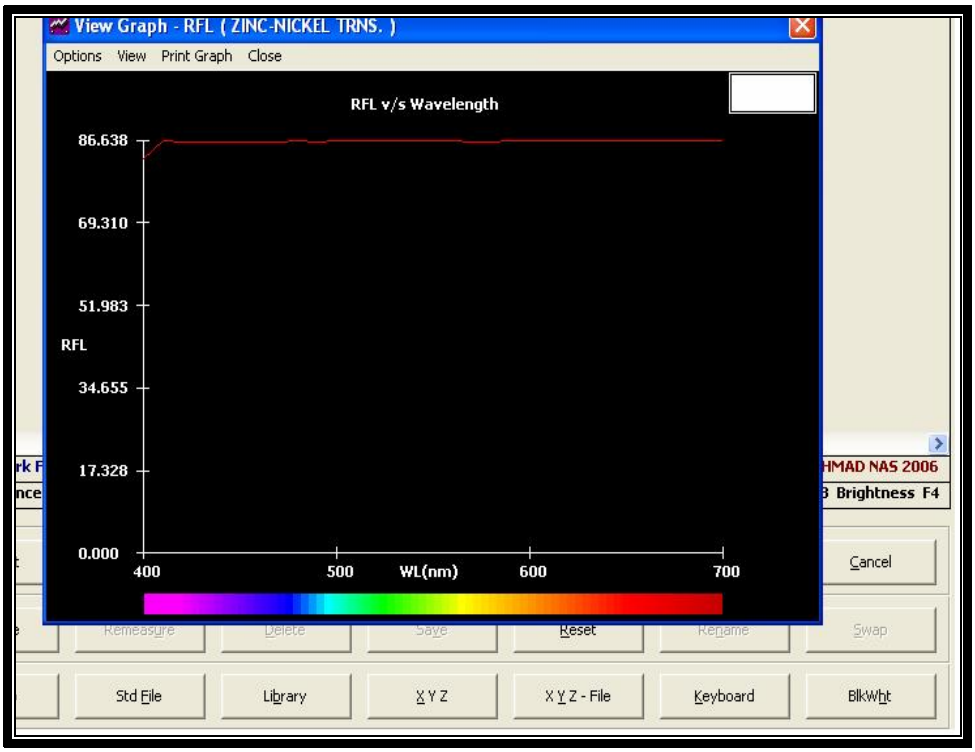

Figure (4.87) Transmissivity Zn-Ni

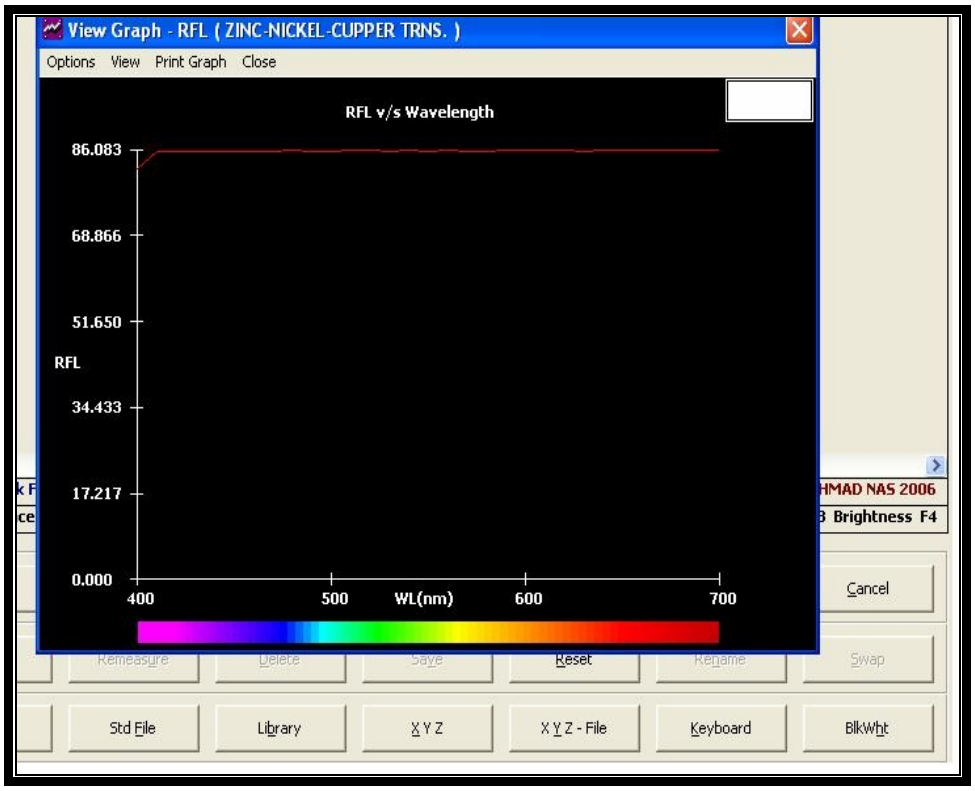

Figure (4.88) Transmissivity Zn-Ni-Cu

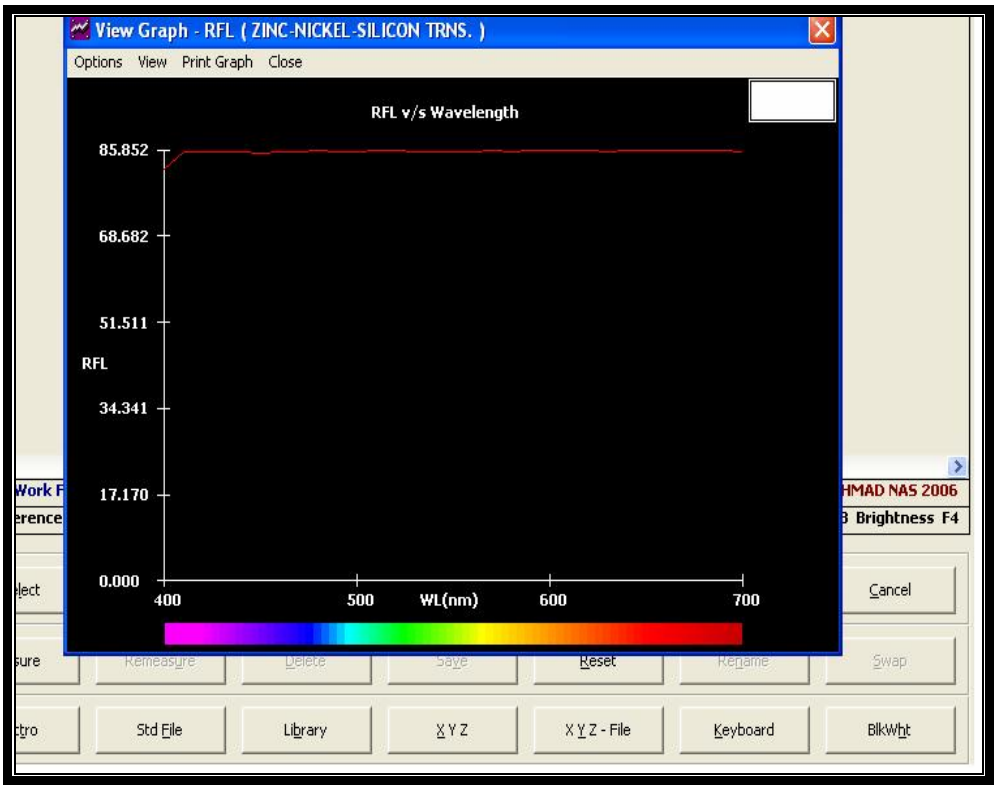

Figure (4.89) Transmissivity Zn-Ni-SiO_2

When the reflectance values are small they provided a good protection for any targets or spacing and that means less scattering.

The black color for Zn-Ni base system has benefits for many processes which depends upon solar cell the possibility of absorption all wave lengths and reflectance by regular distribution.

Chapter Five

CONCLUSIONS & RECOMMENDATIONS FOR FUTURE WORK

Chapter Five

Conclusions and Recommendations for Future Work

5.1 Conclusions

1- This work was carried out in spite of the facts that, the mechanism of Zn-Ni base coatings is poorly understood, in addition to the difficulty of achieving Ni content in the range of ~14%Ni and the need of practical understanding of the performance on the molecular level. Also whether or not the same simple relations would be obtained from the solutions containing other pairs of metal ions. These coatings, however one industrially,are so important.

2- Incorporated of SiO_2 in Zn-Ni system makes them cheaper than Zn-Ni coatings(which itself is so many times cheaper than Ni-Zn coatings, since it is richer with the cheap metal Zn).

3- The addition of SiO_2 to the Zn-Ni coatings causes a reduction in weight(SiO_2 density =2.6 g/cm^3).

4- In several hostile environments (i.e.) salt spray chamber 24hrs at 35°C,the corrosion rate (mpy) for Zn-Ni-SiO_2 coatings was only 3%,7% and 10% with respect to the corresponding value of the base metal, Zn-Ni and Zn-Ni-Cu coatings respectively. When carried out heat treatment at 200°C 1 hr becomes 3% and 4% as compared with Zn-Ni and Zn-Ni-Cu respectively.

5- Polarization computerize curve (Tafel slope) comes in agreement with the above results, and observed corrosion current for Zn-Ni-SiO_2 in 5% NaCl as 8%,13% and 16% as compared with Zn-Ni,

Zn-Ni-Cu respectively. After heat treatment becomes 7% and 9% compared with Zn-Ni and Zn-Ni-Cu respectively.

6- Zn-Ni-SiO_2 coating once again exhibits a significant corrosion resistance (Tafel slope) in 1% sulfuric acid, the corrosion current was only 5%,22% and 23% as compared with base metal, Zn-Ni and Zn-Ni-Cu respectively. After heat treatment the result becomes 9% and 18% as compare with Zn-Ni and Zn-Ni-Cu.

7- Corrosion rate (mpy) in 1% HCl at 15°C for Zn-Ni-SiO_2 is 3%,9% and 10% as compared with base metal,Zn-Ni and Zn-Ni-Cu respectively, and 3%,8% and 10% when temperature is increased to 35°C ,and 4%,6% and 7% when temperature at 45°C,and 7%,9% and 11% when temperature at 55°C.After heat treatment at 200°C 1hr,the corrosion rate at 15°C for Zn-Ni-SiO_2 was only 7% and 8% as compared with Zn-Ni and Zn-Ni-Cu respectively, when temperature is increased to 35°C it becomes 8%,10%,and when temperature is 45°C it becomes 5%,6% and when temperature is 55°C it becomes 10% and 11%.

8- After 24 hrs at 35°C in humidity environment , Zn-Ni-SiO_2 coating shows less weight loss than base metal, Zn-Ni and Zn-Ni-Cu as 2%,7% and 8% respectively, when temperature increased to 45°C it becomes 1%,6% and 7%and when temperature at 55°C it becomes 3%,11% and 14%.When heat treatment was carried out at 200°C 1hr, the weight loss at 35°C for Zn-Ni-SiO_2 represented only 7%,8%

compared with Zn-Ni and Zn-Ni-Cu, when temperature increased to 45°C the weight loss is 6%and 7%,and when temperature was 55°C it becomes 10%and 13%.

10-The morphology of the coatings obtained by SEM showed less damaged in Zn-Ni-SiO_2 coatings.

11-Thermal shock resistance was greatly improved by the addition of SiO_2,cracking and spalling were observed in other coatings. The weight loss of Zn-Ni-SiO_2 after quenching from 550°C for instance, was only 3% and 5% relative to Zn-Ni and Zn-Ni-Cu respectively.

12- The addition of SiO_2 to the coatings appears to have no effect on surface roughness.

13-Significant improvement in hardness was observed by the addition of SiO_2 to the coatings.

14-Reflectivity of Zn-Ni-SiO_2 was proved to be less (more absorption) than Zn-Ni and Zn-Ni-Cu coatings.

5.2 Suggestions for future work:

Although the present work has covered both the detailed kinetic behavior and microstructure of coated systems and their development during corrosion environment and thermal shock in an ideal condition, there are still some demands which need more work. It is necessary to take into account the following suggestions:

1- Changing the percentage element for coated layer and return testing to evaluation performance.

2- The coating thickness to study the effect of the environment.

3- Identification the parameters determining the adhesion of the coated layer with the base metal.

4- Study the influence of heat treatment in the vacuum environment or under pressure to verify the performance.

5- Study the effect of under-zero temperature on the coating layers.

6- Carried out corrosion a test at another corrosion environments.

7- Study the current produce from solar cells.

REFERENCES

References

1-Watson,S.A.,"Zinc-Nickel Alloy Electroplated Steel Coil and Other Precoated Coil for use by the Automotive Industry", Nickel Development Institute Review Series No.13001 (1988).

2-Porter,F.C., and Stoneman,A.M. and Thithorp,R.G.,Inst.Met.Fin. Ann.Tech.Conf. Paper p.115-133 (1988).

3-Lambert,M.R. and Hart, R.G., "Corrosion Resistance of 0-15% Ni-Zn Alloy Electroplated Coatings" SAE Tech. Paper No.860266 (1986).

4-Crotty,D.,"Zinc Alloy Plating for the Automotive Industry", Met. Fin., Vol. 94 ,No.9,p.54-58,(1996).

5-Babitch,H.and Fatrez,P., "Development of Differential Electrocoated Steel Sheets-Example of Zn/ZnNi",3rd International Conference on Zinc and Zinc Alloy Coated Steel Sheet,Galvatech,p.263-268,Chicago(1995).

6-Willlison,R.m.,"Bethlehem Steel Fine-Tunes Zinc-Nickel Sheet", Advanced Materials &Processes, Vol. 149,No.6 ,p33-34 (1996).

7-Mertens,M.L.A.D.,"Multifunctional Coatings in the Automotive Industry", Met. Fin. , Vol. 96,No. 5,p.10-14 (1998).

8-Baldwin,K.R. and Smith,C.J.E.,"Repair of Metal Coatings Using Environmentally Compliant Brush-Plating Solutions",33rd Aerospace/Airline Plating & Metal Finishing Forum, AESF p.63-71 (1997).

9-Baldwin,K.R.,Smith,C.J.E. and Robinson,M.J.,"A Study Into the Electrodepostion Mechanisms of Zinc-Nickel Alloy From an Acid-Sulfate Bath",Met. Fin., Vol.72,No.2,p. 79-88(1994).

10-Azzerri,N., "Coated Steel Sheets for the European Household Appliance Market",3rd International Conference on Zinc and Zinc Alloy Coated Steel Sheet, Galvatech 95,p.425-432,Chicago(1995).

11-Budman,E.and Sizelove, R.R,"Zinc Alloy Plating", Metal Finishing Guidebook, Met. Fin., Vol. 93, No. 1A.,P.324-329(1995).

12-Lynch,R.F.,Zinc Specifications Grow to Match Advances in Zinc-Coated Steel",ASTM Standardization News, Vol. 23,No, 2,p.17-21(1995).

13-De Giz, M.J., Machado, S.A.S., Avaca, L.A. and Gonzales, E.R., "High Area Ni-Zn and Ni-Co-Zn Codeposits as Hydrogen Electrode in Alkaline Solutions", J.Appl. Electrochem., Vol. 22,p.973-977(1992).

14-Jones, D.A. "Principles and Prevention of Corrosion "., Macmillan Publishing Company., New York., 572 pp.,(1996).

15-Evans, U.R.," The Corrosion and Oxidation of Metals:Scientific Principles and Practical Applications" ,Arnold, London , 4th Edi (1971).

16-W.H. Dennis "Metallurgy of The Ferrous Metals "., Sir Isaac Pitman & Sons Ltd. London., (1963).

17-Henthrone, M.," Chemical Engineering" , vol.14 (1971).

18-Uhlig, H.H.,"Corrosion and Corrosion Control"., John Wily&Sons,3rd ed.,(1985).

19- National Bureau of Standards," Economic Effects of Metallic Corrosion in The United States", Areport to the Congress., (1978).

20-http: // nace.org/nace/content/publicaffairs/cocorrindex.asp.

21- http://www.corrosion –club.com/links.htm

22- K. Lewis, R. Kelly and R. Piascik, "Determination of the Corrosive Conditions Present within Aircraft Lap-Splice Joints", Proc. Of The FAA-NASA Symposium on Continued Airworthiness of Aircraft Structures., Williamsburg,VA., (1998).

23-C. J Slunder and W K Boyd "Zinc : Its Corrosion Resistance "., First edition ., Zinc Institute Inc. (1971).

24- Perry , R.H., and Green , D. W., "Perry's Chemical Engineers Handbook "., 7th ed., McGraw Hill Co., (1997).

25-Metal Handbook Ninth edition vol.13 " Corrosion"., ASM International .,(1987).

26-Andrey P. Jivkov ., Ph.D Thesis , Mechanical engineering department ,Malmo University,Sweden.,(2002).

27-J. E Scully, "The Fundamental of Corrosion ", 2nd ed., Pergamon Press, Oxford, (1975).

28- K.R. Trethewey & J. Chamberlain , " Corrosion for Science and Engineering "2nd ed., Printed in Singapore , (1996).

29-Fontana and Greene "Corrosion Engineering" .,McGraw-Hill,Inc., (1978).

30-J.M. WEST "Electrodepostion and Corrosion Process"., William Clowes and Sons.,(1971).

31-J.M. West, "Basic Corrosion and Oxidation ", 2nd ed.,John Wiley & Sons Inc., (1986).

32-Trethewey , K.R. ., and Chamberlain, J., "Corrosion for Science and Engineering ",Logman Group Ltd., (1996).

33-GamryInstruments.UnitedKigdoEISTheory.
http://www.gamry.com/g2/ftp/download/literature /1999/Eis 300.Zip.

34-Stern, M.., "Corrosion J"., vol. 13 , P.775t ., (1957).

35-Bakhvalov, G.T. and Turkovskaya, A.V., " Corrosion and protection of Metals"., Pergamon Press.,(1965).

36- Herbert H. Uhlig ., "The Corrosion Handbook "., John Wiley & Sons (1948).

37-A.Masih , N. S., Ph.D. Thesis, Chemical Engineering Department, College of Engineering,Baghdad University,(1990).

38- Sherir, L.L., "Corrosion :Metal/Environment reactions", Newnes –Buttenworths., (1976).

39-Steigerwald, R.F. Corrosion J. January, p.1 ., (1968).

40- C. Wagner "Passivity and Inhibition during the Oxidation of Metals at Elevated Temperatures" , Corrosion Science ,5, 751-764 .,(1963).

41- Schweitzer, P. A., "What Every Engineer Should Know About Corrosion", Mareel Deaker,1st ed.,(1987).

42-Mansfeld, F., "Corrosion Mechanisms", Marcel Decker Inc.,(1987).

43-Trethewey.K.R., and Chamberlain, J.,"Corrosion for Science and Engineering", Longman Group Ltd.,(1996).

44-Ailor, W.H., "Handbook on Corrosion Testing and Evaluation", John Wiely & Sons , 1st . Edi (1971).

45-Harvey P. Hack., " Galvanic Corrosion "., ASTM STP 978.,American Society for Testing and Materials ., (1988).

46- Scott D. Henry ., "Corrosion in The Petrochemical Industry "ASM Intrnational., (1999).

47-Laque, F.L. , Marine Corrosion Causes and Prevention , Jone Weily &Sons ,(1975).

48-Tomashov , N.D., "Theory of Corrosion and Protection of Metals", The Macmillan Company .,New York., (1966).

49-Intercorr.International, Inc., An Internet site at www.corrosionsource.com,2001

50- Baboian , R. " Localized Corrosion of Metal Failure –Cause of Metal Failure" , ASTM STP 516 ,American Society for Testing and Materials ,(1972).

51-Robert Baboian "Galvanic and Pitting Corrosion-Field and Laboratory Studies"., ASTM., STP 576 ., Ameriacn Society for Testing and Materials, (1974).

52-Mansfeld, F., "Corrosion Mechanisms", Marcel Decker Inc.,(1987).

53-W. Bolton, “Engineering Materials Technology”, 3rd ed., U.K.,(1998).

54-B. Borgard ., C. Warren, S.S. Somayaji and R. Heidersbach ., " Mechanisms of Corrosion of Steel in Concrete "., In: Corrosion Rates of Steel in Concrete / N.S.Berke V. Chaker and D. Whiting , editors , (STP :1065) ASTM ,Philadelphia , (1990).

55- From the Internet H: /Electroplating/History of Electrochemistry, (2006).

56- Quality Metal Finishing Guide 1,No.1-B "Decorative Precious Metal Plating", Metal Finishing Suppliers Association, Potomac Falls, Virginia ,206 (1998).

57- J. K. Dennis, T.E. Such., "Nickel and Chromium Plating, Newnes-Butterworths, London (1972).

58- www.rschrome.co.uk, (2006).

59- Daniele Gilkes, MSc.Thesis, University of Florida , (2002).

60- "Nuclear Engineering and Technology", Vol.38 No.3, (2006).

61- Manida Teeratananon ," Current Distribution Analysis of Electroplating Reactors and Mathematical Modeling of The Electroplated Zinc-Nickel Alloy", Ph.D.Theses ,Chulalongkorn University ,Chemical Technology, (2004).

62- J.N.Agar, "Diffusion and Convection at Electrodes", Discussion of Faraday Soc.,1, p.27-37 (1947).

63- C.R.Wike and C.W.Tobias ,et al.,"Free-Convection Mass Transfer at Vertical Plates", Chemical Engineering Progress,43,No.12, p663-674 (1953).

64- Bard, J. and Faulkner, R., "Electrchemical Methods", New York, John Wiley&Sons, (1980).

65- Li D.Y.,"Texture Formation in Iron Electrodeposits", Ph.D. Thesis.McGill University , Montereal,Canada (1995).

66- Landolt , D.Electrochim.Acta 39, p 1075 (1993).

67- Hull,R.O.,AM Electroplate Soc.,27, p.52-60 (1939).

68- Li D.Y.,Texture Formation in Iron Electrodeposits, Ph.D. Thesis, McGill University, Montreal, Canada (1995).

69- Bockris J.O'M.and Khan S.U.M., Surface Electrochemistry-A Molecular Level Approach., Plenum Press., New York(1993).

70- Winand R., Fundamentals and Practice of Aqueous Electrometallurgy (Short Course,Coordinator:Demopoulos G.P.), Sponsored by The Metallurgical Society of CIM,Chapter2, (1990).

71- Brenner, A. "Electrodeposition of Alloys", Vol.1&2 , New York ,Academic Press,(1963).

72- Natorski , T.J.,"Zinc and Zinc Alloy Plating in The '90s'", Met.Fin.,Vol.90,No.3, p.15-17 (1992) .

73- Al balat ,R., Gomez,E., Muller, C., Pregonans, J., Saret,M.,Valles,E.,"Journal of Applied Electrochemistry", Vol.21 p.44-49 (1991).

74- Refference Graham Tonge,Tonger&Taylor Ltd.,United Kingdom (2000).

75- David Grotty and Robert Griffin," Performance Characteristics of Zinc Alloy", Plating &Surface Finishing , (1997).

76- Paul C. Wynn ,"Zinc Nickel Electroplating in the New Millennium" ,Atotech UK Limited , United Kingdom (2001).

77- Paul C. Wynn , "Internal Communication " , Atotech UK Ltd..,(2001).

78- Yanagawa et al. US Patent 4 , 877, 496 (1989).

79- Test Methode ASTM B 117 American Society for Testing and Materials ,(2004).

80- D.Block and C.V. Bishop US Patent 5,417,840 (1995).

81- P.C. Wynn & C.V. Bishop,"Replacing Hexevalent Chromium in Passivations on Zinc Plated Parts", Products Finishing , US Publication, (2001).

82- K.R. Baldwin and C.J.E. Smith, Trans.Inst.Met.Finish.,74, 202, (1996).

83- W.H.Safranek , Plate.Surf.Finish.,85,45 (1997).

84- J.S.Hadley , "Replacements for Cadmium",Omi-Imasa Europe-Hertogen-Bosch.,The Netherlands (2006).

85- Razak Lajis ,"The Effects of Cadmium", National Poison Centre, University of Sains Malaysia ,(2006).

86- U.S.Department of Labor ,"Cadmium Helth Effects" ,(2006).

87- A.Ashur,and I.E.Klein , Plat.Surf.Finish ,83,58 (1996).

88- V.C. McMillan,"Electrodeposited Zinc-Nickel as An Alternative to Cadmium Plating for Aerospace Application",NASA ,(1991).

89- Boeing Environmental Technotes.,"Update on CadmiumPlating Alternatives ", Vol. 10, No.3, (2005).

90- The Massachusetts Toxics Use Reduction Institute,"Non-Cyanide Plating Processes ", University of Massachusetts, Toxics Use Reduction Institut .,(1994).

91- Dr.Keith O.Legg,"Overview of Chromium and Cadmium Alternative Technologies",ASM International, Ohio and IOM Communications Ltd.,UK (2002).

92- Alan Gardner.,"High Performance Alternative to Hexavalent Chromium Passivation of Plated Zinc and Zinc Alloys", Society of Automotive Engineers, (2001).

93- P.Hulser "Chromium (VI),Free Passivating Basecoat for Deltacoll on Zinc and Zinc Alloys" SurTec GmbH,Germany (2005).

94- Birgit Sonntag and Venkatesh Sundaram,"Substitution of Cr(VI)- Containing Chromate Coatings by the European Automobile Industry", Atotech GmbH Berlin,Germany (2005).

95-Commission Decision of 27 June 2002, Amending Annex II of Directive 2000/53/EC of the European Parliament and of The Council on End-of-Life Vehicles, C 2238 (2002).

96- L.Thiery and N.Pommier.,"Hexavalent Chromium-Free Passivation Treatments in the Automotive Industry", Corenty SAS.,France (2004).

97- Lambert, M.R.Hart, R.G. and Townsend , H.E., "Corrosion Mechanism of Zn-Ni Alloy Electrodeposited Coatings" SAE Tech.Paper No.831817, (1983).

98- Kazuo Kondd and Zennosuke Tanaka,"Atomic Force Microscopy Study on Growth of Zinc-Nickel Electrodeposits", ISIJ International,Vol.38 p.778-780 (1998).

99- Kubaschewski O.,"Binary Alloy Phrase Diagram " , 2nd edition, Editor-in Chief : Massalski T.B. ,ASM,1795 (1991).

100- Mackowiak J.and Short N.R.,Int'l.Metals Reviews,1,1(1979).

101- Hall,D.E.,Plating Surf.Finish.,71 (1983).

102- Romachar ,T.L. Electroplating 1,p.165 (1959).

103- Swathirajan,S. J.Electroanal .Chem. p.211-221 (1987).

104- Bruet-Hotellaz,and Marolleau ,"Strcture of Zinc-Nickel Alloyelectrodeposits" , France;Journal of Materials Sciences 34 .,p.881-886 (1999).

105- Swiatakz : "Non-Equilibrum Phase Composition of Electrodeposted Zn-Ni Alloys", Department of Chemical Engineering , University "La Sapienza" Italy (2004).

106- G.D.Wilcox and D.R.Gabe,"Electrodeposited Zinc Alloy Coatings,Corrosion Science", (1993).

107- Craig V.Bishop,Lawrence Emch,"Effects of Zinc Nickel Alloy Composition",Dale Block of McGean-Rocho and Frank Freitas Central Metal Finishing,AESF Svr/Fin'98, (1998).

108- F.Elkhatabi,M.Benballa,M.Sarret,C.Muller, "Dependence of Coating Characteristics on Deposition Potential for Electrodeposited Zn-Ni Alloys" ,University of Barecelona , Spain, Electrochimica Acta,44, p 1645-1653 (1999).

109- S.Swathirajan, J.Electroanal. Chem.., p211-221 (1987).

110- H.Dahms,I.M.Croll,J.Electrochem.Soc.112 (1965).

111- J. Balej, J. Divisek , H. Schmitz, J. Mergel, J. Appl. Electrochem. 22,705 (1992).

112- Nobuyuki Koura,"Electrodepostion of Amorphous Zn-Ni Alloy from an Organic Solvent Added $ZnCl_2$-$NiCl_2$-EMIC Ambient –Temperature Molten Salt Bath", Tokyo University of Sience, Japan (2005).

113-Gomez,E.and Valles E.,"First Stages in Zinc Deposition" in "Progress in the Understanding and Prevention of Corrosion",eds.J.M. Costa and A.D.Mercer ,The Institute of Materials, p.343-349 (1993).

114-Ohtsubo,H.,Sogo,H.,Nakai,K. and Ohmori,Y.,"Zn-Ni Electrodepostion on Low Carbon Steel Substrate", ISIJ Int.,Vol.37,No.5 p.512-518 (1997).

115- Tsuru,T.Kobayashi,S.,Akigama,T.,Fukushima H.,Gogia,S.k.and Kamme l,R., "Electrodepostion Behaviour of Zinc-Iron Group Metal Alloys from a Methanol Bath", J.Appl.Electrochem.,Vol.27,p.209-214 (1997).

116- Elkhatabi,F.,Barcelo,G.,Sarret,M.and Maller,C.,"Electrochemical Oxidetion of Zinc+Nickel Alloys in Ammonium Baths",J.Electroanal.Chem.,Vol.419N p.71-76 (1996).

117- Ramesh Bapu,G.,Devaraj,G.,Ayyapparaju, J. and Subramanian, R. "Electrodeposition of Zinc-Nickel Alloys", Met.Fin., Vol 85, No.2 , p.49-50 (1987).

118- Domnikov,L.,"Electrodepostion of Zinc-Nickel Alloys", Met.Fin.,Vol.63,No.3 p.63-67 (1965).

119- Tsuda,T.and Kuremoto,T. U.S. Patent 4-249-999 (1981).

120- Zaki,N.Metal Fin. 87, (6), p.57-60 (1989).

121- Kalantary,M.R. Plating Surf.Finish.,71, p.80-88 (1994).

122- Basker Veeraragharan,Hansung Kim,Branko Popov, "Optimization of Electroless Ni-Zn-P Deposition Process:Experimental Study and Mathematical Modeling", Electrochimica Acta 49 p.3143-3154 (2004).

123- Hyounsoo Park, "The Role of Texture and Morphology in Optimizing the Corrosion Resistance of Zinc-Based Electrogalranized Coating", Ph.D Thesis , Department of Metallurgical Eng,University of Montereal ,(1997).

124- Wang Zhao-Lun,Yang Yo-Xiang,Chen Ya-Ru,"A Study on Electroplating of Zinc-Nickel With HEDP", JCSE the Journal of Corrosion Science and Engineering, Vol. 7 ISSN ,1466-8858 (2005).

125- Swaminatha P.Kumaraguru ,Basker Veeraraghavan,and Branko N.Popv ,"Development of An Electroless Method to Deposit Corrosion-Resistant Silicate Layers on Metallic Substrates",J.Electrochemical Society,1539(7) B253-259 (2006).

126- C.Muller,M.Sarret,M.Beuballa,"Complex Agents for a Zn-Ni Alkaline Bath", J.Electroanalytical Chemistry 519,85-92 (2002).

127- N.poper , "Studies on Electrodeposited Zn-Ni-X(X=Cu,Cd,Fe and SiO_2) Coating As a Replacement for Cadmium Coatings", University of South Carolina,Department of Chemical Engineering ,(2004).

128- Toshiaki Ohtsuka , "Ellipsometric Study of the Initial Layer Formation of the Preferential Zn Deposition in Zn-Ni Electroplating" ,Nagoy Institute of Technology , Japan, ISIJ International , Vol.35,No.7 p 892-899 (1995).

129- Paul Wynn, "Multi-Lyer Sacrificial Coatings", Atotech U.K. (2004).

130- Kh.M.S.,C.C.Koch and P.S.Fedkiw, J.Electrochem.Soc.,151, C103-C111 (2004).

131-Prabhu Ganesan,Swaminath P.Kumaragurun and Branko N.popov;"A Novel Approch to Deposit Compositionally Modulated Zn-Ni Maltilayer as a Replacement for Cadmium Coating",University of South Carolina.,(2005).

132- Bertling,S.,"Corrosion –Induced Metal Runoff External Constructions and Its Environmental Interaction", Ph.DThesis, Royal Institute of Technology,Stockholm (2005).

133-OdnevallWallinder,I.,Bertling,S.,Herting,G.,Leygraf,C.,Heijerick,D.,Berggren,D.& Koundakjian ,P., "Release of Chromium,Nickel Andiron from St.Steel Exposed Under Atmospheric Conditions and The Environmental Interaction of These Metals", Brussels:Eurofer,Swedon (2004).

134- Graedel,T.E.,"Copper Patinas Formed in The Atmosphere ",ll. Aqualitative Assessment of Mechanisms Corrosion Science ,Vol.27, p.721-740 (1987).

135- Odnevall Wallinder,I.,Verbiest,P.He,W.& Leygraf,C.,"Effect of Exposure Direction and Inclination on The Runoff Rates of Zinc and Copper Roofs", Corrosion Science,Vol.42 , p.1472-1487 (2000).

136- Johan Aslund,"Release Rates and Environmental Impact of Zinc-Nickel Coating in The Automotive Industry", M.Sc.Thesis,Stockholm,Sweden (2006).

137- Baldwin,K.R,C.J.E. and Robinson ,M.J., "Cathodic Protection of Steel by Electrodeposited Zinc-Nickel Coating",Corrosion,Vol.51, p232-940 (1995).

138- N.Worauaychai, N.Tareelap,C.Nitipanyawong, "Zinc-Nickel Alloy Electroplating in Alkaline Electrolyte for Corrosion Resistance Improvement", Thailand (2004).

139- Shibuya, A.,Kurimoto, T.,Hoboh, Y.and Usuki, N., "Development of Ni-Zn Alloy Plated Steel Sheet" Trans.ISIJ,Vol.23 p.923-929 (1983).

140- Suzuki,I."Corrosion-Resistance Coatings Technology", Marcel Dekker,Inc., New York (1989).

141- Algirdas Selskis,Laima,Iganas,Rimantas, "Corrosion of Zn and Zn Alloy Electrodeposits:Morphology and Strcture Changes", Chemija No.3, p17-25 ,Italy (2004).

142- F.J.Fabri Miranda,I.C.P.Margarit,O.R.Mattos,O.E.Barcia,R.Wiart, Corrosion,55,732 (1999).

143- A.M.Simoes,M.J.F.Marques,M.E.Almeida, "Corrosion Resistance of Electrodeposited Zinc-Nickel Coatings", Instituto Superior Tecnico/Chemical Engineering Dep.,Portugal (2004).

144-" Novel Non Chrome Processes for The Protection of Metal Substrate" ,(2004).

145- Basker Vecraraghavan,Bala Haven,Dragan Slarkov,Swaminatha Prabhu,Branko Popov and Bob Helmann,"Development of Novel Electrochemical Methode to Deposit High Corrosion Resistance Silicate Layers on Metal Substrate"., J.Electrochemical and Solid-State Letters,6 (2) B4-B8 (2003).

146-Byoung-Yong ,Chang and Su-Moon Park ,"Relative contribution of Ni^{+} and Zn^{+} Reduction Currents to Anomalous Electrodepostion of Zn-Ni Alloys", Journal of Electrochemical Society, 151 (12) C786-C788 (2004).

147-Mottate T.,Proc.of the International Conference of Zinc and Zinc Alloy Coated Steel Sheet (GALVATECH) .The Iron and Steel Institute of Japan ,Tokyo,625 (1989).

148- Chassaing ,E.Quang ,K.Vu.,and Wuart,R.Journal Appl . Electrochem . ,19, p.893 (1989) .

149-Murali Ramasubramanian ,"Studies on Alloys and Composites That Undergo Anomalous Codeposition ",Center for Electrochemical Engineering,University of South Carolina(1998).

150-C.J.E.Smith ,K.R.Baldwin, Some Cadmium Replacements for Use on Aircraft Components Product Finishing ,p.12-18 (1992).

151-K.R.Baldwin,C.J.E.Smith, Advances in Replacements for The Cadmium Plating of Aerospace Fasteners and Components",Wire Industry,p. 667-677 (1997).

152- ASTM, Phase Diagram ,(2004).

153-Hall,E.O., The Deformation and Ageing of Mild Steel:III Discussion of Results, Proc.Phys.Soc.London,Vol.B64 p.747-753 (1951).

154-Petch,N.J., The Cleavage Strength of Polycrystals ,J.Iron Steel Inst.,Vol.174, p.25-28 (1953).

155-Vlad C.M.,Proc.TMS Symposium on Zinc-Based Steel Coating System(Krauss G.and Matlock D.K.eds),Detroit,Michigan,129, p.7-11 (1990).

156-Alfantazi A.M.,A Study on The Synthesis,Characterization and Properties of Pulse-Plated Ultrafine-Grained Zn-Ni Alloy Coatings,Ph.D.Thesis,Queen's University,Kingston , Ontario (1994).

157-S.M.C Fernandes,L.V.Ramanathan , Rare Earth Oxide Coatings to Decrease High Temperature Degradation of Chromia Forming Alloys ,Mat.Res.,Vol.7,No.1 (2004).

158-Liana Roman, Rodica Stancu, Valentina Filippi, Carmen Raducanu, Catalin Cristescu,"Studies on Zn-Ni-P Alloy Electrodepostion"Mechanical Engneering Reesearch Institute Bucharest,2002.

159-ASM, Metals Handbook,9th ed.,Vol.1,(1978).

160-C.A.Keyser,Materials Science in Engineering,4th ed.,USA (1986).

161-A.Bakri,The Technology of Temperature Resistance Alloys, Ph.D .Thesis, C.I.T.England (1984).

162-H.W.Chatfield,The Science of Surface Coating , London (1962).

163- http://en.wkipedia.org/wiki/acid-rain. (2007).

164-F.R.Foulkes,Electrochemistry Course Notes,Chapter 21,(1999).

165-M.Stern and A.L.Geary,J.Electrochem.Soc.104-1,p.56 (1957).

APPENDIX

(Appendix A) [21]

Region / Industry	Cost of Corrosion	Reference
Aircraft Industry (North America)	$13 billion per year	IAR Flyer, Spring 2000 Edition, NRC Institute for Aerospace Research (Canada). V.S. Agarwala: "Corrosion Detection and Monitoring - A Review", Paper No. 271, Corrosion 2000, NACE International, 2000.
Aircraft, Military (United States of America)	$ 3 billion per year	V.S. Agarwala: "Corrosion Detection and Monitoring - A Review", Paper No. 271, Corrosion 2000, NACE International, 2000.
Aircraft (lost revenue when grounded for corrosion maintenance/repairs)	$100,000 per day	IAR Flyer, Spring 2000 Edition, NRC Institute for Aerospace Research (Canada).
Air Force and Navy – Australia	>$50 million per year	Web site of Defense Science and Technology Organization (DSTO, Australia)
Army - US	$10 billion per year (estimate)	M. Youson: "Invisible Enemy", Engineering, September 2003.
Army - US	$2 billion per year, related to painting and paint removal (estimate)	M. Youson: "Invisible Enemy", Engineering, September 2003.
Australia	about 2% of GDP.	Materials World, December 2001, p.30.
Australia	around $8 billion in 1982	R. Francis: "Beating Rust on Farm Buildings", published on web site of Australian Corrosion Association Inc.

Automobiles in Finland	about US$160 per car yearly (about US$300 million in total per year)	Studies conducted in the 1990's by the Finnish Road Administration, published at www.tieh.fi/winter.htm
Automobiles (USA)	0.25% of GNP attributed to motor vehicle corrosion (in 1998)	Materials Performance, March 2002, p.31.
Automobiles (USA)	$23.4 billion per year cost to American consumers due to: increased manufacturing costs, repairs and maintenance, depreciation. (Costs of reduced safety not included)	http://www.corrosioncost.com/ **"Corrosion Costs and Preventive Strategies in the United States"**, Report by CC Technologies Laboratories, Inc. to Federal Highway Administration (FHWA), Office of Infrastructure Research and Development, Report FHWA-RD-01-156, September 2001.
Bridges (USA Highway Bridges)	$30 billion (1999 dollars) to remediate corrosion-induced structural deficiencies	Materials Performance, March 2002, p.31.
Coast Guard, United States, Aircraft	$20 million per year	Lee Ann Tegtmeier: "U.S. Coast Guard Treads in Deep Water", Overhaul & Maintenance Magazine (May 1, 2002).
Concrete, reinforced	link to separate page	
David statue by Michelangelo – restoration	around $500,000 (estimate)	L. McLaren: "Bath time for David", in The Globe and Mail, October 1, 2002.
Easter Island Statues 	around $10 million in restoration costs (note that the tourism industry associated with these statues reportedly generates several million dollars each year)	link to separate page for further details

Eiffel Tower (Paris) 	1989 refurbishment costs of 200 million FF. About 50-60 tons of paint are applied every 7 years by some 25 painters, as corrosion protection for the > 7 thousand ton steel structure. Corrosion damage is a major consideration in the maintenance / refurbishment requirements.	Articles by A. Roith, University Bayreuth and M. Martin, IZA published at www.uni-bayreuth.de and www.iza.com
Gas Pipeline Industry (North America)	$80 million per year purchased in coatings to coat new pipelines and recoat existing pipelines (1993 reference).	P. Cavassi and M. Cornago: "The Cost of Corrosion in the Oil and Gas Industry", JPCL, May 1999, pp30-40. (Background Section on p.34, with additional references.)
 Golden Boy Statue - restoration project, Winnipeg, Canada	$ 6 million (cost estimate) for corrosion related repairs	M. O'Malley: "Winnipeg's Golden Boy", CBC News Online, October 8, 2002.
Helicopters - US Army (1998 estimate)	$ 4 billion spent on corrosion repairs (estimate)	MTTC News, Volume 8, Issue 9 (August 19, 2003), under article "Corrosion costs eat up DOD budget".
Japan	0.8-1.0 % of GNP (1997 estimate of direct corrosion costs)	National Institute for Materials Science (Japan).
Military – USA	more than $ 20 billion per year (as reported by GAO)	MTTC News, Volume 8, Issue 9 (August 19, 2003), under article "Corrosion costs eat up DOD budget".

Military cargo trucks - USA	$850 per truck in replacement parts in the fifth service year. Anticipated to escalate to $17,500 per truck in the 11th service year	1998 TACOM study referenced in Eastern Michigan University Press release dated June 8, 2005 and titled "EMU Coatings Research Institute continues war effort against corrosion".
Navy - USA 	Around 25 % of total fleet maintenance budget (estimate) spent on corrosion prevention and control	United States General Accounting Office, Report No. GAO-03-753, 2003.
Nuclear reactors - a particular problem of voluminous corrosion product formation on in-reactor steel components	£100 million per annum	"Jack Harris column" in the journal Materials World (September 2004 issue).
Oil and Gas (Agip)	about $0.40 per barrel of oil produced, the economic impact of corrosion	P. Cavassi and M. Cornago: "The Cost of Corrosion in the Oil and Gas Industry", JPCL, May 1999, pp30-40.
Oil and Gas (North Sea production platforms)	60% of all maintenance costs related to corrosion, directly or indirectly (1993)	P. Cavassi and M. Cornago: "The Cost of Corrosion in the Oil and Gas Industry", JPCL, May 1999, pp30-40. (Background Section on p.34, with additional references.)
Pipelines (Gas and Liquid Transmission, USA)	~ $7 billion	http://www.corrosioncost.com/ **"Corrosion Costs and Preventive Strategies in the United States"**, Report by CC Technologies Laboratories, Inc. to Federal Highway Administration (FHWA), Office of Infrastructure Research and Development, Report FHWA-RD-01-156, September 2001.

United States of America	Approximately $300 billion per year, for metallic corrosion (about 4% of GNP or >$1000 per person). More than one third of costs considered avoidable using existing know-how and technology.	Batelle news release, 1996.
Roads, Sidewalks, Bridges Toronto (Canada)	$110 million is to be spent by this city on the repair of roads, sidewalks and bridges in 2005 ... with a backlog of $235 million deferred due to budget constraints.	K. McGran's article "On the road to ruin?", Toronto Star, February 5, 2005, pB4-B5.
Statue of Liberty (USA) 	> $200 million restoration project (1986), largely necessitated due to corrosion damage, with significant internal galvanic corrosion damage.	Baboian, R. et al: "The Statue of Liberty Restauration", NACE International, Houston, 1990.
Stray Current Corrosion (USA)	5% of total corrosion costs in USA, with most costs arising from electrified DC transit system operations.	"Electrolytic Corrosion in DC Powered Transit Systems," IIT Research Institute, Chicago, IL, 8 Reports Prepared for the National Cooperative Transit Research and Development Program (NCTRP) Project 48-1, TRB, National Research Council, Washington DC, 1985-1987.
Switzerland	3-5% of GNP per year, or 10-15 billion Swiss Franks per year	EMPA web site (dated 1999).

United States of America	Approximately $300 billion per year, for metallic corrosion (about 4% of GNP or >$1000 per person). More than one third of costs considered avoidable using existing know-how and technology.	Batelle news release, 1996.
United States of America	$279 billion per year (direct costs), corresponding to 3.2 percent of the U.S. GDP. Indirect costs to the user (society costs) were conservatively estimated to be equal to the direct costs.	http://www.corrosioncost.com/ **"Corrosion Costs and Preventive Strategies in the United States"**, Report by CC Technologies Laboratories, Inc. to Federal Highway Administration (FHWA), Office of Infrastructure Research and Development, Report FHWA-RD-01-156, September 2001.
United States of America (historical note)	$5 billion, in 1941	Akron Chemline (Newsletter of the Akron Section of the American Chemical Society), April 1996
Water Infrastructure	link to separate page	
Water and Wastewater Pipeline Failures in Australia (aging pipeline system)	$250 million per year. Further cost increases expected as the already aging system gets older.	CSIRO news release, 18 September 2001, (Ref. 2001/207).
more to follow ...		

(Appendix B) [90]

Cyanide Process	Alternative	PRODUCT QUALITY			
		Corrosion Protection	Finish Appearance	Chromate Colors	Ductility
Zinc[1]	Zinc Alkaline	(+) Good, greater protection in difficult to rinse areas	(+) Good brightness	Full line available	(+) Good, may be reduced at higher thickness
	Zinc Acid Chloride	(+) Good, but less protection in difficult to rinse areas	(+) Excellent brightness and leveling	Full line available	(−) Higher brightener levels may reduce ductility (+) little hydrogen embrittlement
Cadmium[1]	Cadmium Neutral or Acid Sulfate	(+) Good	(+) Satisfactory	Full line available	(+) Good, little hydrogen embrittlement
	Cadmium Acid Fluoborate	(+) Good	(+) Satisfactory	Full line available	(+) Good, little hydrogen embrittlement
	Zinc Nickel Alkaline	(+) Excellent with chromate conversion coating	(+) Good	Specialized chromates: bronze, yellow, iridescent, black	(+) More ductile than acid zinc
	Zinc Nickel Acid	(+) Good	(+) Good brightness at higher efficiency	Specialized chromates: bronze, yellow, iridescent, black	(−) Less ductile due to higher brightener levels
	Zinc Cobalt Acid	(+) Good	(+) Excellent (+) Provides deep uniform black without use of silver	Specialized chromates: bronze, yellow, iridescent, black	(+) Fair, lower hydrogen embrittlement than alkaline
	Zinc Cobalt Alkaline	(+) Good	(+) Provides deep uniform black without use of silver	Specialized chromates: bronze, yellow, iridescent, black	(+) Better than acid bath
	Zinc Iron Acid or Alkaline	(+) Good, not recommended for high temp. applications	(+) Provides deep uniform black without use of silver	Black, others limited based on bath conditions	(+) Good
	Tin Nickel Acid or Near Neutral	(+) Good resistance to corrosion and tarnish	(+) Can be decorative in appearance	N/A	(+) Good
	Tin Zinc Acid, Alkaline or Neutral	(+) Good with chromate applied (+) Does not undergo bimetallic corrosion	(−) Fair	Limited to yellow	(+) Excellent (soft deposit)
Copper	Copper Alkaline	N/A	(+) Good appearance	N/A	(+) Good
	Copper Acid Sulfate or Fluoborate	N/A	(+) Good appearance (+) Excellent leveling	N/A	(+) Good to Excellent
	Copper Pyrophosphate	N/A	(+) Good, fine grained and semi-bright	N/A	(+) Good

Notes: 1. Alkaline and acid zinc may also be used as cadmium cyanide plating substitutes.
2. N/A = Not Applicable

Alternative	PROCESS		GENERAL COMMENTS
	Plating Uniformity	Process Considerations	
Zinc Alkaline	(+) Good, uniform in high and low density areas (+) Good throwing power	(-) Narrow optimum operating range of bathparameters	(-) Lower conductivity than acid zinc (+.) Better for some forming operations (-) Harder to plate on cast iron and carbonitrided steel
Zinc Acid -Chloride	(-) Variable with current density	(-) Liners necessary in steel or porous tanks (+) High cathode efficiency at high current densities (-) Agitation required	(+) Higher conductivity results in energy savings (-) Bleedout of entrapped plating solution may limit use for complex parts (+) Plates readily on cast iron and carbonitrided steel
Cadmium Neut/Acid Sulfate	(-) Poor throwing power	(-) Liners required for acid, preferred for neutral	(-) High toxicity, low discharge limits for cadmium; not preferred toxics use reduction (TUR) option
Cadmium Acid Fluoborate	(-) Poor throwing power	(+) High cathode efficiency at high current densities (+) Good stability	(+) Good data on use available - widely used in barrel plating (-) High toxicity, low discharge limits for cadmium; not preferred TUR option
Zinc Nickel Alkaline	(+) More uniform thick-ness and alloy distribution than acid Zn Ni (+) Good throwing power	(-) Chiller required to maintain optimum temperature (-) Slower plating speed than acid Zn Ni (+) Chemistry similar to alkaline Zn	(+) Good corrosion properties maintained after forming and heat treating (-) May contain chelators
Zinc Nickel Acid	(-) Poor thickness distribution, alloy variation from high to low current density	(-) Requires additional inert anodes and segregated rectification (+) Faster plating speed than alkaline Zn Ni	(+) Good corrosion properties maintained after forming and heat treating (-) May contain ammonia or chelators
Zinc Cobalt. Acid	(-) Poor throwing power (-) Variable with current density	(+) Good plating speed (+) High cathode efficiency	(+) No silver required for black chromating (-) May contain chelators
Zinc Cobalt 'Alkaline	(+) More uniform than acid ZnCo	(-) Lower efficiency than acid ZnCo	(+) No silver required for black chromating (-) May contain chelators
Zinc Iron Acid or Alkaline	(+) Good throwing power	(-) Iron content must be controlled to prevent blistering	(+) No silver required for black chromating (-) May contain chelators
Tin Nickel Acid/Near Neutral	(+) Deep throwing power	(-) Chiller required (-) Lined tanks recommended	(+) Good hardness (between Ni and Cr) and wear resistance, low contact resistance (+) Ability to retain oil film for lubrication
Tin Zinc Acid, Alkaline or Neutral	(-) Poor throwing power (+) Excellent covering power	(-) Chiller required	(+) Excellent solderability properties
Copper Alkaline	(+) Better throwing power than cyanide	(+) Operating pH range 8.0 to 10.5	(+) Can be used as heat treat maskants (+) Less corrosive (+) May be used as strike bath
Copper Acid Sulfate or Fluoborate	(-) Less macrothrowing power than alkaline (+) more microthrowing power than alkaline	(-)Lined tanks and appropriate anode basketsrequired (+) Fluoborate allows use of higher current densities	(+) Good use data available (-) Corrosive on coatings and some substrates
Copper Pyro-phosphate	(+) Good throwing power	(+) Operating pH 8.0 to 8.8 (-) More sensitive to organic contaminants than acid Cu (-) May require longer plating time	(+) May be used as strike bath (-) May contain ammonia

Appendix C1

Dataset #0000

Copy! Format

#	X	Y
1	-1.975	-3.775e-1
2	-1.950	-3.064e-1
3	-1.925	-2.805e-1
4	-1.900	-2.559e-1
5	-1.875	-2.285e-1
6	-1.850	-2.082e-1
7	-1.825	-1.866e-1
8	-1.800	-1.647e-1
9	-1.775	-1.432e-1
10	-1.750	-1.288e-1
11	-1.725	-1.061e-1
12	-1.700	-0.937e-1
13	-1.675	-0.781e-1
14	-1.650	-0.667e-1
15	-1.625	-0.569e-1
16	-1.600	-0.482e-1
17	-1.575	-0.406e-1
18	-1.550	-0.339e-1
19	-1.525	-0.274e-1
20	-1.500	-0.170e-1
21	-1.474	-0.004e-1
22	-1.449	0.203e-1
23	-1.424	0.439e-1
24	-1.399	0.698e-1
25	-1.374	0.974e-1
26	-1.349	1.263e-1
27	-1.324	1.568e-1
28	-1.299	1.890e-1
29	-1.274	2.210e-1
30	-1.249	2.506e-1
31	-1.224	2.753e-1
32	-1.199	2.954e-1
33	-1.174	3.033e-1
34	-1.149	2.847e-1
35	-1.124	2.298e-1
36	-1.099	1.367e-1
37	-1.074	0.613e-1
38	-1.049	0.329e-1
39	-1.024	0.206e-1
40	-0.999	0.141e-1
41	-0.974	0.114e-1

start GPES Manager: Manu... EN 12:11

Electroplating Zn-Ni (data polarization curve)

Appendix C2

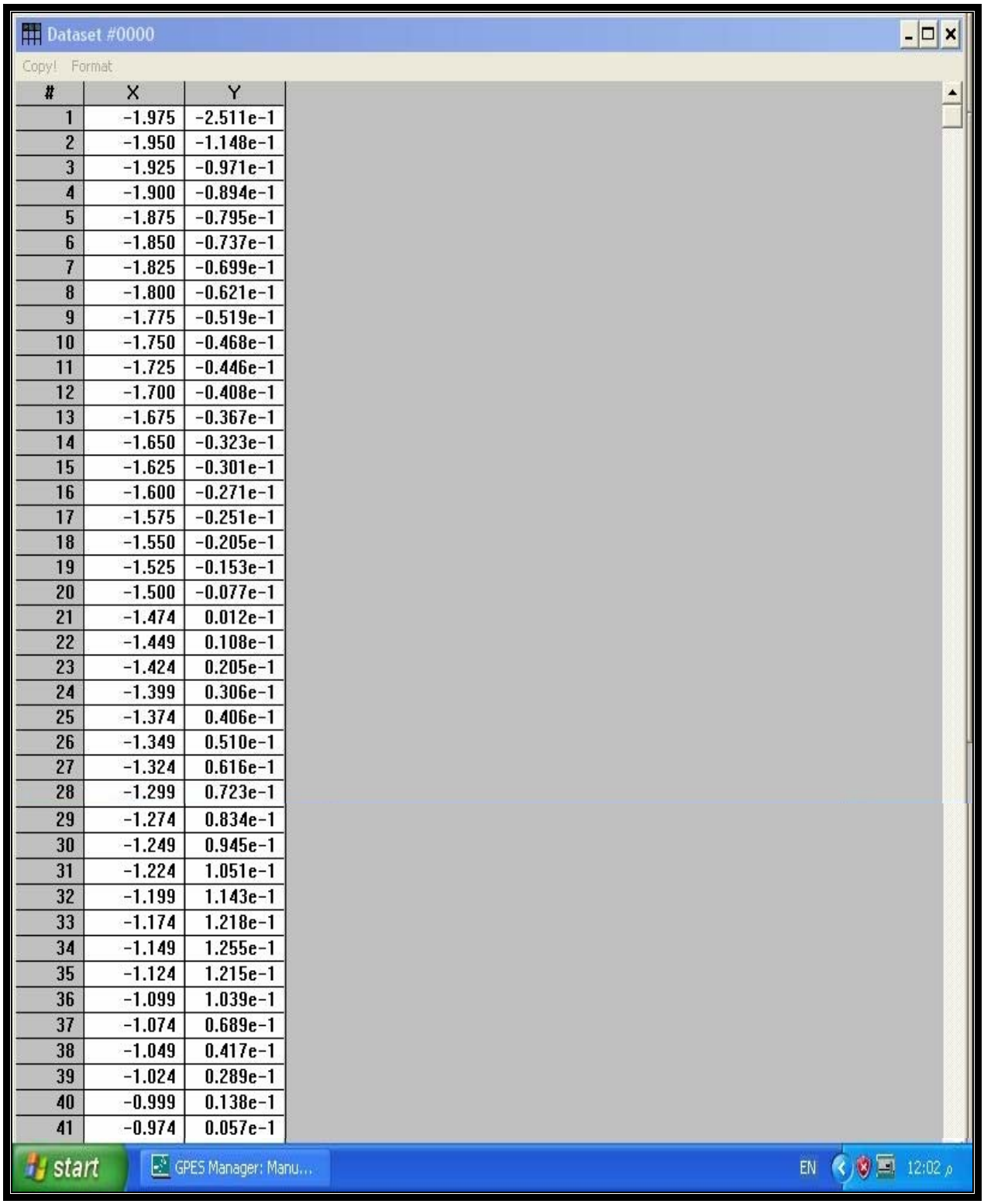

#	X	Y
1	-1.975	-2.511e-1
2	-1.950	-1.148e-1
3	-1.925	-0.971e-1
4	-1.900	-0.894e-1
5	-1.875	-0.795e-1
6	-1.850	-0.737e-1
7	-1.825	-0.699e-1
8	-1.800	-0.621e-1
9	-1.775	-0.519e-1
10	-1.750	-0.468e-1
11	-1.725	-0.446e-1
12	-1.700	-0.408e-1
13	-1.675	-0.367e-1
14	-1.650	-0.323e-1
15	-1.625	-0.301e-1
16	-1.600	-0.271e-1
17	-1.575	-0.251e-1
18	-1.550	-0.205e-1
19	-1.525	-0.153e-1
20	-1.500	-0.077e-1
21	-1.474	0.012e-1
22	-1.449	0.108e-1
23	-1.424	0.205e-1
24	-1.399	0.306e-1
25	-1.374	0.406e-1
26	-1.349	0.510e-1
27	-1.324	0.616e-1
28	-1.299	0.723e-1
29	-1.274	0.834e-1
30	-1.249	0.945e-1
31	-1.224	1.051e-1
32	-1.199	1.143e-1
33	-1.174	1.218e-1
34	-1.149	1.255e-1
35	-1.124	1.215e-1
36	-1.099	1.039e-1
37	-1.074	0.689e-1
38	-1.049	0.417e-1
39	-1.024	0.289e-1
40	-0.999	0.138e-1
41	-0.974	0.057e-1

Electroplating Zn-Ni-Cu (data polarization curve)

Appendix C3

Dataset #0000

Copy! Format

#	X	Y
1	-1.975	-3.076e-1
2	-1.950	-2.516e-1
3	-1.925	-2.198e-1
4	-1.900	-1.988e-1
5	-1.875	-1.814e-1
6	-1.850	-1.652e-1
7	-1.825	-1.483e-1
8	-1.800	-1.351e-1
9	-1.775	-1.213e-1
10	-1.750	-1.087e-1
11	-1.725	-0.963e-1
12	-1.700	-0.841e-1
13	-1.675	-0.740e-1
14	-1.650	-0.658e-1
15	-1.625	-0.566e-1
16	-1.600	-0.505e-1
17	-1.575	-0.439e-1
18	-1.550	-0.364e-1
19	-1.525	-0.271e-1
20	-1.500	-0.161e-1
21	-1.474	-0.030e-1
22	-1.449	0.111e-1
23	-1.424	0.267e-1
24	-1.399	0.433e-1
25	-1.374	0.607e-1
26	-1.349	0.771e-1
27	-1.324	0.921e-1
28	-1.299	1.099e-1
29	-1.274	1.295e-1
30	-1.249	1.487e-1
31	-1.224	1.663e-1
32	-1.199	1.785e-1
33	-1.174	1.803e-1
34	-1.149	1.675e-1
35	-1.124	1.428e-1
36	-1.099	1.111e-1
37	-1.074	0.786e-1
38	-1.049	0.400e-1
39	-1.024	0.171e-1
40	-0.999	0.104e-1
41	-0.974	0.076e-1

start GPES Manager: Manu... EN 02:37

Electroplating Zn-Ni-SiO_2 (data polarization curve)

$$gmd^{(29)} = \frac{\Delta g}{area \times day}$$

$$mm/y^{(29)} = \frac{gmd}{2.74 * density}$$

$$mpy^{(29)} = \frac{mm/y}{0.0254}$$

$$i^{(29)} = \frac{\Delta g \times n \times 96487}{time * a * area} \times 10^{6}$$

gmd……Grams per square decimeter per day

mm/y ……...Millimeters per year

mpy……Mils per year

Appendix E1

Dataset #0000

Copy! Format

#	X	Y
1	0.050	0.020e-1
2	0.025	0.020e-1
3	-0	0.020e-1
4	-0.025	0.019e-1
5	-0.050	0.018e-1
6	-0.075	0.017e-1
7	-0.100	0.017e-1
8	-0.125	0.016e-1
9	-0.150	0.015e-1
10	-0.175	0.014e-1
11	-0.200	0.013e-1
12	-0.225	0.012e-1
13	-0.250	0.010e-1
14	-0.275	0.009e-1
15	-0.300	0.008e-1
16	-0.325	0.007e-1
17	-0.350	0.006e-1
18	-0.375	0.005e-1
19	-0.400	0.004e-1
20	-0.425	0.003e-1
21	-0.450	0.002e-1
22	-0.475	0.001e-1
23	-0.501	0.001e-1
24	-0.526	-0e-1
25	-0.551	-0.001e-1
26	-0.576	-0.001e-1
27	-0.601	-0.001e-1
28	-0.626	-0.002e-1
29	-0.651	-0.002e-1
30	-0.676	-0.002e-1
31	-0.701	-0.002e-1
32	-0.726	-0.002e-1
33	-0.751	-0.002e-1
34	-0.776	-0.003e-1
35	-0.801	-0.003e-1
36	-0.826	-0.003e-1
37	-0.851	-0.004e-1
38	-0.876	-0.004e-1
39	-0.901	-0.004e-1
40	-0.926	-0.004e-1
41	-0.951	-0.005e-1
42	-0.976	-0.005e-1
43	-1.001	-0.005e-1
44	-1.026	-0.005e-1
45	-1.051	-0.005e-1
46	-1.076	-0.006e-1
47	-1.101	-0.007e-1
48	-1.126	-0.007e-1
49	-1.151	-0.008e-1
50	-1.176	-0.009e-1
51	-1.201	-0.010e-1
52	-1.226	-0.011e-1
53	-1.251	-0.012e-1
54	-1.276	-0.013e-1

start GPES Manager: Manu... base metal nacl 20-3 ... EN 02:40 م

Tafel(data) for Base Metal in 5% NaCl

Appendix E2

Dataset #0000

Copy! Format

#	X	Y
1	0.050	0.006e-1
2	0.025	0.005e-1
3	-0	0.005e-1
4	-0.025	0.004e-1
5	-0.050	0.004e-1
6	-0.075	0.003e-1
7	-0.100	0.003e-1
8	-0.125	0.002e-1
9	-0.150	0.002e-1
10	-0.175	0.002e-1
11	-0.200	0.001e-1
12	-0.225	0.001e-1
13	-0.250	0.001e-1
14	-0.275	0.000e-1
15	-0.300	-0e-1
16	-0.325	-0.000e-1
17	-0.350	-0.001e-1
18	-0.375	-0.001e-1
19	-0.400	-0.001e-1
20	-0.425	-0.002e-1
21	-0.450	-0.002e-1
22	-0.475	-0.002e-1
23	-0.501	-0.003e-1
24	-0.526	-0.003e-1
25	-0.551	-0.003e-1
26	-0.576	-0.004e-1
27	-0.601	-0.004e-1
28	-0.626	-0.004e-1
29	-0.651	-0.005e-1
30	-0.676	-0.005e-1
31	-0.701	-0.005e-1
32	-0.726	-0.006e-1
33	-0.751	-0.006e-1
34	-0.776	-0.006e-1
35	-0.801	-0.006e-1
36	-0.826	-0.007e-1
37	-0.851	-0.007e-1
38	-0.876	-0.007e-1
39	-0.901	-0.008e-1
40	-0.926	-0.008e-1
41	-0.951	-0.008e-1
42	-0.976	-0.009e-1
43	-1.001	-0.009e-1
44	-1.026	-0.009e-1
45	-1.051	-0.010e-1
46	-1.076	-0.010e-1
47	-1.101	-0.010e-1
48	-1.126	-0.011e-1
49	-1.151	-0.011e-1
50	-1.176	-0.012e-1
51	-1.201	-0.012e-1
52	-1.226	-0.013e-1
53	-1.251	-0.013e-1
54	-1.276	-0.014e-1

start GPES Manager: Manu... zn-ni- nacl x - Paint EN 11:24 ص

Tafel (data) for Zn-Ni in 5% NaCl

Appendix E3

Dataset #0000

Copy! Format

#	X	Y
1	-1.175	-0.030e-1
2	-1.150	-0.021e-1
3	-1.125	-0.016e-1
4	-1.100	-0.013e-1
5	-1.075	-0.010e-1
6	-1.050	-0.008e-1
7	-1.025	-0.007e-1
8	-1.000	-0.006e-1
9	-0.975	-0.005e-1
10	-0.950	-0.004e-1
11	-0.925	-0.003e-1
12	-0.900	-0.002e-1
13	-0.875	-0.002e-1
14	-0.850	-0.002e-1
15	-0.825	-0.001e-1
16	-0.800	-0.001e-1
17	-0.775	-0.001e-1
18	-0.750	-0.000e-1
19	-0.725	-0e-1
20	-0.699	0.000e-1
21	-0.674	0.001e-1
22	-0.649	0.001e-1
23	-0.624	0.001e-1
24	-0.599	0.002e-1
25	-0.574	0.002e-1
26	-0.549	0.003e-1
27	-0.524	0.004e-1
28	-0.499	0.004e-1
29	-0.474	0.005e-1
30	-0.449	0.006e-1
31	-0.424	0.006e-1
32	-0.399	0.007e-1
33	-0.374	0.008e-1
34	-0.349	0.009e-1
35	-0.324	0.011e-1
36	-0.299	0.013e-1
37	-0.274	0.016e-1
38	-0.249	0.018e-1
39	-0.224	0.021e-1
40	-0.199	0.023e-1
41	-0.174	0.026e-1

start GPES Manager: Manu… EN 02:32

Tafel (data) for Zn-Ni-Cu in 5% NaCl

Appendix E4

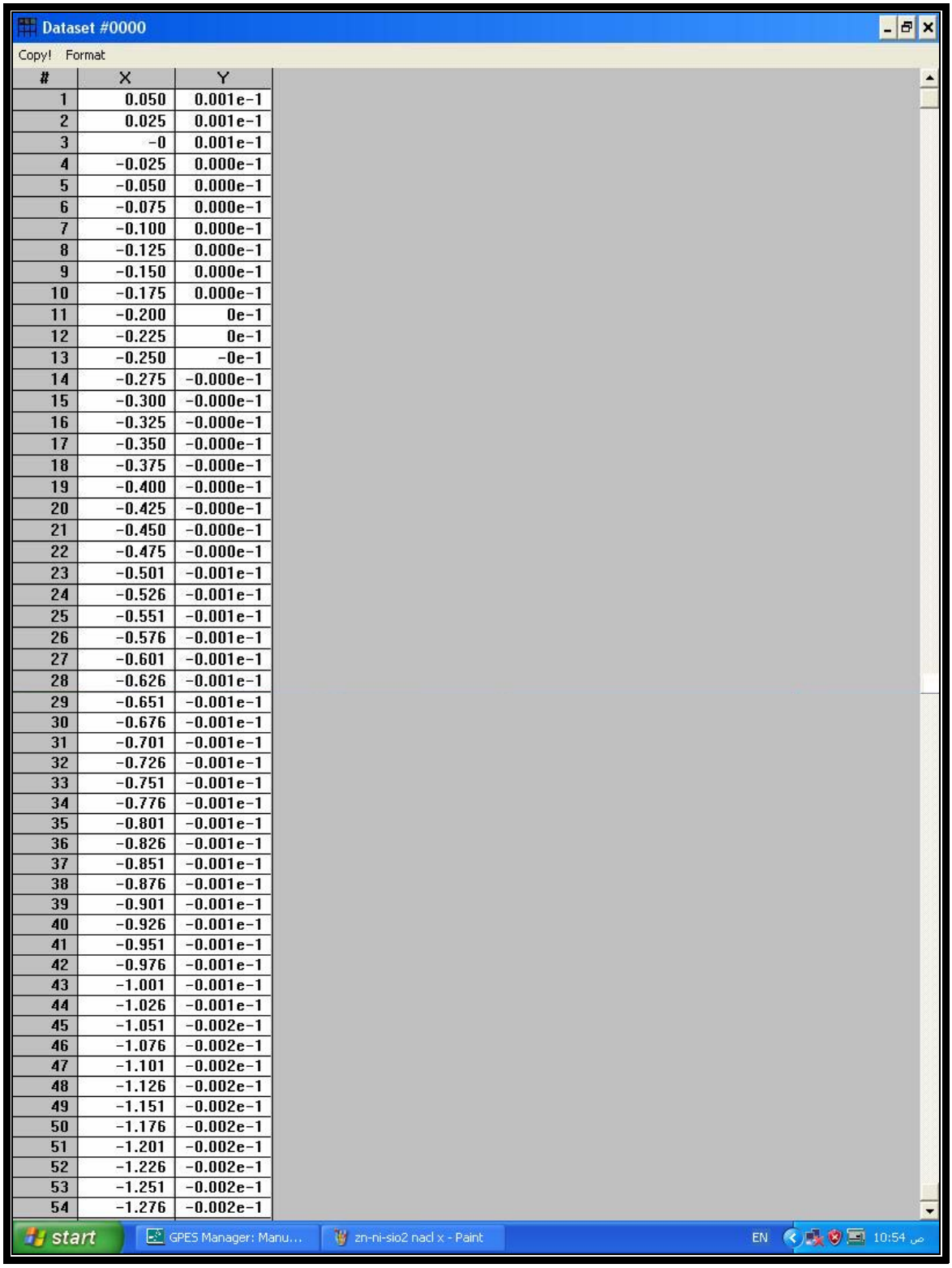

Dataset #0000

Copy! Format

#	X	Y
1	0.050	0.001e-1
2	0.025	0.001e-1
3	-0	0.001e-1
4	-0.025	0.000e-1
5	-0.050	0.000e-1
6	-0.075	0.000e-1
7	-0.100	0.000e-1
8	-0.125	0.000e-1
9	-0.150	0.000e-1
10	-0.175	0.000e-1
11	-0.200	0e-1
12	-0.225	0e-1
13	-0.250	-0e-1
14	-0.275	-0.000e-1
15	-0.300	-0.000e-1
16	-0.325	-0.000e-1
17	-0.350	-0.000e-1
18	-0.375	-0.000e-1
19	-0.400	-0.000e-1
20	-0.425	-0.000e-1
21	-0.450	-0.000e-1
22	-0.475	-0.000e-1
23	-0.501	-0.001e-1
24	-0.526	-0.001e-1
25	-0.551	-0.001e-1
26	-0.576	-0.001e-1
27	-0.601	-0.001e-1
28	-0.626	-0.001e-1
29	-0.651	-0.001e-1
30	-0.676	-0.001e-1
31	-0.701	-0.001e-1
32	-0.726	-0.001e-1
33	-0.751	-0.001e-1
34	-0.776	-0.001e-1
35	-0.801	-0.001e-1
36	-0.826	-0.001e-1
37	-0.851	-0.001e-1
38	-0.876	-0.001e-1
39	-0.901	-0.001e-1
40	-0.926	-0.001e-1
41	-0.951	-0.001e-1
42	-0.976	-0.001e-1
43	-1.001	-0.001e-1
44	-1.026	-0.001e-1
45	-1.051	-0.002e-1
46	-1.076	-0.002e-1
47	-1.101	-0.002e-1
48	-1.126	-0.002e-1
49	-1.151	-0.002e-1
50	-1.176	-0.002e-1
51	-1.201	-0.002e-1
52	-1.226	-0.002e-1
53	-1.251	-0.002e-1
54	-1.276	-0.002e-1

start GPES Manager: Manu... zn-ni-sio2 nacl x - Paint EN 10:54 ص

Tafel (data) for Zn-Ni-SiO_2 in 5% NaCl

Appendix E5

Dataset #0000

Copy! Format

#	X	Y
1	-1.175	-0.022e-1
2	-1.150	-0.014e-1
3	-1.125	-0.011e-1
4	-1.100	-0.008e-1
5	-1.075	-0.007e-1
6	-1.050	-0.006e-1
7	-1.025	-0.005e-1
8	-1.000	-0.004e-1
9	-0.975	-0.004e-1
10	-0.950	-0.003e-1
11	-0.925	-0.003e-1
12	-0.900	-0.002e-1
13	-0.875	-0.002e-1
14	-0.850	-0.002e-1
15	-0.825	-0.002e-1
16	-0.800	-0.001e-1
17	-0.775	-0.001e-1
18	-0.750	-0.001e-1
19	-0.725	-0.001e-1
20	-0.699	-0.001e-1
21	-0.674	-0.000e-1
22	-0.649	-0.000e-1
23	-0.624	0.000e-1
24	-0.599	0.001e-1
25	-0.574	0.001e-1
26	-0.549	0.002e-1
27	-0.524	0.002e-1
28	-0.499	0.002e-1
29	-0.474	0.003e-1
30	-0.449	0.003e-1
31	-0.424	0.003e-1
32	-0.399	0.003e-1
33	-0.374	0.004e-1
34	-0.349	0.004e-1
35	-0.324	0.004e-1
36	-0.299	0.005e-1
37	-0.274	0.006e-1
38	-0.249	0.008e-1
39	-0.224	0.009e-1
40	-0.199	0.011e-1
41	-0.174	0.013e-1
42	-0.149	0.015e-1
43	-0.124	0.018e-1
44	-0.099	0.020e-1
45	-0.074	0.023e-1
46	-0.049	0.025e-1
47	-0.024	0.028e-1

start GPES Manager: Manu... EN 05:24

Tafel (data) for Zn-Ni (Heat Treated) in 5% NaCl

Appendix E6

Dataset #0000

Copy! Format

#	X	Y
1	-1.175	-0.019e-1
2	-1.150	-0.012e-1
3	-1.125	-0.008e-1
4	-1.100	-0.006e-1
5	-1.075	-0.005e-1
6	-1.050	-0.004e-1
7	-1.025	-0.003e-1
8	-1.000	-0.003e-1
9	-0.975	-0.003e-1
10	-0.950	-0.002e-1
11	-0.925	-0.002e-1
12	-0.900	-0.002e-1
13	-0.875	-0.002e-1
14	-0.850	-0.001e-1
15	-0.825	-0.001e-1
16	-0.800	-0.001e-1
17	-0.775	-0.001e-1
18	-0.750	-0.001e-1
19	-0.725	-0.001e-1
20	-0.699	-0.000e-1
21	-0.674	-0.000e-1
22	-0.649	-0e-1
23	-0.624	0.000e-1
24	-0.599	0.001e-1
25	-0.574	0.001e-1
26	-0.549	0.002e-1
27	-0.524	0.002e-1
28	-0.499	0.002e-1
29	-0.474	0.003e-1
30	-0.449	0.003e-1
31	-0.424	0.003e-1
32	-0.399	0.003e-1
33	-0.374	0.003e-1
34	-0.349	0.003e-1
35	-0.324	0.004e-1
36	-0.299	0.005e-1
37	-0.274	0.006e-1
38	-0.249	0.008e-1
39	-0.224	0.009e-1
40	-0.199	0.011e-1
41	-0.174	0.012e-1
42	-0.149	0.014e-1
43	-0.124	0.016e-1
44	-0.099	0.017e-1
45	-0.074	0.019e-1
46	-0.049	0.020e-1
47	Click here to begin	0.022e-1

start GPES Manager: Manu... untitled - Paint untitled - Paint EN 04:24

Tafel (data) for Zn-Ni-Cu (Heat Treated) in 5% NaCl

Appendix E7

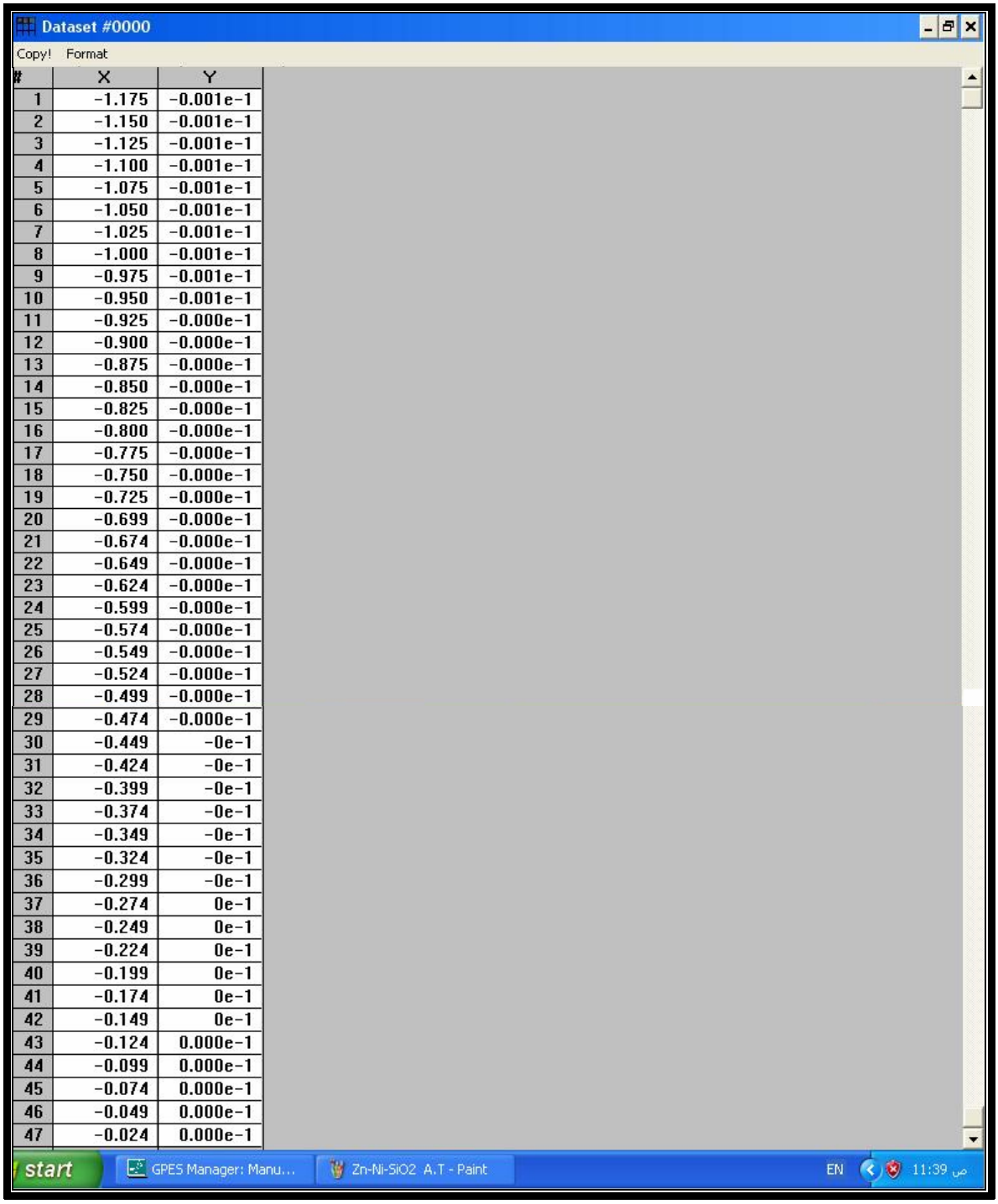

Dataset #0000

Copy! Format

#	X	Y
1	-1.175	-0.001e-1
2	-1.150	-0.001e-1
3	-1.125	-0.001e-1
4	-1.100	-0.001e-1
5	-1.075	-0.001e-1
6	-1.050	-0.001e-1
7	-1.025	-0.001e-1
8	-1.000	-0.001e-1
9	-0.975	-0.001e-1
10	-0.950	-0.001e-1
11	-0.925	-0.000e-1
12	-0.900	-0.000e-1
13	-0.875	-0.000e-1
14	-0.850	-0.000e-1
15	-0.825	-0.000e-1
16	-0.800	-0.000e-1
17	-0.775	-0.000e-1
18	-0.750	-0.000e-1
19	-0.725	-0.000e-1
20	-0.699	-0.000e-1
21	-0.674	-0.000e-1
22	-0.649	-0.000e-1
23	-0.624	-0.000e-1
24	-0.599	-0.000e-1
25	-0.574	-0.000e-1
26	-0.549	-0.000e-1
27	-0.524	-0.000e-1
28	-0.499	-0.000e-1
29	-0.474	-0.000e-1
30	-0.449	-0e-1
31	-0.424	-0e-1
32	-0.399	-0e-1
33	-0.374	-0e-1
34	-0.349	-0e-1
35	-0.324	-0e-1
36	-0.299	-0e-1
37	-0.274	0e-1
38	-0.249	0e-1
39	-0.224	0e-1
40	-0.199	0e-1
41	-0.174	0e-1
42	-0.149	0e-1
43	-0.124	0.000e-1
44	-0.099	0.000e-1
45	-0.074	0.000e-1
46	-0.049	0.000e-1
47	-0.024	0.000e-1

Tafel (data) for Zn-Ni-SiO_2 (Heat Treated) in 5% NaCl

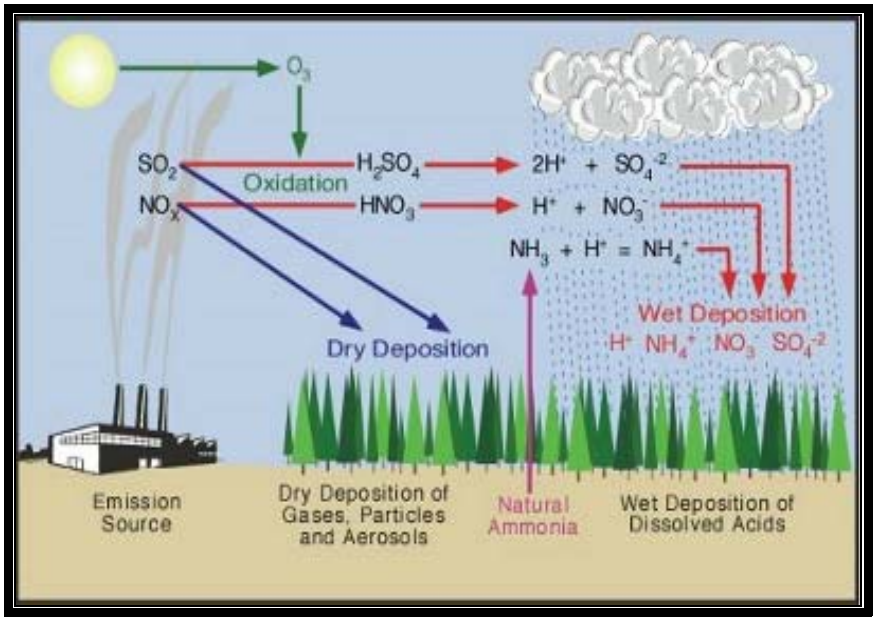

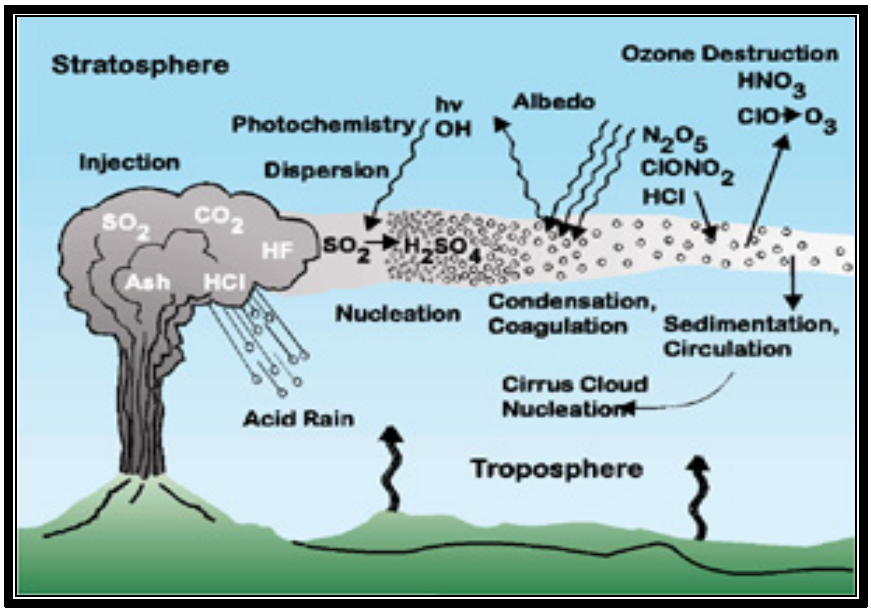

Formation of Acid Rain(163).

Appendix G1

Dataset #0000

Copy! Format

#	X	Y
1	0.025	0.688e-1
2	-0	0.613e-1
3	-0.025	0.582e-1
4	-0.050	0.546e-1
5	-0.075	0.515e-1
6	-0.100	0.482e-1
7	-0.125	0.448e-1
8	-0.150	0.412e-1
9	-0.175	0.376e-1
10	-0.200	0.344e-1
11	-0.225	0.307e-1
12	-0.250	0.274e-1
13	-0.275	0.240e-1
14	-0.300	0.207e-1
15	-0.325	0.175e-1
16	-0.350	0.142e-1
17	-0.375	0.109e-1
18	-0.400	0.077e-1
19	-0.425	0.046e-1
20	-0.450	0.015e-1
21	-0.475	-0.015e-1
22	-0.501	-0.045e-1
23	-0.526	-0.073e-1
24	-0.551	-0.101e-1
25	-0.576	-0.127e-1
26	-0.601	-0.153e-1
27	-0.626	-0.181e-1
28	-0.651	-0.207e-1
29	-0.676	-0.233e-1
30	-0.701	-0.257e-1
31	-0.726	-0.294e-1
32	-0.751	-0.324e-1
33	-0.776	-0.353e-1
34	-0.801	-0.376e-1
35	-0.826	-0.401e-1
36	-0.851	-0.435e-1
37	-0.876	-0.460e-1
38	-0.901	-0.482e-1
39	-0.926	-0.507e-1
40	-0.951	-0.554e-1
41	-0.976	-0.586e-1
42	-1.001	-0.621e-1
43	-1.026	-0.638e-1
44	-1.051	-0.664e-1
45	-1.076	-0.729e-1
46	-1.101	-0.761e-1
47	-1.126	-0.768e-1
48	-1.151	-0.824e-1
49	-1.176	-0.859e-1
50	-1.201	-0.883e-1
51	-1.226	-0.933e-1

start GPES Manager: Manu... Base Metal in acid x - ... EN 03:47

Tafel (data) for Base Metal in 1% H_2SO_4

Appendix G2

Dataset #0000

Copy! Format

#	X	Y
1	0.050	0.121e-1
2	0.025	0.110e-1
3	-0	0.101e-1
4	-0.025	0.095e-1
5	-0.050	0.091e-1
6	-0.075	0.088e-1
7	-0.100	0.084e-1
8	-0.125	0.080e-1
9	-0.150	0.075e-1
10	-0.175	0.071e-1
11	-0.200	0.066e-1
12	-0.225	0.062e-1
13	-0.250	0.057e-1
14	-0.275	0.052e-1
15	-0.300	0.047e-1
16	-0.325	0.042e-1
17	-0.350	0.037e-1
18	-0.375	0.032e-1
19	-0.400	0.026e-1
20	-0.425	0.020e-1
21	-0.450	0.014e-1
22	-0.475	0.009e-1
23	-0.501	0.003e-1
24	-0.526	-0.004e-1
25	-0.551	-0.011e-1
26	-0.576	-0.018e-1
27	-0.601	-0.026e-1
28	-0.626	-0.033e-1
29	-0.651	-0.041e-1
30	-0.676	-0.050e-1
31	-0.701	-0.058e-1
32	-0.726	-0.067e-1
33	-0.751	-0.076e-1
34	-0.776	-0.085e-1
35	-0.801	-0.093e-1
36	-0.826	-0.101e-1
37	-0.851	-0.110e-1
38	-0.876	-0.118e-1
39	-0.901	-0.128e-1
40	-0.926	-0.138e-1
41	-0.951	-0.148e-1
42	-0.976	-0.155e-1
43	-1.001	-0.162e-1
44	-1.026	-0.170e-1
45	-1.051	-0.177e-1
46	-1.076	-0.184e-1
47	-1.101	-0.192e-1
48	-1.126	-0.200e-1
49	-1.151	-0.208e-1
50	-1.176	-0.216e-1
51	-1.201	-0.225e-1
52	-1.226	-0.235e-1
53	-1.251	-0.244e-1
54	-1.276	-0.250e-1

start GPES Manager: Manu... zn-ni h2so4 x - Paint EN 12:50

Tafel (data) for Zn-Ni in 1% H_2SO_4

Appendix G3

Dataset #0000

Copy! Format

#	X	Y
1	0.025	0.363e-1
2	-0	0.325e-1
3	-0.025	0.302e-1
4	-0.050	0.290e-1
5	-0.075	0.270e-1
6	-0.100	0.251e-1
7	-0.125	0.233e-1
8	-0.150	0.220e-1
9	-0.175	0.200e-1
10	-0.200	0.184e-1
11	-0.225	0.169e-1
12	-0.250	0.152e-1
13	-0.275	0.134e-1
14	-0.300	0.117e-1
15	-0.325	0.098e-1
16	-0.350	0.081e-1
17	-0.375	0.063e-1
18	-0.400	0.047e-1
19	-0.425	0.030e-1
20	-0.450	0.012e-1
21	-0.475	-0.005e-1
22	-0.501	-0.022e-1
23	-0.526	-0.040e-1
24	-0.551	-0.059e-1
25	-0.576	-0.078e-1
26	-0.601	-0.098e-1
27	-0.626	-0.118e-1
28	-0.651	-0.138e-1
29	-0.676	-0.157e-1
30	-0.701	-0.182e-1
31	-0.726	-0.202e-1
32	-0.751	-0.224e-1
33	-0.776	-0.251e-1
34	-0.801	-0.272e-1
35	-0.826	-0.298e-1
36	-0.851	-0.315e-1
37	-0.876	-0.349e-1
38	-0.901	-0.364e-1
39	-0.926	-0.390e-1
40	-0.951	-0.419e-1
41	-0.976	-0.438e-1
42	-1.001	-0.491e-1
43	-1.026	-0.510e-1
44	-1.051	-0.536e-1
45	-1.076	-0.553e-1
46	-1.101	-0.589e-1
47	-1.126	-0.616e-1
48	-1.151	-0.638e-1
49	-1.176	-0.673e-1
50	-1.201	-0.683e-1
51	-1.226	-0.703e-1

start GPES Manager: Manu... Zn-Ni IN ACID x - Paint EN 02:36

Tafel (data) for Zn-Ni-Cu in 1% H_2SO_4

Appendix G4

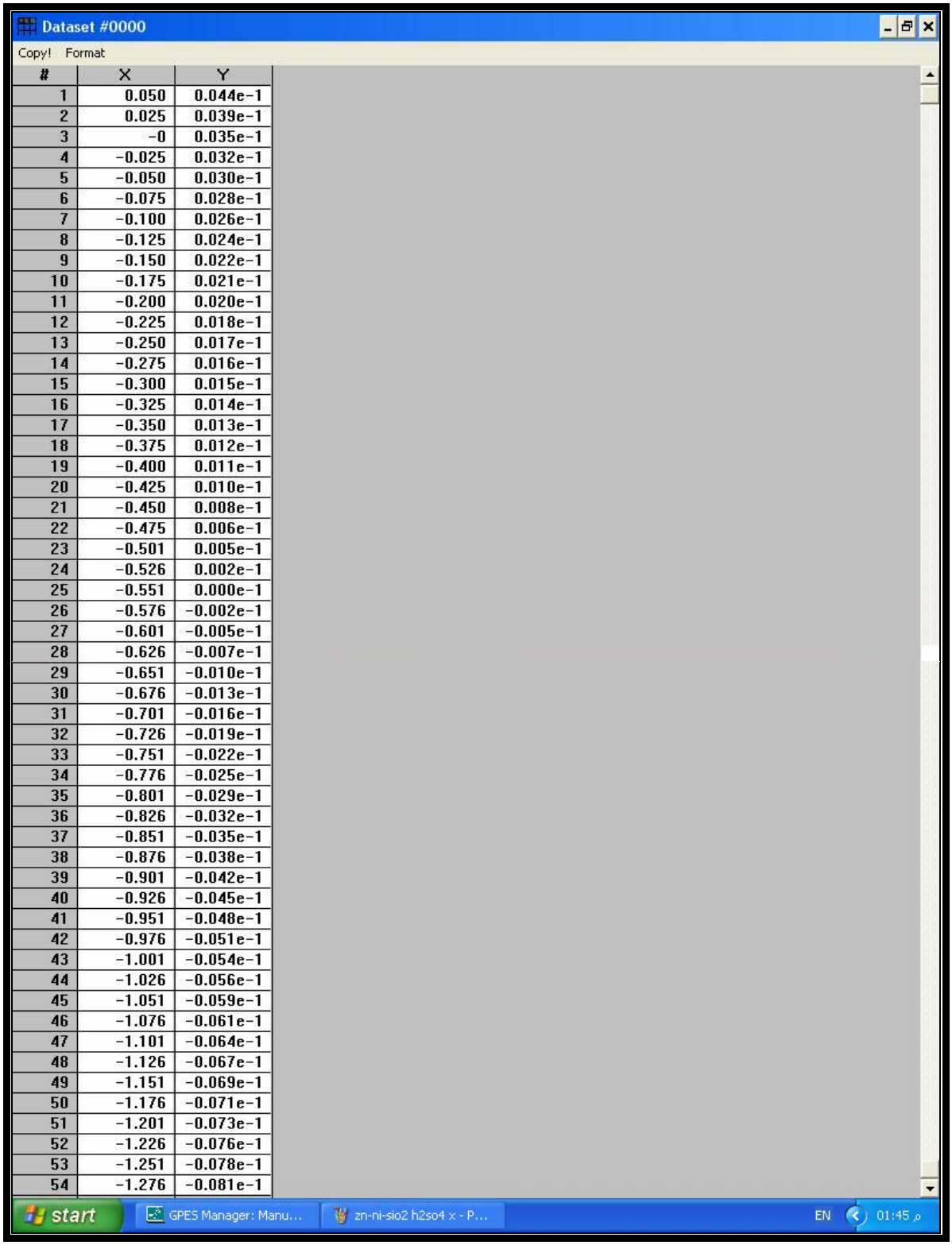

#	X	Y
1	0.050	0.044e-1
2	0.025	0.039e-1
3	-0	0.035e-1
4	-0.025	0.032e-1
5	-0.050	0.030e-1
6	-0.075	0.028e-1
7	-0.100	0.026e-1
8	-0.125	0.024e-1
9	-0.150	0.022e-1
10	-0.175	0.021e-1
11	-0.200	0.020e-1
12	-0.225	0.018e-1
13	-0.250	0.017e-1
14	-0.275	0.016e-1
15	-0.300	0.015e-1
16	-0.325	0.014e-1
17	-0.350	0.013e-1
18	-0.375	0.012e-1
19	-0.400	0.011e-1
20	-0.425	0.010e-1
21	-0.450	0.008e-1
22	-0.475	0.006e-1
23	-0.501	0.005e-1
24	-0.526	0.002e-1
25	-0.551	0.000e-1
26	-0.576	-0.002e-1
27	-0.601	-0.005e-1
28	-0.626	-0.007e-1
29	-0.651	-0.010e-1
30	-0.676	-0.013e-1
31	-0.701	-0.016e-1
32	-0.726	-0.019e-1
33	-0.751	-0.022e-1
34	-0.776	-0.025e-1
35	-0.801	-0.029e-1
36	-0.826	-0.032e-1
37	-0.851	-0.035e-1
38	-0.876	-0.038e-1
39	-0.901	-0.042e-1
40	-0.926	-0.045e-1
41	-0.951	-0.048e-1
42	-0.976	-0.051e-1
43	-1.001	-0.054e-1
44	-1.026	-0.056e-1
45	-1.051	-0.059e-1
46	-1.076	-0.061e-1
47	-1.101	-0.064e-1
48	-1.126	-0.067e-1
49	-1.151	-0.069e-1
50	-1.176	-0.071e-1
51	-1.201	-0.073e-1
52	-1.226	-0.076e-1
53	-1.251	-0.078e-1
54	-1.276	-0.081e-1

Tafel (data) for Zn-Ni-SiO_2 in 1% H_2SO_4

Appendix G5

Dataset #0000

Copy! Format

#	X	Y
1	0.025	0.402e-1
2	-0	0.358e-1
3	-0.025	0.335e-1
4	-0.050	0.314e-1
5	-0.075	0.295e-1
6	-0.100	0.277e-1
7	-0.125	0.259e-1
8	-0.150	0.241e-1
9	-0.175	0.222e-1
10	-0.200	0.205e-1
11	-0.225	0.186e-1
12	-0.250	0.168e-1
13	-0.275	0.149e-1
14	-0.300	0.131e-1
15	-0.325	0.113e-1
16	-0.350	0.094e-1
17	-0.375	0.076e-1
18	-0.400	0.057e-1
19	-0.425	0.039e-1
20	-0.450	0.021e-1
21	-0.475	0.003e-1
22	-0.501	-0.015e-1
23	-0.526	-0.033e-1
24	-0.551	-0.052e-1
25	-0.576	-0.071e-1
26	-0.601	-0.092e-1
27	-0.626	-0.114e-1
28	-0.651	-0.135e-1
29	-0.676	-0.156e-1
30	-0.701	-0.178e-1
31	-0.726	-0.199e-1
32	-0.751	-0.221e-1
33	-0.776	-0.245e-1
34	-0.801	-0.267e-1
35	-0.826	-0.289e-1
36	-0.851	-0.309e-1
37	-0.876	-0.334e-1
38	-0.901	-0.360e-1
39	-0.926	-0.380e-1
40	-0.951	-0.405e-1
41	-0.976	-0.425e-1
42	-1.001	-0.446e-1
43	-1.026	-0.469e-1
44	-1.051	-0.491e-1
45	-1.076	-0.516e-1
46	-1.101	-0.546e-1
47	-1.126	-0.575e-1
48	-1.151	-0.594e-1
49	-1.176	-0.624e-1
50	-1.201	-0.649e-1
51	-1.226	-0.670e-1

start | GPES Manager: M... | Zn-Ni-Cu A,T in a... | Zn-Ni- A,T in acid ... | Zn-Ni-second A,T ... | EN | 11:15 ص

Tafel (data) for Zn-Ni(Heat Treated) in 1% H_2SO_4

Appendix G6

Dataset #0000

Copy! Format

#	X	Y
1	0.050	0.090e-1
2	0.025	0.080e-1
3	-0	0.072e-1
4	-0.025	0.067e-1
5	-0.050	0.062e-1
6	-0.075	0.058e-1
7	-0.100	0.054e-1
8	-0.125	0.050e-1
9	-0.150	0.047e-1
10	-0.175	0.043e-1
11	-0.200	0.040e-1
12	-0.225	0.036e-1
13	-0.250	0.033e-1
14	-0.275	0.030e-1
15	-0.300	0.026e-1
16	-0.325	0.023e-1
17	-0.350	0.019e-1
18	-0.375	0.016e-1
19	-0.400	0.012e-1
20	-0.425	0.009e-1
21	-0.450	0.006e-1
22	-0.475	0.002e-1
23	-0.501	-0.001e-1
24	-0.526	-0.005e-1
25	-0.551	-0.009e-1
26	-0.576	-0.013e-1
27	-0.601	-0.017e-1
28	-0.626	-0.022e-1
29	-0.651	-0.027e-1
30	-0.676	-0.033e-1
31	-0.701	-0.039e-1
32	-0.726	-0.045e-1
33	-0.751	-0.051e-1
34	-0.776	-0.058e-1
35	-0.801	-0.065e-1
36	-0.826	-0.072e-1
37	-0.851	-0.080e-1
38	-0.876	-0.087e-1
39	-0.901	-0.094e-1
40	-0.926	-0.101e-1
41	-0.951	-0.107e-1
42	-0.976	-0.115e-1
43	-1.001	-0.121e-1
44	-1.026	-0.127e-1
45	-1.051	-0.134e-1
46	-1.076	-0.140e-1
47	-1.101	-0.146e-1
48	-1.126	-0.152e-1
49	-1.151	-0.159e-1
50	-1.176	-0.165e-1
51	-1.201	-0.172e-1
52	-1.226	-0.182e-1
53	-1.251	-0.190e-1
54	-1.276	-0.197e-1

start | GPES Manager: Manu... | zn-ni-sio2 h2so4 x - P... | zn-ni-cu h2so4 x - Paint | EN | 12:32

Tafel (data) for Zn-Ni-Cu (Heat Treated) in 1% H_2SO_4

Appendix G7

Dataset #0000

Copy! Format

#	X	Y
1	0.025	0.033e-1
2	-0	0.028e-1
3	-0.025	0.026e-1
4	-0.050	0.024e-1
5	-0.075	0.022e-1
6	-0.100	0.021e-1
7	-0.125	0.020e-1
8	-0.150	0.018e-1
9	-0.175	0.017e-1
10	-0.200	0.015e-1
11	-0.225	0.014e-1
12	-0.250	0.012e-1
13	-0.275	0.011e-1
14	-0.300	0.009e-1
15	-0.325	0.008e-1
16	-0.350	0.006e-1
17	-0.375	0.004e-1
18	-0.400	0.003e-1
19	-0.425	0.001e-1
20	-0.450	-0.001e-1
21	-0.475	-0.002e-1
22	-0.501	-0.004e-1
23	-0.526	-0.005e-1
24	-0.551	-0.007e-1
25	-0.576	-0.008e-1
26	-0.601	-0.010e-1
27	-0.626	-0.011e-1
28	-0.651	-0.013e-1
29	-0.676	-0.015e-1
30	-0.701	-0.017e-1
31	-0.726	-0.019e-1
32	-0.751	-0.021e-1
33	-0.776	-0.023e-1
34	-0.801	-0.026e-1
35	-0.826	-0.028e-1
36	-0.851	-0.031e-1
37	-0.876	-0.033e-1
38	-0.901	-0.036e-1
39	-0.926	-0.038e-1
40	-0.951	-0.041e-1
41	-0.976	-0.043e-1
42	-1.001	-0.046e-1
43	-1.026	-0.050e-1
44	-1.051	-0.053e-1
45	-1.076	-0.057e-1
46	-1.101	-0.059e-1
47	-1.126	-0.061e-1
48	-1.151	-0.063e-1
49	-1.176	-0.067e-1
50	-1.201	-0.070e-1
51	-1.226	-0.072e-1

start GPES Manager: Manu... Zn-Ni-SiO2 a.t in aci... EN 09:48 ص

Tafel (data) for Zn-Ni-SiO_2 (Heat Treated) in H_2SO_4

Appendix H1

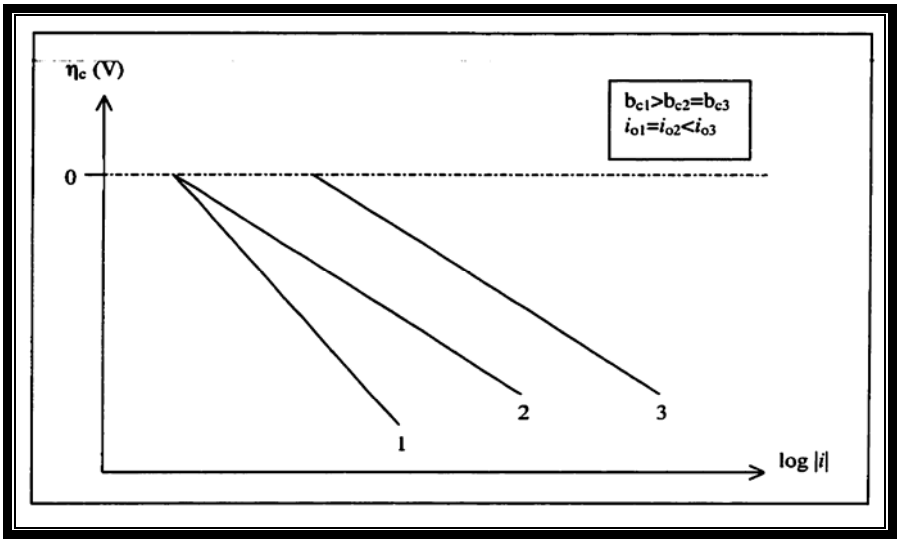

Figure (H1) Hypothetical cathodic Tafel plots [164]

when an examination of some hypothetical Tafel plots figure (H1) show that more active materials will have higher i_o (curve 3 has the highest i_o and as such is most active at low η) . Materials with indistinguishable to values but with different Tafel values will have different activities .

At high η the reaction rates will differ and the more active materials can be distinguished by their corresponding current densities .The higher the current density for a given overpotential is indicative of the more active material .As depicted for a given η_x curve 2 has a higher activity than curve 1 given that they both have similar i_o values. Similarly ,for materials with the same Tafel slopes the higher the current density for a given overpotential the more active the material (curve 3 is the most active for a given η_x) [164].

Appendix H2

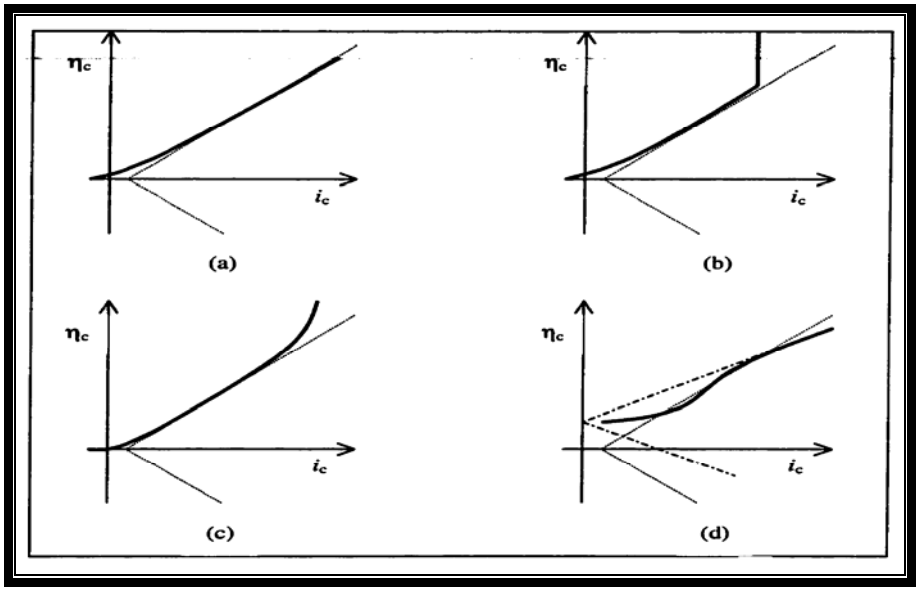

Figure (H2) Possible η -log i phenomena for a non-corroding electrode system $Z^{+}+e^{-} \leftrightarrow Z$ (line …..) [165]

a) Activation polarization.
b) Activation polarization and concentration polarization with limiting current.
c) Resistance polarization.
d) Second electrochemical (corrosion) process

$M^{+}+e^{-} \leftrightarrow M$ (line …..)

Appendix I1

Reflectance Values of : ZINC-NICKEL

WL(nm)	Reflectance	WL(nm)	Reflectance	WL(nm)	Reflectance	WL(nm)	Reflectance
360	0.000	460	9.895	560	9.503	660	10.026
370	0.000	470	9.673	570	9.244	670	10.153
380	0.000	480	10.826	580	9.629	680	9.818
390	0.000	490	10.282	590	10.266	690	10.576
400	7.658	500	10.494	600	10.027	700	10.503
410	9.499	510	10.472	610	8.953	710	0.000
420	9.330	520	10.981	620	9.430	720	0.000
430	9.639	530	10.546	630	9.066	730	0.000
440	9.340	540	10.299	640	9.172	740	0.000
450	10.184	550	9.906	650	9.817	750	0.000

Close

Zinc-Nickel

Appendix I2

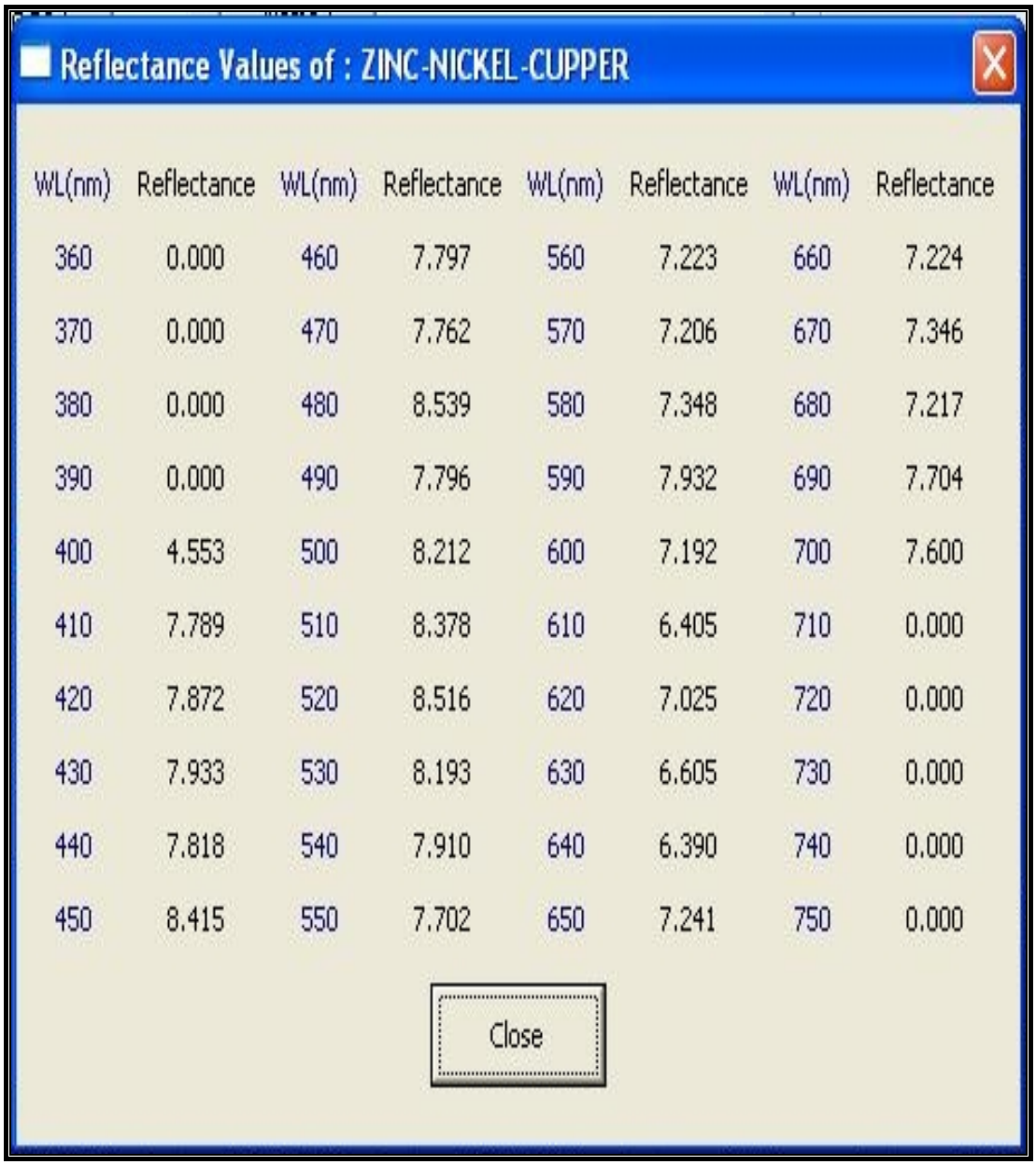

WL(nm)	Reflectance	WL(nm)	Reflectance	WL(nm)	Reflectance	WL(nm)	Reflectance
360	0.000	460	7.797	560	7.223	660	7.224
370	0.000	470	7.762	570	7.206	670	7.346
380	0.000	480	8.539	580	7.348	680	7.217
390	0.000	490	7.796	590	7.932	690	7.704
400	4.553	500	8.212	600	7.192	700	7.600
410	7.789	510	8.378	610	6.405	710	0.000
420	7.872	520	8.516	620	7.025	720	0.000
430	7.933	530	8.193	630	6.605	730	0.000
440	7.818	540	7.910	640	6.390	740	0.000
450	8.415	550	7.702	650	7.241	750	0.000

Zinc-Nickel-Cupper

Appendix I3

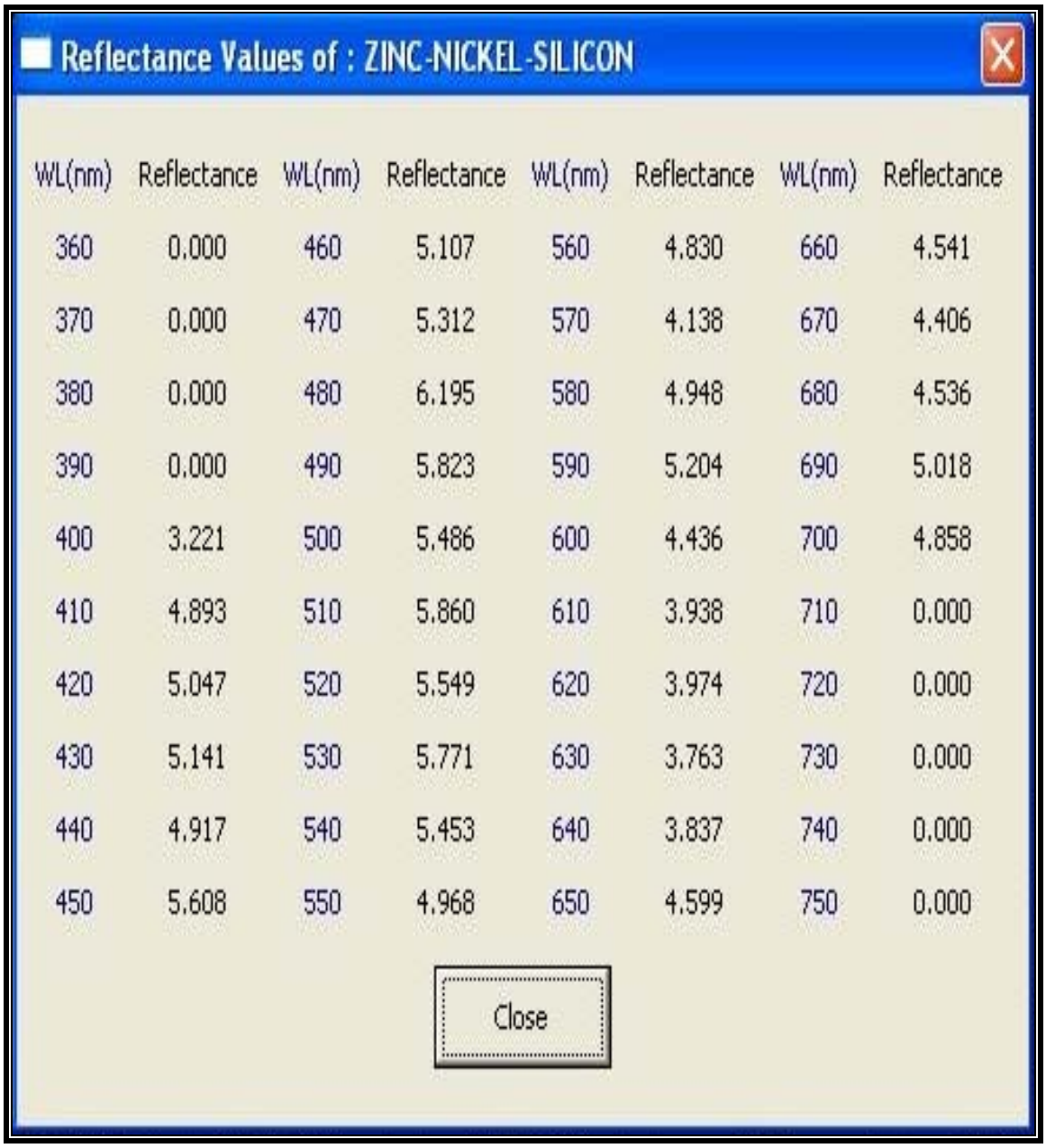

WL(nm)	Reflectance	WL(nm)	Reflectance	WL(nm)	Reflectance	WL(nm)	Reflectance
360	0.000	460	5.107	560	4.830	660	4.541
370	0.000	470	5.312	570	4.138	670	4.406
380	0.000	480	6.195	580	4.948	680	4.536
390	0.000	490	5.823	590	5.204	690	5.018
400	3.221	500	5.486	600	4.436	700	4.858
410	4.893	510	5.860	610	3.938	710	0.000
420	5.047	520	5.549	620	3.974	720	0.000
430	5.141	530	5.771	630	3.763	730	0.000
440	4.917	540	5.453	640	3.837	740	0.000
450	5.608	550	4.968	650	4.599	750	0.000

Zinc-Nickel-Silicon

وقد أظهرت إختبارات الرطوبة (Humidity environment) التي أجريت للنماذج قبل وبعد المعاملة الحرارية, فمثلاً كان الفقدان في الوزن لطبقات $Zn\text{-}Ni\text{-}SiO_2$ في درجة 55 °C ولمدة 24 hrs تمثل فقط 10% ، 13 % مقارنةً بطبقات Zn-Ni , Zn-Ni-Cu .

في اختبارات التآكل في حامض الكبريتيك المخفف (1%) كان تيار التآكل المحسوب بطريقة تافل يمثل 5% ،22% ، 23% مقارنة بالمعدن الأساس وطبقات الطلاء . وهذا يُظهر مرة" أخرى قدرة هذه الطبقة على الحماية في أوساط مختلفة .

وقد أبدت هذه الطبقة قابلية على الحماية (Protective) في أوساط أخرى مثل حامض الهيدروكلوريك المخفف (1%) بدرجات 15 ، 35 ،45، 55°C قبل وبعد المعاملة الحرارية ،أذ كانت مقاومة التآكل (mpy) تمثل 7%،9% و 11% فقط مقارنة بالمعدن الاساس وبقية طبقات الطلاء.

في أختبارات الصدمة الحرارية التي اجريت من درجات حرارية مختلفة (250 , 300, 350, 400 ,450, 500, 550 °C) بفواصل 50 °C وأخماد في الماء وبفواصل زمنية (15 min) أظهرت طبقة $Zn\text{-}Ni\text{-}SiO_2$ لدونة وتلاصق عالية ، أذا كان الوزن المفقود (هو مقياس لتكسر وتقشر طبقات الطلاء) 3%،5% مقارنة ببقية طبقات الطلاء.

كما بينت قياسات خشونة السطح Surface Roughness لطبقات الطلاء بان اضافة SiO_2 لاتؤثر على هذه الخشونة.

اما اختبارات الانعكاسية Reflectivity والنفوذية Transmissivity لطبقات الطلاء لقياس الامتصاصية absorptivity والانعكاسية لهذه الطبقات فقد بينت ان اضافة SiO_2 سببت زيادة في النفوذية وقللت الانعكاسية (لطبقة الطلاء الاولى) بمعنى امتصاصية عالية.

المستخلص

بات معروفا في الوقت الحاضر ان الطلاء بطبقة Zn-Ni يعطي خواصا تطبيقية في صناعات واسعة مثل صناعات الفضاء Aerospace Industries.

البحث الحالي يمثل محاولة لادخال تحسينات اضافية على خواص هذه الطلاءات على الرغم مما يكتنف عمليات الترسيب الكهربائي لهذه الطلاءات المهمة من غموض وقلة المعلومات المتوفرة في آلياتها.

وهنالك صعوبات أخرى تتمثل في أختيار مكونات المحلول الكهربائي بالكيفية التي تعطي طبقة حماية انودية (Sacrificial) وذلك بالحصول على نسبة 14% Ni .كما انه ليس معلوما فيما أذا كانت نفس العلاقات البسيطة يصح استعمالها في الحالات التي يكون في المحلول ازواج اخرى من الايونات.

في البحث الحالي تم ترسيب طبقات جديدة من Zn-Ni و Zn-Ni-Cu وكذلك $Zn\text{-}Ni\text{-}SiO_2$ على نماذج من الفولاذ الواطئ الكاربون باستخدام تقنية Potentistatic في وسط خامل من النتروجين ثم تم استخدام الاشعة السينية X-ray fluorescent للتحليل الكيميائي.

ان اعتماد البحث الحالي على محاولة تطوير اداء طبقة الطلاء Zn-Ni وليس Ni-Zn يمثل اختيارا للطلاء الارخص, أما اضافة SiO_2 فهي الاخرى تقلل الكلفة مرة ثانية وتقلل الوزن أذ ان كثافتة في حدود ($2.6\ gm/cm^3$) وهذا يمثل أقصى متطلبات صناعة الفضاء.كما ان هذه الطلاءات تخلو من السمية وصديقة للبيئة مقارنة بالكادميوم والكروم.

تم اجراء أختبار الصلادة الدقيقة Microhardness لطبقات الطلاء والمعدن الاساس وكانت النتائج واضحة بتفوق طبقة الطلاء $Zn\text{-}Ni\text{-}SiO_2$.

جرت أختبارات التآكل باستعمال الرذاذ الملحي (Salt Spray Chamber) بتركيز 5% NaCl بدرجة حرارة° C 35 ولمدة 24 hrs وضغط 1 bar للمعدن الاساس(الفولاذ الواطى الكاربون) وطبقات الطلاء ,أظهرت طبقة الطلاء $Zn\text{-}Ni\text{-}SiO_2$ مقاومة عالية للتآكل في الوسط الملحي مقارنة بالطلاءات الاخرى.أذ كان معدل التآكل (mpy) لطبقة $Zn\text{-}Ni\text{-}SiO_2$ يمثل 3%,7% و10% فقط مقارنة بالمعدن الاساس و Zn-Ni وZn-Ni-Cu .

في اختبارات الاستقطاب (منحنيات تافل)المقاسة أليا باستخدام تقنية Potentistatic في نفس الوسط الملحي , جاءت النتائج مرة أخرى تشير الى تفوق طبقة $Zn\text{-}Ni\text{-}SiO_2$,أذ كان تيار التآكل يمثل 9%,15% و18% مقارنة بالمعدن الاساس وطبقات الطلاء.

جمهورية العراق
وزارة التعليم العالي والبحث العلمي
جامعة بابل
كلية الهندسة

تَطويرألطلاء ألكهربائي لنِظام ذو أساس Zn-Ni ألمُسْتَخدَم في صِناعات الفضّاء

أطروحة مقدمة

الى

قسم هندسة المواد في كلية الهندسة جامعة بابل

كجزء من متطلبات نيل درجة دكتوراه فلسفه في

هندسة المواد

مقدمة من قبل

محمد عبد المهدي محمد حسين

إشراف

أ.د عبد الواحد كاظم راجح

أ.م.د فاضل محمد حسون

أ.م.د فرقد فائق محمد سعيد

٢٠٠٧ ١٤٢٨